X-641-71-184
PREPRINT

MULTI-COLOR PHOTOMETRY OF SUPERGIANTS AND CEPHEIDS

THOMAS KELSALL

MAY 1971

GSFC
GODDARD SPACE FLIGHT CENTER
GREENBELT, MARYLAND

MULTI-COLOR PHOTOMETRY OF SUPERGIANTS AND CEPHEIDS

by
Thomas Kelsall

Dissertation submitted to the Faculty of the Graduate School
of the University of Maryland in partial fulfillment
of the requirements for the degree of
Doctor of Philosophy
1971

ABSTRACT

Title of Thesis: Multi-color Photometry of Supergiants and Cepheids

Thomas Kelsall, Doctor of Philosophy, 1971

Thesis directed by: Roger A. Bell, Associate Professor of Astronomy

The results of photometry of supergiants and cepheids in a seven filter system are presented. A color index is used in combination with other colors to produce four indices freed from the effects of interstellar reddening. These four indices give measures of the Balmer discontinuity, effects of the metallic line absorption in the violet region of the spectra, break in the spectrum across the G-band, and the strength of the cyanogen band head at 4216Å.

The separation of supergiants from stars of other luminosity classes is possible. This is performed by a non-linear mapping of the colors onto an M_v,$\log T_e$ H-R diagram.

Population discrimination for cepheids appears impossible from a study of the colors. However, it is shown that the values of various color-color loop areas can be used to distinguish cepheids of Pop. I and Pop. II. This procedure is superior as it is independent of interstellar reddening.

The Balmer discontinuity index for supergiants and cepheids is insensitive to the effects of line blanketing. We speculate that this will allow for a precise calibration in terms of gravity. The strengths of the metallic line absorption and CN absorption are strongly correlated.

No obvious correlation is found between galactic position and

and chemical composition, as indicated from the strength of the metallic line index.

DEDICATION

I dedicate this thesis to two gentlemen who gave me much for which I am thankful --

my father

Mr. Bernard Kelsall

my teacher and friend

Dr. Uco Van Wijk

ACKNOWLEDGEMENTS

I offer sincere thanks to Dr. Roger A. Bell, my advisor, for the giving of his critical insights, time, and patience.

I am grateful to Dr. Nicholas U. Mayall, Director of Kitt Peak National Observatory,+ for the opportunity to use the facilities of his observatory. I also thank the observatory staff for their assistance and friendliness, and in particular, Dr. David L. Crawford, Mrs. Jeannette Barnes, and Mr. J. C. Golson.

For the reading of the manuscript and helpful advice I thank the Drs. Donat Wentzel and Michael A'Hearn.

Acknowledgement is made to Dr. Richard J. Drachman and Dr. Bengt Strömgren for their many useful discussions.

Mr. Andrew Butz and Mr. Charles Mahaffey gave aid in the reading of the charts, proof reading of the punched data, and numerous other assistances for which I am thankful.

To my wife Ann I offer appreciation for the aid given, both direct and indirect.

+Operated by the Association of Universities for Research in Astronomy, Inc., under contract with the National Science Foundation.

TABLE OF CONTENTS

LIST OF TABLES

Table | Page

LIST OF FIGURES

Figure Page

Figure Page

Figure — Page

CHAPTER I

INTRODUCTION

1-1. Preamble

The study of cepheids starts with the visual recognition of the variability of δ Cep by Goodricke in 1784, and continues through the present day. The data is of great usefulness, and is applied to a variety of problems - determination of galactic structure, compositional discrimination between galactic systems, evaluation of the extra-galactic distance scale, verification of evolutionary stellar models, etcetera. In this introductory chapter no attempt is made to summarize all the available data and their interpretations. We limit ourselves to an abbreviated discussion of a selected set of facts, observational and theoretical, representative of our knowledge; and, to a statement of this investigation's goals. A more complete picture of cepheid research is given in the works of Aller (1954), Christy (1966a, 1968), Kraft (1960, 1963, 1965), Ledoux and Walraven (1958), Payne-Gaposchkin (1954), Rosseland (1954), and Zhevakin (1963).

1-2. Theoretical Work and Its Motivational Basis

We begin with a review of cepheid theory, as it gives us an understanding of the type of stars involved and introduces concepts utilized in the interpretation of the raw observational data.

As is characteristic of astronomy the first attempts to explain variable star phenomena were geometric in structure. A main contender was the binary star hypothesis. However, by the 1920's the body of observational data could not be explained by a single, encompassing,

goemetric theory. A correct theory must explain the following:

(a) the nearly linear relationship between absolute magnitude and the log of the period;

(b) the Doppler shifting of the spectral lines with phase;

(c) the mirror image in time and structure of the light and velocity curves (maximum light at minimum recessional velocity, and the converse);

(d) in the mean a smooth progression of light curve forms with period;

(e) the time invariance of the periods;

(f) the phase-dependent changes in the spectrum, which closely mimic at each phase a class of sharp-line, non-variable stars (the pseudo-cepheids which we refer to today as supergiants);

(g) the correlation of light amplitude with period;

(h) the strong, linear correlation between light and velocity amplitudes;

(i) the restriction of the cepheids to a narrow region in the H-R diagram.

On the basis of these data the main theoretical thrust was directed toward a pulsational solution. With the strengthening of the concept that stars doubtless possess spherical symmetry, the main emphasis was directed toward pure radial pulsational theories. The major credit in promulgating these ideas must be given to Eddington.

On relatively simple arguments we can relate the expected periods of pulsating stars with their internal structure. The period should be related to a characteristic length, the diameter of the star, and the

time needed for a compressional wave to traverse that distance --

$$P \propto 2R/\bar{v}, \tag{1-1}$$

where P is the period, R the radius, and $\bar{v}$ a mean sound velocity in the star. In the quasi-static, adiabatic limit we have --

$$v = \sqrt{\gamma p/\rho}\ , \tag{1-2}$$

where γ is the ratio of specific heats, p is the pressure, and ρ the gas density. For an equilibrium, gaseous sphere with zero pressure at the surface, so surface integrals vanish, the virial theorem gives for the potential energy --

$$-W = 3\int p dV = 3\int (p/\rho)dm = 3\int (v^2/\gamma)dm$$

or

$$-W \sim 3\bar{v}^2 M/\gamma \tag{1-3}$$

where M is the mass of the star. From simple potential theory we have --

$$-W = 3GM^2/((5-n)*R) = kGM^2/R\ , \tag{1-4}$$

where n is the polytropic index, and G the constant of gravity. Using Eqs. (1-3) and (1-4) in Eq. (1-1) gives --

$$P \propto 2\sqrt{(3/\gamma G)}*\sqrt{(1/k)}*R^{3/2}M^{-1/2}\ . \tag{1-5}$$

As k increases with the degree of central concentration, Eq. (1-5) predicts that P decreases for a fixed M and R. Substituting the equality --

$$M = 4\pi R^3 \bar{\rho}_\odot \bar{\rho}/3\bar{\rho}_\odot$$

in Eq. (1-5) we develop the well-known period density relationship --

$$P\sqrt{(\bar{\rho}/\bar{\rho}_{\odot})} \propto 2\sqrt{(3/\gamma k)}/\sqrt{(4\pi G\bar{\rho}_{\odot}/3)} = Q \ . \qquad (1\text{-}6)$$

The constant Q is often referred to as the pulsation constant. With $\rho_{\odot}$ equal to 1.5 gr/cm^3, n equal to 3 ($\rho_c/\bar{\rho} = 55$), and γ equal to 5/3, we find Q = 0.039. This value is very close to results from the most sophisticated calculations for the cepheids.

Dimensional arguments, while powerful in their ability to illuminate basic physical relationships, are incapable of demonstrating the dynamical causes of pulsation. The demand of the dynamics for a periodic solution is shown by a crude first order theory as applied to a homogeneous star. For any point r in the star undergoing small, radially synchronous pulsations, Newton's equation of motion is --

$$\ddot{r} = -g - \rho^{-1}dp/dr \ , \qquad (1\text{-}7)$$

g being the instantaneous value of the gravitational acceleration. Expanding r about its equilibrium value (r_o), recognizing the assumed homogeneous configuration, and assuming adiabatic pulsations so $p \sim \rho^{\gamma}$ we have --

$$r = r_o(1+\delta(t))$$

$$g = g_o(1+\delta)^{-2} \sim g_o(1-2\delta)$$

$$\rho = \rho_o(1+\delta)^{-3} \sim \rho_o(1-3\delta)$$

$$p = p_o(1+\delta)^{-3\gamma} \sim p_o(1-3\gamma\delta),$$

where $\delta(t)$ is a time-dependent function. Substituting in Eq. (1-7), and dropping terms of order δ^2 and higher gives --

$$\ddot{\delta} + [g_o(3\gamma-4)/r_o]\delta = 0$$

or

$$\ddot{\delta} + K\delta = 0 \ , \qquad (1\text{-}8)$$

where use is made of the equilibrium relation --

$$dp_o/dr_o = -g_o\rho_o \ .$$

The general solution to Eq. (1-8) is of the periodic form --

$$ae^{i\sqrt{k^*}t} + be^{-i\sqrt{k^*}t} \ ,$$

but considering only real displacements we can write --

$$\delta = \text{const.}*\sin(\sqrt{k^*}t) = \text{const.}*\sin(2\pi t/P) \ .$$

Here P, the period of the oscillations, is given by --

$$P = [3\pi/(G\rho_o(3\gamma-4))]^{\frac{1}{2}} \ , \qquad (1\text{-}9)$$

as $g_o/r_o = 4\pi G\rho_o/3$. In this case, an evaluation gives a Q of the order of 0.10. A more rigorous analysis using for the star model a polytrope of index 3 gives a value for Q of 0.039.

A multiplicity of investigations of adiabatic pulsations was

performed from 1874 (the time of Ritter's original suggestion that gaseous spheres might be pulsationally unstable) up through the early 1950's. A classic and virtually terminal discussion along these lines is well represented by Epstein's work (1950). Epstein incorporated a number of features into his models corresponding to the increased awareness of the physical characteristics of giant stars. The models possess large radii and luminosities, and high central temperatures and degrees of central concentration. In addition, distinct from the older models, the chemical composition more nearly approximates present day estimates for the mass fractions of hydrogen, helium, and the heavy elements. The investigation shows beyond doubt that only the external portions of the star are effective in governing the basic form of the pulsations. The pulsational amplitudes are virtually zero at the center, and largest at $r \sim R$. As the stars are of a centrally condensed type, the mass involved in the larger amplitude excursions is one-tenth or less of the total mass of the star. For a wide range of reasonable physical parameters the pulsational constant, Q, is nearly invariant, and of value 0.035 ± 0.005. The ratio of first harmonic period to the fundamental period is 0.69, in good agreement with the existing data.

A salient feature of Epstein's work, and all prior investigations, is its inability to account for the persistence of the pulsations. That the escapement mechanism is the variation of nuclear energy release is untenable because of the non-participation of the central regions in the oscillations. Damping times are so precipitously short, amounting to hundreds of years, the possibility of ever observing a variable star is excluded. And all these calculations fail in explaining the "cepheid phase lag", the occurrence of light maximum a quarter

of a period after minimum radius.

What motivated theorists to continue their labors, as the returns while exciting were meager? To be sure, geometric model solutions to the problem could in no way account for the list of observational characteristics, but neither could the preliminary theoretical pulsational models. The impetus to continue was the fruitful observational search for corroborative evidence of the pulsational hypothesis.

One of the most compelling pieces of direct evidence for pulsations is the observational verification of the $P\sqrt{\rho} = Q$ relation. The ingredients needed are the masses, radii, and periods of the stars. We can determine the masses and radii by using the relations --

$$(R/R_\odot)^2 = (L/L_\odot)(T_{e\odot}/T_e)^4$$

$$M/M_\odot = (L/L_\odot)^{-3-b}$$

to give

$$\bar{\rho}/\bar{\rho}_\odot = M/M_\odot/(R/R_\odot)^3 \ ,$$

where the constant b in the mass-luminosity equation is usually taken to be near zero (see, for example, Payne-Gaposchkin and Gaposchkin (1938)). The values of T_e and L are observables, although some assumptions are required to obtain them from the raw observational data. From the determined values of ρ and P we find a Q of approximately 0.09 for the cepheids, and a wide variety of other variables. While this value is in disagreement with most theoretical determinations, it is noted that the discrepancy can easily result from minor errors in the values assigned to T_e, and less critically, to the luminosity.

Baade (1926) proposed a test of the pulsational hypothesis using color, light, and velocity measures. From the color observations it is possible to obtain bolometric corrections (BC's) and effective temperatures. From the measured visual light magnitudes (m) at any two phase points the ratio of the radii at the two points is given by --

$$R_2/R_1 = \text{Anti-log}((m_1+BC_1-m_2-BC_2-10*\log(T_{e_2}/T_{e_1}))/5). \qquad (1\text{-}10)$$

From the velocity curve, assuming the star to be a radial pulsator, we have --

$$R_2/R_1 = (R_1+\delta R_{12})/R_1 = [R_1 + d\int_{\phi_1}^{\phi_2} (v_r-\bar{v}_r)d\phi]/R_1 , \qquad (1\text{-}11)$$

where d is the limb-darkening correction term (usually taken as 24/17), and v_r, $\bar{v}_r$ are the observed and the average observed radial velocities, respectively. Using R_1 as the unit of length, the results from Eqs. (1-10) and (1-11) are comparable, and if equal, the idea of radial pulsation is supported. The first attempts were inconclusive, and the realization grew that the primary difficulty resides in the evaluations of the BC's and T_e's. Wesselink (1946) modified Baade's method by pointing out that if the two phase points are points of equal color, which are assumed to represent points of equal temperatures, the difference in light can be attributed purely to radius variations. Under this assumption Eqs. (1-10) and (1-11) are combined to give --

$$(m_1-m_2) = 2.17*[d\int_{\phi_1}^{\phi_2} (v_r-\bar{v}_r)d\phi]/\bar{R}$$

$$\Delta m = 2.17*\Delta D/(\bar{R}/d) \ . \qquad (1\text{-}12)$$

Wesselink's formulation gives, with few exceptions, excellent confirmatory results. For illustration, the application to δ Cep is shown in Fig. 1.1. From the slope of the curve, and with d = 24/17, the mean radius of δ Cep is found equal to thirty-nine solar radii.

Schwarzschild (1938) argued that a strenuous test of the pulsation hypothesis would be the demonstration that the light curve can be directly predicted from a knowledge of the velocity curve. His derivation of the test is not amenable to simplified presentation. Suffice it to say that starting from the fundamental equation --

$$L = -(16\pi r^2\sigma T^3/3\kappa\rho)dT/dr \ ,$$

and using the equation of motion to give the density variations in terms of the radius variations, we are able to find an expression relating the luminosity $L(\phi)$, in units of $\bar{L}$, to quantities derivable from the velocity curve - $\dot{r}$, $\ddot{r}$, and $r-\bar{r}$. The final expression contains three free parameters, which fortunately can be specified with reasonable precision by recourse to simple physical arguments. The application of this method to δ Cep is shown in Fig. 1.2. The observed and predicted curves are in excellent agreement.

In 1919 Shapley and Nicholson (1919) argued that an unambiguous test of pulsation would be found in observations showing a tight relationship between line asymmetries and Doppler velocities. The definitive application of the idea was delayed for thirty-three years,

but finally given in the excellent work of van Hoof and Deurinck (1952). They devised, from a reduction of high dispersion (2.9 Å/mm) spectra of η Aql, two independent tests from studying two separate sub-groups of the weak Fe I lines. The first test is the consideration of the weak Fe I lines lying on the linear portion of the curve of growth. At each phase point, seven weak, narrow lines in the range 4376 Å to 4587 Å are reduced, normalized, and averaged. The averaging procedure greatly reduces measurement errors. On visual inspection alone the correspondence between predictions - blue excess on expansion, red on contraction - and observations is good. Detailed calculations, which incorporate the effects of the pulsation hypothesis, strengthen the impression of an agreement to present the fact of agreement. In addition the line shapes for equal but opposite velocities are mirror images of one another. Illustrative results are shown in Fig. 1.3. As a check, a repeat of the above is performed on the Fe I lines situated on the horizontal portion of the curve of growth. In this case, profile averaging is impossible, so lines must be considered individually. The results are as satisfactory as in the first test .

As the observations inexorably point to the correcteness of the pulsational hypothesis, the theories must be deficient in some essential ingredient. A physical process that is, as Eddington (1930) said, "fantastic in an ordinary engine but not necessarily so in a star". The resolution came through the works of Zhevakin (see Zhevakin (1963) for a comprehensive review), and Cox and Whitney (1958) who found that the necessary destabilization results from the conversion of thermal energy into mechanical energy in the surface ionization zones of hydrogen and helium ($10^4 \lesssim T \lesssim 10^5$ °K).

In the main body of a star ($T \gtrsim 10^5$ °K) the opacity obeys a

Kramer's type law --

$$\kappa = \kappa_0 \rho^{\alpha} T^{\beta} ,$$

where $\alpha \sim +1$ and $\beta \sim -3.5$. Upon compression the temperature rises, the opacity decreases, and heat energy leaks out. This loss of heat on compression reduces the pressure during the expansion stage, and subsequently damps out the pulsation - a mechanism referred to as "radiative damping". The process in the hydrogen and helium ionization zones is most different, as the contribution of these zones to the pulsations is to balance the negative dissipation of the deeper adiabatic layers. The valving action of the ionization zones results from two distinct processes. Compressional heating goes not into the raising of the temperature but into the ionization of the medium. Thus, these regions are cooler than their surroundings and can absorb heat. This process is signaled by a decrease in the ratio of the specific heats ($\gamma \rightarrow 4/3$), and is called the "gamma effect". It might better be called the "C_p effect", as it is the increased heat capacity of the ionization regions that aid in the driving. The C_p or gamma effect is most pronounced in the second helium ionization zone, and is unimportant in the hydrogen ionization zone, which is closer to the surface, thinner, and contains appreciably less mass. In addition, on compression the opacity increases, α and β are both positive, and energy is stored up in these zones. This is called the "kappa effect". Both the gamma and kappa effects work in unison to increase the pressure upon subsequent expansion, and thus help maintain the pulsations. The relative dissipative effects of the deep adiabatic layers and the outer

ionization zones, for a particular model taken from Christy (1968), are shown in Fig. 1.4.

The complete set of equations, in Lagrangian form and standard notation, governing the pulsations are

equation of motion: $$\partial^2 r/\partial t^2 = -GM_r/r^2 - (4\pi r^2)\partial P/\partial M_r \qquad (1\text{-}13)$$

continuity equation: $$\partial r/\partial M_r = 1/(4\pi r^2 \rho) \qquad (1\text{-}14)$$

radiative diffusion: $$L_r = -(64\pi^2 acr^4 T^3/3\kappa)\partial T/\partial M_r \qquad (1\text{-}15)$$

energy equation: $$\partial L_r/\partial M_r = (P/\rho^2)\partial\rho/\partial T - \partial E/\partial t \qquad (1\text{-}16)$$

equation of state: $$P = k\rho T/\mu H + aT^4/3 \qquad (1\text{-}17)$$

internal energy/gram: $$E = 3kT/2\mu H + aT^4/\rho + I, \qquad (1\text{-}18)$$

where I is the ionization energy. The subsidiary relation giving kappa as a function of ρ,T and composition is usually in the form of a table. It is important to note that while the equations are coupled, the first two are related to the mechanicalfeatures and the second two to the thermal features of the stellar configuration. In the energy equation the nuclear energy generation is not included, because all studies show the region of interest is only the outer envelope ($T \lesssim 10^6$ ^oK). The complement to the radiative transport equation, the convective transport equation, is not shown. The question of the inclusion of time dependent convection is most complex, and an adequate prescription

is yet to be formulated. A recent attempt is that by Unno (1967). A normal set of surface boundary conditions are --

$$M_r = M: \quad P = 0; \quad d(T^4)/d\tau = T^4/A \ ,$$

where τ is the optical depth ($d\tau = -\kappa dM_r/4\pi r^2$) and the constant A is usually taken to be 2/3 so the temperature distribution satisfies Eddington's gray atmosphere approximation. The interior boundary is defined by --

$$T = \text{constant } (\sim 10^6\ ^oK) \text{ or } M_r = \text{constant } (\sim 0.5M): \quad \partial r/\partial t = 0; \quad L = L_o \ ,$$

where L_o is the luminosity emanating from the interior.

The methods of abstracting information from Eqs. (1-13) through (1-16) are referred to in the literature by a useful, descriptive nomenclature. The names, major features, and a particular modern study of these procedures are as follows;

(a) Linear, adiabatic - The structure equations are linearized ($r(t) = r_o(1+\delta r(t))$, etc.), the ones describing the thermal properties are eliminated by imposing the adiabatic condition $P \propto \rho^\gamma$, and a single second-order differential equation developed for the pulsations - Epstein (1950);

(b) Linear, quasi-adiabatic - The same as in (a), except that the adiabatic solutions are used to estimate the non-adiabatic effects by substituting into the thermal equations - Baker and Kippenhahn (1965);

(c) Linear, non-adiabatic - The four linearized structure equations are solved in their entirety - Cox (1963);

(d) Full, non-adiabatic - The structure equations are attacked without approximation - Christy (1964).

A full review of all the theoretical work is not feasible. We limit our discussion below to a single, current, comprehensive investigation.

Recently, Stobie (1969a, b, c), in a series of beautifully presented papers, has studied the effects of variations in the five prime parameters - mass, luminosity, effective temperature, helium content (Y), and heavy metal content (Z) - on theoretical cepheid models. The parameter list really contains only four, as the effects of Z variations are minor, and any reasonable ($0.02 \lesssim Z \lesssim 0.06$) value is adequate to the discussion. The calculations include radiation pressure and the three ionization zones of hydrogen and helium, but neglect convective transport. The ommission of convection restricts commentary to the high and mid-T_e region of the cepheid instability strip in the H-R diagram. There are seven observational controls imposed on the theoretical models --

(a) location of the strip's high T_e boundary;

(b) position of the strip in the M_V, (B-V) diagram;

(c) form of the M_V-logP relation;

(d) dependence of the velocity amplitude with period;

(e) correlation of (B-V) with period;

(f) location of secondary bumps on the light curves;

(G) occurence of the famous cepheid phase lag.

The choice of the basic parameters in ref. (1969b) is taken from evolutionary model calculations. For this choice the cepheid model

results disagree with the observational data, and no adjustment of the parameters, within the frame-work of the evolutionary calculations, can achieve consistency. However, the results can be made compatible with the observations by increasing the light to mass ratio. In ref. (1969c) a reduction of approximately two in mass from the evolutionary calculations is made, and the effects on the cepheid models analyzed. The mass is the most likely candidate for change as it is the one parameter not accessible to observational evaluation. The results of the new study are most encouraging.

The controls sensitive to Y - the strip's high-T_e boundary, its overall location in the M_V, (B-V) diagram and the positioning of the equal-period lines, M_V-logP relation (mainly the zero point), and the (B-V)-logP correlation - all indicate a Y of approximately 0.45. In fact, the comparison between the theory and the observations is improved for a Y of 0.45 in the M_V-logP case, if use is made of Geyer's (1970) recent re-evaluation of the zero point. Stobie compared his results with Kraft's older M_V-logP relation. The location of the secondary bump is fine - bump on the descending portion for $7^d < P < 10^d$, at light maximum for $P \sim 10^d$, and on the ascending part of the light curve for $P > 10^d$. The velocity amplitudes and their inter-relationship with period is improved. The famous cepheid phase lag test is inconclusive. This feature is the most difficult to match theoretically, but the situation is satisfactory.

This reduction in mass from that expected from evolutionary calculations has also been noted by Christy (1966b), who studied pulsational models for δ Cep and η Aql. He could get good agreement with the observations only for masses ~ 2 times smaller than those

predicted from evolutionary models. The justification for this mass reduction is usually made by invoking mass loss during a star's evolution. But is this absolutely essential? We note that even for the sun the effects of line absorption translate into an equivalent reduction in g of approximately thirty percent in the cool photosphere, as has been calculated for the Fe II ions by Lambert (1968). In the cepheid ionization zones the temperature is appreciably higher, the upper atomic levels of hydrogen and helium are populated, and resulting line absorption may easily account for some of the needed reduction in g. Obviously, this effect is restricted to the outer layers as it is negligible in the deeper, hotter, adiabatic regions. It should also be noted that part of the difficulty may arise from errors in the opacities used in the model calculations.

1-3. Basic Cepheid Parameters from Observations

We understand a group of variable stars if we can interpret observational measures to give us period, luminosity, radius, mass, composition, and evolutionary status. In this section we describe the evaluations of these prime characteristics, along with some derived inter-relationships. We discuss the pure photometric observations in 1-4.

The periods of well observed cepheids are specified to a remarkable precision, seven to nine significant figures. This stems from the long time of study as compared to the characteristic pulsational periods - e.g., eighty years as compared to ten days. As is usual we define the period as the time between sucessive light maxima. If we let T be the time of maximum light (Julian days), T_o be an arbitrary time of initial maximum, P_1 be a first approximation to the period,

then a predicted time of maximum after N cycles is --

$$T = T_0 + P_1 * N \ .$$

A study of the residuals, $T_{obs} - T_{cal}$, as a function of time gives us all the data necessary for correcting P_1. In practice this procedure is sufficient for a majority of the cepheids. For a small number, a better fit to the time of maxima is --

$$T = T_0 + P_1 * N + a * N^2 \ ,$$

so

$$P = T_{N+1} - T_N = P_1 + 2a * N + a \ .$$

Again a study of the residuals allow for the evaluation of the constants P_1 and a. In the main a is very small ($\sim 1^d.0 \times 10^{-6}$). We note that neither of the above representations is a physical statement, they are just convenient fitting expressions. However, a secular term is reasonable. The cepheid phenomena is an evolutionary stage of a short-lived massive star. The evolutionary studies indicate a star traverses the instability strip in 10^7 to 10^4 years, depending on the star's mass (4 to 9 $M_\odot$). During the traversal the period varies by approximately a third. Thus, detectable secular changes in the period of the order of seconds per year are to be expected.

A most striking cepheid relationship is the correlation between luminosity and period, the period-luminosity (P-L) law. This was first noted by Miss Leavitt around the the turn of the century in her study of cepheids in the Small Magellanic Cloud (SMC). The P-L relation for

almost any magnitude - photovisual, photographic, the B, V magnitudes of the UBV system, etc. - is of the form --

$$m = a + b*\log P \ , \qquad (1\text{-}19)$$

for a wide range in logP. The magnitude m is most often taken as the magnitude of the intergrated mean intensity. Non-linear logP terms in Eq. (1-19) should be small. We can demonstrate this by a crude calculation. We assume that in the mean a cepheid can be represented by a black-body at a particular temperature (T_{bb}). As cepheids of longer period are in the mean cooler, decreasing $\log T_{bb}$ is equivalent, in a rough sense, to increasing logP. We calculate for values of $\log T_{bb}$ the bolometric, B, and V magnitudes. Now physically Eq. (1-19) probably best represents the variation of M_{bol} with period. If such is the case and the B luminosity is a constant fraction of the bolometric luminosity for all $\log T_{bb}$ (logP), then the B magnitude would also vary linearly with logP. For pure black-bodies this is an impossibility. The true change of the B magnitude with $\log T_{bb}$, assuming $M_{bol} = \text{const.} \log T_{bb}$, is shown in upper left panel of Fig. 1.5 as the solid line, with arbitrary normalization so the M_{bol}, dashed line, and the B curves are equal at T = 7000 ^{o}K. In the lower left panel of Fig. 1.5 the results for V are shown. The prediction from this simple calculation is that there should be a discernible downward turn at low $\log T_{bb}$ (large logP) values. This is in good agreement with the photometric P-L relations for V and B determined from a combined study of cepheids in our galaxy, SMC, LMC, M31, and NGC 6822 by Sandage and Tammann (1968). The Sandage-Tammann results are shown in the right panels

of Fig. 1.5, where the dashed line represents the straight line which passes through the greatest segment of the respective P-L curves.

The usefulness of the P-L relation is contingent upon precise evaluations of the zero point, a, and slope, b, in Eq. (1-19). The paucity of absolute magnitudes, in any photometric system, for cepheids in our galaxy precludes the simultaneous determination of these constants. The usual assumption has been that the slope can be taken from the extensive observations of cepheids in the SMC. This ad hoc assumption is now reasonably well supported by the observational (Sandage and Tammann 1968) and theoretical (Stobie 1969b) results. Though the observational results are still a little unsettled, especially for V, as can be seen in Table 1.1.

Some of the deviation in the slope determinations results from the small samples, the assumed form of internal absorption corrections in the SMC, and the intrinsic difficulties working with faint stars. But the major problem is probably the presently impossible task of selecting a homogeneous and representative sampling of cepheids - i.e., cepheids which are chemically similar, pulsating in the same mode or combination of modes, and are non-binaries. This problem is most likely illustrated by the differing results found by the Gaposchkin's (1966) when they separately analyzed cepheids with maxima preceding the minima by 0.3P ($= \bar{\Phi} - \phi$) and less, and cepheids with $\bar{\Phi} - \phi > 0.3$ (solutions #2 and #3 in their Table 9).

Once the slope of the P-L relation is known the galactic cepheids can be employed in two methods to give the zero point. The first and older method is through the study of the proper motions and radial velocities. A recent investigation is by Geyer (1970). Geyer first

analyzed the proper motions of one hundred and eighteen cepheids, broken up into five distance groupings. From each grouping the solar motion, $S_{\odot}(PM)$, is found. The analysis incorporates into its structure a distance scale determined by an assumed value of the zero point. As a second step the solar motion is evaluated from the radial velocities, $S_{\odot}(RV)$, a procedure which is distance scale independent. If the distance scale, based on the assumed zero point value, in finding $S_{\odot}(PM)$ is correct, the $S_{\odot}(PM)$ should equal $S_{\odot}(RV)$. If the equality is not found, the distance scale must be corrected by the factor $S_{\odot}(PM)/S_{\odot}(RV) = \lambda$, or equivalently a correction made to the zero point of $5\log\lambda$.

A second method, by Kraft (see Kraft (1960) and references therein), is constructed from UBV data on the five cepheids in five different galactic clusters. Assuming chemical homogeneity the main-sequences of the clusters are fitted to the Hyades standard, thus giving the clusters' (B-V) reddening excesses. Assuming a ratio for the total to selective absorption, we find the distance moduli. These data give directly the absolute magnitudes for the associated cepheids. On the further assumption that the slope of the mean P-L relation is the same as for cepheids in the SMC the zero point is easily evaluated from the data on the five cluster cepheids to give the P-L relation --

$$M_V = -1.67 - 2.54*\log P \ .$$

Geyer would modify the zero point to -1.88.

A variation on the use of the cluster cepheids in our galaxy is that employed by Sandage and Tammann (1968). Their analysis is not governed by considering Eq. (1-19) as being fundamental. They determine

a best mean P-L relation for cepheids in our and other galaxies, using the cluster cepheids in our galaxy as a control on the distance moduli of the external galaxies. The control procedure is to adjust the moduli until the scatter in the P-L diagram shows no systematic differences relative to the cluster cepheids. Their results have already been presented in the right panels of Fig. 1.5.

A third, and rather novel, approach is that taken by Fernie (1964, 1965, 1967c). Starting with the prime equation --

$$M_{bol} = M_{bol_\odot} - 5\log(R/R_\odot) - 10\log T_e + 10\log T_{e_\odot} ,$$

he introduces observable quantities through a series of substitutions. These substitutions are as follows:

$$(1) \quad \log T_e = -0.168*(B-V) + 3.87$$

and

$$M_{bol} = M_V - 0.36*(B-V) - 0.09 ,$$

which are derived from a combination of spectrophotometry and a study of model atmospheres (Oke 1961);

$$(2) \quad \log(R/R_\odot) = 0.558*\log P + 1.260 ,$$

a result of studying the radii derived from use of Wesselink's method (Fernie 1968b);

$$(3)\quad T_{e_\odot} = 5800\ ^{o}K$$

and

$$M_{bol_\odot} = 4.^{m}72\ ,$$

the solar constants (Allen 1963). Using these secondary relations in the expression for M_{bol} gives --

$$M_V = -2.56 + 2.04*(B-V) - 2.79*\log P\ . \qquad (1\text{-}20)$$

However, the observations indicate a $\partial V/\partial(B-V)$ which is color dependent, and of value $2.79 - 1.55*(B-V)$. Using this as the coefficient for $(B-V)$ in the above gives --

$$M_V = -2.56 + 2.79*(B-V) - 1.55*(B-V)^2 - 2.79*\log P\ . \qquad (1\text{-}21)$$

Applying Eq. (1-21) to the eight cepheids with well determined M_V's in binaries, associations, and clusters it is found that the average residual is not zero. However, minor improvements in the coefficients of Eq. (1-21) can be made to force the average residual to zero. The final period-luminosity-color (P-L-C) equation is --

$$M_V = -2.55 + 2.73*(B-V) - 1.60*(B-V)^2 - 2.85*\log P\ . \qquad (1\text{-}22)$$

Fernie makes a series of secondary checks on Eq. (1-22) and finds it is in excellent agreement with observations. To reduce Eq. (1-22) to a simple P-L relation we use the correlation --

$$(B-V) = 0.24 + 0.49*\log P \ ,$$

so Eq. (1-22) becomes --

$$M_V = -1.99 - 1.89*\log P - 0.38*(\log P)^2. \qquad (1\text{-}23)$$

Geyer's investigation indicates a small change in the zero point to -2.05 is needed. The non-linearity in Eq. (1-23) is obvious, but is it real? In form it produces a curvature opposite from our simple black-body analog to the cepheids, and it is in disagreement with the results of Sandage and Tammann (1968). It does agree with the results of Payne-Gaposchkin and Gaposchkin (1966). However, Sandage and Tammann consider the Gaposchkins' results to be vitiated by their over correcting for internal reddening in the SMC. A final resolution will have to await the time when the number of cepheids with good M_V's and intrinsic colors is sufficient to calculate from them alone the form of the P-L-C and P-L relations.

A resume of the M_V evaluations is shown in columns two, three, and four of Table 1.2.

A major source of information on radii is from the application of Wesselink's method. The method is not without difficulties, and sometimes gives startling and ambiguous answers. The procedure rests on two suppositions that are not necessarily met in every case. The first assumption is that points of equal color are identical to points of equal temperature. But this is refuted by the observation that color-color plots in any photometric system are not lines, but loops. It is incumbent on us to make a most judicious choice of color. Invariably,

in the UBV system the color (B-V) is the one chosen, as all observational data indicate this to be better than (U-B) as an index of temperature. A second assumption is that the relative separation of the photosphere and the line-forming reversing layer remains constant during the pulsation. Abt (1959b) considers this condition is satisfied only if the pulsational expansion is twenty to hundred times the atmospheric scale height, an expected situation for the bulk of the classical cepheids. However, Christy (1968) finds from his non-linear model representation for β Dor that the motion of the photospheric layers is approximately ten percent less than for the line forming region. This differential motion requires the Wesselink radius be reduced by ten percent. A third obstacle in utilization is observational, as the radial velocity and photometric observation are almost inevitably performed at different epochs, and by different observers. This difficulty is surmountable only if the velocity and photometric results can be matched in phase to within $0^{p}.01$, otherwise the radius determinations are severely degraded (Fernie and Hube 1967). Overall the expected accuracy of Wesselink radii is of the order of ten to fifteen percent.

As stressed by Reddish (1955), a fundamental relation should exist between period and radius. Fernie (1964, 1965, 1968b) has analyzed the set of best determined radii and finds a strong correlation between period and radius (this relation was used above in deriving Eq. (1-20)) --

$$\log(R/R_{\odot}) = 0.558*\log P + 1.260 \ . \qquad (1\text{-}24)$$

The dispersion about this linear relation is markedly larger for a fraction (1/3) of the cepheids than would be expected on any set of reasonable premises. Fernie then makes the ad hoc assumption that the stars with large deviations - η Aql, W Sgr, β Dor, X Cyg - are pulsating in other than the fundamental mode, and adjusts their periods by dividing by 0.71, the ratio of the first overtone to the fundamental. For one star, U Car, the adjustment is made assuming the star is pulsating in the third overtone. This process greatly reduces the scatter, but whether any legerdemain of this nature is a valid indicator of overtone pulsation is, we believe, debatable. In fact, in one instance, for β Dor, the situation is ambiguous. Fernie gives a value of 79 $R_\odot$. Christy (1968) using recent data finds a radius of 69 $R_\odot$, which he further reduces by ten percent as mentioned above, to give a final value of 62 $R_\odot$. Evading the issue whether the ten percent reduction is applicable to all cepheids with periods near ten days, Christy's evaluation are both very close to the value of 65 $R_\odot$ predicted by Fernie's P-R relation (Eq. (1-24)).

A period-radius relation can be derived reasoning as Fernie did in creating his P-L relation. From the usual expression for M_{bol} we have the instantaneous relation --

$$5*\log(R/R_\odot) = -M_{bol} - 10*\log T_e + \text{Const.}_\odot, \qquad (1\text{-}25)$$

into which we substitute

$$M_{bol} = M_V + a_1*(B\text{-}V) + a_2$$

and

$$\log T_e = b_1*(B\text{-}V) + b_2 \quad .$$

Averaging over a pulsational cycle gives --

$$5*\langle\log(R/R_\odot)\rangle = -\langle M_V\rangle - (a_1+10b_1)*\langle B-V\rangle + (\mathrm{Const}_\odot - a_2 - 10b_2) \quad . \qquad (1\text{-}26)$$

Assuming an ensemble average is obtained upon substituting the mean relations --

$$\langle M_V\rangle = c_1*\log P + c_2$$

and

$$\langle B-V\rangle = d_1*\log P + d_2 \ ,$$

we have

$$5*\langle\log(R/R_\odot)\rangle = (-c_1 - a_1d_1 - 10b_1d_1)*\log P + (\mathrm{Const.}_\odot - a_2 - 10b_2 - c_2 - a_1d_2 - 10b_1d_2). \qquad (1\text{-}27)$$

Accepting Sandage and Tammann's expressions for M_{bol} and $\log T_e$, correcting their Eq. (7) for $\langle B\rangle - \langle V\rangle$ by 0.02 to make it correspond more closely to $\langle B-V\rangle$ (Kraft 1961), and linearizing their $\langle M_V\rangle$ - log P ridge line ($\langle M_V\rangle = -1.50 - 2.73*\log P$) we find upon substituting into Eq. (1-27) that --

$$\langle\log(R/R_\odot)\rangle = 0.655*\log P + 1.131 \ . \qquad (1\text{-}28)$$

Investigators often give rather small error estimates for their values of the coefficients a_1, a_2, etc.; but a comparison of results between equally competent researchers reveals that systematic errors can be larger than the quoted internal errors. It is expected that the mean errors of the constants in Eq. (1-28) can easily be of the order of

±0.1. A comparison between Eqs. (1-24) and (1-28) is shown in columns five and six of Table 1.2.

The masses of the cepheids can be inferred from the pulsational equation --

$$P*\sqrt{(\rho/\rho_{\odot})} = P*(M/M_{\odot})^{\frac{1}{2}}*(R/R_{\odot})^{-\frac{3}{2}} .$$

Christy's (1968) theoretical results indicate that a reasonable expression for Q is of the form --

$$Q = A*(M/M_{\odot})^{-\frac{1}{4}}*(R/R_{\odot})^{\frac{1}{4}} . \qquad (1\text{-}29)$$

Substituting Eq. (1-29) into the pulsational equation, and letting $\log(R/R_{\odot}) = a_1*\log P + a_2$ gives --

$$\log(M/M_{\odot}) = (7/3*a_1 - 4/3)*\log P + 7/3*a_2 + 4/3*\log A . \qquad (1\text{-}30)$$

We note that Eq. (1-30) predicts a <u>decrease</u> in mass with period for all a_1 less than 4/7 (0.571). If we accept Fernie's P-R relation, we would have this result; and the same would occur whether Q is a pure constant, or obeys the observational relationship with period as determined by Kraft (1963) [$\log Q \sim 0.1*\log P$ + Const.]. To circumvent this difficulty, and as the radius results are comparable to those found by Fernie, we use Eq. (1-28) for the variation for logR with logP. To fix the constant A in Eq. (1-29) we take Q = 0.042 at a period of two days, forcing agreement with the observed ratio (Oosterhoff 1964, Leotta-Janin 1967) of first overtone to fundamental (P_1/P_0 = 0.71) for short period cepheids.

The final expression for $\log(M/M_{\odot})$ is --

$$\log(M/M_{\odot}) = 0.195*\log P + 0.570 \ . \qquad (1\text{-}31)$$

An alternative estimation procedure is to make use of the mass-luminosity relationship. For the zero-age-main sequence we have, from the work of Kelsall and Strömgren (1966), for a composition appropriate for young Pop. I stars (X = 0.60, Y = 0.36, Z = 0.04) --

$$M_{bol} = 3.53 - 8.44*\log(M/M_{\odot}) \ .$$

Assuming the cepheids lie one magnitude above their initial ZAMS position, and using the appropriate subsidiary equations from Sandage and Tammann we find the above equation results in the relation --

$$\log(M/M_{\odot}) = 0.344*\log P + 0.475 \ . \qquad (1\text{-}32)$$

A comparison of the mass estimates derived from the equations developed here, the evolutionary calculations of Iben (1965, 1966a,b,c) and the pulsational calculations for a helium content of 0.45 by Stobie (1969c) is shown in columns seven through ten of Table 1.2. On the whole the discrepancies at any period are tolerable, never exceeding forty one percent.

The more direct method of mass determination from the study of binary motions can not presently be carried out for cepheids. Thiessen (1956) interpreted the 27 day variation in the light of the A5 supergiant BM Cas as arising from a cepheid companion. Under this

assumption the cepheid mass would be approximately twenty three times that of the sun. The data is scant, and the analysis therefore of doubtful quality. For those cepheids with distinquishable physical companions (δ Cep (Fernie 1966a, Worley 1966, Vitrichenko and Tsarevskii 1969), α UMi (Fernie 1966b), ℓ Car (Fernie 1967b)) the separations are so great that the orbital periods are too long to be useful in mass determinations. There is the exciting double cepheid CE Cas a and CE Cas b in the galactic cluster NGG 7790. Both are cepheids with the nearly equal pulsational periods of $5^d.14$ (a) and $4^d.47$ (b). But here the orbital period is minimally hundred thousand years. An analysis by Sandage and Tammann (1969) incorporating a study of the stars' magnitudes and colors, and a comparison with evolutionary tracks, is only capable of indicating a mass ratio - $M_b/M_a \tilde{=} 1.007$.

However, the observational determination of cepheid masses looks promising. Lloyd Evans (1968) has recently re-evaluated the frequency of spectroscopic binaries among classical cepheids. The study makes use of the variability of the radial velocity, and the verified correlation between photometric anomalies and binary occurrence. Lloyd Evans finds that at least fifteen percent of all cepheids are spectroscopic binaries. This estimate is almost an order of magnitude larger than that suggested by Abt (1959a) in an earlier discussion.

To capitalize on this situation will require a substantial amount of observational work. Two new techniques can be of great aid. Griffin (1967, 1969) has constructed a photoelectric radial-velocity spectrometer capable of determining six to eight velocity measures per hour, with a precision of approximately one kilometer per second. This tremendous enhancement of the data gathering rate is such as to make a

large, systematic program feasible. In addition, it may be possible to rise above the statistical limitation of spectroscopic binary mass analysis by the use of space-scanning photometers (Rakos 1965, Franz 1966). With a scanning photometer we could detect close, faint binaries which are "lost" in more conventional procedures due to the intrinsic brightness of the cepheids.

The growth of photographic spectroscopy, and the desire to fathom the complexities of cepheid behavior were coeval. Much of the spectroscopic results for the cepheids was, however, of a transitory nature, but a significant portion of the researches were of such merit that they are still cited in the most current investigations. We here briefly review the more salient findings. For a more complete review, with extensive reference citations, see Kraft (1960).

Radial velocities have been determined by workers since the 1890's. Large, ambitious, and precise programs have been carried out by men such as Joy, Jacobsen, Sanford, and Stibbs (see Lloyd Evans (1968) for detailed references). At present there is data for some two hundred cepheids of all types. There is a strong linear correlation between light and velocity amplitude up to a velocity amplitude of ~ 50 km/sec and light amplitude of $\sim 1^{m}.5$, after this point the velocity amplitude increases more slowly with the light amplitude (maximum light amplitude is $\sim 2^{m}.0$). The velocity and light curves are virtual mirror images of one another, with maximum velocity at minimum light, etcetera. Though there does appear a systematic phase lag in the velocity of $\sim 0^{p}.1$ with respect to the light variations. The radial velocity data in conjunction with photometry allows for the determination of radii, as we have seen above. A second major use of the velocity data is the

detection of companions.

At classification dispersions ($\sim$ 100 Å/mm) the spectra of cepheids very closely resembles that of their non-variable counterparts, the supergiants. This feature is agreed upon by even the most astute observers. At light maximum the cepheids, independent of period, are equivalent to F5 - F8 Ib stars. Anomalies are noticeable, particularly in stars with periods greater than five days, in that the hydrogen lines are conspicuously stronger than expected from the estimate of the spectral type from the metal lines. There is also a slight enhancement in the Ti II and Fe II lines. At light minimum the spectral types go toward the later types smoothly with period.

High dispersion (2 - 20 Å/mm) work gives much data on line shapes. It is found that the profiles can be accounted for by invoking the effects arising from the geometry of pulsation, "level effects" resulting from a velocity gradient in the atmosphere, and phase dependent turbulence (micro and macro) strengths. The inclusion of rotational effects appears unnecessary on the basis of evolutionary arguments (Kraft 1966). The model atmosphere analyses utilizing the high dispersion results show that the physical parameters T_{exc}, T_{ion}, P_e and turbulent velocities are similar to those of supergiants at the same equivalent spectral type. There are two interesting transitory instances during the pulsational cycle where the cepheids differ markedly from the supergiants. One is the peculiar doublings in the low excitation lines of Fe I, Ti II and H, which apparently indicates that material is falling back onto the star. Second is the anomalous behavior of the Ca II emission. In essence the emission is just totally distinct from that observed in the supergiants. This is most puzzling

for it is then difficult to argue for a common mode of origin, yet every other indicator points to the great similarities in the atmospheric structures. As an example of the divergence, if we calculate the absolute magnitudes for cepheids via the Wilson-Bappu procedure the prediction is that the cepheids are two to three magnitudes brighter than is conceivable by any other mode of magnitude evaluation.

Our more pressing interest in the elemental abundances for cepheids is not well satisfied by the present literature. An indirect argument that indicates solar or Hyades like metal abundances is the virtual similarity of the cepheid spectra as compared to normal supergiants. More substantive work during the last decade is slight. Three southern cepheid variables have been meticulously studied by Bell and Rodgers. While their analyses do incorporate the assumption of approximate solar metal abundances, by a system of ingenious checks and balances they are able to insure that a systematic indication of over or under abundance will be correct. For κ Pav, which is probably of old Pop. I type, they find a deficiency in [Fe/H] of -0.42, and for elements synthesized by slow neutron capture the [s.n.c./Fe] is $\approx$ -1.0 (Rodgers and Bell 1963, 1968b). For β Dor they find no inconsistency with the idea of solar abundances, though the line strengths for Eu II are anomalous (Rodgers and Bell 1964). In a first paper on ℓ Car they report finding a lithium line at 6707 Å, a "first" for cepheids. The strength of the line indicates a [Li] of -0.4 (Rodgers and Bell 1968a). This implies an abbreviated extent for the photospheric convection layer, otherwise the lithium would have been burned up. In a second paper (Bell and Rodgers 1969), heralding for them the use of computer synthesized spectra, they are able to determine differentially the near

equivalence in metal abundances for ℓ Car and δ CMa, with some likelihood that ℓ Car possesses a higher abundance of metals, but still in the Hyades range. Abt et al. (1966) have analyzed the short period cepheid TV Cam. In TV Cam the metal lines appear weak. In addition, the star's light amplitude is large for its period. This combination led some to propose that if the SMC cepheids were similar to TV Cam, their large light amplitudes relative to their periods could be explained on the basis of chemical anomalies. This appears to be incorrect from the Abt et al. work, for they find TV Cam is of normal metal abundance. The weakening of the metal lines can be explained by a low value for the micro-turbulent velocity. However, it is admitted by them that the erection or rejection of an hypothesis on the basis of a single star is of dubious value.

1-4. Intrinsic Colors

The precise removal of interstellar-reddening effects is of paramount importance, if observed colors are to attain their maximum usefulness. There are numerous methods used by observers, but we here described briefly the four predominant procedures.

A useful assumption is that a particular color for the cepheids is constant at maximum light, independent of period. This is reasonable as it reflects the observed constancy of spectral type at light maximum. The determination of a color excess is simply obtained from the observations under this assumption, if we know, either by analysis or substantial qualitative evidence, the value of the particular color at light maximum. Once a color excess is found, all other excesses maybe deduced if color excess ratios are known. This procedure has been used by Gascoigne and Eggen (1957) for classical cepheids. They

took (P-V) = 0.25 at light maximum, a value indicated by the SMC cepheids.

An interesting study which indpendently demonstrates the reasonableness of near color constancy of (P-V) at light maximum is that of Stibbs (1955). The distance modulus of a cepheid is given by --

$$(m-M) = 5*\log(r) + X_1*E_1(r,b) - 5 \ ,$$

where E_1 is the selective absorption in the six-color system as a function of distance and galactic latitude, and X_1 is the known ratio of total to selective absorption in the six-color system. The functional dependence of E_1 on distance and galactic latitude can be found from a galactic obscuration model (Stibbs chose a model by ' Parenago). Given an obscuration model, we have all that is needed for a self-consistent, boot-strap determination of E_1. We first determine the distance modulus using the m from the observations and the calculated absolute magnitude, assuming the correctness of the P-L relation. The second step is to guess at r, derive E_1 from the obscuration model, and calculate an (m-M). We compare the calculated (m-M) to the observational evaluation, and continue to guess at r until the two determinations for (m-M) are identical. The resultant E_1 is only as precise as the obscuration model, and the assumption that the P-L relation is valid for any particular star. Once E_1 is given we use it in the relation --

$$(P-V) = (P-V)_{obs} - (X_1/X)*E_1 \ ,$$

where X is the ratio of total to selective extinction in the P,V system.

From a study of approximately thirty cepheids it is found that --

$$(P\text{-}V)_{max} = 0.17 + 0.18*\log P \ .$$

In the range $1.2 \leq \log P \leq 2.0$ the above relation gives a $(P\text{-}V)_{max}$ close to the observed SMC value of 0.25.

A second method is that employed by Kron (1958), and Kron and Svolopoulos (1959). In the six-color system (UVBGRI) the F through K5 supergiants are dispersed in a (V-B) versus (R-I) diagram by reddening, which moves a star's color away from the thermal locus, as is shown in Fig. 1.6. Breaking the stars up into subgroups the evaluation of an adequate mean reddening line in the diagram is possible. To fix the position of the thermal locus as simply the blue boundary of the scattered points is imprecise, as even the brightest and nearest supergiants are probably reddened. Kron emphasizes the idea that stars at the higher galactic latitudes are the least reddened, and thus a best choice is to position the thermal locus slightly to the blue side of these high latitude stars. His thermal locus is shown in Fig. 1.6 as the solid line. On the assumption that at each phase point a cepheid's colors are equivalent to those of a supergiant, the color excess at any phase point can be estimated. The final color excess for a cepheid is the average value of all excesses at a number of phase points (usually ten evenly spaced points are sufficient).

A third procedure is that proposed by Kraft (1963). The combination of Γ and UBV photometry in a two step process is capable of giving accurate intrinsic colors for cepheids. Gamma photometry measures the G-band strength in a manner insensitive to the effects of reddening.

There is a smooth and strong correlation between the Γ magnitude and the MK spectral type for supergiants. To derive an intrinsic (B-V), $(B-V)_o$, relationship with respect to spectral type, use is made of the cepheids in galactic clusters. At many phases Γ and (B-V) are observed. From a knowledge of the E_{B-V}, as derived from the B stars in the clusters, the observed (B-V) is simply converted to $(B-V)_o$. The spectral type at each phase is assigned from the observed value of Γ. By this procedure Kraft developes a $(B-V)_o$ versus spectral type relation. To determine the E_{B-V} for any cepheid, or supergiant, we first assign a spectral type from the value of Γ; second, we read off the associated $(B-V)_o$, and then simply take the difference between the observed (B-V) and $(B-V)_o$. This procedure is illustrated in Fig. 1.7. A criticism of Kraft's results is that the (B-V) excesses found from the B stars in the clusters are not directly applicable to the cepheids. This is an inherent problem in a broad-band system where the color excesses are a function of spectral type. Corrections to Kraft's work taking into account the variation of E_{B-V} with spectral type are given by Fernie (1963). A additional refinement is the allowance for the variation of E_{B-V} with phase for a cepheid. This improvement has been performed by Nikolov (1967a,b). In these last investigations attempts are also made to determine $(U-B)_o$ for both cepheids and supergiants through a relationship connecting E_{B-V} to E_{U-B}.

A final method is one, originally proposed by Becker (1938), which tries to eliminate the effects of reddening by an appropriate combination of colors. The procedure is best recognized by the construction of Q in the UBV system --

$$Q = (U-B) - 0.72*(B-V) ,$$

where the coefficient of (B-V) is simply the slope of the reddening line in the (U-B), (B-V) diagram. By this process Q becomes statistically independent of reddening. Similar reddening free colors have been used by the Walravens (1960) in their five-color system, and by Strömgren (1966) in his four-color work. This is the method used in our investigation and is discussed subsequently.

1-5. Aims of the Investigation

Having determined intrinsic colors in a photometric system we search for internal systematics, and for correlations with stellar properties. In the UBV system the internal relations linking color and period, and blue amplitude and position in the instability strip are primary findings. Deviations from the mean relations are useful as indicators of chemical anomalies, and in detecting unseen companions. Using external information we are able to calibrate (B-V) with $\log T_e$, and form a meaningful P-L relation, so as to give us the unambiguous location of the cepheid strip in the H-R diagram. This information is of great use in creating theoretical pulsation models, and in evaluating the correctness of theoretical evolutionary tracks. Much similar information is gathered by other broad pass-band photometric systems.

Further ground based photometry is justified only if it is performed within the framework of a photometric system designed primarily to evaluate basic physical parameters in a reasonably direct manner. The composite photometric system of this investigation satisfies this prime condition. We have four major objectives for a further investigation of the photometric properties of cepheids and supergiants.

The four-color system of Strömgren (1966) allows one color to be used to eliminate the effects of interstellar reddening, and uses the remaining two color indices to give data on the strength of the Balmer discontinuity (gravity) and the abundance of metals. This system is used here in conjunction with the three-color system of Crawford (1961). Crawford's system gives two colors relevant to the study of supergiant and cepheid stars. The colors measure the strength of the G-band and the break in the spectrum caused by the CN band head at 4215 Å. With this composite system we try to do the following:

(1) Find where the cepheids and supergiants fit in the Strömgren system, in order to complement the careful studies for main-sequence stars;

(2) Ascertain whether the composite system is an adequate survey tool, in the sense that it is possible to segregate stars, particularly supergiants, into their respective luminosity classes;

(3) Determine if the strong, unexplained, correlation between metal, and C and N abundances for main sequence stars as found by van den Bergh and Sackmann (1965) is also evidenced in supergiants and cepheids;

(4) Use the Strömgren metal index to investigate variations in relative metal abundances in cepheids and supergiants as a function of galactic location.

The complete satisfaction of the first point is not possible. The colors of this investigation are neither identical to or transformable to the standard Strömgren system. However, the range in the Balmer and metal indices for the stars studied are far larger than the

deviations between our systems at any fixed color, or spectral type. Thus, the difficulty is of little importance for delineating gross features and in the interpretation of the indices, but it is bothersome when comparing minor details.

Relevant to the last objective, Conti and Deutsch (1966, 1967) raise the issue that differences of Strömgren's metal index between similar stars do not necessarily arise solely from relative metal abundance differences. Their objection is that the differences can arise from variations in the micro-turbulent velocities. This point is critical, for if true it vitiates the use of the metal index. The micro-turbulent velocities for the supergiants are appreciable, have strengths correlated with spectral type, possess a substantial dispersion at any one spectral type, and vary in a quasi-periodic manner for any one star (Rosendhal 1970). The micro-turbulent velocities are phase dependent for the cepheids. Strömgren points out that even if the Conti and Deutsch proposition is true, the trouble can be unimportant if the micro-turbulence is not an independent parameter. The problem is addressed in a quantitative manner in the studies by Barry (1967), McNamara (1967), Kraft et al. (1968), and Chaffee (1970) for main-sequence stars. Their sum opinion refutes, except in a few cases, the Conti and Deutsch hypothesis. As Rosendahl (1970) finds much qualitative similarity in his rough model of micro-turbulent motion in supergiants as compared to Chaffee's for main-sequence stars, we are encouraged to believe that use of Strömgren's metal index is viable.

The body of this study is broken up into six self-contained chapters. In Chapter II we discuss the characteristics of the filters

and the method of data gathering. Chapter III is devoted to the data reduction process. Particular emphasis is placed on the method of the meshing of the various observational runs, which were carried out over a period of two and one-half years. The reduction procedure is designed to give the best possible results for the standard stars. The standard star results are graphed to show the difficulty of any transformations between the observational system and the standard Strömgren system.

Chapter IV gives the primary results for the supergiants stars in terms of colors freed from the effects of inter-stellar reddening. In addition, the color excess for each star is determined by reference to a simple linear thermal locus in a particular color-color diagram. Some comments are made on the difficulty of the physical interpretation of the colors on the Crawford photometric system.

A major aim of this investigation is the possibility of separating the supergiant stars from those of other luminosity classes. This problem is attacked in Chapter V. The mean color curves for luminosity classes V through I are developed. The data on the supergiants come from this investigation alone. Data on the other luminosity classes are implemented by transformation of data from the work of other investigators. A study of various color-color curves indicate that precise separation of I-II stars is impossible. However, we find that a mapping of the mean color curves over into a H-R diagram gives some improvement in luminosity class discrimination. This mapping is called the 'supercolor' method.

The basic cepheid results are presented in Chapter VI. New periods are determined from analysis of published V data in combination

with our visual magnitude results. The periods for five of the program cepheids have discernably varied from the values listed in the General Catalog of Variable Stars (Kukarkin et al., 1958). The cepheid colors are shown to be similar to those for the supergiants. A new and novel population discriminant is found through a study of selected color-color loop areas. This discriminant has the advantage of being unaffected by interstellar absorption. Color excesses are determined from an analysis of the location of the color-color loops in a G,(b-y) diagram relative to a simple linear thermal locus. This thermal locus is virtually identical to that found independently for the supergiants. The correlation between Strömgren's (b-y) color and (B-V) is linear, and indicates that effective temperatures can be well determined.

Chapter VII concludes the presentation with interpretations relying on the combination of supergiant and cepheid data. The supercolor method is re-introduced and applied to the data of individual stars. The method is found to locate the average position of a cepheid in the vicinity of the instability strip, and to separate approximately two-thirds of supergiants from all other classes of stars. The correlation between metallic and CN absorption is pronounced. The value of the Balmer discontinuity index is shown to be insensitive to the effects of line blanketing. No clear correlation between galactic location and chemical composition is shown by the supergiants or cepheids.

TABLE 1.1

SLOPE OF THE P-L RELATION FOR SMC CEPHEIDS.

Source	V	B
Arp (1961)	-2.47	-2.23
Kron & Gascoigne (1965)	-2.95	-----
Payne-Gasposchkin & Gasposchkin (1966)	-----	-2.13
Sandage & Tammann (1968)	-2.73‡	-2.40‡

‡Slope of the straight line which best fits the P-L ridge line data given in their Table A1.

TABLE 1.2

PHYSICAL PROPERTIES OF CLASSICAL CEPHEIDS.

		M_V		$R/R_\odot$			$M/M_\odot$		
Period	Kraft[‡]	Sandage & Tammann[§]	Fernie	Fernie	Eq. (1-28)	Eq. (1-31)	Eq. (1-32)	Iben	Stobie (Y=0.45)
2^d	$-2^m.64$	$-2^m.37$	$-2^m.65$	27	21	4.2	3.8	4.3	3.2
5	-3.66	-3.38	-3.56	45	39	5.1	5.1	5.6	4.6
10	-4.42	-4.20	-4.32	66	61	5.8	6.4	7.0	5.4
20	-5.18	-5.06	-5.15	97	96	6.7	8.1	8.6	6.1
50	-6.20	-6.22	-6.36	161	175	8.0	11.	11.	7.8

[‡] with zero corrected according to Geyer (1970).

[§] from their Table A1 (Sandage and Tammann 1968).

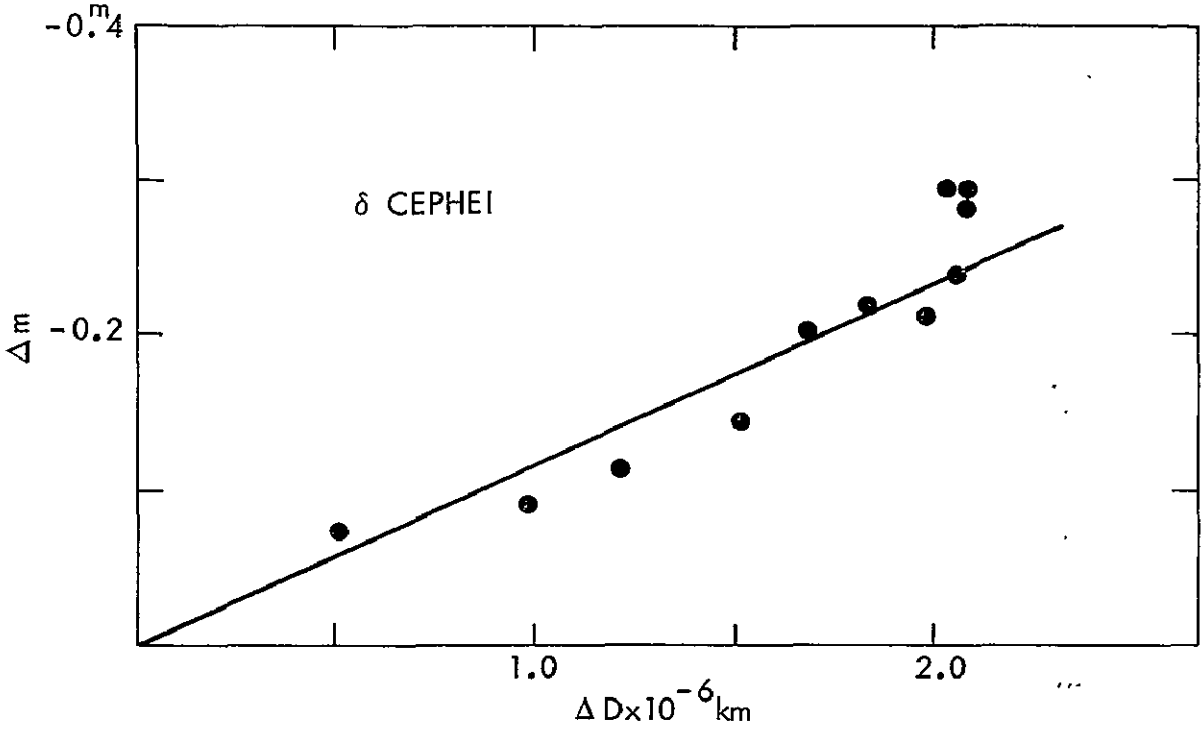

Fig. 1.1 Magnitude differences versus relative surface displacements at points of equal color for δ Cep.

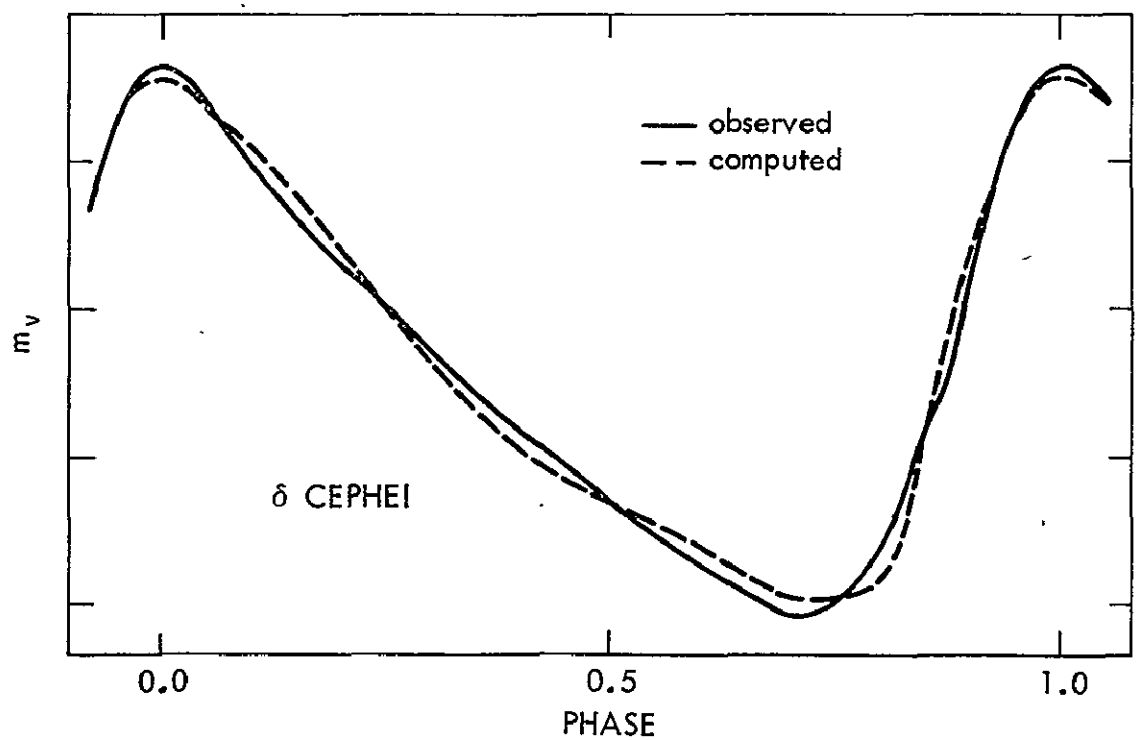

Fig. 1.2. Comparison of the observed and computed light curves for δ Cep.

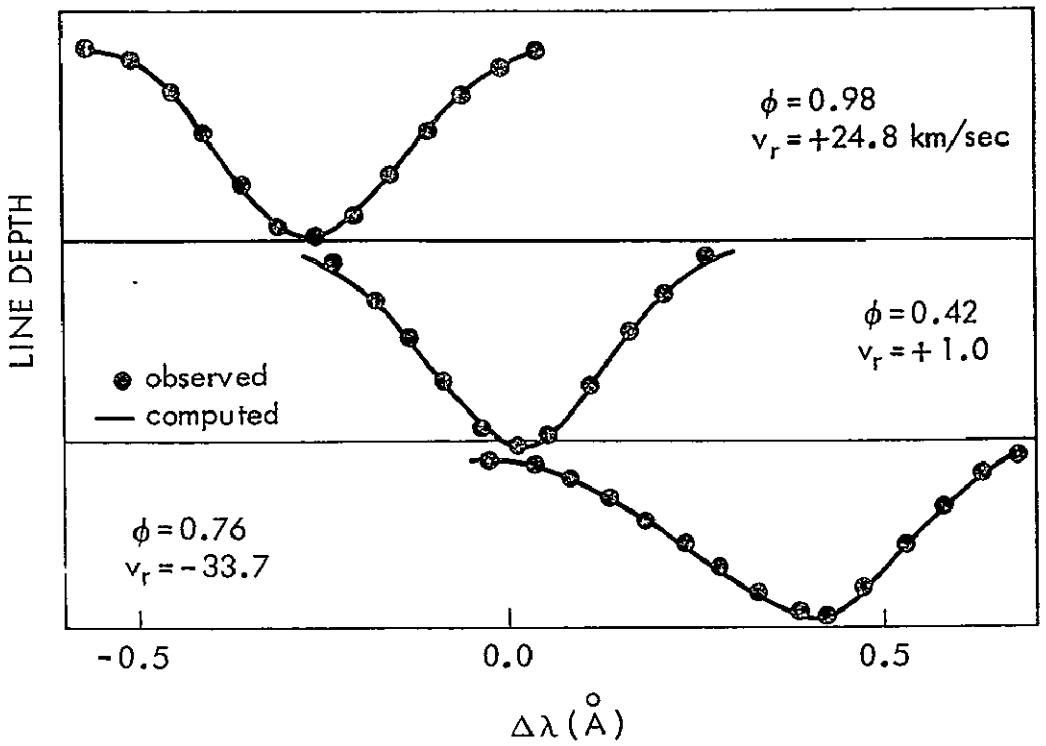

Fig. 1.3. Observed and computed line profiles for weak Fe I lines in η Aql.

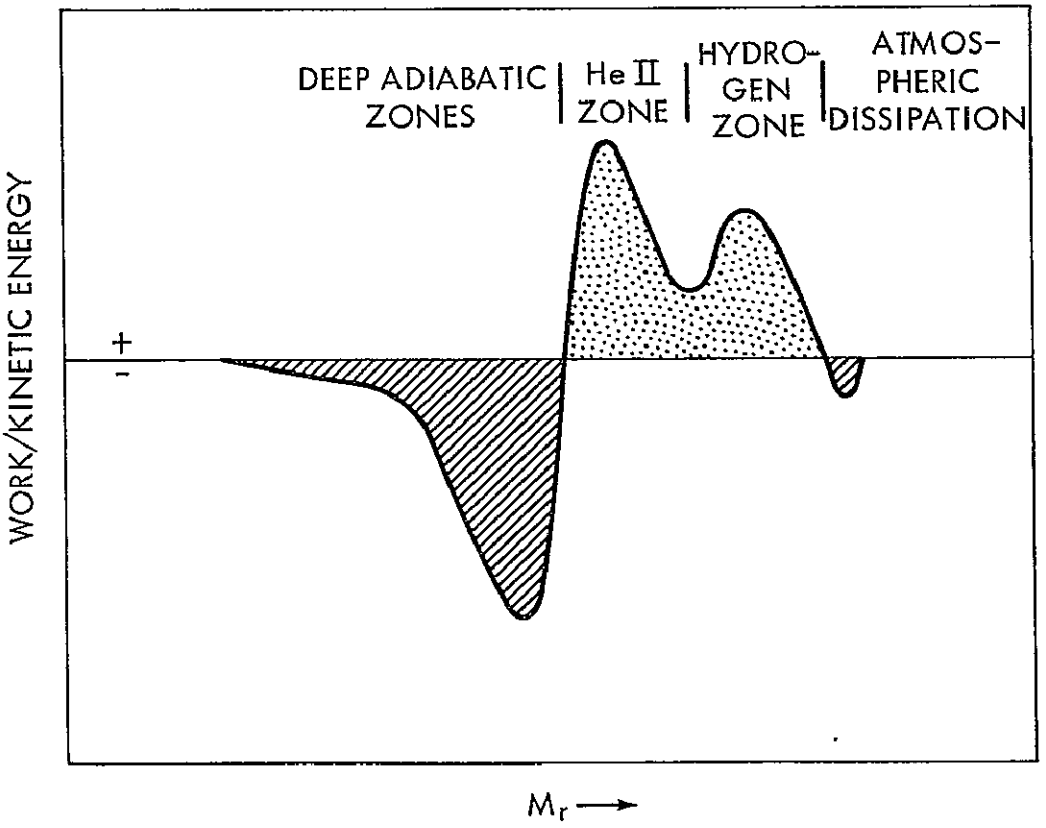

Fig. 1.4. Contribution of various regions in a star to the maintenance of pulsation.

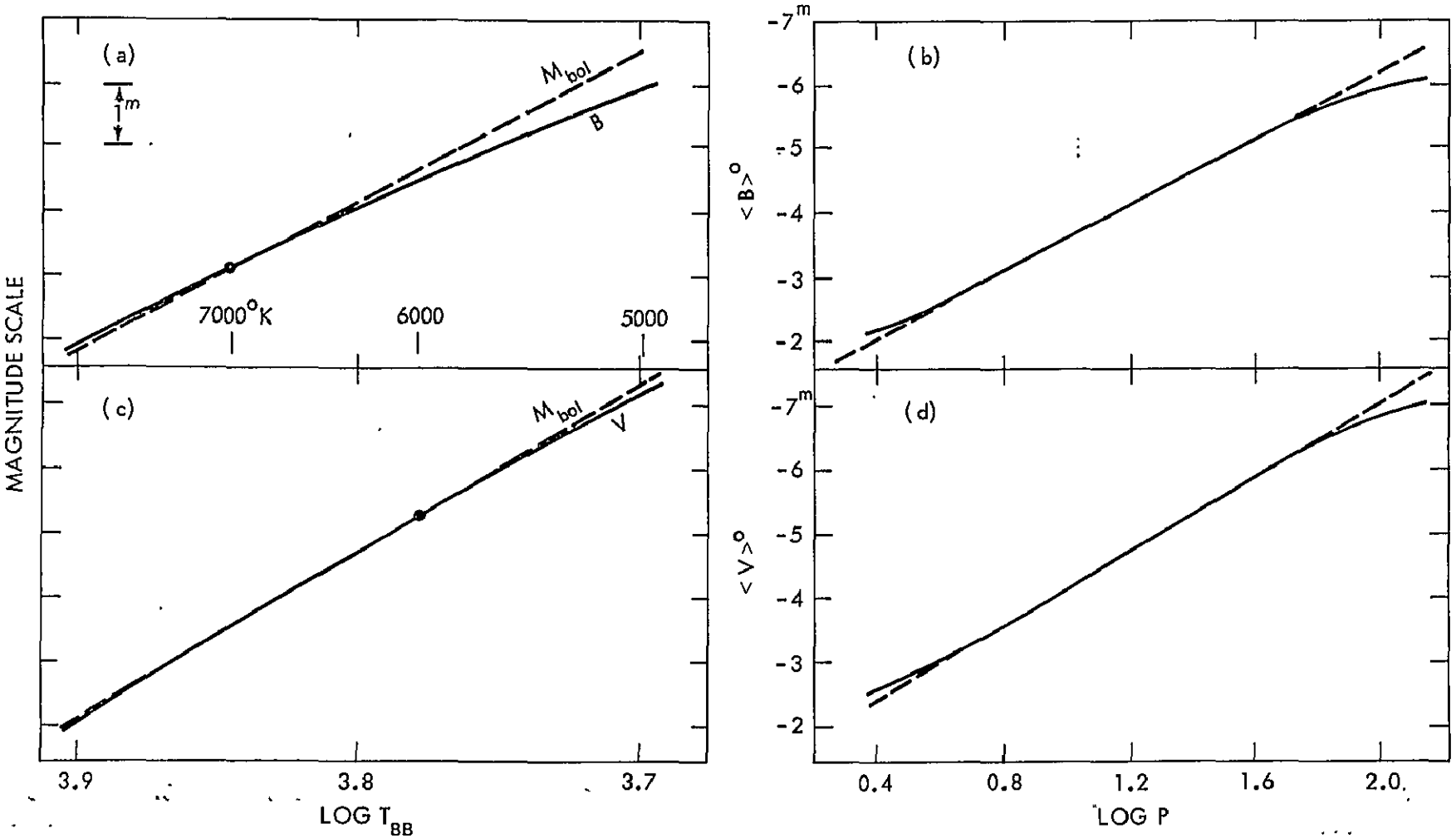

Fig. 1.5. Variation with temperature of the V and B magnitudes for black-bodies (left panels). The observed dependence of the mean V and B magnitudes with period (right panels).

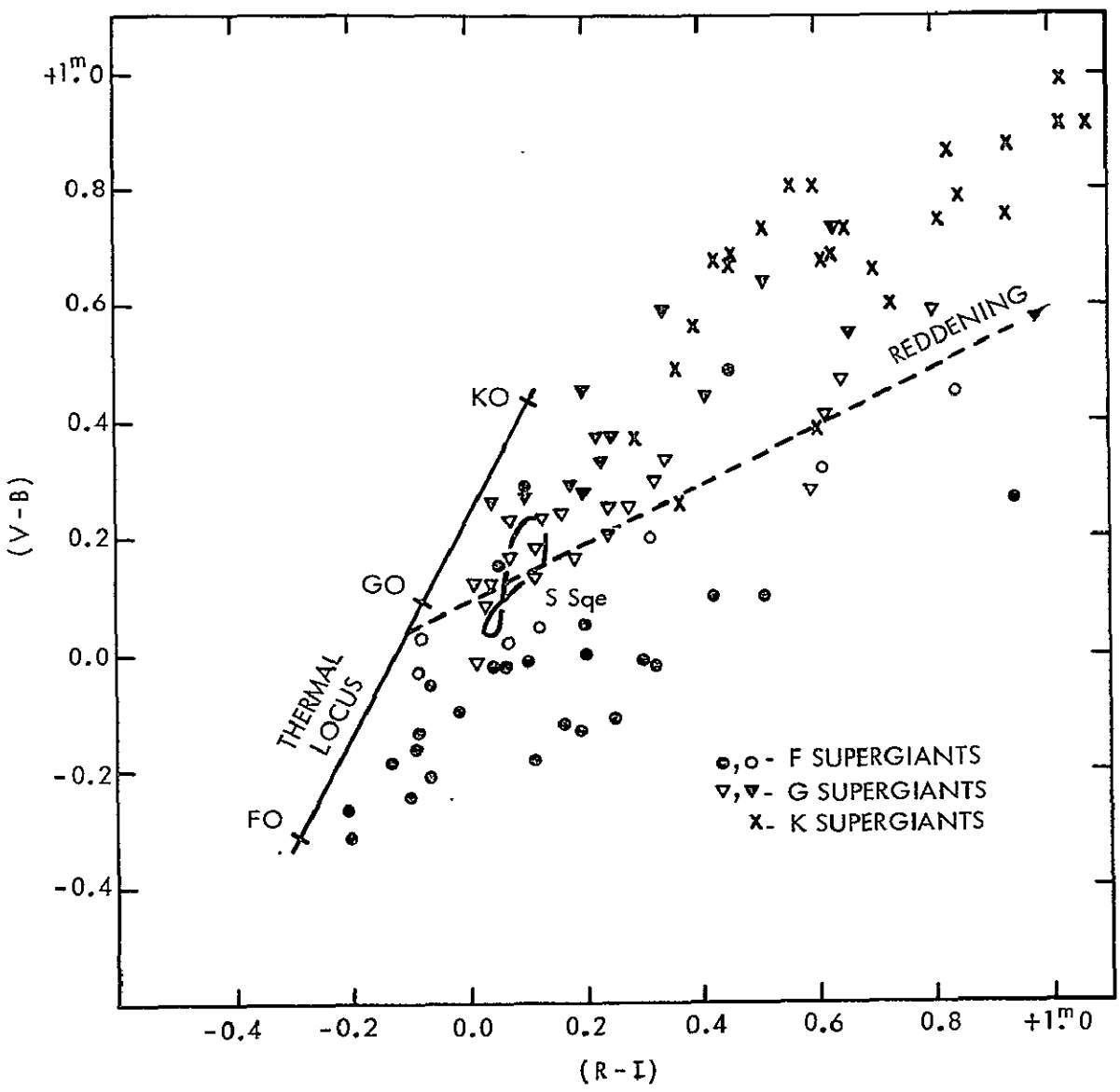

Fig. 1.6. Location of the F, G and K supergiants and the cepheid S Sge in a six-color (V-B),(R-I) diagram.

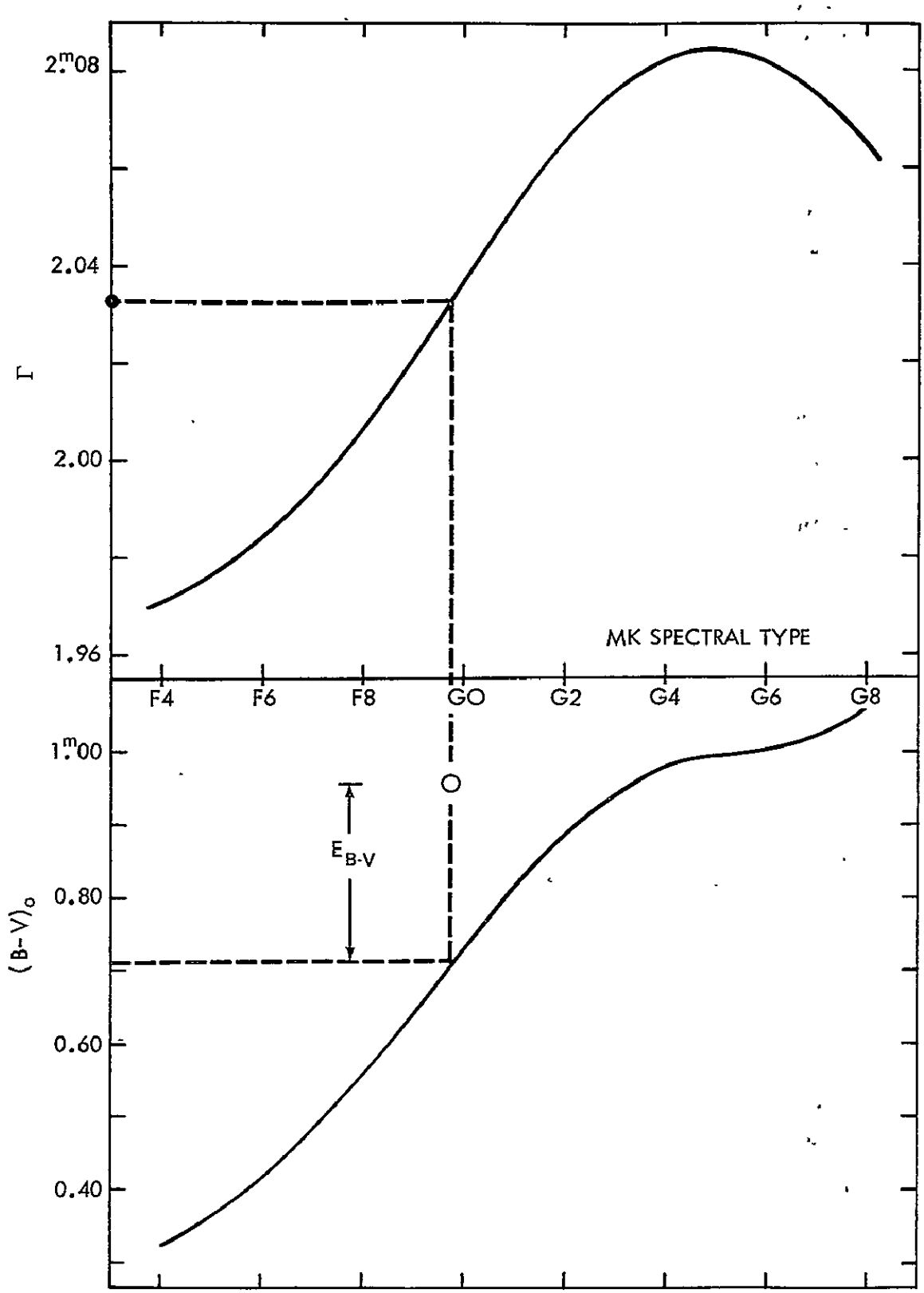

Fig. 1.7. Determination of the (B-V) color excess through the use of Γ photometry.

CHAPTER II

THE OBSERVATIONS

2-1. The Filters

The observational system contains seven filters. Four are similar to those forming the Strömgren uvby photometric system. These include an ultra-violet glass filter (u), and three - violet (v), blue (b), and yellow (y) - interference filters. The remaining three filters are those of Crawford's photometric system. These last filters (A, B, and C) are narrow pass-band interference filters, all located within the short wavelength base of 200 Å extent centered about 4275 Å.

The transmission characteristics of the filters were measured twice during the period of the observations. The measurements were taken in June 1964 and November 1966 on the Cary spectrometer at the Kitt Peak National Observatory (KPNO) office in Tucson, Arizona. The two transmission scans indicate no evidence of aging effects, which sometimes are bothersome when dealing with interference filters. The transmission curves for the seven filters are shown in Fig. 2.1. The figures show only the regions where the transmission is measurable, but the full scan for each filter covers the range from 3000 Å to 7500 Å to make sure there exist no red leaks, etcetera. Pertinent filter characteristics are presented in Table 2.1.

The uvby filters, KPNO uvby set #2, are not those used by Strömgren, KPNO uvby set #1, in defining his photometric system. In fact, they are not even 'duplicates' in the sense of being ordered from the initial

source to the original specifications. They are close facsimiles produced by Baird-Atomic, Inc. of Cambridge, Massachusetts. In Table 2.2 the two sets of uvby filters are compared. The b filter is the most different, but it is the differences in the v filter which, as we shall see in section 3.4, cause the two uvby systems to be linked by non-linear transformations.

2-2. Equipment and Data Gathering

The observations were carried out over a period of approximately two and a half years, starting in June of 1964. The dates of the individual observational runs and other related information is compiled in Table 2.3. All the observations were made at the Kitt Peak installation of the KPNO.

Two different sixteen inch telescopes were used. Both instruments are off-axis mounted, possess Cassegrain optical systems, and are manufactured by Boller and Chivens. They are scaled down versions of the #1 thirty six inch and the eighty two inch Kitt Peak telescopes, with focal ratios of 13.5 and 7.6, respectively.

The optical arrangement of the single-channel photometers is of a standard format - focal plane diaphragm, movable beam-interceptor mirror with its associated small angle microscope, field lens, filter bolt, fuzed quartz window, and photomultiplier in a dry ice, refrigerated box (see Johnson (1962), Fig. 1, for the standard instrument arrangement).

The focal plane diaphragms were selected each night on the basis of seeing conditions. It was sometimes necessary, if the seeing improved or deteriorated, to change the diaphragm during the course of a night. As the star fields are not dense the changing of the diaphragm size had no detectable effects, except on the magnitude of the sky readings. The

majority of the observations were made with a diaphragm diameter of approximately fifteen seconds of arc, with an occasional use of diaphragms of eight or thirty seconds of arc diameter.

The detectors used were RCA 1P21 photomultipliers, cooled with dry ice. The dry ice was packed into the refrigeration box at least two hours before the beginning of each night's run, and replenished throughout the night as needed. The tubes were operated at a working voltage of nine hundred volts.

The constant-amplified photomultiplier output is accumulated for a preset time interval by a discretized, variable-gain, integrator module, and the resultant value of the integrated charge on an RC circuit is recorded on a standard twelve inch Honeywell strip chart recorder. The gain steps on the integrator module are in units of 0.500 magnitudes, with a total range of 10 magnitudes. Response settings are designated A1, A2,...,A6;B1,....,B6; C1,....,C6; D1,....,D6. The response at A6 is approximately equal to that at B1, etc.. The gain calibration of the integrator module consists of determining the difference in the response at A6 as compared to that at B1, at B6 compared to C1, and at C6 as compared to D1. This is easily implemented, and was done twice during each observational run and average values of the gain calibration used in the reduction of that run.

The observation of a star was executed in the following manner: integrated star readings (ten seconds) of filters y, b, v, u, A, B, C; sky readings on C, B, A; hour angle and MST noted on the chart; sky readings on u, v, b, y; star readings of y, b, v, u, A, B, C. For bright stars the sky readings are eliminated. For faint stars double-symmetric readings for each filter are made. The gain step for each filter is

chosen so that the height of the chart response is greater than, or equal to sixty percent of the maximum reading possible on the chart. The sky readings were taken at a single gain setting ten times more sensitive then the most sensitive filter gain setting, or at the maximum possible gain (D6) when this ten times ratio was impossible. This procedure in effect reduces the chart reading errors (±0.1%) in the sky deflections by a factor of ten relative to chart reading errors in star deflections, and thus are more appropriate to the level of the sky contribution. The larger sky deflections also aid in detecting instances when a faint star has been inadvertently positioned in the diaphragm. It is also easier to discern from the telescope anomalous behavior in the sky deflections.

A cleaned up replica of an observation of a single star is shown in Fig. 2.2.

A total of 1619 observations were made, of which 701, 303, and 615 are on standard, ordinary, and variable stars, respectively. The average number of star and sky deflections per observation are 16.2 and 3.7, respectively. This number of deflections indicates that the telescope was devoted exclusively to observations approximately forty percent of each night. The remainder of the time was spent in choosing the next star to be observed, locating and centering the star in the diaphragm, annotating the strip chart, etc.. The reduction procedure is discussed in the next chapter.

TABLE 2.1

TRANSMISSION CHARACTERISTICS OF THE FILTERS USED IN THIS INVESTIGATION.

Filter	$\langle\lambda\rangle$	Half Power Mid-wavelength	Full Power Half-width
y	5493Å	5492Å	118Å
b	4700	4700	48
v	4108	4106	71
u	3455	3453	192
A	4377	4375	40
B	4279	4277	43
C	4166	4165	27

TABLE 2.2

COMPARISON OF THE TRANSMISSION CHARACTERISTICS

OF uvby FILTER SETS NO. 1 AND NO. 2.

Filter Set	Peak Trans.	Wavelength of Peak Trans.	Half-trans. Points	Central Wavelength	Full Trans. Half-width
		--- y Filter ---			
1	52%	5521Å	5355, 5598Å	5476Å	243Å
2	72	5498	5378, 5612	5495	234
		--- b Filter ---			
1	47	4668	4588, 4762	4675	174
2	85	4700	4655, 4745	4700	90
		--- v Filter ---			
1	46	4094	4007, 4205	4106	198
2	60	4110	4038, 4169	4104	131
		--- u Filter ---			
1	44	3433	3267, 3647	3457	380
2	37	3451	3267, 3641	3454	374

TABLE 2.3

SUMMARY OF THE OBSERVATIONAL RUNS AT KITT PEAK NATIONAL OBSERVATORY.

	Observation Dates							
	June '64		Dec. '64	Feb. '65				
	6/3-15	Oct. '64	Jan. '65	Mar. '65	Oct. '65	Feb. '66	Nov. '66	
	6/18-21	10/17-26	12/29-1/10	2/26-3/7	10/12-22	2/17-26	11/2-16	Totals
Total Nights in Run	17	10	13	10	11	10	15	86
Expected Useful Nights	12	7	6	6	8	6	9	54
Useful Nights	12	$6\frac{1}{2}$	0	$7\frac{1}{2}$	6	$5\frac{1}{2}$	6	$43\frac{1}{2}$
Useful/Total	0.71	0.65	0.00	0.75	0.54	0.55	0.40	0.51

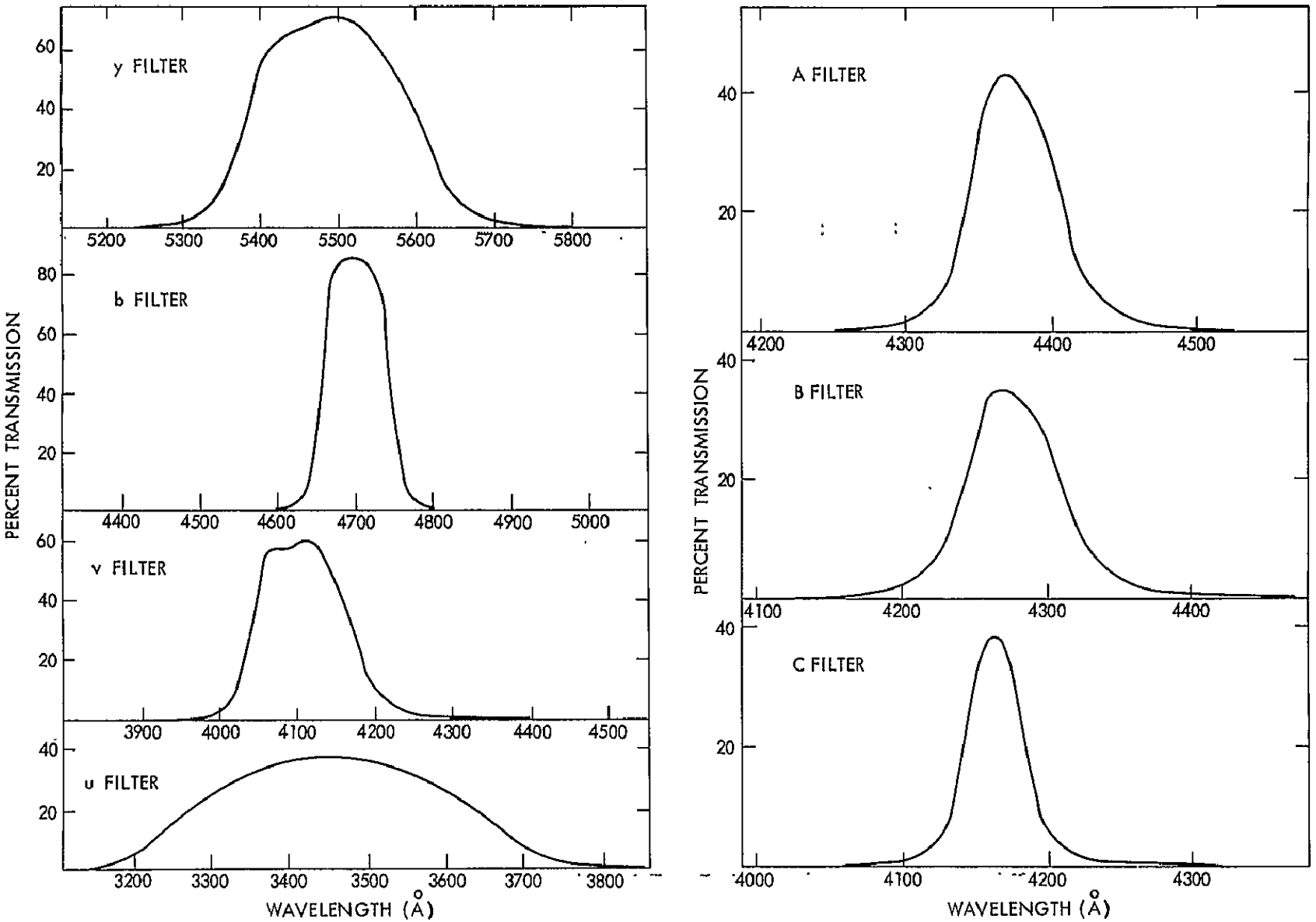

Fig. 2.1. Transmission scans for the filters used in this investigation.

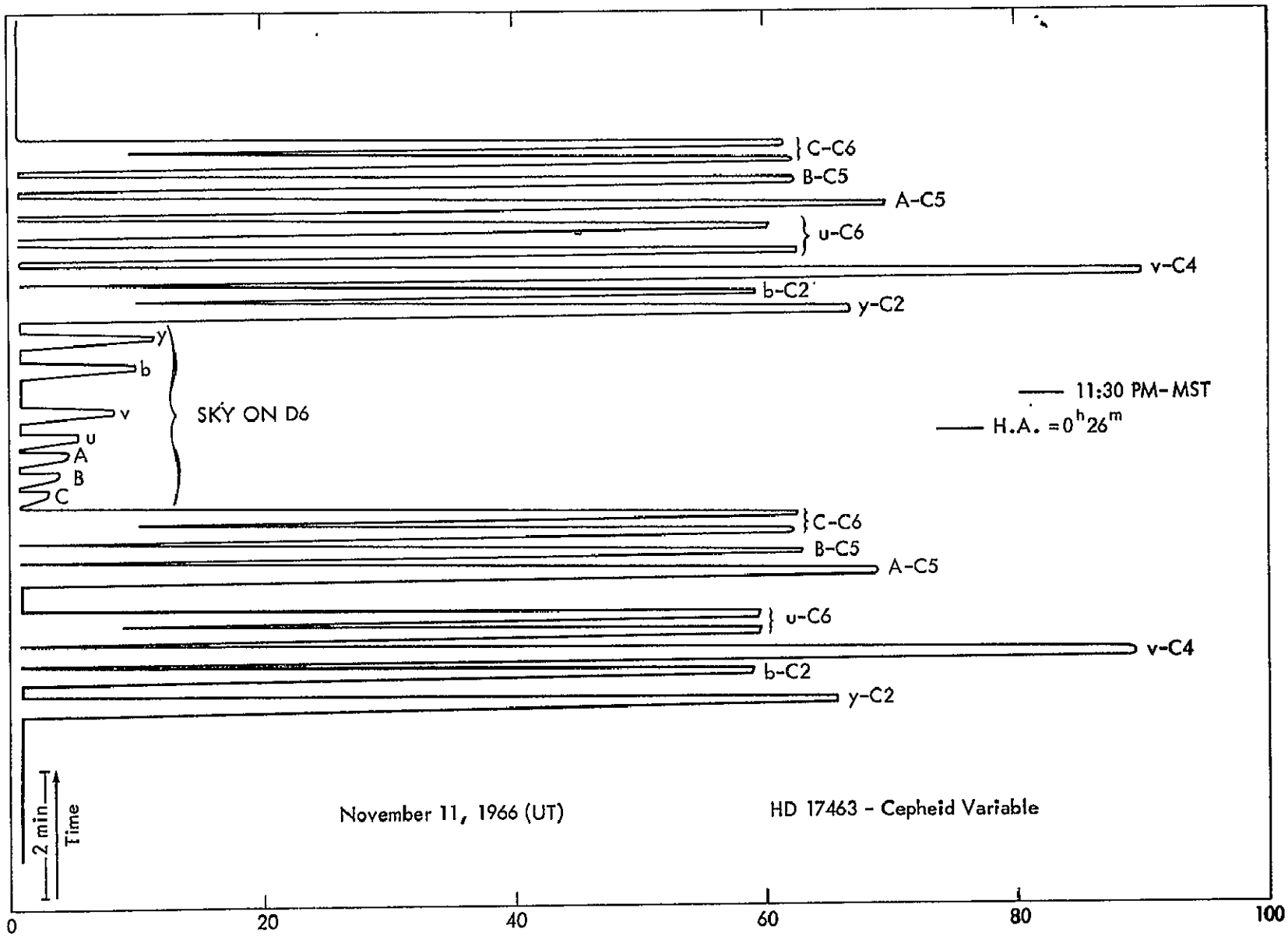

Fig. 2.2. A replica of the strip chart recording representing the observation of a single star.

CHAPTER III

THE STANDARD SYSTEM

3-1. Photometric Quantities

Initially, we hoped to reduce our data making direct use of the uvby standards listed in the Strömgren-Perry catalog (1962), and in the supplemental standard star data lists prepared by KPNO. For the ABC system it is necessary to construct a standard system, as no standard values have been published by Crawford. However, after a preliminary reduction of the first observational results (June 1964) it became obvious that the uvby data gathered using the four-color filter set #2 is not directly comparable with the Strömgren system as defined by the Strömgren-Perry catalog. The transformations connecting the observational system to the Strömgren system are non-linear, of high dispersion, and strongly (b-y)-color dependent. These difficulties preclude the usefulness of the Strömgren system's results in the data reduction, and demand that the observational system be totally self-contained.

We need a reduction procedure which incorporates the disjointed observation runs into a coherent body of observational quantities. To accomplish this a variety of schemes were tried, all of which produce observational systems which agree within the determined mean error of a single observation for any specified color. The two-stage, bootstrap process described below is the one that produces the smallest error per observation for every color.

The observational quantities are the following:

y - a photovisual magnitude determined totally by the response of the y filter. It is adjusted so as to agree in the mean with the V given in the Yale Bright Star (YBS) catalog (1964).

c_1 - a color index created from the difference of two colors, $c_1 = (u-v) - (v-b)$. The value of c_1 is strongly correlated to the strength of the Balmer discontinuity.

m_1 - a color index which measures the effects of metal line absorption in the violet band as compared to the essentially metal clear regions in the blue and yellow bands. The index is formed by the difference (v-b) - (b-y).

b-y - a blue minus yellow color, similar to (B-V), which is relatively insensitive to metal content.

G - a color formed from (B-A), which measures the break in the spectrum across the G-band.

N - the color defined by (C-B), which detects the break in the spectrum arising from the CN-band head at 4216 Å.

3-2. Basic Processing Procedure

Prior to discussing the overall reduction procedure, we describe the mechanism of reducing the data for a single star, and the reduction of all the star data on a single night.

For a single star the individual filter intensity readings are transformed to a common gain setting (A1) via the gain calibration of the integrator module. This is also done for the sky deflections. The sky deflections are then subtracted from the appropriate filter deflections.

For example, the raw data depicted in Fig. 2.2 give the following sky-corrected filter deflections - 2 for y, v, and b; 4 for u; 2 for A and B; and 4 for C. Each of these deflections are converted into magnitudes, and the filter magnitudes are averaged. The magnitudes are averaged as the major source of the differences in the deflections for a single filter result from variations in the optical depth of the atmosphere. These optical depth variations are reflected as linear perturbations in the magnitudes, this is not true for the deflections. The average magnitudes are utilized in forming the desired photometric quantities. These quantities are corrected to zero air mass in the manner described below.

To reduce a night's data the first step is the formation of single star data in the manner outlined above. After all star colors are reduced to zero air mass the individual differences between the calculated colors and the standard colors are determined. These differences are averaged to produce the commonly-called night corrections. Strömgren and KPNO observers find it is often possible to detect a time variation in the night corrections. These variations can be quite discontinuous. For example, it might be better to use one set of night corrections for all observations between 8 PM and 1 AM, and another set from 1 AM to dawn. We find no obvious time discontinuities in the night corrections, probably a result of using a minimum number of standard star observations per night. For each night we use only a single, gross set of night corrections. Once the set of night corrections are determined, all individual colors of the standard stars are improved by the addition of the appropriate night correction to the zero air mass color.

We note that in the first stage of the homogenization process the correction to zero air mass is performed using average extinction coefficients, and not the extinction coefficients determined for a particular night. These coefficients are the averages determined from all the extinction star observations gathered in the six runs from June 1964 to November 1966. At a high altitude observatory with clear skies it is better to use average extinction coefficients. In Table 3.1 the average coefficients are displayed. The results in row two of the table are those formed from the average magnitude coefficients. It is noteworthy that these are virtually identical to the color coefficient averages found from the extinction star, or the total standard star color data. This equivalence is a strong indicator of the stability of the absolute sensitivity in the photometric equipment, and the superb quality of the photometric nights at KPNO. The variation of the average magnitude coefficients with wavelength is smooth, and agrees reasonably well with a Rayleigh like λ^{-4} dependence. This is illustrated in Fig. 3.1, where a λ^{-4} dependent extinction coefficient is shown by the solid line (normalized to agree with the observational results at 4375 Å, the A filter). The large value of k at 5480 Å (y) is discordant with the KPNO average and the Rayleigh curve. No simple explanation is possible, but it is true that a recent re-evaluation of k(y) by KPNO does indicate a higher value is more appropriate, something of the order of 0.14 to 0.16. In the first stage of the overall reduction the averages shown in row three of Table 3.1 are the relevant ones.

3-3. Construction of the Observational System's Standards

To start the homogenization of the runs, a particular initial group

is chosen. This is found to be a non-critical choice, and the February-March run of 1965 was used. The nights in this run are reduced following the scheme given above. At the end of the run's reduction the colors for each star are averaged over all the nights observed. To these averages a constant is added so that in the mean they agree with the standards in common with the Strömgren uvby system, and the V system given in the YBS. The resulting colors and magnitude are then retained as those standard values which are the basis for the determination of the night corrections. The whole procedure is repeated, and new provisional standard values produced. This iterative boot-strapping is ceased when the (n-1)-iterate's standard values agree with the n-iterate's standard values to better than $0^{m}.001$ in all quantities for all stars.

The next step is to meld this run with yet another. The June 1964 run is chosen. The average values of the February-March 1965 run are used in the first iteration as the standard values. At the end of the first iteration standard values are formed from the June 1964 stars alone. These are adjusted so that in the mean, as determined from stars observed at least three times in February-March 1965 and three times in June 1964, they are in agreement with the February-March 1965 run. Using these June 1964 results as the standards the whole procedure is iterated until the $0^{m}.001$ level of agreement is reached.

At this juncture the February-March 1965 run and the June 1964 run standards are joined into a weighted standard star system, and used as the basis for coalescing the October 1964 run. The mean zero point adjustment is made only through stars observed at least three times in October 1964 and three times in the combined February-March 1965 plus June 1964 standard star catalog.

The above process slowly meshes the runs in the following order: February-March 1965, June 1964, October 1964, October 1965, February 1966, and November 1966. After this level of coherence is obtained, all the runs are processed at a single time and iterated three times to produce a single smoothed standard star catalog. This preliminary smoothed total catalog of standard values differs in the mean from the six run merged total catalog by less than $0^{m}.001$ in all quantities.

To obtain the final standard star results the following last stage of the boot-strap reduction procedure is performed. The stars from all the runs were processed in a single group. The only distinction from the previous stage is that on each night both the night corrections and the extinction coefficients for all quantities are determined from the standard star data. The average of these coefficients for all the nights in all the runs is listed in row four of Table 3.1. This total reduction of all the data was iterated three times to yield the final standard photometric quantities. The final results are presented in Table 3.2.

3-4. Final Comments

Some general supplemental comments are relevant. The two stage reduction procedure described was written by the author in Fortran IV language, and run on the IBM 360/91 at GSFC.

The probable errors for the observational quantities are listed in Table 3.3. It is encouraging that the accuracy attained in this study is comparable to that of the Strömgren-Perry results, for in the latter case observational nights of dubious quality could be totally removed as they were working with a much more extensive set of data than in this investigation, where it is essential to use every bit of information

gathered. It is to be stressed that no subjective weighting factors were used in the reduction, and all indications are that any such manipulation are ineffective in changing the results listed in Table 3.2.

In Figs. 3.2 through 3.5 comparisons between the observational photometric system and that of Strömgren's uvby system, and the V system in the YBS are shown. The differences in the δ versus (b-y) plots are in all cases formed by subtracting this investigation's results from those of the external system's. It is impossible, as has been remarked before, to make transformations of high accuracy from this system to the Strömgren system, except perhaps for the color (b-y). The case of representing V by the y magnitude is quite satisfactory. However, there is the striking anomalous point for the G5 V star HR 7504. This star was observed on eight nights, and its value of y is $5^{m}.990 \pm 0.003$ pe. There is no possibility of misidentification, which leads us to the conclusion the star has significantly varied since the YBS catalog was compiled. The entry in the YBS catalog does not appear to be in error as the value of $6^{m}.2$ is given in other contemporary sources. The average difference of (V-y) is $-0^{m}.0094$ if the non-photoelectric V observations are included (+'s in Fig. 3.2), and $-0^{m}.0067$ if only the photoelectric determinations of V are considered. Thus, some improvement in making y match V could be made by the systematic subtraction of 0.0067. However, as this is below the listed accuracy of the YBS catalog, the y results remain as machine computed throughout the discussion.

TABLE 3.1

THE COLOR-EXTINCTION COEFFICIENTS.

	k(y)	$k(c_1)$	$k(m_1)$	k(b-y)	k(G)	k(N)
KPNO Averages Determined Using uvby Set No. 1.	0.12	0.181	0.052	0.060		
Averages Developed from the Average Magnitude Coefficients.	0.161	0.180	0.066	0.054	0.020	0.032
Averages Formed from the Extinction Star Color Data.	0.160	0.178	0.067	0.052	0.021	0.031
Averages Formed from the Total Standard Star Color Data.	0.156	0.180	0.067	0.058	0.018	0.036

TABLE 3.2

OBSERVATIONS OF THE STANDARD STARS.

HD	SPECTRAL TYPE	Y	C1	M1	B-Y	NO. OBS.	G	N	NO. OBS.
571	F2II	5.038	1.074	0.138	0.269	12	0.001	0.396	10
6961	A7V	4.357	0.957	0.234	0.085	10	-0.105	0.352	1
9826	F8V	4.110	0.437	0.158	0.348	82	0.079	0.360	82
10476	K1V	5.239	0.378	0.300	0.512	4	0.216	0.385	4
18331	A1V	5.188	1.040	0.163	0.054	4			
19373	G0V	4.065	0.418	0.168	0.385	14	0.108	0.353	14
21120	G8III	3.616	0.472	0.328	0.538	3	0.188	0.537	2
26574	F2III	4.082	0.765	0.249	0.177	2			
27022	G5III	5.281	0.443	0.279	0.509	17	0.169	0.487	16
27309	A SI	5.392	0.521	0.210	-0.092	7			
30652	F6V	3.198	0.396	0.185	0.287	6	0.039	0.386	6
31398	K3II	2.681	0.229	0.817	0.941	17	0.407	0.814	16
39587	G0V	4.405	0.333	0.178	0.378	19	0.114	0.357	17
48329	G8IB	3.002	0.213	0.702	0.855	17	0.326	0.868	16

TABLE 3.2

(CONTINUED)

HD	SPECTRAL TYPE	Y	C1	M1	B-Y	NO. OBS.	G	N	NO. OBS.
57669	K0III	5.220	0.326	0.590	0.771	3	0.297	0.811	3
58715	B7V	2.916	0.782	0.113	-0.033	11			
58946	F0V	4.192	0.616	0.150	0.216	9	-0.029	0.393	4
62345	G8III	3.581	0.425	0.363	0.575	64	0.213	0.583	58
62721	K5III	4.853	0.428	0.769	0.889	10	0.424	0.652	9
67006	A2V	4.835	1.068	0.174	0.013	5			
73262	A0V	4.170	1.062	0.170	0.003	18			
78362	F5&A5	4.675	0.686	0.261	0.211	5	-0.025	0.432	4
79439	A5V	4.823	0.860	0.210	0.111	5			
82885	G8IV-V	5.418	0.423	0.241	0.498	2	0.213	0.412	1
83425	K3III	4.676	0.432	0.650	0.803	3	0.360	0.631	3
D89484	K0IIIP	2.019	0.401	0.446	0.693	4	0.261	0.565	3
91316	B1IB	3.879	-0.060	0.015	-0.014	4			
102870	F8V	3.601	0.445	0.160	0.363	16	0.086	0.373	15

TABLE 3.2

(CONTINUED)

HD	SPECTRAL TYPE	Y	C1	M1	B-Y	NO. OBS.	G	N	NO. OBS.
103095	G8VI	6.442	0.198	0.215	0.477	10	0.172	0.339	8
103287	A0V	2.465	1.076	0.163	0.009	2			
103578	A3V	5.556	1.072	0.194	0.059	9			
107328	K1III	4.979	0.532	0.505	0.701	3	0.267	0.594	3
111812	G0III	4.942	0.442	0.173	0.438	29	0.120	0.381	29
113139	F2V	4.940	0.565	0.177	0.239	19	-0.011	0.392	8
120315	B3V	1.893	0.279	0.089	-0.071	4			
122563	G0VI	6.222	0.542	0.109	0.629	2	0.120	0.442	2
127762	A7III	3.069	0.979	0.204	0.106	5			
130109	A0V	3.756	1.044	0.153	0.004	17	-0.123	0.336	2
142860	F6IV-V	3.859	0.412	0.146	0.318	17	0.051	0.372	5
143107	K3III	4.145	0.428	0.577	0.745	11	0.317	0.667	11
143761	G2V	5.418	0.373	0.156	0.391	11	0.113	0.338	11
159181	G2II	2.809	0.451	0.319	0.597	13	0.190	0.500	13

TABLE 3.2

(CONTINUED)

HD	SPECTRAL TYPE	Y	C1	M1	B-Y	NO. OBS.	G	N	NO. OBS.
182640	F0IV	3.368	0.710	0.187	0.193	4	-0.030	0.388	2
182835	F2IB	4.661	1.465	0.093	0.406	12	-0.004	0.424	12
185758	G0II	4.397	0.499	0.255	0.481	70	0.143	0.481	70
186427	G5V	5.989	0.401	0.188	0.409	8	0.139	0.356	8
186791	K3II	2.708	0.209	0.779	0.935	13	0.401	0.790	13
187013	F5V	5.005	0.450	0.147	0.311	4	0.029	0.395	4
192514	A3III	4.843	1.283	0.157	0.067	11			
192713	G2IB	5.165	0.317	0.404	0.631	3	0.193	0.618	3
194093	F8IB	2.230	0.912	0.317	0.375	4	0.077	0.477	4
202109	G8II	3.215	0.298	0.428	0.602	23	0.217	0.688	23
210027	F5V	3.772	0.440	0.175	0.284	5	0.028	0.390	5
211336	F0IV	4.198	0.752	0.206	0.170	13	-0.053	0.382	9
212943	K0III	4.788	0.457	0.415	0.634	2	0.244	0.531	2
217014	G5V	5.453	0.396	0.234	0.407	4	0.144	0.388	4

TABLE 3.3

STANDARD STAR PROBABLE ERRORS.

Quantity	Kelsall	Strömgren-Perry
y	0.0070	
c_1	0.0089	0.0085
m_1	0.0082	0.0071
b-y	0.0044	0.0057
G	0.0055	
N	0.0051	

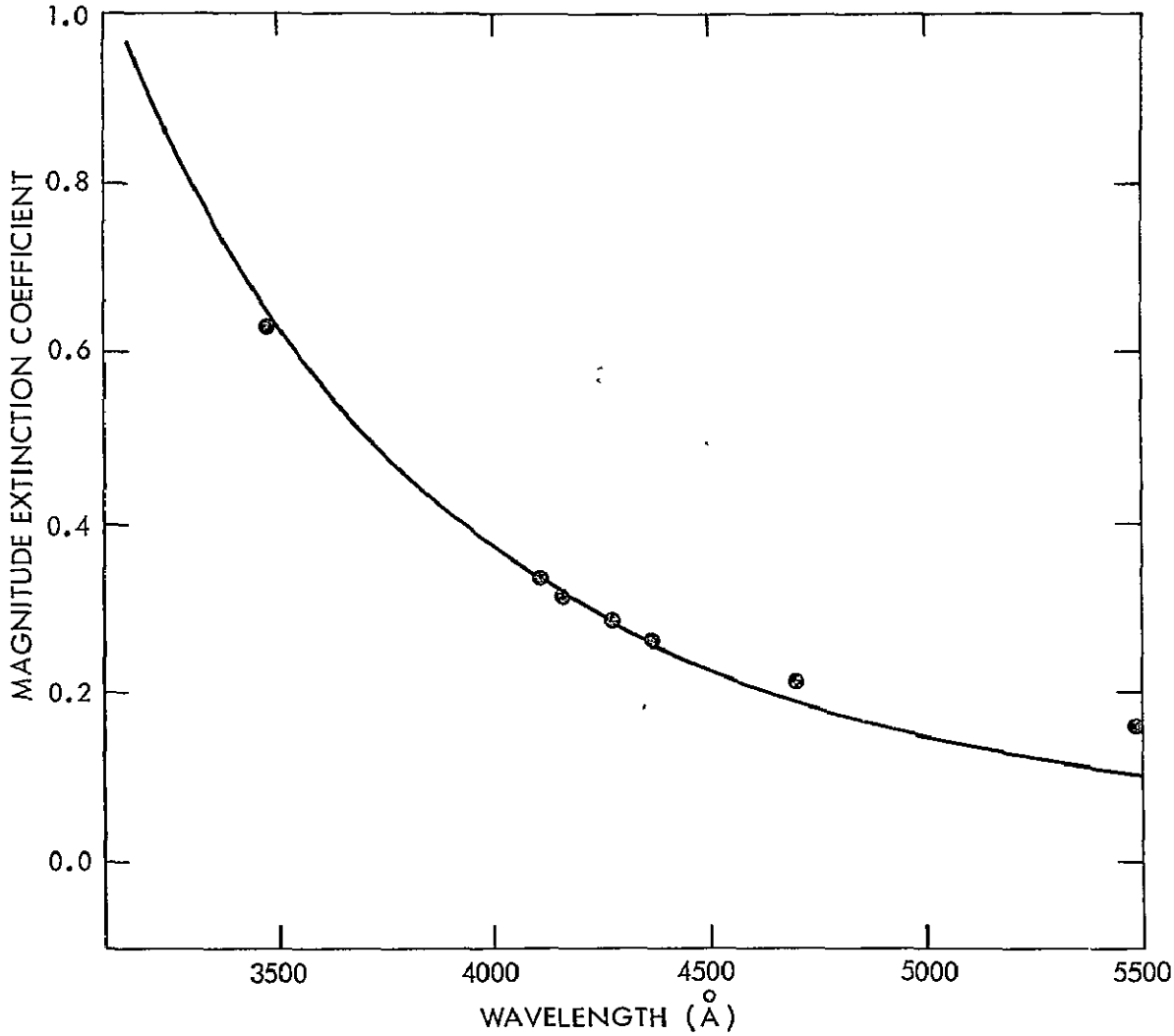

Fig. 3.1 Variation of the extinction coefficient with wavelength. The solid curve is the Rayleigh extinction curve normalized to the observations at 4375Å.

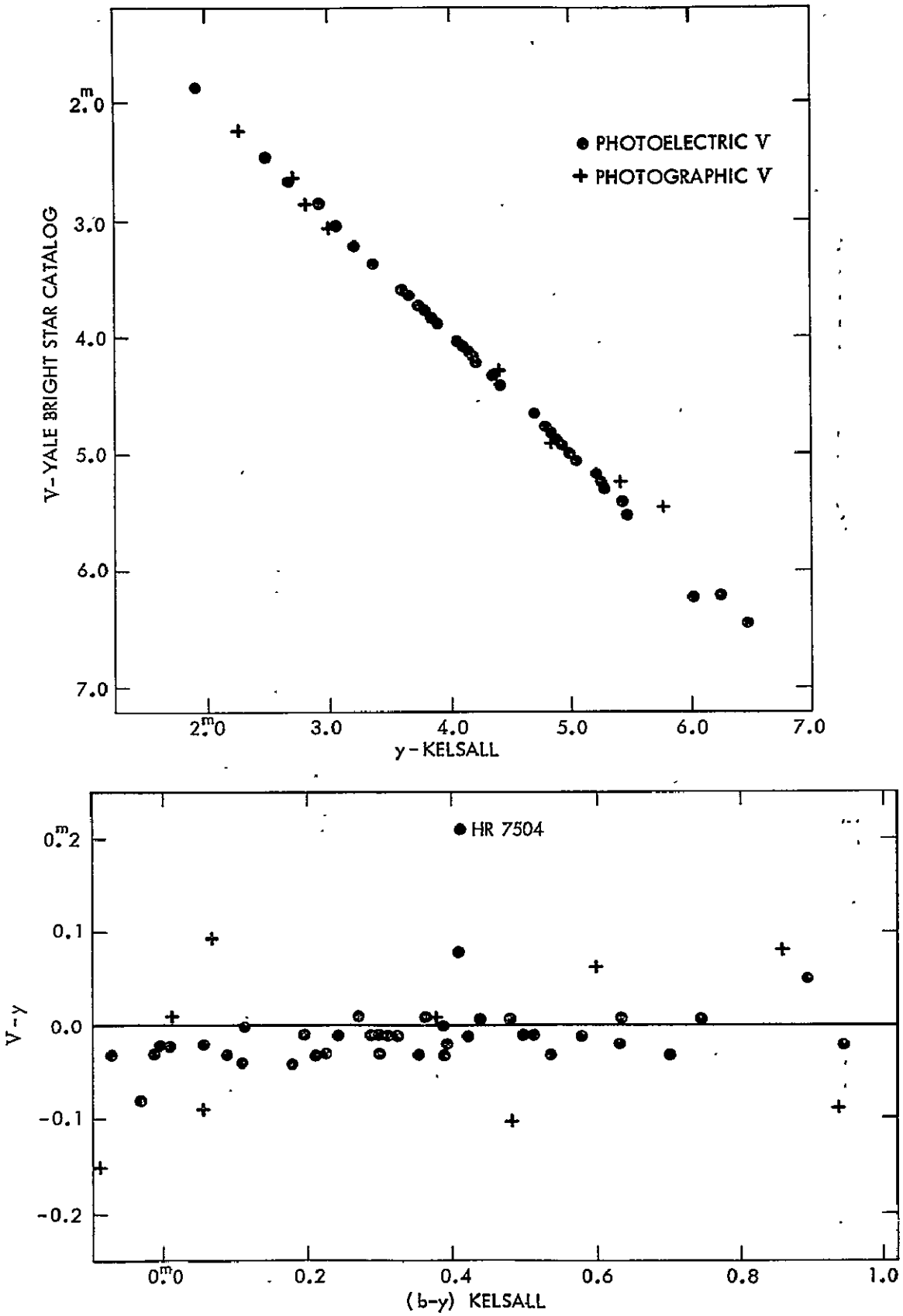

Fig. 3.2 Comparison of V from YBS to the y observed in this investigation.

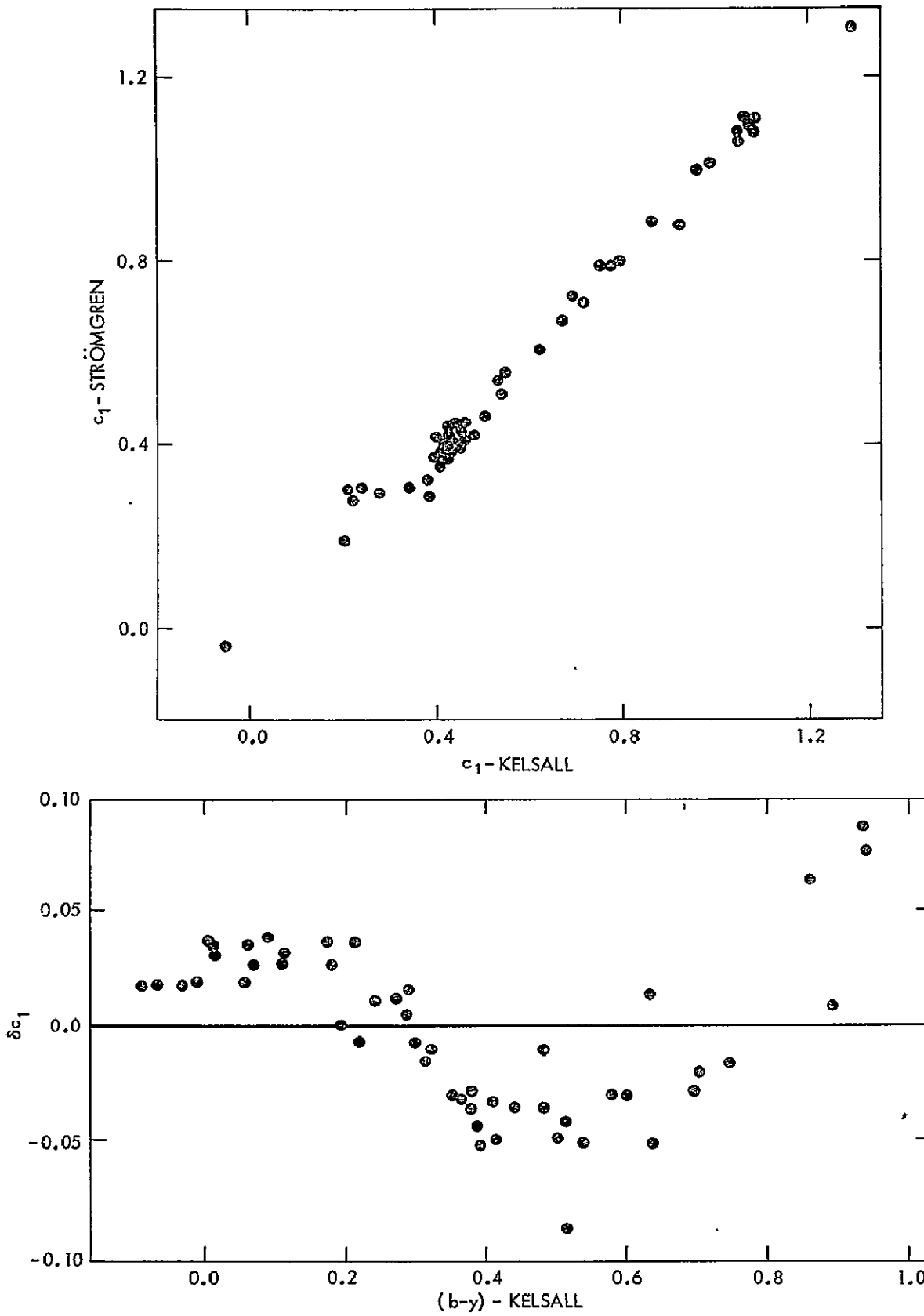

Fig. 3.3 Comparison of c_1's from the Strömgren-Perry catalog to those observed in this investigation.

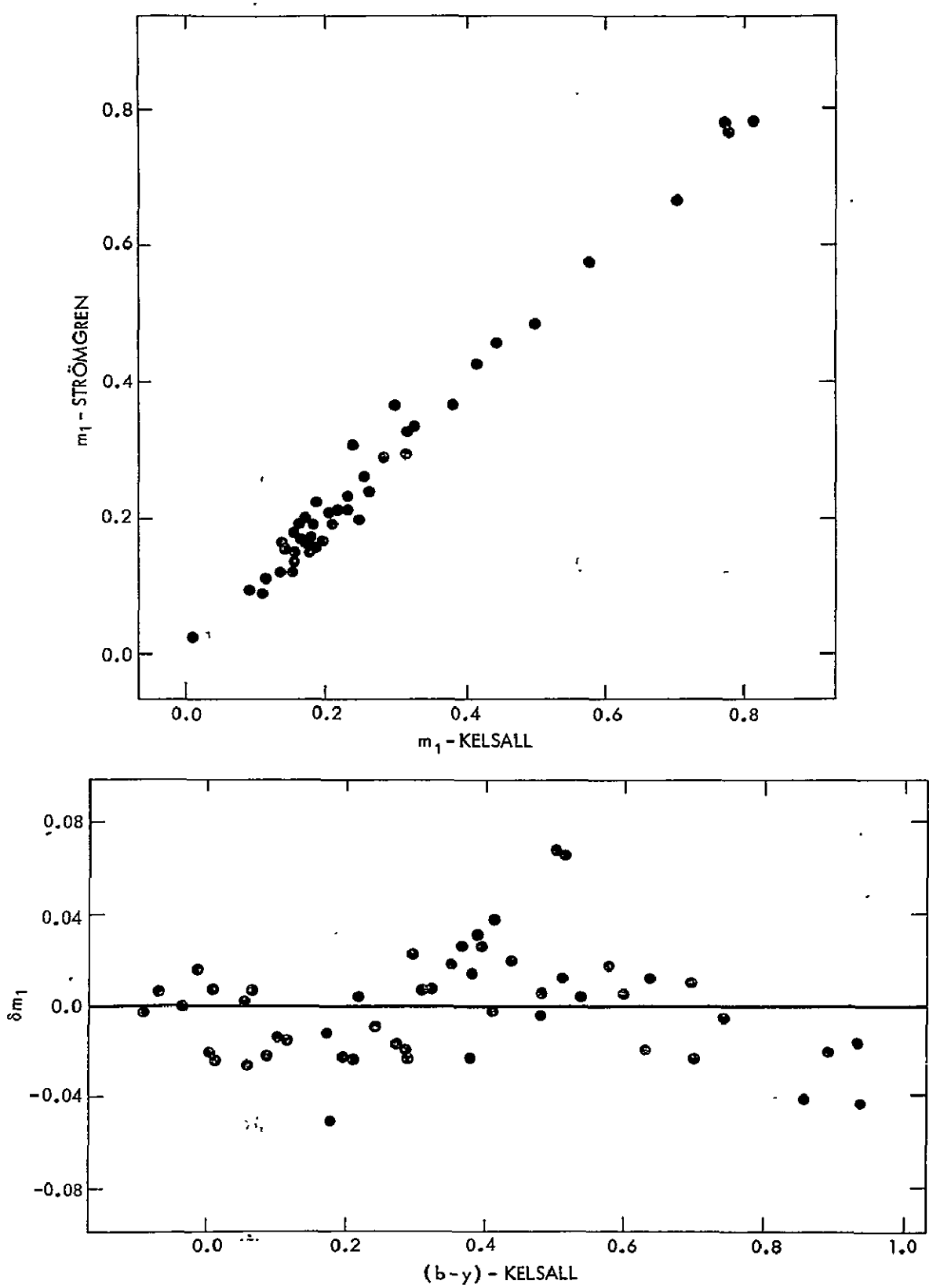

Fig. 3.4 Comparison of the m_1's from the Strömgren-Perry catalog to those observed in this investigation.

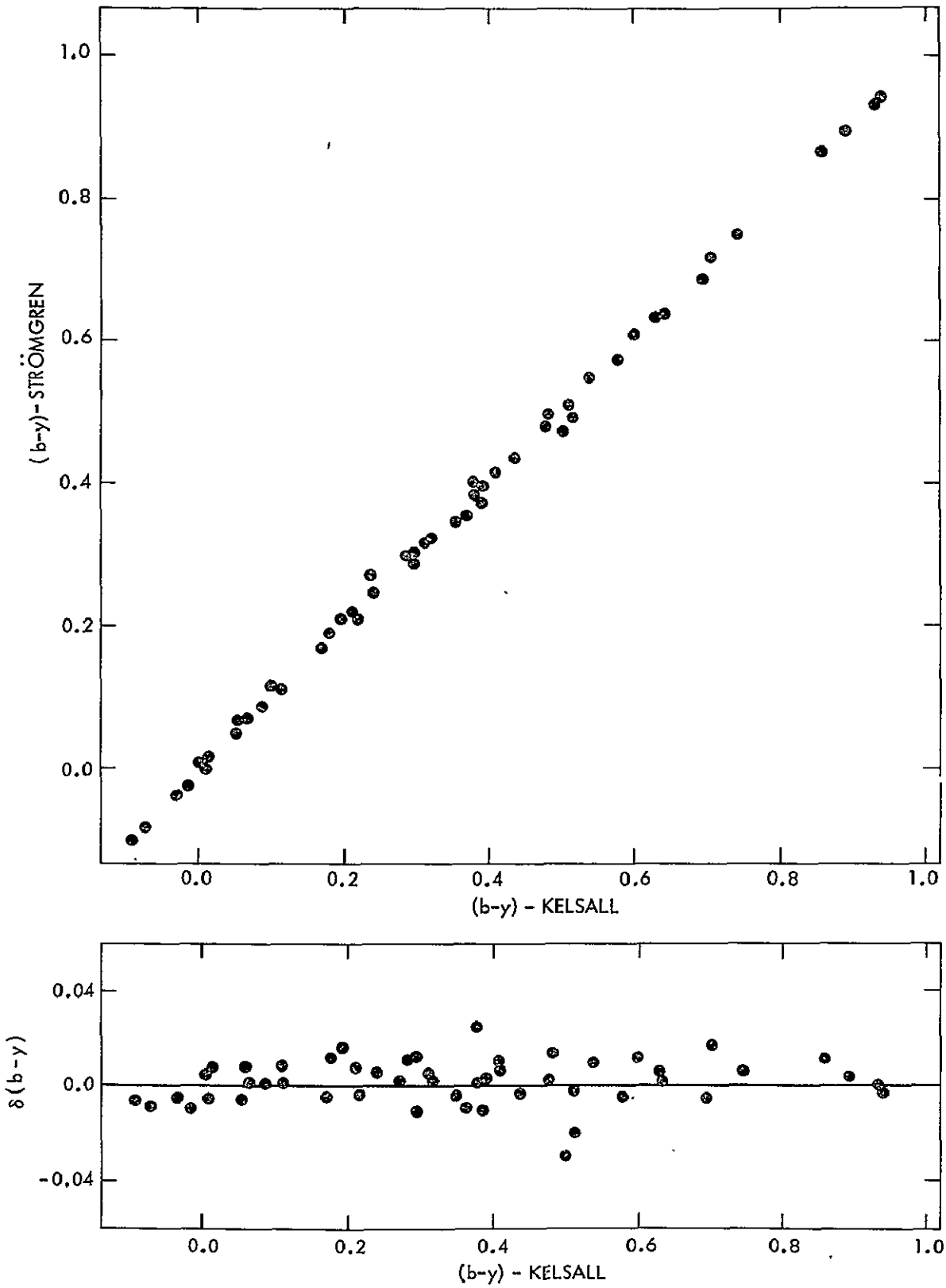

Fig. 3.5 Comparison of the (b-y)'s from the Strömgren-Perry catalog to those observed in this investigation.

CHAPTER IV

ORDINARY STAR RESULTS

4-1. Reduction and Results

Once the standard system is established, data reduction is straightforward. For each night the intensity readings are transformed into the basic photometric quantities by the procedure described in section 3-2. To these quantities air mass and night corrections are added. The appropriate extinction coefficients and night corrections are obtained from the analysis of the standard star data on that night.

Table 4.1 lists the final results for the ordinary (i.e., nonvariable) stars in this program. The spectral types are from the compilation by Jaschek et al. (1964). A number of stars require individual discussion, and this specific commentary is contained in the notes appended to the table.

4-2. Mode of Analysis

The major body of the ordinary star results is devoted to supergiant stars. These stars suffer much interstellar reddening. The effects of the interstellar reddening on supergiants is seen as the scatter in the plot of c_1 versus (b-y) shown in Fig. 4.1. For the G and K stars there is a discernible envelope, which probably delineates the reddening-free, thermal locus. This simple pattern is immediately confused by the configuration of the interwoven A and F stars. As we shall see later, c_1 is a parabolic function of (b-y), or spectral type. The question that must be settled is how best to eliminate the effects of reddening.

As mentioned in section 1-4 a standard technique used in eliminating the reddening from a multi-color program is to plot a particular color-color diagram. Then from an analysis of the least reddened stars (near-by or high latitude stars), and those for which the reddening is reasonably well-known (cluster or association members), a thermal locus can be determined. Once the thermal locus is known, color excesses can be procured for any one of the chosen colors. The deduction of all other color excesses is possible, if the color excess ratios are known with respect to one of the chosen colors. This last step requires external knowledge of the nature of the interstellar reddening as a function of wavelength, or spectral type information so reddening lines can be deduced from the photometric data itself. This procedure is quite adequate, but it does introduce a number of systematic effects which we wish to circumvent. Firstly, the thermal locus is a line delineating an unreddened boundary presumed to be true for all stars. This assumption that the thermal locus is dispersionless is not necessarily correct. Secondly, the shape of the thermal locus cannot be well defined unless the distribution of unreddened, or slightly reddened, stars is sufficiently dense along its total path in the color-color diagram. Finally, the positioning of the locus is often subjective. These three effects can introduce hidden systematic errors in the deduced color excesses for the other colors.

Another method of suppressing reddening effects is exemplified by the construction of Q in the UBV system. To illustrate this procedure we consider a system composed of the three observed quantities c_1, c_2, and c_3. Any c is a composite of c_0, the intrinsic value of c, E(c), the

c's color excess, and e(c), the observational error. We drop e(c) from the discussion for convenience. If the color excess ratios, $E(c_1)/E(c_3)$ and $E(c_2)/E(c_3)$, are known, we can construct two reddening free quantities. We denote these by bracketed symbols. The unreddened quantity associated with c_1 is --

$$[c_1] = c_1 - E(c_1)/E(c_3)*c_3$$

or

$$[c_1] = c_1 - \alpha*c_3$$

As each color is equal to its intrinsic value plus the reddening excess we have --

$$[c_1] = c_{1_0} - \alpha*c_{3_0} + (E(c_1) - \alpha*E(c_3)),$$

which reduces to --

$$[c_1] = c_{1_0} - \alpha*c_{3_0}.$$

Similarly for the other color we have --

$$[c_2] = c_{2_0} - \beta*c_{3_0},$$

where β is the ratio $E(c_2)/E(c_3)$. The bracketed quantities contain the effects of the interstellar reddening only through the coefficients α and β. In the construction of the bracketed colors no reliance is made on knowing the location of a thermal locus. This process sacrifices one color to remove the interstellar reddening effects. The desirable characteristics of c_3, the sacrificed color, are that it be reasonably neutral as an indicator of stellar physical variables, and that the needed reddening excess ratios be less than unity. The color (b-y) of this investigation satisfies these demands, being mainly determined by stellar effective temperature.

The virtues of forming the bracketed quantities are that the dispersionless thermal locus is not introduced, mean lines can be determined statistically, and all stars regardless of their amounts of reddening can be included in the analysis of fundamental relationships. While it is difficult to argue for the overall superiority of this procedure on strong grounds, its intuitive neatness is very appealing.

4-3. Color Excess Ratios

The determination of the color excess ratios is carried out in three different ways - firstly, through use of the wavelength dependence of interstellar reddening and the filter characteristics; secondly, by an analysis of the cepheid colors at maximum light as functions of (b-y); and, finally, by the fitting of the bracketed quantities for the Ib supergiants with the color excess ratios left as free parameters. These three methods give rather dispersive answers, indicating the difficulty of obtaining good color excess ratios. Our hope is that an average of the results is meaningful, as the three methods are distinct, and each contains errors of different kinds.We discuss each of these methods in more detail below.

The effective wavelength of a filter, λ_e, is defined by the standard relation --

$$\lambda_e = \int \lambda * F(\lambda) * T(\lambda) * S(\lambda) * d\lambda \Big/ \int F * T * S * d\lambda \ ,$$

where $F(\lambda)$ is the filter transmission, $T(\lambda)$ is the telescope plus photometric equipment response function, and $S(\lambda)$ is the stellar distribution function. In our case $F(\lambda)$ is well known from the spectrometer scans. Using reasonable functions for T and S it is found by numerical experimen-

tation that effective wavelength is most insensitive (±3 Å) to these functions, except for the u filter. The difficulty with the u filter is that it lies in the region where the photomultiplier response is rapidly varying, and thus the determination of the effective wavelength is rather difficult as the responses of the individual tubes used are unknown. As a compromise we define $\lambda_e(u)$ with T and S set equal to one at all wavelengths. The values of the effective wavelengths are listed in Table 4.2. The color excess ratios are determined by coupling a knowledge of the effective wavelengths with the results of Nandy (1964, 1965, 1966, 1967), and of Boggess and Borgman (1964) on the variation of the interstellar reddening with wavelength. The results of this are presented in Table 4.3. The large scatter in the ratios for c_1 and m_1 is disappointing. The scatter in the ratios for G and N are much smaller, a reflection of the appreciably shorter wavelength baselines for these colors.

At maximum light the cepheids represent a class of stars of nearly identical spectral characteristics, independent of period. Thus, the scatter of cepheid colors at maximum light in any color-(b-y) diagram can be mainly attributed to the effects of interstellar reddening. We take advantage of this situation by determining the best linear relations between the various colors and (b-y). Clearly, the slopes of these straight lines are the desired color excess ratios. The findings of such a study for the program cepheids are given in Table 4.4.

A final method is to employ all the supergiant data. The procedure is the following. The spectral types are taken as reliable, independent information. This is a judicious choice as the assignment of spectral type has the desired advantage of being relatively unaffected by interstellar reddening. Digitizing the spectral types so A0 = 0.0, A1 = 1.0,

...., K5 = 35.0 transforms them to a numerical coordinate, X. The reddening free colors we use in the analysis are --

$$[c_1] = c_1 - \alpha_{c_1} *(b-y),$$

$$[m_1] = m_1 - \alpha_{m_1} *(b-y),$$

$$[G] = G - \alpha_G *(b-y),$$

and

$$[N] = N - \alpha_N *(b-y),$$

where $\alpha_{c_1} = E(c_1)/E(b-y)$, etcetera. Each of the bracketed quantities are fitted by an eighth order power series in X, with the alphas left as free parameters. The dispersions about the fitting lines are investigated as functions of the alphas. The normalized sum of the deviations squared about the fitting lines are shown as functions of alpha in Fig 4.2. The graph demonstrates that for each of the bracketed colors there is a "best" alpha. These best alphas are indicated by arrows on the graphs and are listed in Table 4.5. The broadness of the curves of normalized S with alpha for $[c_1]$ and $[m_1]$, and the sharpness in the curves for the cases of [G] and [N] are directly understandable in terms of the broadness and narrowness of the associated wavelength baselines. We accept these alphas as representative of the most appropriate statistical values for the color excess ratios.

The final adopted values for the color excess ratios are the weighted averages of the above three sets of results. The subjective weightings applied are - 2 for the cepheid results, 1 for the interstellar-λ_e

findings, and 1 for the free parameter fitting answers. These adopted values and those used by Strömgren (1966), and Williams (1966), in their investigations are shown in Table 4.6.

4-4. Bracketed Colors Versus Spectral Type

Using the adopted color excess ratios the Ib supergiant results are fitted by an eighth order power series in the digitized spectral type coordinate, X, by the method of least squares. There are two reasons for using an eighth order power series fit. First, the order introduces a degree of high frequency smoothing. Second, in the free parameter variation method of section 4-3 it was found that a high order fit was needed to ensure a smooth relation of S with alpha, and make the best alphas independent of the order of the fitting series. A least squares fitting procedure is invalid in the strict sense, as X is both disjoint in nature and not error free. We use the method as a convenience. While there have been some attempts to formulate a meaningful method of fitting in a double error coordinate system, we employ the heuristic method of reversal for final smoothing. That is, we fit the spectral type as a function of the color within the workable limits F0 to K0 where the data is sufficient, and combine these results with the reversed fit, the colors as functions of the spectral type. The final curve for any color is the weighted average (W = 2 for the color as a function of spectral type, and W = 1 for the spectral type as a function of color) of the two results, with a little assist from the scanty data for stars earlier than F0. The adopted relations are shown as solid lines in Fig. 4.3; the crosses are the fit of the color as a power series in X; the filled ellipses are the fit of the spectral type by a power series in the color. The rms

dispersions at any spectral type are $0^{m}.081$, 0.064, 0.021 and 0.030 for $[c_1]$, $[m_1]$, [G] and [N], respectively.

4-5. Intrinsic Values for (b-y) and G

The recovery of the intrinsic values for (b-y) and G as functions of spectral type can be made using the (B-V) color excess data from the UBV results. Buscombe (1964) lists in a catalog of supergiant and cepheid results the E(B-V)'s for seventy-two of the supergiant stars observed in this program. This data is sufficient to position a thermal locus in a G,(b-y) diagram.

In Fig. 4.4 G is plotted against (b-y). The figure indicates that a suitable thermal locus is a straight line. But its position cannot be precisely specified. To locate the zero point of a straight thermal locus we assume that E(b-y) = 0.70*E(B-V). Such a relationship is consistent with our present understanding of the variation of the interstellar extinction with wavelength. For the seventy-two stars with known E(B-V) we can calculate $(b-y)_o$ and G_o, as E(G) = 0.105*E(B-V). Fitting the data for these seventy-two stars to a linear relation gives the dashed line in Fig. 4.4. This line has a slope of 0.532, which is close to the value of 0.510 found by Williams in his study of long period ($P \geq 10^{d}$) cepheids.

For the dependence of $(b-y)_o$ and G_o on spectral type we process the reddening-free colors in a manner commonly used in nuclear physics. Regarding the spectral type as a channel entry we perform a smoothing of the insufficient and "noisy" data by forming the averages over a number of channels, and position this average value at the weighted mean channel location. While the use of moving averages eliminates fine detail, its advantage is to enhance systematic trends which might otherwise be lost

in the bouncy data. As a check, the run of the moving averages are compared for consistency with the single channel averages where there are sufficient points in a single channel. In Fig. 4.5 the mean eye-fitted $(b-y)_o$ and G_o lines are shown. The triangles in the figure are single channel averages, while the squares are the moving averages. It is clear that there is no glaring inconsistency between the two averaging processes. In fact, in this case the moving averages are probably not essential to the discussion, but as this procedure is used later, its introduction here is warranted. The mean line results are not entirely in accord with the straight line thermal locus found in the G,(b-y) plot, as transferral of the separately determined $(b-y)_o$ and G_o points onto this plot produces a slight bulge to the left of the straight line near KO. However, this discord is not significant. The point here is that adequate color excesses are retrievable. These excesses calculated using the thermal locus of Fig. 4.4 are listed in the last column of Table 4.1.

4-6. Physical Meaning of [G] and [N]

The physical interpretation of the photometric parameters associated with the Strömgren system is well supported by the investigations of Strömgren and his collaborators. Such an admirable situation does not exist for the case of the colors [G] and [N].

In a recent study of atmospheric simulation models by Bell and Rodgers (1969) it is pointed out that the Griffin and Redman (1960) photometric index n is a satisfactory cyanogen strength criterion. Thus, to reduce the proverbial multiplicity of correlative graphs, so common to photometric studies, we substantiate our claim that [N] is a CN strength indicator by a plot of n versus [N] in Fig. 4.6. On the whole the agreement

is satisfying, though the scatter is quite large. The mean n and [N] curves with spectral type are similar in shape, though n peaks at an earlier type (G8) than does [N] (KO).

Photometric studies of the G-band strength for supergiants are lacking, except for Kraft's Gamma photometry. Kraft notes that a perusal of the MK standard spectra indicates the G-band strength reaches a maximum in the middle G stars for luminosity class I. His Gamma photometry reproduces this characteristic quite well. The color [G] is a measure of the CH contribution to the G-band as shown by Bell and Rodgers. However, its variation with spectral type is not well correlated with the visual aspects of the spectra used as the classification criteria in the MK scheme. In particular, [G] has not attained a maximum even by spectral type K5. We note, however, that the G-band strength is often determined from plates of low dispersion, and the contrast on these plates is muted by the spectrograph's instrumental profile and the background of weak lines. In lieu of any objective G-band criterion we will retain the suggestive G notation for the color, but stress that it probably is not an indicator of what many observers would call the G-band strength.

TABLE 4.1

OBSERVATIONS OF THE ORDINARY STARS.

HD/BD	SPECTRAL TYPE	Y	C1	M1	B-Y	NO. OBS.	G	N	NO. OBS.	E(B-Y)
HD 4362	G0IB	6.414	0.502	0.308	0.682	3	0.198	0.492	3	0.152
HD 6474	G0IA	7.639	0.647	0.353	1.089	2	0.250	0.575	2	0.585
HD 7927	F0IA	4.998	1.467	0.049	0.479	3	0.035	0.391	3	0.299
HD 8906	F3IB	7.127	1.294	0.145	0.493	2	0.046	0.423	2	0.289
HD 8992	F6IB	7.780	0.970	0.179	0.595	2	0.055	0.512	2	0.406
HD 9022	K3III	6.899	0.489	0.644	0.915	1	0.391	0.675	1	
HD 9250	G0IB	7.183	0.632	0.247	0.929	3	0.200	0.530	3	0.493
HD 9366	K3IB	6.915	0.242	0.804	1.242	2	0.421	0.850	2	0.351
HD 10494	F5IA	7.283	1.511	0.009	0.870	2	0.087	0.462	2	0.706
HD 11092	K5IABB	6.569	0.173	0.812	1.396	1	0.496	0.821	1	0.369
HD 11800	K5IB	7.794	0.292	0.651	1.360	1	0.507	0.800	1	0.288
BD 59 366	A0IB	8.623	0.629	0.047	-0.161	3				
HD 12014	K0IB	7.719	0.279	0.703	1.307	2	0.424	0.873	2	0.433
BD 59 389	F0IB	9.048	1.601	-0.030	0.776	1	0.001	0.417	1	0.800

TABLE 4.1

(CONTINUED)

HD/BD	SPECTRAL TYPE	Y	C1	M1	B-Y	NO. OBS.	G	N	NO. OBS.	E(B-Y)
HD 14662	F7IB	6.282	0.872	0.211	0.552	3	0.094	0.479	3	0.246
HD 16901	G0IB	5.452	0.624	0.315	0.556	3	0.140	0.486	3	0.130
HD 17378	A5IA	6.251	1.366	-0.075	0.677	3	0.025	0.422	1	0.601
HD 17506	K3IB	3.771	0.217	0.789	1.075	3	0.421	0.835	2	0.119
HD 17958	K3IA	6.223	0.145	0.797	1.379	2	0.491	0.805	2	0.358
HD 17971	F5IA	7.738	1.385	0.056	0.740	2	0.079	0.475	2	0.547
HD 18391	G0IA	6.936	0.531	0.360	1.304	2	0.280	0.624	2	0.806
HD 20123	G5II	5.048	0.431	0.308	0.742	2	0.219	0.579	2	0.183
HD 20902	F5IB	1.809	1.090	0.190	0.304	2	0.019	0.423	2	0.096
HD 23230	F5II	3.798	0.968	0.197	0.266	3	0.002	0.413	3	0.087
HD 25030	K1IB	8.605	0.498	0.624	0.945	2	0.392	0.768	1	0.012
HD 25056	G0IB	7.049	0.752	0.201	0.799	3	0.170	0.474	3	0.391
HD 25305	A2IB	8.909	0.828	0.238	0.175	2				
HD 25291	F0II	5.053	1.459	0.132	0.336	4	-0.017	0.406	4	0.235

TABLE 4.1

(CONTINUED)

HD/BD	SPECTRAL TYPE	Y	C1	M1	B-Y	NO. OBS.	G	N	NO. OBS.	E(B-Y)
HD 26630	G0IB	4.148	0.566	0.273	0.608	2	0.156	0.503	2	0.162
HD 31118	K5IB	7.087	0.284	0.848	1.121	4	0.471	0.695	4	0.052
HD 31964	F0IAP	3.053	1.274	0.061	0.395	5	0.018	0.389	2	0.225
HD 31910	G0IB	4.046	0.525	0.323	0.548	5	0.166	0.499	4	0.052
HD 33299	K1IB	6.722	0.348	0.545	1.037	3	0.335	0.823	3	0.289
HD 36673	F0IB	2.590	1.476	0.193	0.104	2	-0.034	0.344	2	0.000
HD 36891	G3IB	6.113	0.417	0.365	0.630	3	0.197	0.570	3	0.085
HD 37819	F5IB	8.120	0.667	0.238	0.371	2	0.015	0.475	1	0.201
HD 38247	G8IAB	6.635	0.215	0.693	1.019	3	0.346	0.862	3	0.235
HD 38808	G3IBII	7.554	0.453	0.306	0.649	3	0.208	0.536	3	0.081
HD 39416	G3IBII	7.516	0.383	0.382	0.650	2	0.183	0.566	2	0.148
HD 39866	A2IB	6.360	1.498	0.028	0.257	2				
HD 39970	A0IA	6.000	0.557	-0.042	0.345	2				
HD 39949	G2IB	7.251	0.531	0.292	0.705	2	0.174	0.545	2	0.248

TABLE 4.1

(CONTINUED)

HD/BD	SPECTRAL TYPE	Y	C1	M1	B-Y	NO. OBS.	G	N	NO. OBS.	E(B-Y)
HD 40297	A0IB	7.267	0.953	-0.017	0.256	2				
HD 43282	G5IBII	7.744	0.373	0.444	0.848	2	0.252	0.718	1	0.243
HD 44033	K3IB	5.652	0.381	0.870	0.974	2	0.470	0.688	1	0.000
HD 44990	F7IAB	6.066	0.388	0.456	0.752	3	0.192	0.625	2	0.266
HD 45829	K0IAB	6.661	0.236	0.714	1.004	2	0.363	0.863	2	0.170
HD 46300	A0IB	4.522	0.982	0.085	0.042	4	-0.057	0.366	1	
HD 47731	G5IB	6.442	0.383	0.430	0.667	3	0.224	0.630	3	0.064
HD 48616	F5IB	6.852	1.039	0.186	0.513	2	0.041	0.479	2	0.329
HD 58439	A2IB	6.242	1.257	0.035	0.240	2				
HD 58526	G3IB	5.991	0.472	0.380	0.547	2	0.170	0.511	2	0.039
HD 59067	G8IB	5.864	-0.004	0.096	0.430	2	0.040	0.449	1	0.218
HD 67594	G2IB	4.368	0.413	0.435	0.561	2	0.203	0.546	2	0.000
HD 71952	K0IV	6.247	0.458	0.391	0.619	4	0.247	0.521	3	0.000
HD 74395	G2IB	4.640	0.492	0.298	0.507	2	0.132	0.498	1	0.085

TABLE 4.1

(CONTINUED)

HD/BD	SPECTRAL TYPE	V	C1	M1	B-Y	NO. OBS.	G	N	NO. OBS.	E(B-Y)
HD 77912	G8IBII	4.565	0.387	0.419	0.632	4	0.223	0.648	4	0.018
HD 84441	G0II	2.973	0.484	0.268	0.505	4	0.149	0.479	3	0.036
HD 87737	A0IB	3.533	0.963	0.060	0.036	2				
HD 96436	G7	5.528	0.421	0.339	0.588	5	0.215	0.453	4	
HD 111631	M0.5V	8.472	0.083	0.730	0.813	3				
HD 128750	K2	5.929	0.418	0.463	0.671	4	0.265	0.585	4	
HD 134083	F5V	4.954	0.455	0.143	0.295	1	0.032	0.394	1	
HD 148743	A7IB	6.519	1.539	0.115	0.247	3	-0.029	0.391	2	0.142
HD 149757	O9.5V	2.579	-0.081	-0.013	0.104	1	-0.041	0.401	1	
HD 161796	F3IB	7.111	1.526	0.199	0.287	4	0.041	0.411	4	0.015
HD 163506	F2IA	5.448	1.418	0.119	0.227	2	0.014	0.407	2	0.003
HD 163800	O8	6.985	-0.084	-0.038	0.270	1	-0.020	0.424	1	
HD 168913	F9IB	5.615	0.722	0.233	0.136	1	-0.067	0.386	1	0.088
HD 171635	F7IB	4.778	0.898	0.272	0.357	2	0.070	0.457	2	0.037

TABLE 4.1

(CONTINUED)

HD/BD	SPECTRAL TYPE	Y	C1	M1	B-Y	NO. OBS.	G	N	NO. OBS.	E(B-Y)
HD 172365	F9IB	6.362	0.724	0.232	0.499	2	0.102	0.463	2	0.149
HD 173638	F2IBII	5.716	1.489	0.110	0.404	1	-0.021	0.444	1	0.339
HD 174104	G0IB	8.370	0.549	0.204	0.458	1	0.120	0.435	1	0.046
HD 179784	G5IB	6.685	0.409	0.363	0.921	1	0.273	0.697	1	0.289
HD 180028	F6IB	6.934	0.929	0.147	0.549	1	0.078	0.460	1	0.282
HD 180583	F6IBII	6.055	0.814	0.205	0.361	1	0.027	0.449	1	0.156
HD 182296	G3IB	7.023	0.458	0.367	0.868	2	0.228	0.708	2	0.334
HD 183864	G2IB	7.329	0.579	0.204	0.839	2	0.181	0.524	2	0.418
HD 187203	G0IB	6.445	0.714	0.227	0.609	2	0.152	0.491	2	0.173
HD 187299	G5IABB	7.136	0.198	0.410	1.080	2	0.280	0.751	2	0.494
HD 226223	F6IB	9.159	0.848	0.187	0.406	1	-0.010	0.484	1	0.313
HD 190113	G5IB	7.839	0.404	0.438	0.954	1	0.308	0.728	1	0.244
HD 331777	F8IA	7.923	0.970	0.304	0.942	2	0.186	0.526	2	0.548
HD 190446	F6IB	8.219	0.794	0.202	0.345	2	0.050	0.392	2	0.073

TABLE 4.1

(CONTINUED)

HD/BD	SPECTRAL TYPE	Y	C1	M1	B-Y	NO. OBS.	G	N	NO. OBS.	E(B-Y)
HD 190323	G0IAAB	6.849	0.880	0.344	0.514	2	0.115	0.518	2	0.138
HD 190403	G5IBII	5.731	0.416	0.239	0.470	2	0.175	0.418	2	0.000
HD 191010	G3IB	8.171	0.424	0.318	0.623	2	0.203	0.558	2	0.059
HD 191423	O9V.	8.060	-0.085	-0.022	0.188	1	-0.038	0.392	1	
BD 37 3827	F3IB	8.134	1.427	0.074	0.649	1	0.059	0.456	1	0.473
HD 192909	K3IBII	3.959	-0.242	0.544	0.989	2	0.335	0.618	2	0.222
HD 192876	G3IB	4.248	0.450	0.361	0.672	1	0.194	0.581	1	0.151
HD 193370	F5IB	5.160	1.019	0.204	0.413	3	0.054	0.443	3	0.157
HD 193469	K5IB	6.375	0.067	0.656	1.250	1	0.409	0.715	1	0.393
HD 195295	F5II	4.014	1.068	0.189	0.250	2	0.010	0.414	2	0.045
HD 195324	A1IB	5.864	1.193	-0.032	0.384	2				
HD 195593	F5IAB	6.214	1.106	0.103	0.684	3	0.047	0.503	3	0.551
HD 196093	K2IB	4.588	-0.550	0.428	1.073	2	0.298	0.640	2	0.437
HD 196725	K3IB	5.659	0.232	0.769	0.940	2	0.378	0.796	2	0.041

TABLE 4.1

(CONTINUED)

HD/BD	SPECTRAL TYPE	Y	C1	M1	B-Y	NO. OBS.	G	N	NO. OBS.	E(B-Y)
HD 200102	G1IB	6.629	0.479	0.301	0.654	2	0.192	0.527	2	0.129
HD 200905	F5IB	8.312	1.304	0.162	0.498	2	0.025	0.442	2	0.349
HD 200905	K5IB	3.683	0.138	0.794	1.026	3	0.421	0.724	3	0.049
HD 202314	G2IB	6.163	0.367	0.418	0.699	2	0.242	0.644	2	0.062
HD 204022	GCIB	7.430	0.609	0.307	0.973	2	0.245	0.570	2	0.437
HD 204867	G0IB	2.914	0.572	0.303	0.511	1	0.146	0.498	1	0.052
HD 205349	K1IB	6.229	0.207	0.752	1.180	2	0.411	0.883	2	0.290
HD 206312	K1II	7.127	0.387	0.520	0.772	1	0.271	0.797	1	0.087
HD 206778	K2IB	2.377	0.170	0.823	0.938	2	0.397	0.807	2	0.000
HD 206859	G5IB	4.336	0.348	0.479	0.710	2	0.254	0.708	2	0.047
HD 207089	K0IB	5.272	0.250	0.587	0.876	2	0.317	0.772	2	0.113
HD 207260	A2IA	4.265	0.965	-0.035	0.426	2				
HD 207489	F5IB	7.229	1.062	0.177	0.430	4	0.072	0.458	4	0.160
HD 207647	G4IB	7.017	0.381	0.388	0.749	2	0.195	0.649	2	0.256

TABLE 4.1

(CONTINUED)

HD/BD	SPECTRAL TYPE	Y	C1	M1	B-Y	NO. OBS.	G	N	NO. OBS.	E(B-Y)
HD 207673	A2IB	6.480	1.054	-0.015	0.355	2				
HD 208606	G8IB	6.125	0.277	0.565	1.042	2	0.314	0.831	2	0.350
HD 209481	O9V	5.542	-0.110	-0.028	0.138	1	-0.038	0.367	1	
HD 209750	G2IB	2.938	0.474	0.404	0.571	2	0.194	0.538	2	0.009
HD 210221	A3IB	6.116	1.332	0.018	0.327	2				
HD 210745	K1IB	3.370	0.190	0.778	0.992	4	0.384	0.893	4	0.098
HD 214680	O9V	4.927	-0.150	0.030	-0.054	1	-0.068	0.360	1	
HD 216206	G4IB	6.246	0.398	0.406	0.696	3	0.234	0.636	3	0.081
HD 216946	K5IB	4.981	0.196	0.838	1.156	2	0.461	0.775	2	0.126
HD 217476	G0IA	4.998	0.487	0.431	0.960	12	0.207	0.591	12	0.519
HD 218356	K0IBP	4.761	0.144	0.549	0.834	3	0.294	0.675	3	0.114
HD 219135	G0IB	7.620	0.622	0.242	0.677	3	0.174	0.502	3	0.210
BD 60 2532	F7IB	8.305	0.849	0.154	0.751	3	0.100	0.503	3	0.508
HD 221861	K0IAB	5.835	0.288	0.540	1.176	3	0.333	0.826	3	0.489

TABLE 4.1

(CONTINUED)

HD/BD	SPECTRAL TYPE	Y	C1	M1	B-Y	NO. OBS.	G	N	NO. OBS.	E(B-Y)
HD 222574	G0II	4.805	0.523	0.297	0.493	2	0.156	0.453	2	0.000
HD 223047	G5IB	4.964	0.285	0.425	0.696	3	0.208	0.656	3	0.147
HD 224014	F8IAP	4.584	0.861	0.350	0.680	3	0.146	0.504	3	0.288
HD 224165	G8IB	6.005	0.320	0.495	0.731	2	0.257	0.718	2	0.068

COMMENTS

WE REFER TO THE SOURCES JASCHEK ET AL (1964), GENERAL CATALOG OF VARIABLE STARS (KUKARKIN ET AL 1958), AND THE YALE CATALOG OF BRIGHT STARS (1964) BY THE SYMBOLS J, GCVS, AND YBS, RESPECTIVELY. THE COLORS CORRECTED FOR INTERSTELLAR REDDENING ARE DENOTED BY A ZERO.

BD 59 389 - THE COLORS (B-Y)0, G0, AND N0 ARE ALL A TRIFLE LOW FOR ITS SPECTRAL TYPE, BUT THERE IS ONLY ONE OBSERVATION FOR THIS FAINT (Y = 9.0) STAR.

HD 17509 - HAS A B COMPANION, D = 28", BUT NO EFFECT IS OBVIOUS IN THE RESULTS.

HD 23230 - LISTED AS POSSIBLE VARIABLE IN GCVS, NO EVIDENCE IN THE RESULTS THAT IT IS OTHER THAN A F5II STAR.

HD 25030 - THE VALUE OF C10 IS HIGH FOR A K1IB STAR, BUT THE STAR IS FAINT AND THE PHOTOMETRY SHOWS APPRECIABLE SCATTER.

TABLE 4.1

(CONTINUED)

HD 26630 - SPECTROSCOPIC BINARY AND DOUBLE (DELTA-M = 7.5, D = 15"), BUT PHOTOMETRICALLY IT APPEARS AS AN ORDINARY G0IB STAR.

HD 37819 - PHOTOMETRY IS OF GOOD QUALITY, C10 LOW AND M10 HIGH FOR A F5II STAR.

HD 38247 - PHOTOMETRY SHOWS LARGER SCATTER THAN EXPECTED FOR A STAR WITH A Y = 6.6. ALL INDICES WOULD BE BETTER UNDERSTOOD IF THE SPECTRAL TYPE WERE CHANGED FROM G8 TO K0.

HD 44990 - THIS IS THE CEPHEID T MON, P = 27 DAYS.

HD 59067 - INDICES ASKEW FROM EFFECTS OF B COMPANION (DELTA-M = 2. D = 1").

HD 163506 - LISTED IN GCVS AS V441 HER, A SEMIREGULAR VARIABLE WITH A POSSIBLE PERIOD OF 70 DAYS. NO EVIDENCE IN THE PHOTOMETRY WHICH IS OF GOOD QUALITY AND IN ACCORD WITH THE GIVEN CLASSIFICATION, F2IA.

HD 168913 - GIVEN AS EITHER A6V OR F9IB IN J (A M IN YBS). PHOTOMETRICALLY C10 AND M10 ARE COMPATIBLE WITH EITHER ASSIGNMENT, WHILE THE VALUES FOR (B-Y)0, G0, AND N0 ARE IN BETTER ACCORD WITH A6V.

HD 182296 - THE INDICES N0 AND M10 ARE HIGH FOR ITS SPECTRAL TYPE. POSSIBLY OVER ABUNDANT IN METALS, C, AND N.

HD 187299 - THE C10 IS LOW FOR ITS SPECTRAL TYPE, ALL OTHER INDICES ARE NORMAL.

HD 190113 - LISTED AS G5I0 OR G8V IN J, PHOTOMETRY SUPPORTS THE G5IB LISTING.

HD 190323 - THE VALUE OF C10 IS APPROXIMATELY 0.3 TOO LARGE FOR ITS SPECTRAL TYPE, ALL OTHER COLORS ARE WITHIN REASONABLE LIMITS FROM 'NORMAL'.

TABLE 4.1

(CONTINUED)

HD 190403 - LISTED AS G5IB-II, G5II, OR K1V IN J. THE RESULTS HERE ARE MORE CONSISTENT WITH THE LUMINOSITY CLASS V ASSIGNMENT, BUT NOT WITH A SPECTRAL TYPE AS LATE AS K1.

HD 192909 - ALGOL TYPE VARIABLE, LISTED AS K3IB-II + B IN J. THE EFFECTS OF THE COMPANION ARE PRONOUNCED, PARTICULARLY ON C10 AND NO WHICH ARE LOW.

HD 196093 - LISTED AS K2IB + B IN J, QUITE OBVIOUS FROM THE PHOTOMETRY.

HD 200905 - A SPECTROSCOPIC BINARY, NO EFFECTS OBVIOUS IN THE RESULTS.

HD 202314 - ALL COLORS WOULD BE MORE CONSISTENT IF THE SPECTRAL TYPE WERE CHANGED FROM G2 TO G5.

HD 208606 - A SPECTROSCOPIC BINARY, NO EFFECTS OBVIOUS IN THE RESULTS.

HD 210745 - A SPECTROSCOPIC BINARY, NO EFFECTS OBVIOUS IN THE RESULTS.

HD 216946 - SUSPECTED VARIABLE IN GCVS, PHOTOMETRICALLY IT APPEARS NORMAL.

HD 217476 - DEFINITELY VARIABLE, DATA IS INSUFFICIENT TO DETERMINE A PERIOD BUT IT IS OF THE ORDER OF HUNDREDS OF DAYS.

HD 222574 - LISTED AS VARIABLE IN J, AND A POSSIBLE VARIABLE IN GCVS, LOOKS NORMAL PHOTOMETRICALLY.

HD 224014 - THE VARIABLE STAR 7 RHO CAS, PHOTOMETRICALLY IT APPEARS AS A NORMAL F8IA STAR.

TABLE 4.2

EFFECTIVE WAVELENGTHS

Filter	λ_e	λ_e^{-1}
u	0.3455μ	$2.894\mu^{-1}$
v	0.4108	2.434
b	0.4700	2.128
y	0.5482	1.824
A	0.4377	2.285
B	0.4279	2.337
C	0.4166	2.400

TABLE 4.3

COLOR EXCESS RATIOS FROM EXTERNAL SOURCES.

Source/Region	$E(c_1)/E(b-y)$	$E(m_1)/E(b-y)$	$E(G)/E(b-y)$	$E(N)/E(b-y)$
Nandy				
Cygnus	+0.142	-0.129	+0.142	+0.156
Perseus	-0.065	-0.274	+0.087	+0.134
Cassiopeia	+0.050	-0.014	+0.114	+0.200
Cepheus	+0.016	-0.192	+0.135	+0.129
Boggess & Borgman	+0.242	-0.098	+0.151	+0.170
Averages	+0.077±0.105	-0.141±0.088	+0.126±0.023	+0.158±0.026

TABLE 4.4

COLOR EXCESS RATIOS DETERMINED

FROM CEPHEIDS AT MAXIMUM LIGHT

$E(c_1)/E(b-y) = +0.188$

$E(m_1)/E(b-y) = -0.145$

$E(G)/E(b-y) = +0.150$

$E(N)/E(b-y) = +0.124$

TABLE 4.5

COLOR EXCESS RATIOS DETERMINED

FROM FREE PARAMETER FITTING

$E(c_1)/E(b-y) = +0.084$

$E(m_1)/E(b-y) = -0.076$

$E(G)/E(b-y) = +0.173$

$E(N)/E(b-y) = +0.178$

TABLE 4.6

FINAL ADOPTED COLOR EXCESS RATIOS

Source	$E(c_1)/E(b-y)$	$E(m_1)/E(b-y)$	$E(G)/E(b-y)$	$E(N)/E(b-y)$
Kelsall	+0.135	-0.125	+0.150	+0.145
Strömgren	+0.20	-0.18		
Williams	-0.009	-0.261	+0.106	+0.109

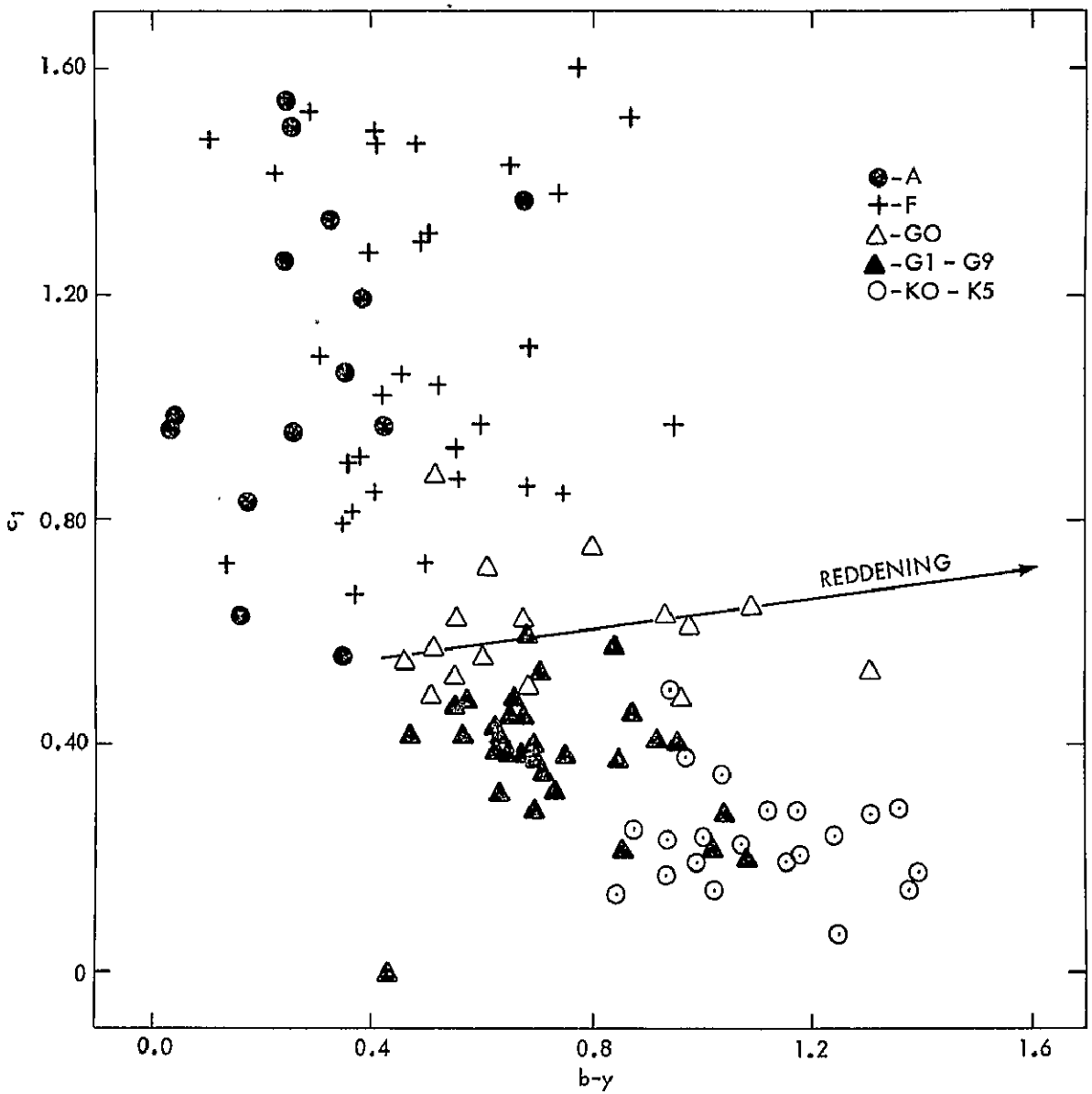

Fig. 4.1 The c_1,(b-y) diagram for A-K supergiants.

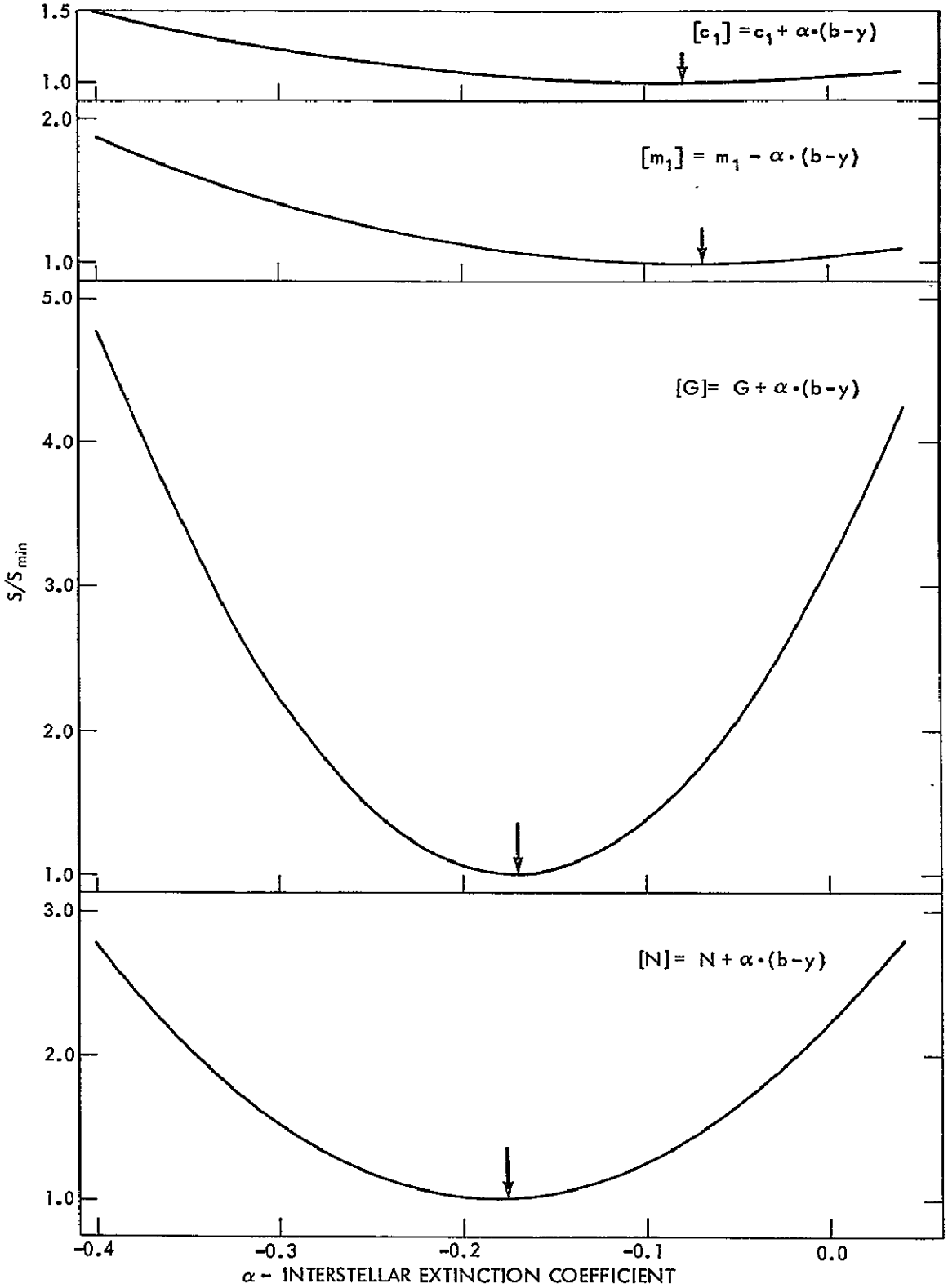

Fig. 4.2 Variation of the normalized sum of the deviations squared with the interstellar extinction coefficient, α, for the reddening-free colors.

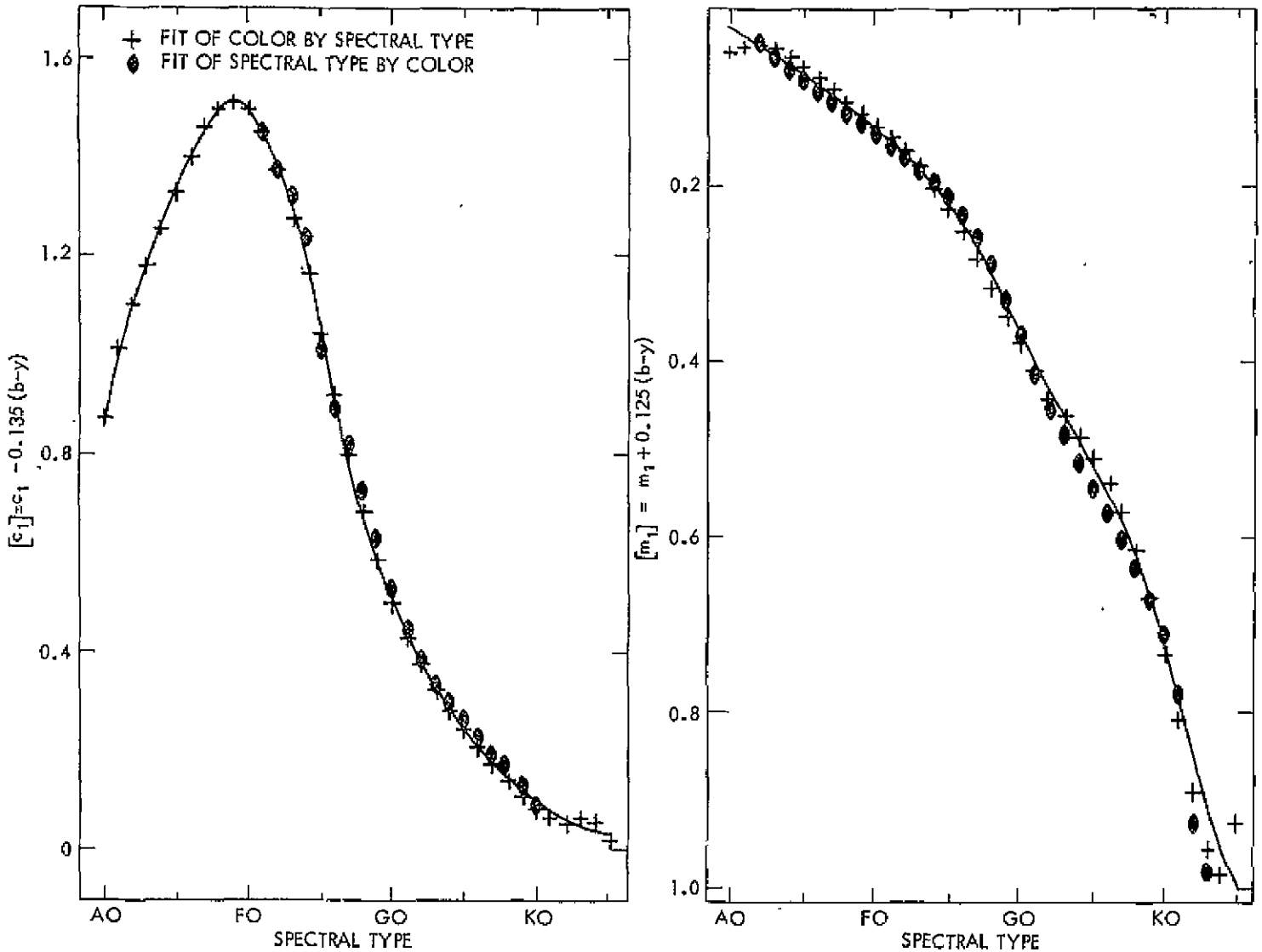

Fig. 4.3(a) The adopted reddening-free colors for the supergiants as a function of spectral type.

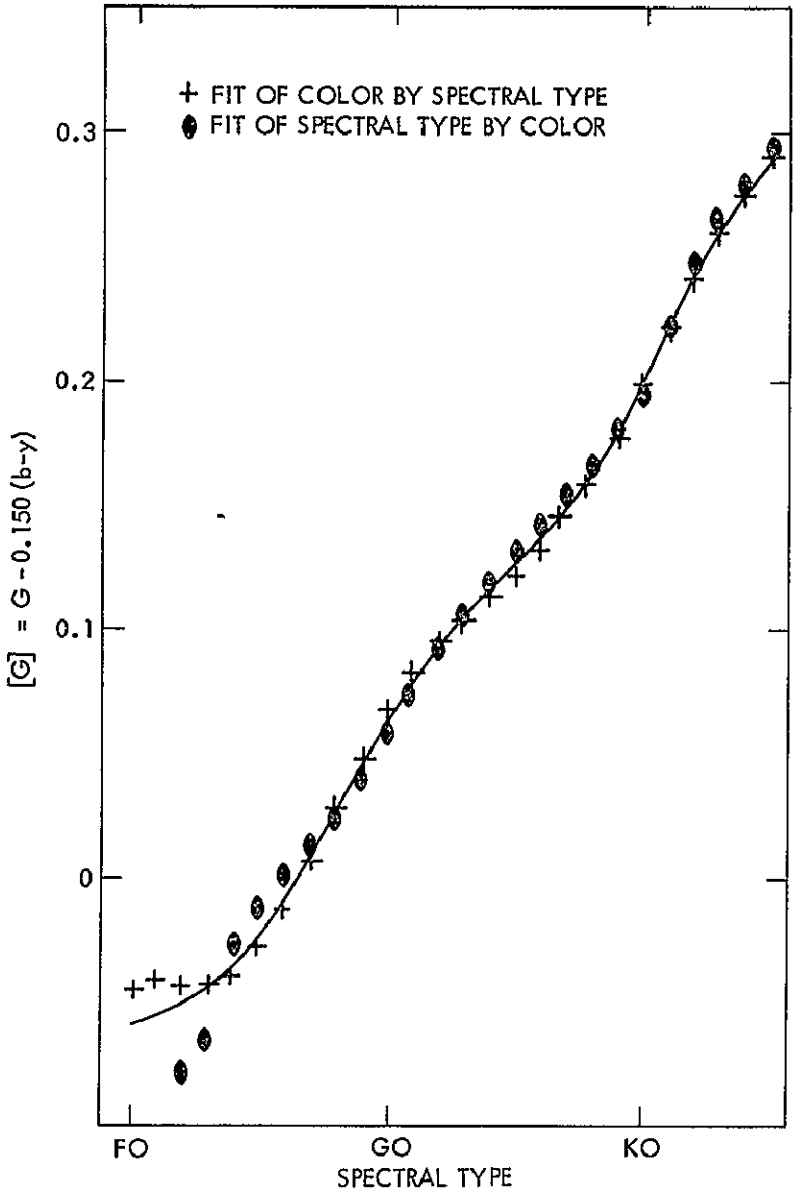
+ FIT OF COLOR BY SPECTRAL TYPE
FIT OF SPECTRAL TYPE BY COLOR
0.3
0.2
0.1
0
[G] = G - 0.150 (b-y)
FO
GO
KO
SPECTRAL TYPE

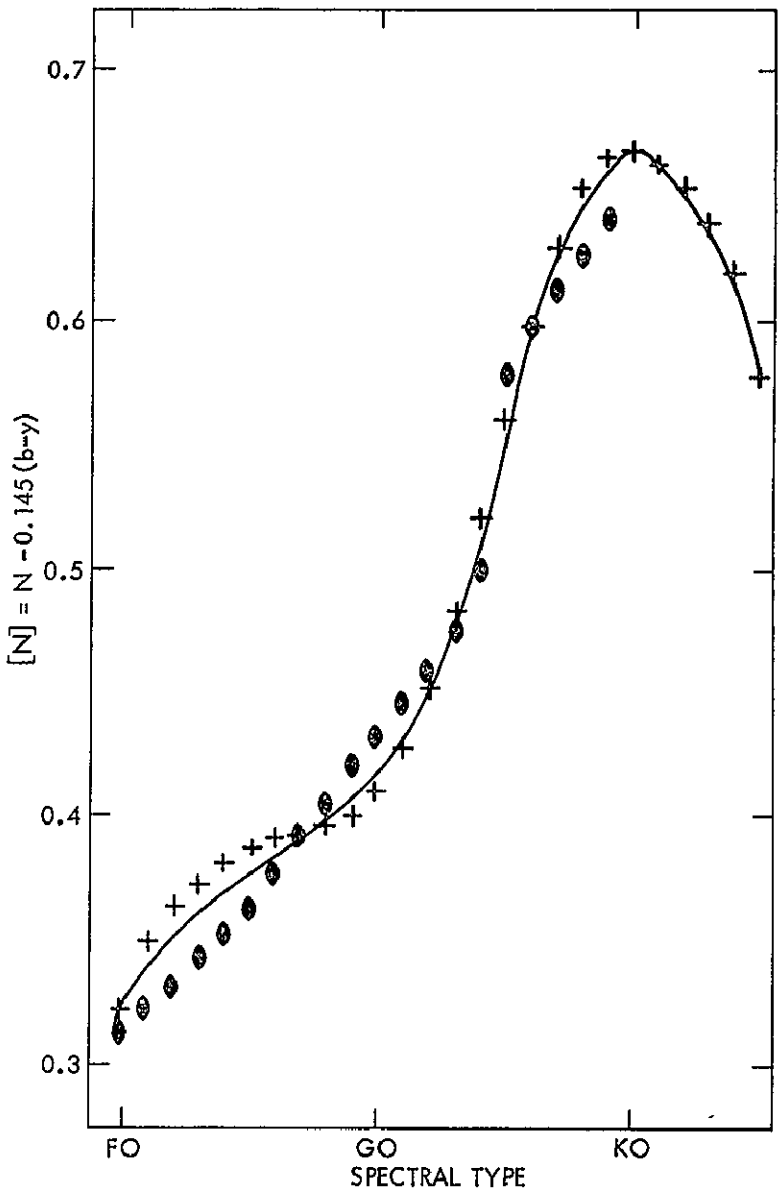
0.7
0.6
0.5
0.4
0.3
[N] = N - 0.145 (b-y)
FO
GO
KO
SPECTRAL TYPE

Fig. 4.3(b)

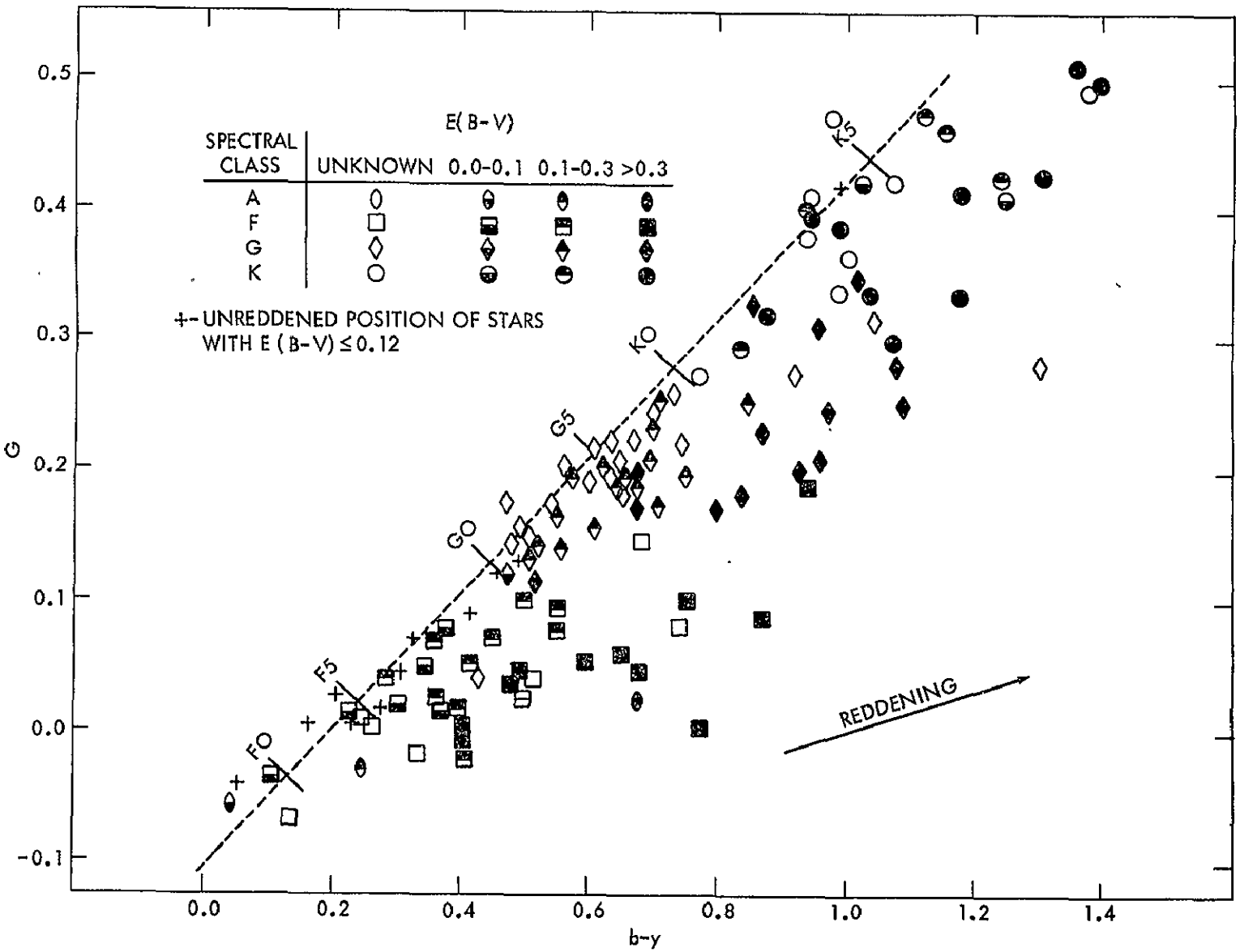

Fig. 4.4 The G,(b-y) diagram for supergiants. The adopted thermal locus is shown as a dashed line.

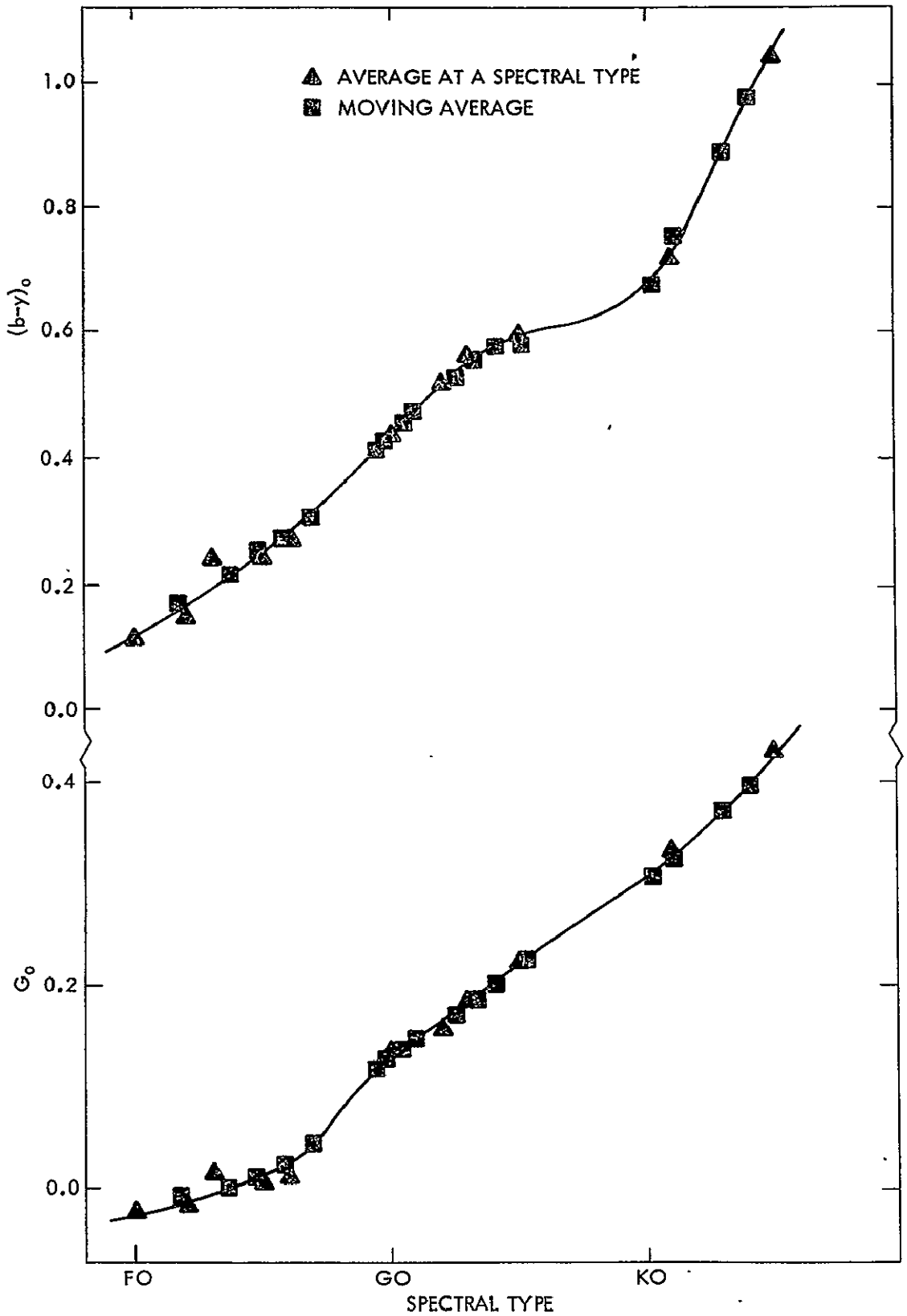

Fig. 4.5 Relationship between the intrinsic colors G_o and $(b-y)_o$ for supergiants and spectral type.

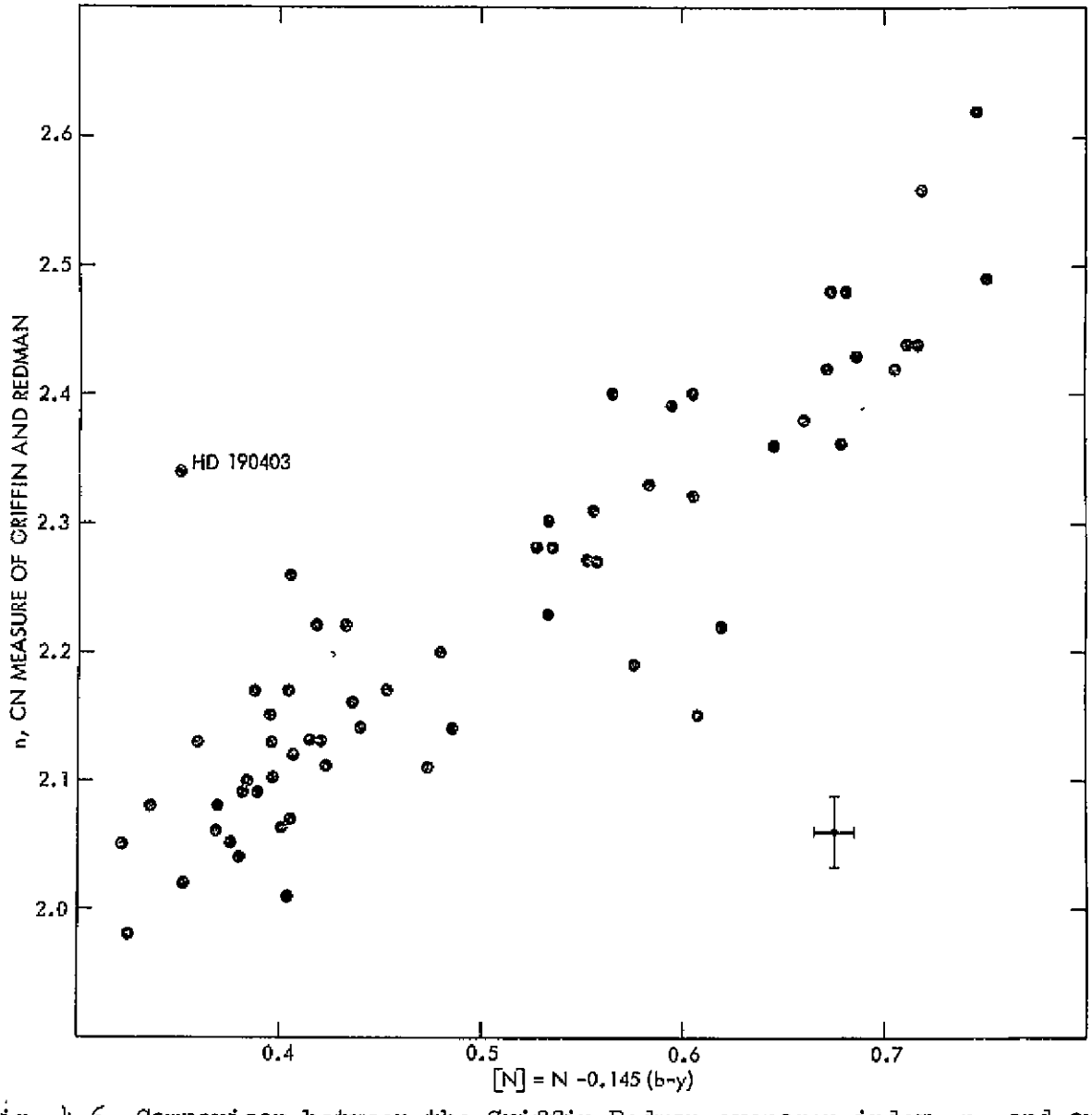

Fig. 4.6 Comparison between the Griffin-Redman cyanogen index, n, and our [N].

CHAPTER V

LUMINOSITY CLASSIFICATION

5-1. Objective and Procedure

One goal of the present investigation is to determine the capability of this photometric system in distinguishing the supergiants from the other luminosity classes. The system's usefulness as a galactic survey tool is greatly enhanced, if this is possible.

We find for each luminosity class the mean color relations with spectral type. A comparison of the separations between the mean color curves, either as functions of spectral type or anyone color, and the errors of measurement show that at least the classes I and II cannot be distinguished. Construction of "supercolors" from quadratic expressions in the mean colors produces a discrimination level superior to that from the use of any pair of colors.

5-2. Source of the Data

The data contained in this study on stars of luminosity classes V through II is insufficient to yield satisfactory color-spectral type relationships. To extend the data on these luminosity classes we incorporate by transformation the data contained in the studies by Strömgren, and Williams. Previously we noted that transformations of high quality are impossible. However, here we restrict the use of the transformed quantities to the simple determination of mean colors, and do not use them in a search for internal correlations. The transformations are adequate for this more limited task.

The best procedure is to transform the bracketed quantities directly. The transformation relations for $[c_1]$ and $[m_1]$ for Strömgren-Perry catalog stars are shown in Fig. 5.1. The expressions for the transformation curves are --

$$[c_1]_K = 0.016 + 0.981*[c_1]_S - 0.012*[c_1]_S^2 ,$$

and

$$[m_1]_K = 0.027 + 0.825*[m_1]_S + 0.205*[m_1]_S^2 .$$

The transformation probable errors are $0^m.022$ and $0^m.013$, respectively. We note the smallness of the zero point and the coefficient of the non-linear term in the $[c_1]$-transformation. As the range in $[c_1]$ is large these aspects of the transformation indicate that our values for $[c_1]$ will be close to those on Strömgren's standard system. This is clearly not true for the value of $[m_1]$. The relations between $[c_1]$, $[m_1]$, [G], and [N] of Williams and those of this study are illustrated in Fig. 5.2. The transformation equations are --

$$[c_1]_K = 0.090 + 0.637*[c_1]_W + 0.268*[c_1]_W^2,$$

$$[m_1]_K = 0.654 + 1.069*[m_1]_W + 0.343*[m_1]_W^2,$$

$$[G]_K = 0.151 + 0.929*[G]_W - 0.572*[G]_W^2 ,$$

and

$$[N]_K = 0.128 + 1.027*[N]_W + 0.130*[N]_W^2 .$$

The probable errors of transformation are $0^m.055$, $0^m.024$, $0^m.007$, and $0^m.009$, respectively. The error in the $[c_1]$ transformation is so large that Williams' results are dropped from the discussion; except for the luminosity class II stars where the data is so scant that every point must

be preserved. The transformation difficulties reflect the complexity of the stellar spectra. The difficulties also emphasize the necessity of carefully matching filters when using an intermediate band-pass system.

A listing of the information used from the Strömgren-Perry catalog and Williams' article is given in an appendix.

It is obvious that color-spectral type relationships for luminosity classes V through II will be less certain than the trends found for supergiants, whose data comes from this investigation alone. However, the uncertainties introduced through the transformations of the external data are within tolerable limits, and the resulting curves are doubtless adequate.

5-3. Color-Spectral Type Relationships

For the supergiant colors the data is sufficient over the spectral type range A5 through K5 so a power series fit in the digitized spectral type coordinate, X, can be made. For the other luminosity class colors it is necessary to make use of moving averages, as in section 4-5. The exceptions to this restriction are the following:

(1) $[c_1]$ for class V stars in the spectral type range A8 to K5 is adequately represented by an eighth order power series in X;

(2) $[m_1]$ for class V stars is suitably given by an eighth order power series in X;

(3) $[c_1]$ and $[m_1]$ for class III stars are matched by an eighth order power series in X.

As the handling of some of the data is subjective, we give the details below.

The smoothing curves (solid lines) for $[c_1]$, [G], and [N] for luminosity class V stars are shown in Fig. 5.3. The power series fit to the full data is denoted by the dots. In the [N] case we see how a high power series fit minimizing the rms deviations introduces bumps, which are probably spurious and need to be smoothed by some sensible intuitive process.

For class IV stars the values of $[c_1]$ and $[m_1]$ cannot be assigned on the basis of the photometric data at the later spectral types. Here an additional expediency is used. The K0 IV - K5 IV results are simply the values found by averaging the class V and class III values (crosses). For [G] and [N] the data is totally inadequate. As the average values formed from the class V and class III results fit the situation as well as any other set of values, these average values are accepted for the class IV stars. The curves are presented in Fig. 5.4.

The smoothed [G] and [N] curves for class III stars are plotted in Fig. 5.5. The turnover in [N] at K3.5 is weakly indicated by the data. This turnover is in accord with the results of Griffin and Redman (1960).

For the class II stars the data is so meager that use of moving averages is of no help, so eye-fitted curves through the raw data are made. In each of the color plots in Fig. 5.6 the class Ib results are shown as a dashed curve. The data points for the class II stars do not distribute themselves about the class Ib line, indicating that photometrically these two classes are distinguishable, if only marginally.

The final over-all results are presented in Table 5.1, and Figs. 5.7 and 5.8. The dispersions about the mean curves are listed in Table 5.2. The $[c_1]$ and $[m_1]$ dispersions for the luminosity class II stars are of doubtful value as the eye-fitted curves stressed the author's results,

while the dispersions are calculated from all the data.

5-4. Supergiant Discriminants

To determine photometric discriminants, all possible color-color graphs were made using the mean colors for the spectral type range A5 through K5. These graphs also included the two constructed colors [u-v] and [u-b]. These two colors are formed using the relations --

$$[u-v] = [c_1] + [m_1],$$

and

$$[u-b] = [c_1] + 2.0*[m_1].$$

The four best segregating curves are shown in Fig. 5.9. In all curves the I-II segregation is virtually impossible to make, and the I-II-III confusion is in many regions quite pronounced. The $[c_1]$ versus [G] curve is the most superior single curve, and when combined with the [u-v] versus [G] curve good discrimination can be made in the ranges $-0.05 \leq [G] \leq 0.10$, and $0.175 \leq [G] \leq 0.300$. For the later spectral types the [G] versus [N] and/or the $[m_1]$ versus [N] curves are useful adjuncts. However, segregation on the basis of the colors alone is below expectations. As all the data was used in making up these curves, it is impossible to determine by any meaningful internal means how well luminosity class segregation can be performed on the basis of the color-color discriminants alone.

Luminosity class segregation can be performed by mapping the mean color curves into the disjointed, luminosity-class, lines in an M_V,logT_e HR diagram. Such a mapping is possible through an equation quadratic in the mean colors.

We first break the mean color-spectral type information up into three segments - A5-F7, F7-G7, and G7-K5. The need for partitioning results from the number of confluences in the mean color lines. For example, in the A5-F7 range the $[c_1]$ lines are cleanly separate for the various luminosity classes, the [G] lines are close through out the range, and the $[m_1]$ and [N] curves are entangled in the neighborhood of F0. The desire that the mapping results be clean demands that there be a limited number of muddying complications contained in the mean color data. For each of these segments we fit M_v simultaneously for all luminosity classes by a single expression in the mean colors $[c_1]$, $[m_1]$, [G], and [N]. That is --

$$M_v(\text{spectral type, luminosity class}) = a_o + \sum_{i=1}^{4} a_i * \text{color}_i + \sum_{i=1}^{4}\sum_{j=i}^{4} c_{ij} * \text{color}_i * \text{color}_j . \qquad (5\text{-}1)$$

In Eq. (5-1), color_i stands for a mean color at a particular spectral type, and for a particular luminosity class. The color_1 is $[c_1]$, etcetera. An equation equivalent to that for M_v is found for $\log T_e$. As these mappings are not calibrations in a strict sense, for convenience and clarity we refer to the results as "supercolors". The results from these rather peculiar constructions are shown in Fig. 5.10. The solid curves represent the M_v data of Blaauw (1963), and the $\log T_e$ calibration of Johnson (1966). The solid curves cover the spectral range A5 through K5 for each luminosity class. The points are the fits achieved using the mean colors for A5 to K5 in a single equation in each of the

three spectral type segments. The agreement is most encouraging. The fitting dispersions are approximately $0^{m}.7$ and 0.008 in M_V and log T_e, respectively. The I-II-III confusion evidenced in the mean color graphs is eliminated in the supercolor diagram. This is a partial vindication of a procedure which might at first appear to be an overly extensive use of the mean colors. However, it is clear that the coefficients in the supercolor equations are basically amplifying terms which enhance small differences in the colors, in order that the results match the imposed calibration conditions. As the calibrations are the disjoint, luminosity-class magnitude and effective temperature curves, the mappings are expected to be unstable to minor perturbations relative to the mean color lines. This feature is probably further magnified by the lack of physical content in the form of the supercolor equations. A redeeming aspect may be the inclusion of the cross-color terms, the utilization of a feature which is hard to grasp through color-color plots. Though the expected sensitivity of supercolor equations to input is a restrictive limitation, the procedure may still be worthwhile when applied to indiscriminantly gathered survey photometry data. We return to this supercolor method in Chapter VII, where we give the results of the method when it is applied to individual stars.

TABLE 5.1

THE MEAN REDDENING-FREE COLORS FOR ALL LUMINOSITY CLASSES.

SPECTRAL TYPE	LUMINOSITY CLASS V	IV	III	II	I	LUMINOSITY CLASS V	IV	III	II	I
	C1 = C1 - 0.135*(B-Y)					M1 = M1 + 0.125*(B-Y)				
B0	-0.027					0.027				
B1	+0.065					0.047				
B2	0.174					0.064				
B3	0.283					0.077				
B4	0.390					0.088				
B5	0.495	0.439				0.098	0.116			
B6	0.600	0.589				0.108	0.118			
B7	0.706	0.728				0.118	0.123			
B8	0.812	0.847				0.129	0.128			
B9	0.911	0.970				0.141	0.138			
A0	0.995	1.042	1.028		0.874	0.153	0.150	0.134		0.018
A1	1.049	1.079	1.084		1.013	0.166	0.163	0.148		0.029
A2	1.068	1.080	1.116		1.103	0.178	0.177	0.162		0.038
A3	1.047	1.055	1.125		1.179	0.188	0.190	0.176		0.047
A4	1.018	1.024	1.115		1.254	0.197	0.200	0.188		0.057
A5	0.980	0.980	1.088	1.475	1.330	0.203	0.203	0.198	0.118	0.068
A6	0.935	0.939	1.050	1.470	1.401	0.207	0.205	0.204	0.127	0.081
A7	0.886	0.885	1.003	1.450	1.460	0.208	0.207	0.208	0.136	0.093
A8	0.824	0.830	0.951	1.425	1.499	0.207	0.208	0.210	0.146	0.107
A9	0.758	0.782	0.895	1.380	1.511	0.205	0.207	0.210	0.155	0.119

TABLE 5.1

(CONTINUED)

SPECTRAL TYPE	LUMINOSITY CLASS V	IV	III	II	I	V	IV	III	II	I
F0	0.693	0.728	0.837	1.325	1.495	0.201	0.205	0.209	0.165	0.132
F1	0.630	0.680	0.779	1.257	1.450	0.197	0.202	0.207	0.175	0.145
F2	0.570	0.640	0.723	1.170	1.376	0.194	0.199	0.206	0.186	0.160
F3	0.516	0.590	0.668	1.060	1.293	0.191	0.196	0.206	0.210	0.178
F4	0.468	0.540	0.617	0.952	1.191	0.191	0.191	0.206	0.227	0.197
F5	0.427	0.495	0.570	0.844	1.033	0.192	0.191	0.209	0.248	0.220
F6	0.391	0.455	0.526	0.735	0.912	0.196	0.195	0.214	0.264	0.245
F7	0.362	0.422	0.486	0.633	0.804	0.202	0.204	0.220	0.283	0.275
F8	0.338	0.395	0.452	0.556	0.701	0.210	0.220	0.228	0.300	0.305
F9	0.319	0.365	0.423	0.494	0.603	0.219	0.234	0.237	0.319	0.339
G0	0.305	0.355	0.398	0.445	0.511	0.228	0.248	0.248	0.338	0.375
G1	0.297	0.340	0.377	0.408	0.436	0.238	0.262	0.260	0.354	0.408
G2	0.292	0.335	0.362	0.378	0.379	0.245	0.270	0.273	0.372	0.439
G3	0.292	0.329	0.350	0.352	0.331	0.253	0.277	0.288	0.390	0.466
G4	0.294	0.324	0.344	0.327	0.291	0.260	0.280	0.304	0.407	0.492
G5	0.298	0.319	0.341	0.304	0.254	0.272	0.283	0.323	0.428	0.518
G6	0.302	0.310	0.340	0.284	0.220	0.276	0.288	0.346	0.455	0.545
G7	0.306	0.305	0.342	0.265	0.186	0.288	0.304	0.375	0.490	0.577
G8	0.309	0.305	0.343	0.248	0.152	0.304	0.330	0.410	0.535	0.616
G9	0.309	0.302	0.343	0.232	0.121	0.328	0.384	0.455	0.580	0.664
K0	0.306	0.301	0.338	0.217	0.095	0.362	0.437	0.511	0.637	0.722
K1	0.292	0.310	0.328	0.202	0.078	0.408	0.503	0.579	0.697	0.795
K2	0.281	0.296	0.311	0.187	0.062	0.468	0.564	0.660	0.757	0.862
K3	0.258	0.271	0.284	0.173	0.049	0.545	0.650	0.754	0.820	0.913
K4	0.226	0.238	0.249	0.155	0.041	0.636	0.746	0.857	0.886	0.956
K5	0.185	0.195	0.206	0.142	0.037	0.735	0.850	0.965	0.950	0.996

TABLE 5.1

(CONTINUED)

SPECTRAL TYPE	LUMINOSITY CLASS V	IV	III	II	I	LUMINOSITY CLASS V	IV	III	II	I
	G = G - 0.150*(B-Y)					N = N - 0.145*(B-Y)				
B0	-0.063					0.364				
B1	-0.069					0.362				
B2	-0.077					0.360				
B3	-0.087					0.357				
B4	-0.097					0.354				
B5	-0.105					0.351				
B6	-0.112					0.348				
B7	-0.117					0.345				
B8	-0.122					0.343				
B9	-0.125					0.342				
A0	-0.128	-0.120	-0.111			0.340	0.341	0.342		
A1	-0.130	-0.121	-0.112			0.340	0.341	0.342		
A2	-0.130	-0.122	-0.113			0.340	0.341	0.342		
A3	-0.129	-0.122	-0.115			0.341	0.341	0.341		
A4	-0.127	-0.120	-0.112			0.342	0.341	0.340		
A5	-0.123	-0.116	-0.110	-0.066	-0.052	0.344	0.341	0.339	0.350	0.322
A6	-0.116	-0.110	-0.105	-0.066	-0.053	0.345	0.342	0.338	0.351	0.325
A7	-0.109	-0.104	-0.099	-0.065	-0.054	0.348	0.343	0.338	0.352	0.328
A8	-0.101	-0.096	-0.090	-0.064	-0.055	0.352	0.344	0.337	0.352	0.331
A9	-0.090	-0.085	-0.080	-0.062	-0.056	0.356	0.346	0.337	0.353	0.334

TABLE 5.1

(CONTINUED)

SPECTRAL TYPE	LUMINOSITY CLASS V	IV	III	II	I	V	IV	III	II	I
F0	-0.080	-0.074	-0.069	-0.061	-0.057	0.360	0.348	0.336	0.355	0.337
F1	-0.068	-0.062	-0.056	-0.060	-0.055	0.362	0.348	0.335	0.357	0.341
F2	-0.054	-0.047	-0.040	-0.055	-0.050	0.362	0.348	0.333	0.360	0.353
F3	-0.040	-0.032	-0.025	-0.048	-0.045	0.358	0.345	0.332	0.364	0.362
F4	-0.026	-0.018	-0.011	-0.035	-0.035	0.354	0.342	0.330	0.369	0.371
F5	-0.012	-0.005	+0.002	-0.023	-0.023	0.348	0.338	0.328	0.375	0.379
F6	+0.002	+0.008	0.013	-0.008	-0.008	0.339	0.332	0.326	0.381	0.386
F7	0.016	0.020	0.023	+0.008	+0.008	0.330	0.328	0.325	0.386	0.392
F8	0.028	0.030	0.032	0.025	0.026	0.320	0.322	0.324	0.390	0.399
F9	0.039	0.040	0.040	0.045	0.045	0.310	0.316	0.322	0.395	0.406
G0	0.049	0.048	0.048	0.064	0.064	0.300	0.310	0.321	0.400	0.417
G1	0.057	0.056	0.054	0.079	0.079	0.292	0.306	0.320	0.411	0.433
G2	0.064	0.062	0.061	0.087	0.094	0.286	0.303	0.320	0.427	0.453
G3	0.070	0.068	0.067	0.097	0.105	0.284	0.303	0.323	0.448	0.480
G4	0.075	0.074	0.074	0.106	0.115	0.283	0.306	0.329	0.469	0.513
G5	0.080	0.080	0.081	0.113	0.124	0.284	0.312	0.340	0.502	0.565
G6	0.085	0.088	0.090	0.120	0.134	0.285	0.320	0.355	0.541	0.597
G7	0.092	0.096	0.100	0.128	0.146	0.287	0.332	0.378	0.578	0.623
G8	0.103	0.108	0.112	0.138	0.160	0.289	0.354	0.418	0.612	0.643
G9	0.115	0.121	0.127	0.152	0.177	0.290	0.375	0.460	0.637	0.657
K0	0.131	0.139	0.145	0.170	0.196	0.292	0.398	0.505	0.654	0.668
K1	0.159	0.163	0.167	0.190	0.220	0.294	0.415	0.536	0.666	0.663
K2	0.191	0.192	0.193	0.221	0.243	0.295	0.428	0.561	0.668	0.652
K3	0.221	0.222	0.224	0.250	0.259	0.297	0.436	0.575	0.666	0.639
K4	0.250	0.254	0.258	0.279	0.274	0.299	0.438	0.576	0.661	0.619
K5	0.281	0.288	0.294	0.307	0.290	0.301	0.430	0.560	0.652	0.578

TABLE 5.2

RMS DISPERSIONS IN THE MEAN COLORS

AT ANY SPECTRAL TYPE

Luminosity Class	$[c_1]$	$[m_1]$	[G]	[N]
I	$0^m.081$	$0^m.064$	$0^m.021$	$0^m.030$
II	0.126	0.067	0.021	0.034
III	0.053	0.034	0.013	0.056
IV	0.067	0.017	0.021	0.036
V	0.054	0.017	0.007	0.007

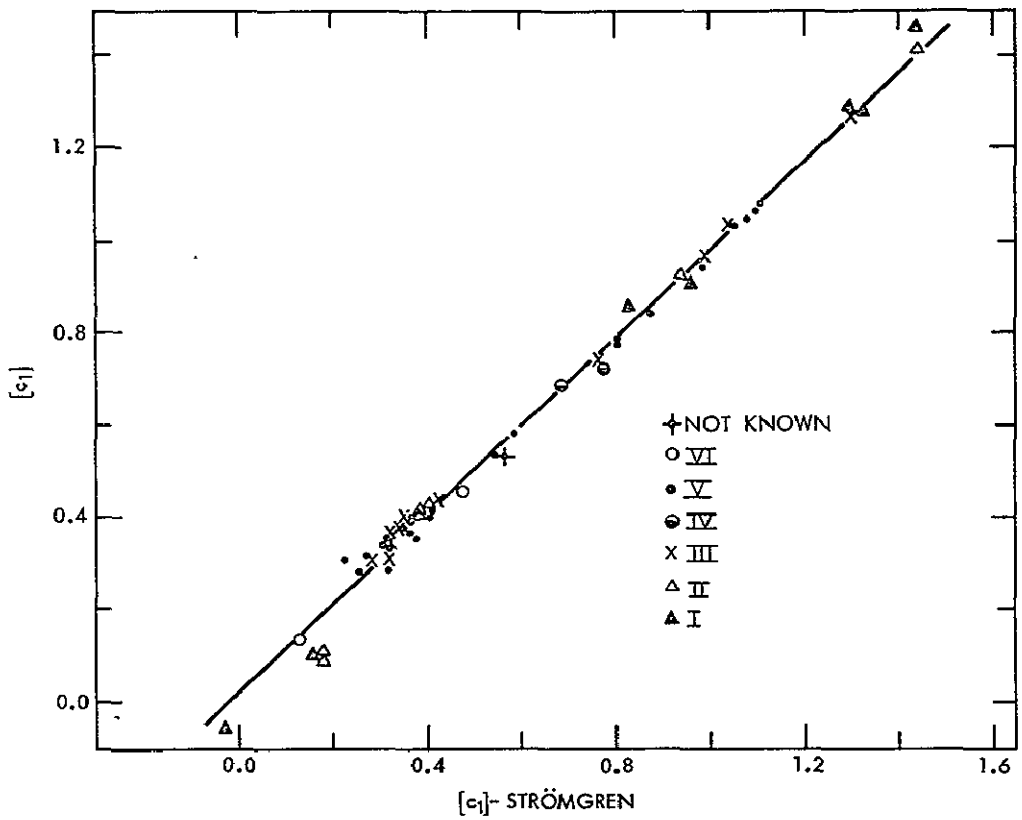

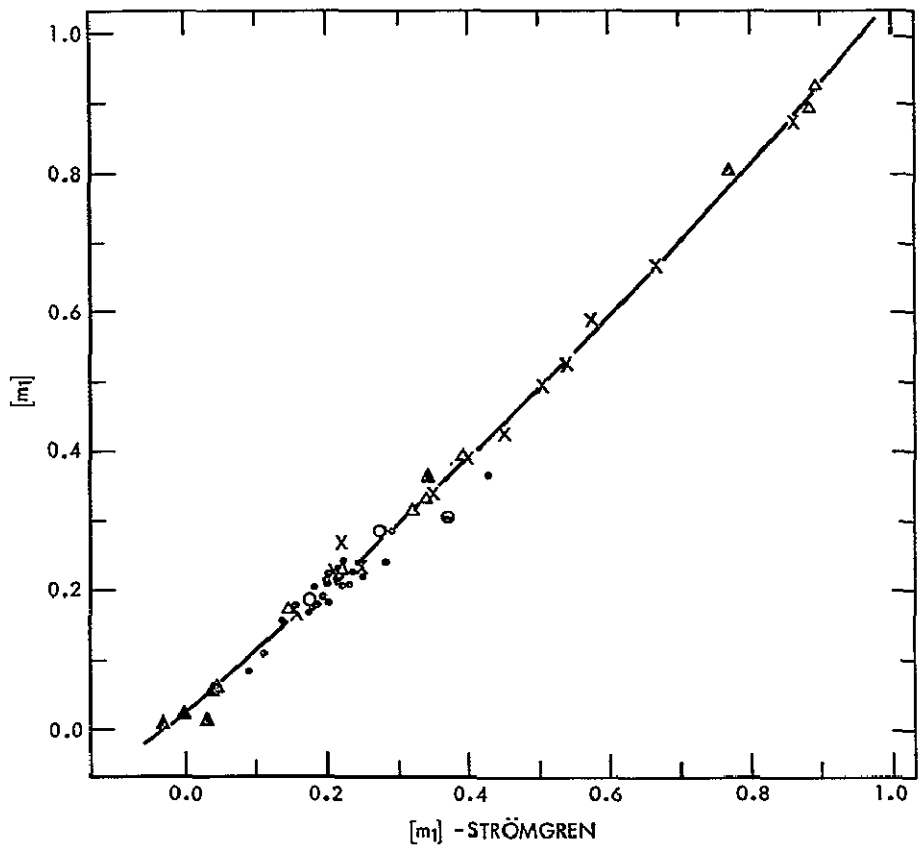

Fig. 5.1 Strömgren to Kelsall transformations for $[c_1]$ and $[m_1]$.

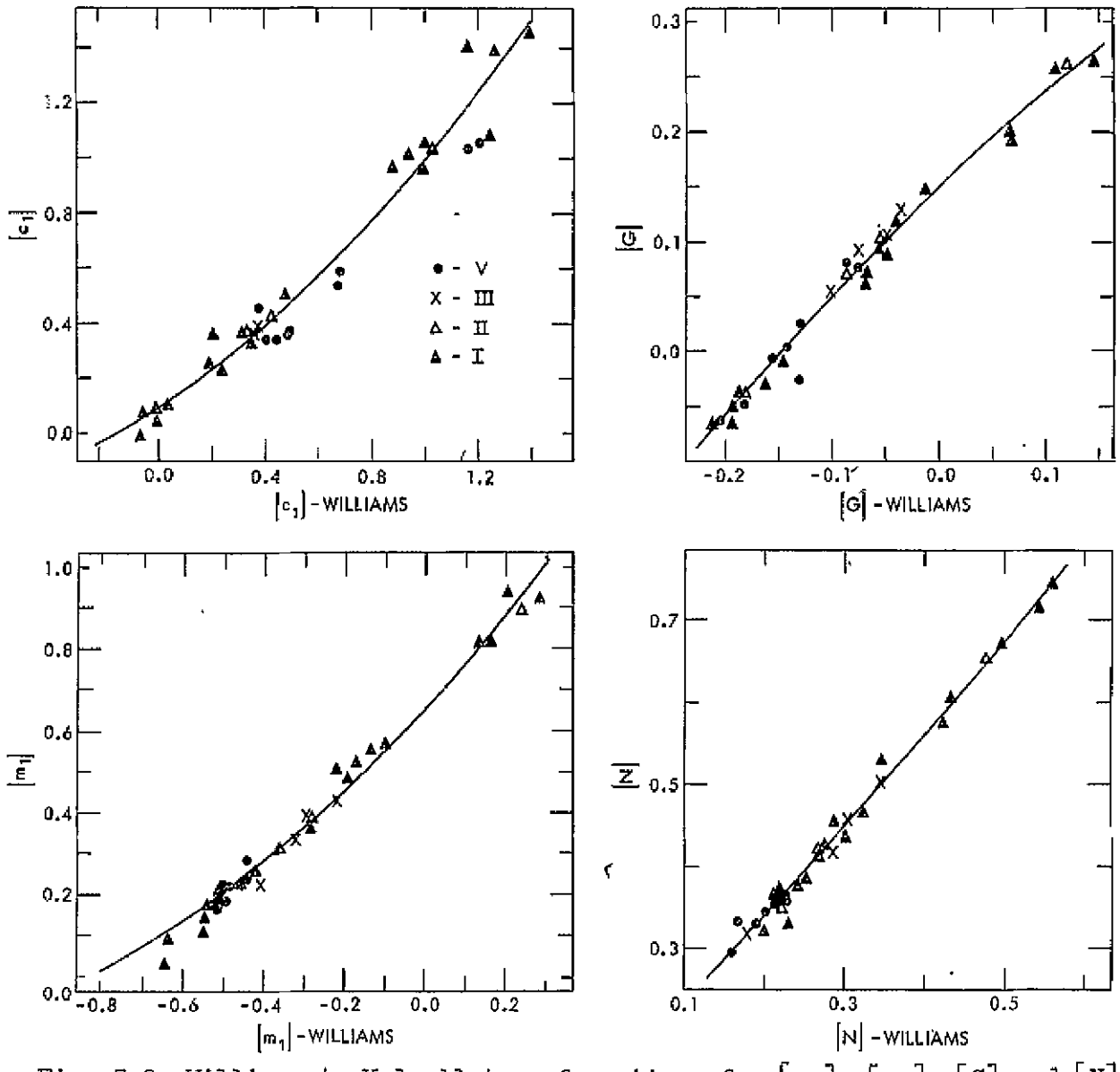

Fig. 5.2 Williams to Kelsall transformations for $[c_1]$, $[m_1]$, [G] and [N].

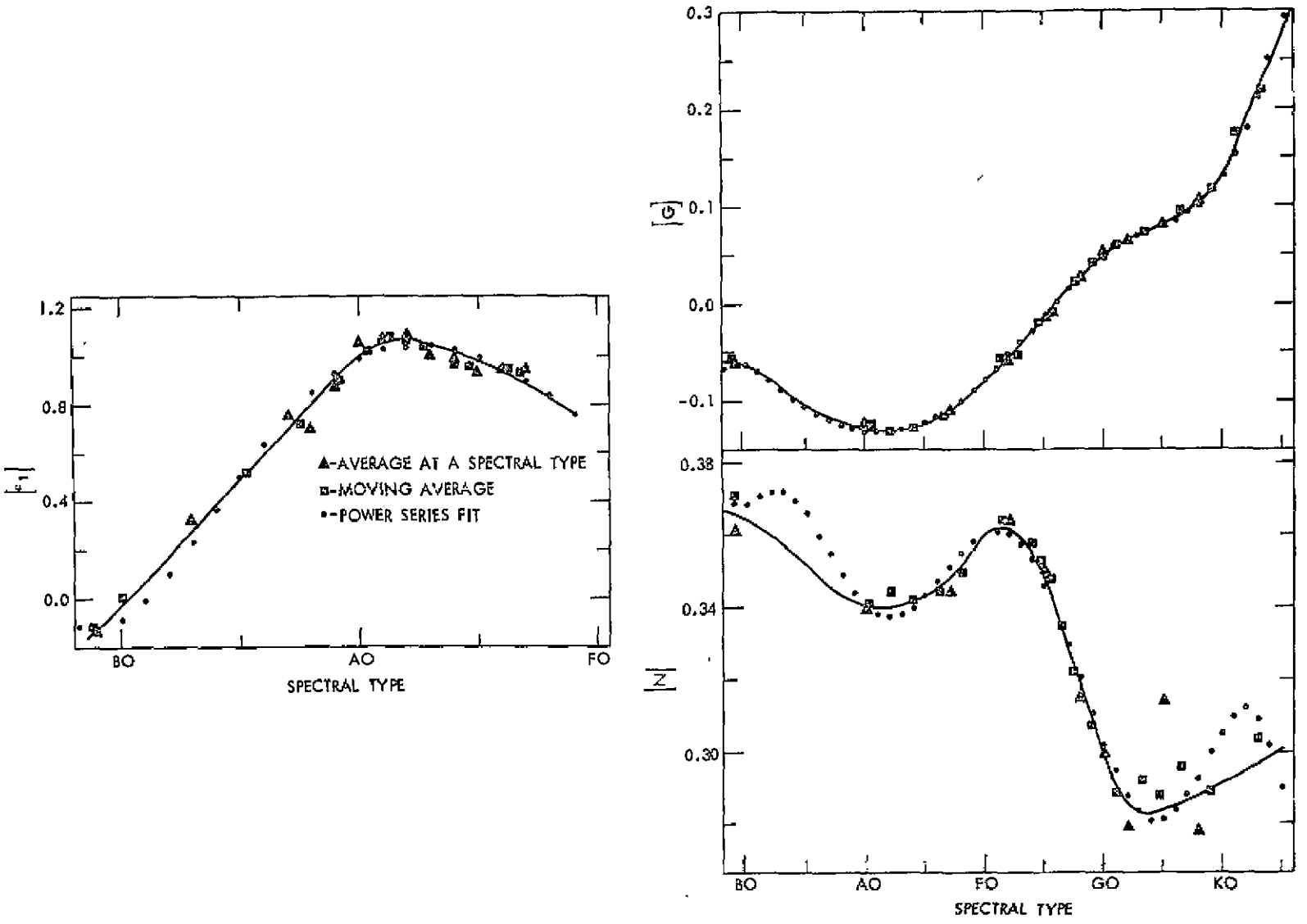

Fig. 5.3 Dependence of $[c_1]$, [G] and [N] on spectral type for luminosity class V stars.

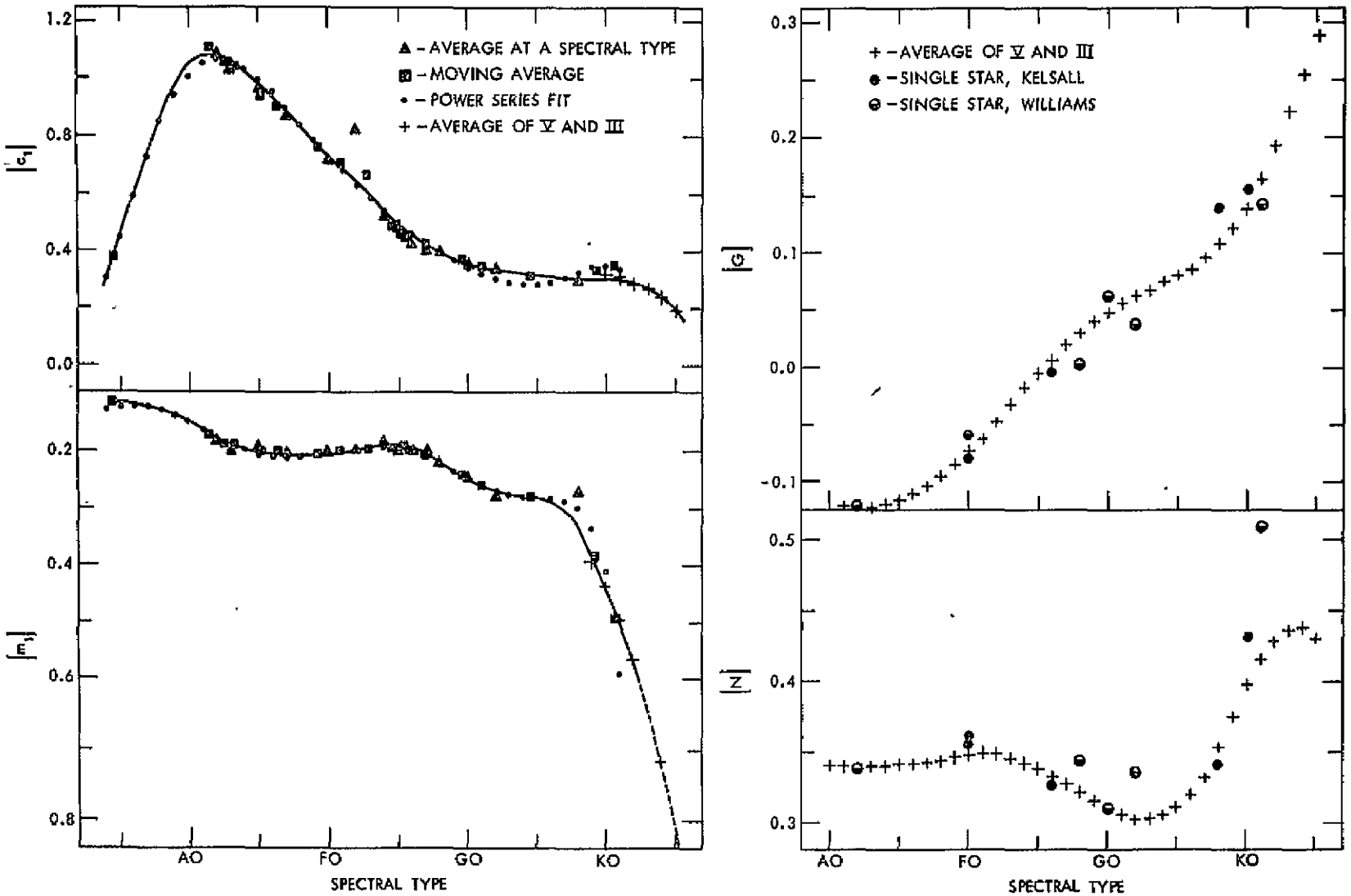

Fig. 5.4 Dependence of $[c_1]$, $[m_1]$, [G] and [N] on spectral type for luminosity class IV stars.

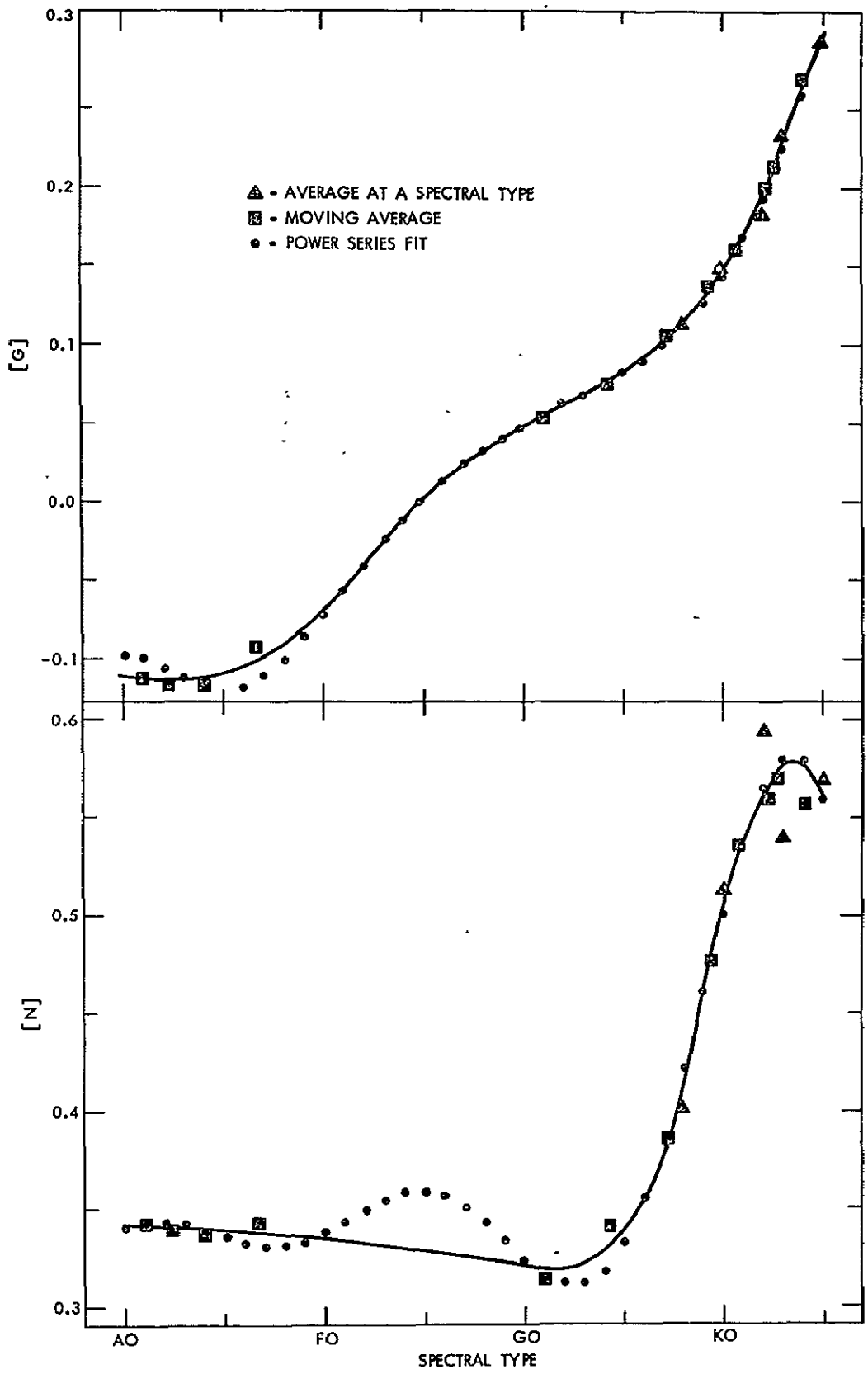

Fig. 5.5 Dependence of [G] and [N] on spectral type for luminosity class III stars.

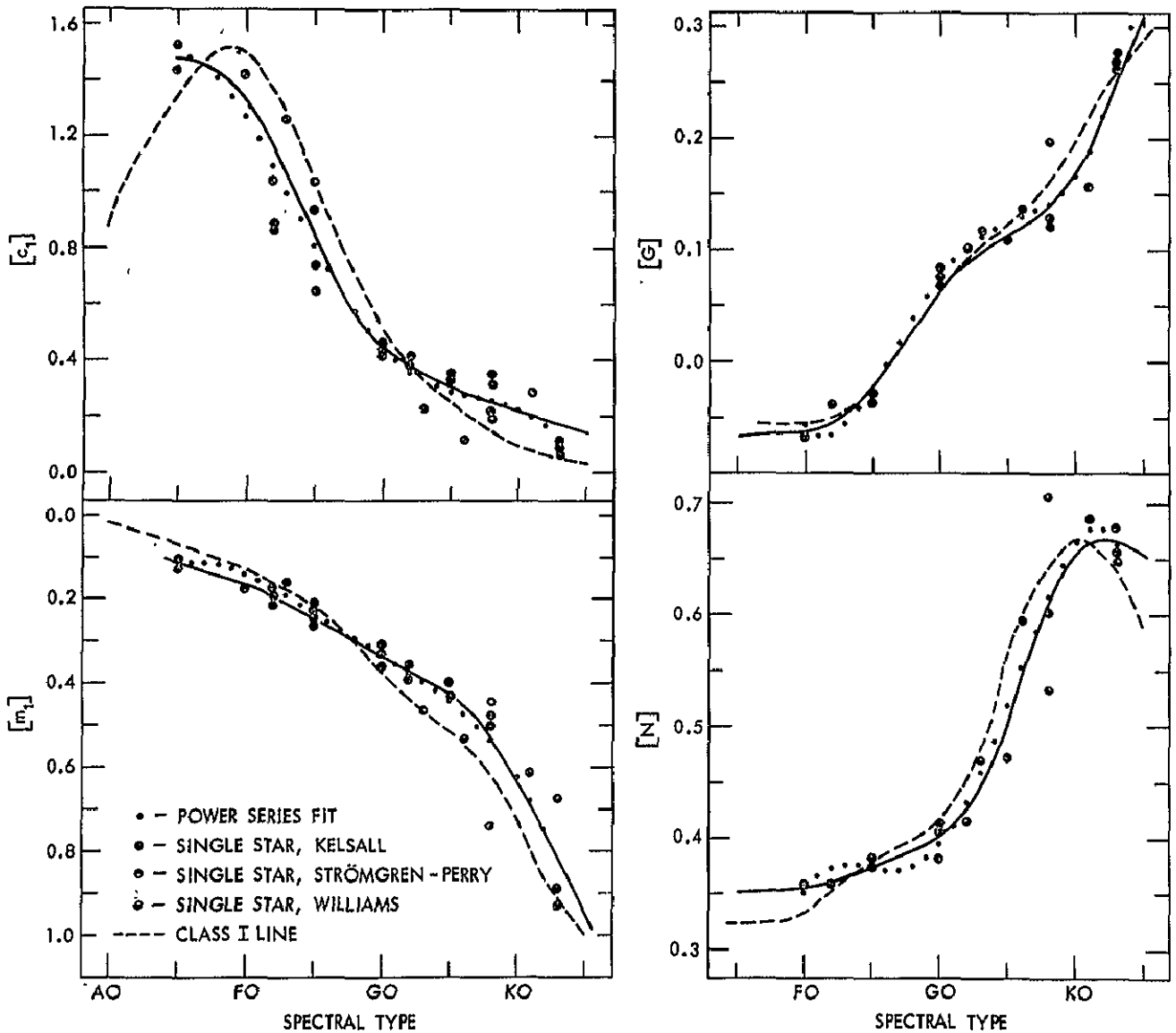

Fig. 5.6 Dependence of $[c_1]$, $[m_1]$, [G] and [N] on spectral type for luminosity class II stars.

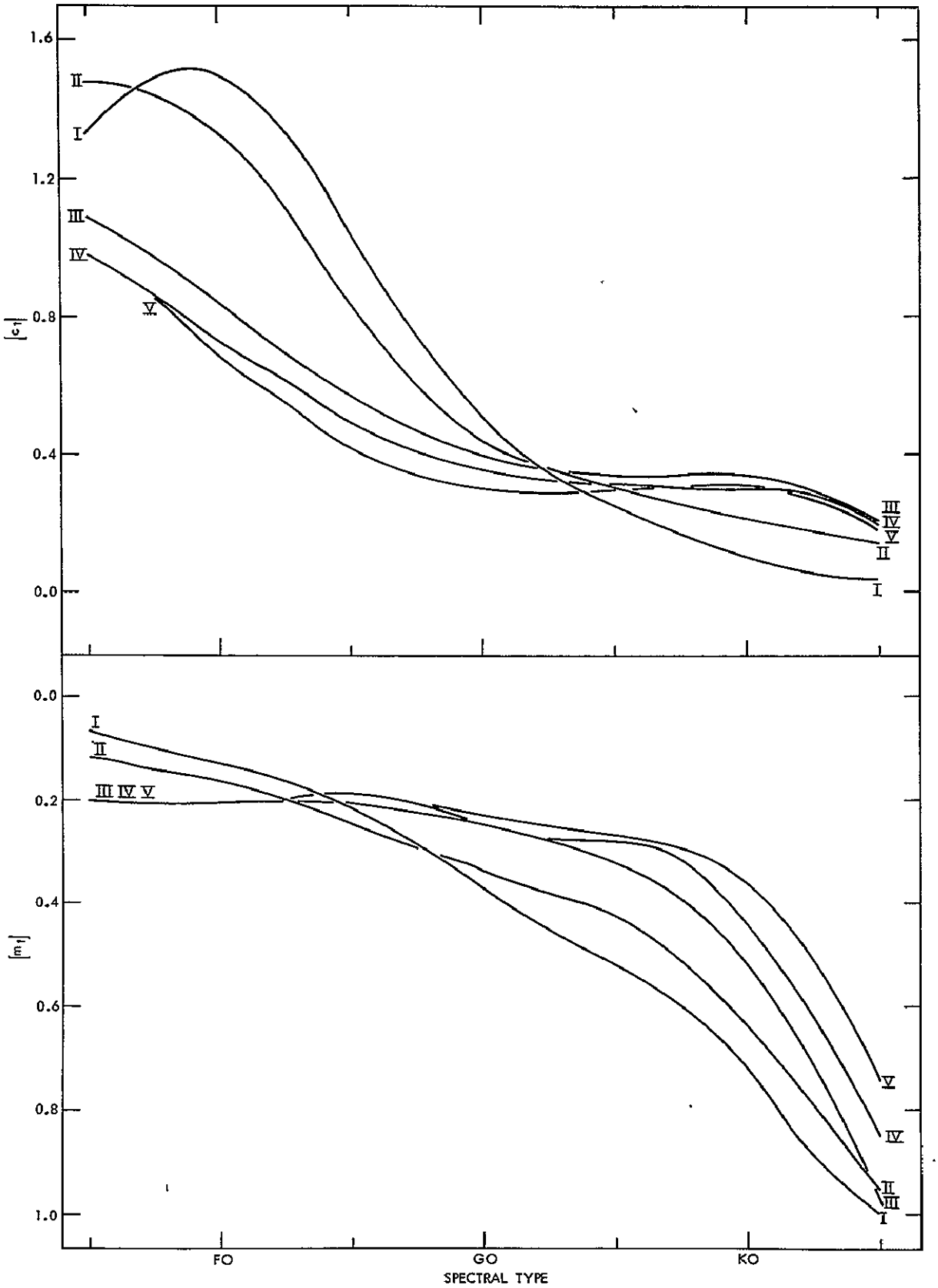

Fig. 5.7 Variation of $[c_1]$ and $[m_1]$ with spectral type for all luminosity classes.

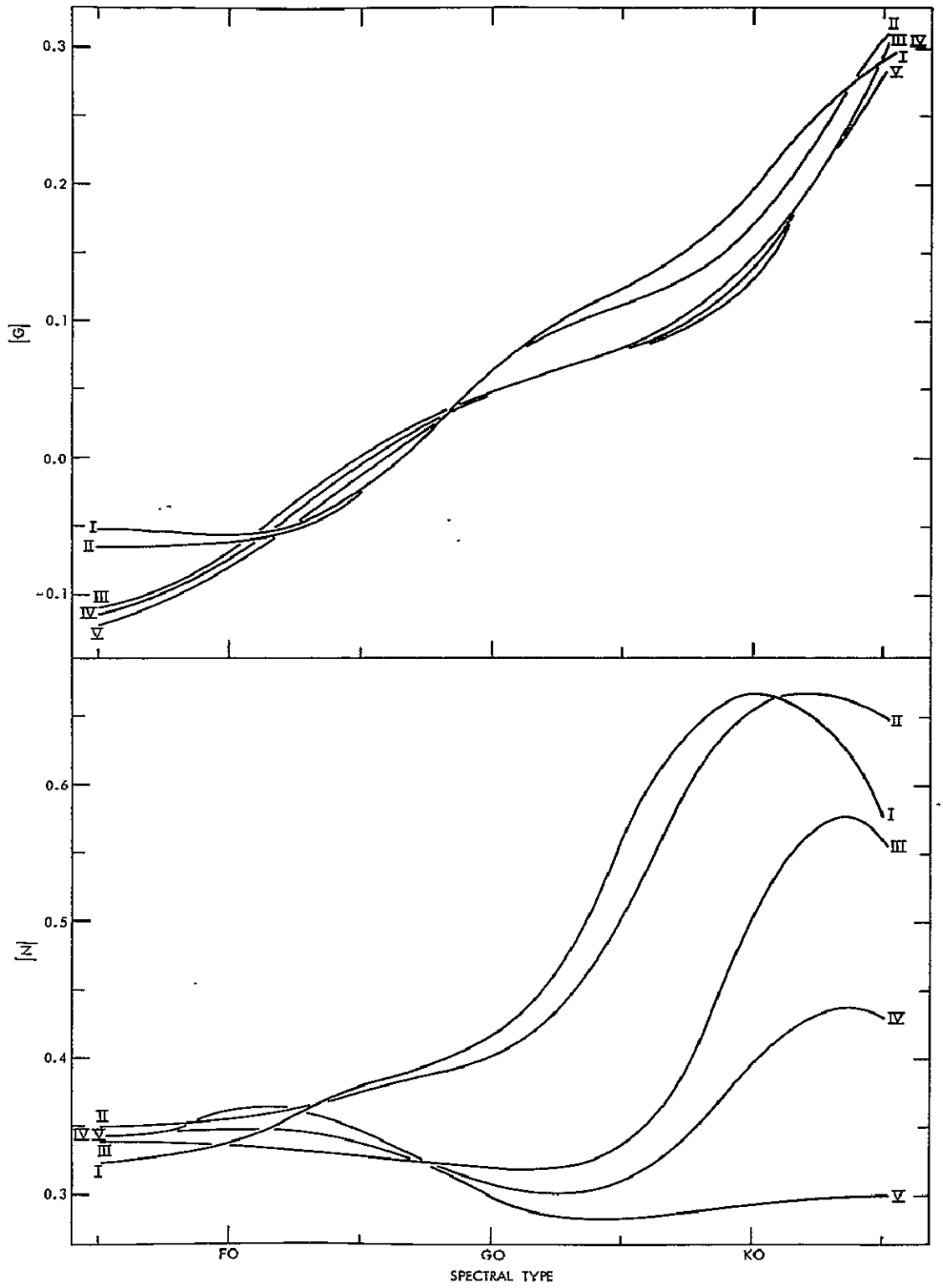

Fig. 5.8 Variation of [G] and [N] with spectral type for all luminosity classes.

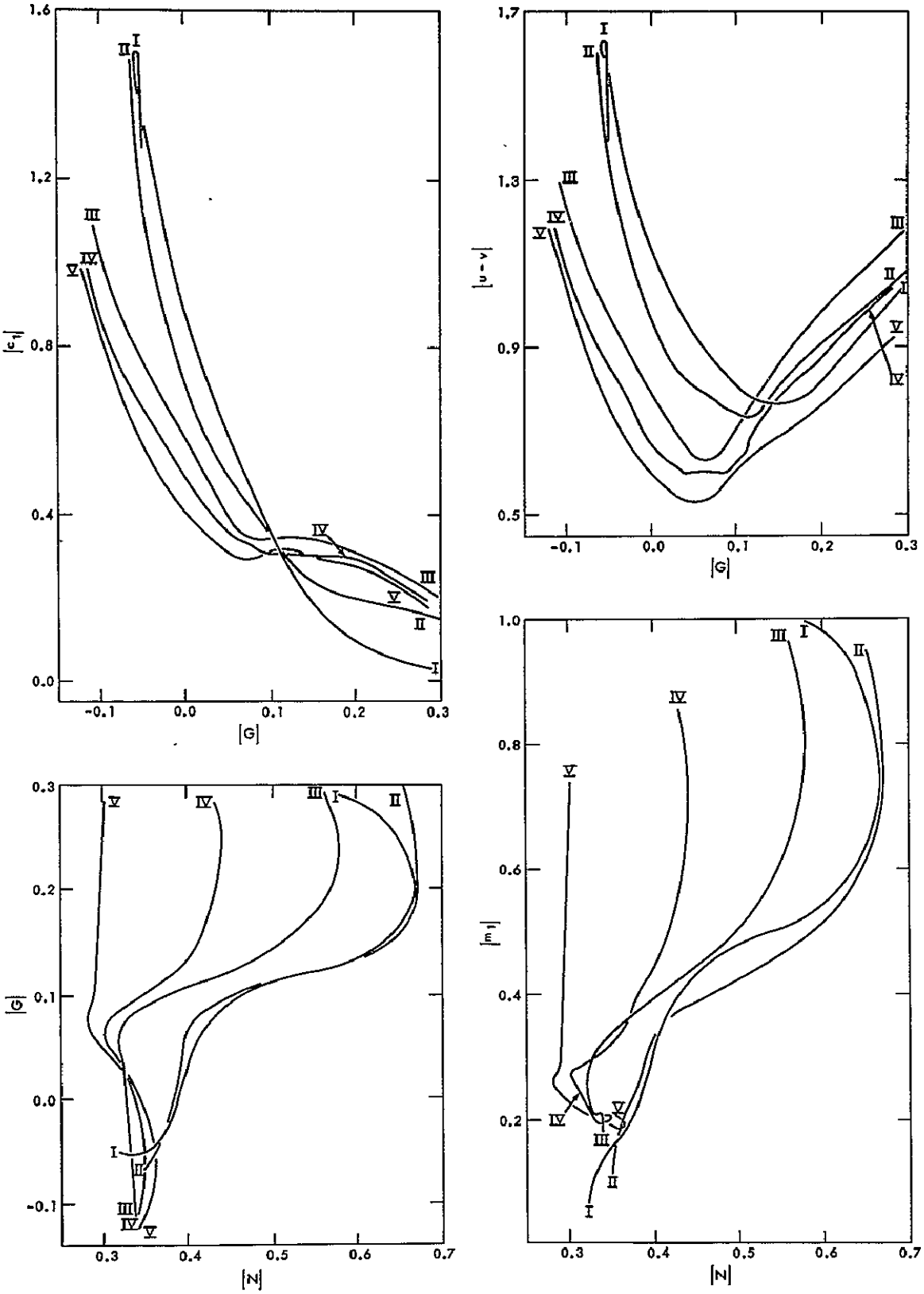

Fig. 5.9 Various color-color diagrams useful in discriminating between luminosity classes.

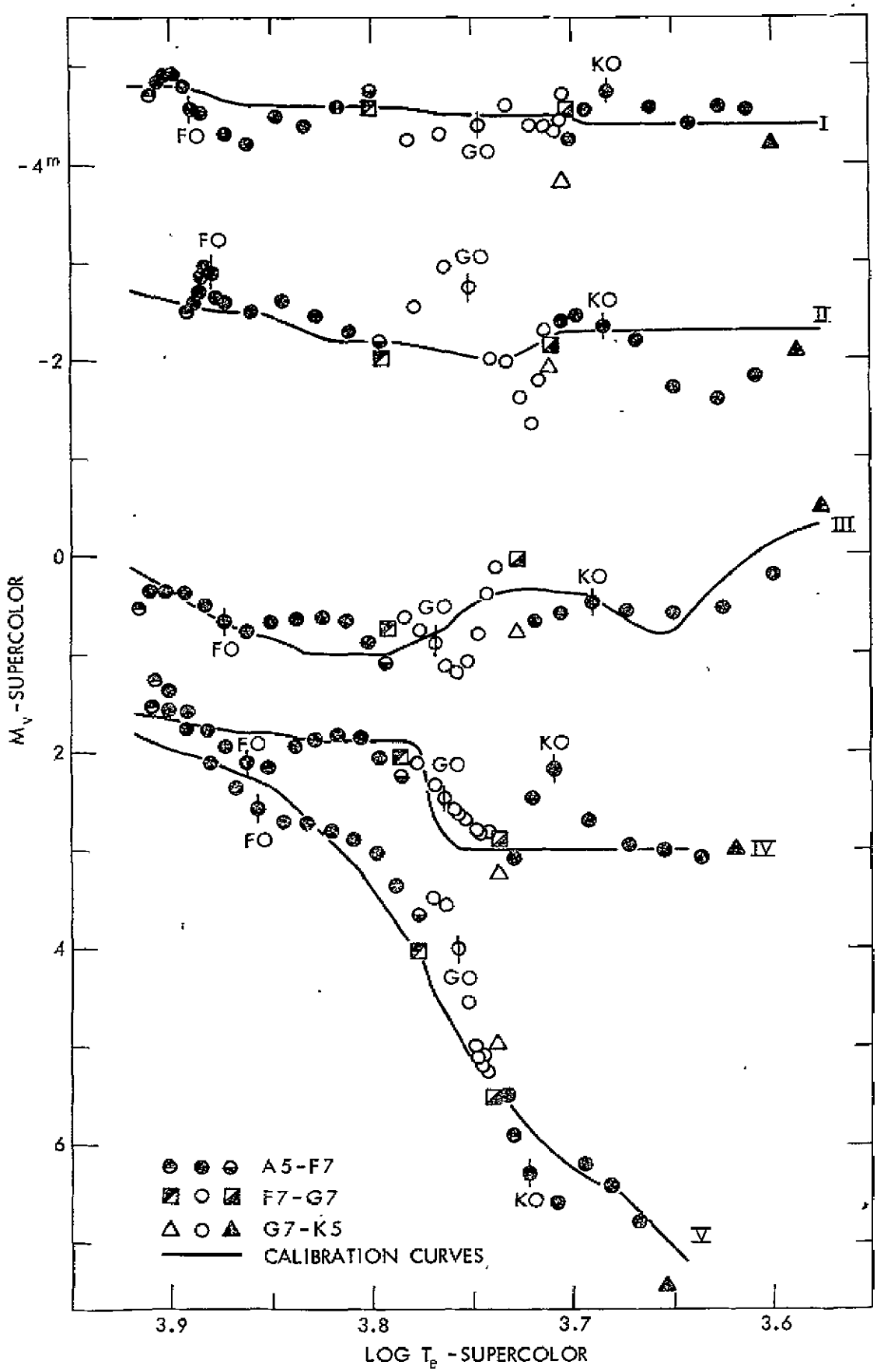

Fig. 5.10 The supercolor H-R diagram. The symbols are the supercolors resulting from using the mean colors at each spectral type over the range A5-K5.

CHAPTER VI

BASIC CEPHEID RESULTS

6-1. Photometry and Data

The cepheid data is collected and reduced in a manner identical to that for the supergiants. Whilst higher accuracy may be obtained using comparison stars, the gain would not warrant the additional observing time. The results are given in Table 6.1. The phases listed are those calculated using the photometric periods and epochs determined from a combination of V and y data as described below. There is on the average 13.1 observations per star.

6-2. The Periods

It is recognized that the cepheid periods are not rigidly time invariant. The compilation of periods in the General Catalog of Variable Stars (GCVS; 1958) is derived basically from photographic results up to 1958. Since 1952 there have been extensive observations made on the UBV system. These results through 1964, transformed to the standard UBV system, are listed in the very fine catalog prepared by Mitchell, Iriarte, Steinmetz, and Johnson (MISJ; 1964). A combination of the V data from MISJ and the y data from this investigation gives new periods of high accuracy.

The method of period determination is to fit the visual magnitude by a Fourier series --

$$V_i = a_o + \sum_{n=1}^{N} [a_n * \sin(2\pi n \frac{t_i - t_o}{P}) + a_{n+1} * \cos(2\pi n \frac{t_i - t_o}{P})], \qquad (6\text{-}1)$$

where n is the harmonic index, N is the maximum number of harmonics in the fit, t_o is the time of the first observation, t_i is the i-th observation time, and P is the period. In the analysis the period is left as a free parameter. For each period the fitting coefficients are calculated by the method of least squares. The best period is defined as that one which minimizes the sum of the deviations squared, S.

We illustrate the procedure by example. In Fig. 6.1 S is plotted against period for the cepheid X Lacertae, using MISJ data only. The interval size in the period scan, ΔP , is chosen so the relative phase change between the first and last observation is less than 0.05 as the period is changed from P to $P + \Delta P$. The upper panel of Fig. 6.1 indicates a minimum in S at approximately 5.44 days. The deep satellite minima result mainly from the blocking of the data into groups, each group being associated with a particular observational program. The computer program, designed by the author to do this analysis, finds the point of deepest minimum. The program then automatically repeats the period scanning in the neighborhood of the deepest minimum with an ever increasing period resolution. This process is continued until the period producing the deepest minimum in S is determined to within five parts in a hundred million. The fine detail is shown in the lower panel of Fig. 6.1, where an unambiguous minimum is found for a period of 5.44389 days.

The following technique is used to combine the V from MISJ with the y of this investigation. The y data is analyzed using the period found from the analysis of the MISJ data alone. From the separate V and y analyses the mean values of the fits, $\langle V \rangle$ and $\langle y \rangle$, are known. To bring y into accord with V, to each y is added the correction term

($\langle V \rangle - \langle y \rangle$). This process is substantially the best that can be done. For while y and V are well correlated for unreddened stars, the broadness of V precludes using this simple correlation for stars as strongly reddened as are the cepheids. Once y is so adjusted the period analysis is repeated using the combined V and y data. The results of this combinational process are shown for four stars in Fig. 6.2 . The stars well represent the full range of situations. As can be seen the y and V data are compatible.

There is no rigorous manner that can specify the accuracy of the determined free-parameter period. However, intuitively we expect the precision to be commensurate with the difficulty of phase positioning arising from the size of the observational error. For example, if the range in V is $0^m.6$, and the observational error is $0^m.012$, the phase location is uncertain to 0.01. This estimate is simply the result of setting $\Delta\phi = (d\phi/dV)*V\text{-error}$. Thus, the expected relative period precision, $\Delta P/P$, for a set of data covering N cycles will be given by --

$$\frac{\Delta P}{P} = \frac{d\phi/dV*V\text{-error}}{\text{no. of cycles}} = \frac{\Delta\phi}{N}. \qquad (6\text{-}2)$$

This intuitive argument for accuracy was checked by performing a number of numerical experiments. The fitting curve for η Aql was taken as true. Random points from this curve were selected, positioned randomly over a time baseline of N cycles, assigned errors of known dispersion, and then analyzed for period. The results for period accuracy bore out the simple argument given above, if the points sufficiently covered the range in phase from 0 to 1.

The results of the period determinations for the thirty program

cepheids are shown in Table 6.2. The data fits in all cases contained three harmonics, i.e., seven fitting coefficients. The accuracy listed in column four of the table probably represents a best situation. The MISJ data contains not only observational errors, but also errors of system transformations. Even making allowances for these difficulties, cepheids W Gem, SZ Tau, SW Tau, and AU Peg have had period decreases, while AL Vir's period has increased over the GCVS periods. The marked variation of AU Peg's period has been noted recently by Kwee (1967).

6-3. Color-Phase Results

The color-phase plots for eight representative cepheids are shown in Figs. 6.3 through 6.10. The phases are those determined from the epochs and periods listed in Table 6.2. The fitting curves for y are not necessarily at a maximum at phase 0.0 as the fits are the results of Fourier analyses of the y data alone, and the y data is often insufficient in determining the time of maximum light. The data appears to be most adequate in delineating the variation of the photometric quantities with phase.

6-4. Comparison with the Supergiants

Photometric comparisons between the cepheids and the supergiants are shown in the graphs of Fig. 6.11, where the photometric data for the cepheids at maximum and minimum light are taken from the fitting curves so as to place all cepheids on an equal footing. On the whole the cepheids duplicate the supergiant results. An exception is the results for $[c_1]$. This discord is most pronounced at maximum light. It is known that the hydrogen lines are strongest then. As $[c_1]$ contains the v magnitude twice, and as the v filter contains H-delta,

part of the trouble with $[c_1]$ may result from the enhancement of H-delta in the cepheids at maximum light over their supergiant equivalents.

Fig. 6.11 also shows that there is no clear photometric discrimination between the classical (Cδ), galactic (C), and Pop. II (CW) cepheids. For while four of the five CW cepheids stand out at maximum light in the $[c_1]$ versus $[m_1]$ plot, the result for AU Peg ($[c_1] = 0.662$, $[m_1] = 0.281$) shows that some of the CW cepheids would be lost photometrically.

6-5. A Population II Discriminant

In the literature cepheid color-color curves are often distinquished by their openness or closedness. This characteristic of the loops is illustrated in Fig. 6.12, where the color-color Lissajous figures in the UBV, six-color, and our composite system are shown. A quantitative measure of a loop's openness would be its area. The index could be either the total or the "signed" area, where the signed area is the area calculated taking into account the direction of circulation around the area's border as the phase goes from 0 to 1.

In Fig. 6.13 the total areas for particular color-color loops in the various systems versus the log of the cepheid periods are shown. We designate the total area of the U versus (B-V) loop by (U,B-V), etcetera. The data shown are the best results for the various photometric systems. For UBV we find no positive population discriminant. The (U,B-V) plot does indicate that the CW cepheids possess systematically larger areas than most of the Pop. I cepheids. Good population discrimination is apparently possible in the six-color and our composite system. The most useful segregation results in our system are

shown in Fig. 6.14. We note that this segregation method is independent of the amounts of interstellar reddening.

One impetus in investigating the color-color areas was a hope that they could be interpreted as thermodynamics-work cycles. The results can not be given a simple quantitative interpretation along such lines. Dr. R. A. Bell (private communication) points out that (b-y) is a temperature indicator, while G depends on pressure and temperature through molecular equilibria. Thus, the (b-y,G) is in a complex manner the area of a (P,T) work cycle. The (c_1,G) is similar, as c_1 is gravity (pressure) dependent. A complete analysis of the results would be most complex.

6-6. (b-y) Color Excesses

The (b-y)-color excesses are calculable once the intrinsic G, (b-y) relation is known. We assume the simple linear relationship --

$$G_o = A*(b-y)_o + B, \qquad (6\text{-}3)$$

and obtain A and B through a two step procedure. The first step is to assume that B is zero in Eq. (6-3), and to take A as a free parameter. For each of the twenty-one Pop. I cepheids the G,(b-y) color-color loop is calculated, at forty phase points, using the Fourier fits to the colors. Each phase point of a particular loop is translated along the G,(b-y) reddening line until it intersects the assumed $G_o,(b-y)_o$ line. The (b-y) translation is the E(b-y) for that point. The true E(b-y) for a star is taken to be the average of the E(b-y)'s at all phase points. This average E(b-y) is applied to each phase point. After all the stars' points are so translated, the rms deviation of the totality of points relative to the assumed $G_o,(b-y)_o$ relation is determined.

The best value for the constant A is that for which the rms deviation is least.

The value for B is fixed by imposing the condition that the average value of E(b-y)/E(B-V) be 0.70. This is identical to the adjustment made to fix the zero point for the supergiants. The values for E(B-V) for the twenty-one cepheids are taken from the compliation by Fernie (1967a). The final $G_o,(b-y)_o$ relation is --

$$G_o^{cep} = 0.543*(b-y)_o - 0.110. \qquad (6-4)$$

This relationship is very close to the supergiant thermal locus given in Fig. 4.4 --

$$G_o^{s.g.} = 0.532*(b-y)_o - 0.106.$$

The E(b-y)'s calculated with either equation differ at most by seven thousandths for any of the twenty-one cepheids.

The slope of the $G_o,(b-y)_o$ relation is in essence the best statistical representation of the orientation of the semi-major axis of the G,(b-y) color-color loops. As a check on the suitableness of the simple linear relation of G_o with $(b-y)_o$, the orientations of the semi-major axes for individual stars were determined. All determinations gave slopes close to the 0.543 value.

The E(b-y)'s calculated using Eq. (6-4) are listed in Table 6.3. No values for the Pop. II cepheids are given. These stars appear to obey the relation --

$$G_o = 0.403*(b-y)_o + B,$$

ut here a precise specification for B is impossible.

6-7. $(b-y)_o$ and the Effective Temperature

Two of the best studied cepheids are δ Cep and η Aql. They constitute the basis for Oke's (1961) calibration of $(B-V)_o$ to θ_{eff}. A comparison of (b-y) and (B-V) as function of phase for these two stars is shown in Fig. 6.15. The (b-y) results have been adjusted so that $\langle b-y \rangle$ equals $\langle B-V \rangle$. The two panels demonstrate the near similar phase variations of (b-y) and (B-V). In Fig. 6.16 $(B-V)_o$ is plotted against $(b-y)_o$. The δ Cep and η Aql data give the relation --

$$(B-V)_o = 0.021 + 1.606*(b-y)_o, \qquad (6\text{-}5)$$

with a fitting probable error of $0^m.021$. Fig. 6.16 also includes the points for X Cyg, the longest period cepheid in the program. While the points for X Cyg lie systematically above the $(B-V)_o/(b-y)_o$ line, the linearity of the relation is obviously preserved even for large $(B-V)_o$. The X Cyg points would lie on the line if the E(B-V) were increased from 0.36, Fernie's value, to 0.42. This value for E(B-V) is within reason as the E(b-y) is 0.283, which predicts an E(B-V) of 0.40.

Oke's calibration relating $(B-V)_o$ to θ_{eff}, modified to include more recent reddening results (Rodgers and Bell 1967), is --

$$\theta_{eff} = 0.651 + 0.337*(B-V)_o. \qquad (6\text{-}6)$$

Substituting Eq. (6-5) into Eq. (6-6) gives --

$$\theta_{eff} = 0.672 + 0.541*(b-y)_o. \qquad (6\text{-}7)$$

The larger coefficient for $(b-y)_o$ over that for $(B-V)_o$ in the expression

for θ_{eff} is compensated for by the higher observational precision possible in the determination of (b-y), and its associated reddening excess.

TABLE 6.1

OBSERVATIONS OF THE CEPHEIDS.

JD (2430000+)	PHASE	Y	C1	M1	B-Y	G	N
		ETA AQL -- 7.1767 DAYS					
8553.933	0.073	3.622	0.924	0.200	0.427	0.043	0.461
8554.878	0.205	3.811	0.761	0.244	0.500	0.097	0.459
8555.919	0.350	3.849	0.707	0.256	0.529	0.125	0.474
8556.895	0.486	4.091	0.608	0.279	0.606	0.171	0.500
8557.881	0.623	4.242	0.563	0.297	0.655	0.166	0.539
8558.833	0.756	4.258	0.575	0.284	0.614	0.145	0.503
8559.883	0.902	3.768	0.791	0.207	0.464	0.074	0.463
8560.895	0.043	3.533	0.955	0.201	0.408	0.045	0.452
8561.890	0.182	3.767	0.798	0.218	0.493	0.091	0.462
8564.872	0.597	4.217	0.558	0.303	0.639	0.187	0.542
8565.898	0.740	4.294	0.547	0.313	0.614	0.172	0.515
8688.594	0.837	3.994	0.646	0.256	0.511	0.107	0.476
8689.594	0.976	3.549	1.000	0.185	0.385	0.040	0.432
9045.601	0.582	4.172	0.520	0.360	0.615	0.155	0.557
		U AQL -- 7.0240 DAYS					
8554.861	0.137	6.251	0.868	0.131	0.676	0.101	0.492
8555.905	0.286	6.339	0.777	0.121	0.735	0.124	0.503
8556.888	0.425	6.585	0.625	0.218	0.770	0.191	0.499
8557.866	0.565	6.724	0.604	0.215	0.814	0.220	0.520
8558.819	0.701	6.843	0.548	0.251	0.801	0.183	0.509
8559.860	0.849	6.500	0.738	0.152	0.694	0.117	0.497
8560.877	0.993	6.071	1.029	0.129	0.576	0.077	0.455
8561.881	0.136	6.264	0.883	0.130	0.673	0.111	0.477
8564.854	0.560	6.696	0.659	0.190	0.830	0.198	0.561
8565.881	0.706	6.842	0.643	0.228	0.812	0.179	0.514
8566.867	0.846	6.500	0.731	0.154	0.693	0.114	0.524
		FF AQL -- 4.4709 DAYS					
8553.801	0.940	5.208	1.025	0.183	0.444	0.037	0.444
8554.812	0.166	5.301	0.947	0.195	0.483	0.052	0.449
8555.763	0.379	5.468	0.862	0.185	0.542	0.094	0.466
8556.764	0.603	5.525	0.820	0.232	0.515	0.105	0.460
8557.754	0.824	5.367	0.913	0.192	0.480	0.062	0.474
8558.753	0.048	5.215	1.049	0.153	0.456	0.040	0.449
8559.744	0.269	5.381	0.926	0.179	0.516	0.081	0.465
8560.752	0.495	5.503	0.796	0.226	0.545	0.075	0.504
8561.760	0.720	5.481	0.860	0.232	0.490	0.081	0.441
8564.748	0.389	5.476	0.848	0.208	0.526	0.073	0.489
8565.758	0.615	5.516	0.847	0.207	0.527	0.107	0.474
8566.746	0.835	5.353	0.918	0.210	0.466	0.054	0.476

TABLE 6.1

(CONTINUED)

JD (2430000+)	PHASE	Y	C1	M1	B-Y	G	N
8688.623	0.095	5.242	1.027	0.191	0.444	0.056	0.449
8689.629	0.321	5.455	0.887	0.218	0.516	0.083	0.466
8692.604	0.986	5.199	1.044	0.188	0.441	0.055	0.441
8694.607	0.434	5.490	0.804	0.199	0.553	0.096	0.461
		FM AQL	--	6.1142 DAYS			
8555.926	0.756	8.595	0.634	0.134	1.009	0.143	0.589
8556.820	0.902	8.124	0.913	0.091	0.816	0.149	0.449
8557.822	0.066	7.986	0.906	0.094	0.804	0.078	0.508
8558.858	0.236	8.206	0.754	0.122	0.906	0.127	0.525
8559.812	0.392	8.343	0.729	0.163	0.949	0.145	0.621
8560.920	0.573	8.542	0.499	0.213	1.006	0.267	0.536
8561.801	0.717	8.634	0.534	0.185	1.009	0.238	0.625
8564.796	0.207	8.154	0.816	0.117	0.894	0.119	0.570
8565.793	0.370	8.327	0.582	0.196	0.936	0.193	0.547
8566.772	0.530	8.529	0.594	0.193	0.971	0.117	0.596
8689.612	0.621	8.649	0.558	0.246	0.981	0.220	0.546
8691.611	0.948	7.920	0.907	0.095	0.796	0.084	0.494
8692.591	0.108	8.061	0.826	0.160	0.818	0.148	0.508
8693.587	0.271	8.221	0.738	0.131	0.921	0.182	0.536
		V496 AQL	--	6.8072 DAYS			
8555.897	0.947	7.603	0.800	0.193	0.703	0.110	0.506
8556.874	0.090	7.642	0.752	0.221	0.710	0.201	0.446
8557.858	0.235	7.725	0.658	0.253	0.765	0.157	0.503
8558.812	0.375	7.827	0.644	0.275	0.783	0.204	0.494
8559.852	0.528	7.940	0.519	0.294	0.820	0.222	0.563
8560.869	0.677	7.925	0.635	0.243	0.827	0.240	0.487
8561.872	0.825	7.773	0.619	0.264	0.735	0.151	0.485
8564.843	0.261	7.748	0.676	0.303	0.724	0.157	0.501
8565.867	0.412	7.845	0.593	0.303	0.792	0.217	0.518
8566.858	0.557	7.975	0.575	0.347	0.789	0.227	0.553
		RT AUR	--	3.7281 DAYS			
8689.003	0.007	5.053	1.114	0.189	0.255	0.0	0.403
8689.972	0.267	5.423	0.801	0.240	0.395	0.077	0.447
8689.997	0.274	5.435	0.800	0.254	0.387	0.078	0.444
8692.938	0.063	5.126	1.024	0.219	0.271	0.013	0.413
8820.763	0.349	5.541	0.733	0.229	0.449	0.103	0.445
8822.744	0.881	5.360	0.894	0.209	0.324	0.035	0.432
8823.754	0.152	5.258	0.930	0.207	0.341	0.027	0.446
8825.775	0.694	5.822	0.660	0.249	0.482	0.118	0.476

TABLE 6.1

(CONTINUED)

JD (2430000+)	PHASE	Y	C1	M1	B-Y	G	N
8826.742	0.953	5.017	1.122	0.167	0.261	-0.008	0.406
9045.985	0.761	5.792	0.617	0.292	0.453	0.103	0.472
9053.005	0.644	5.803	0.628	0.297	0.472	0.123	0.455
9175.757	0.570	5.755	0.627	0.291	0.472	0.130	0.474
9177.791	0.115	5.215	0.974	0.216	0.308	0.023	0.434
9440.944	0.701	5.817	0.678	0.250	0.484	0.133	0.465
9443.958	0.509	5.721	0.633	0.278	0.472	0.134	0.458
		RX CAM	--	7.9124 DAYS			
8687.977	0.494	7.862	0.697	0.235	0.917	0.181	0.551
8688.894	0.609	8.030	0.632	0.288	0.945	0.155	0.589
8689.903	0.737	8.055	0.608	0.280	0.917	0.187	0.520
8691.847	0.983	7.367	1.055	0.108	0.724	0.087	0.499
8692.810	0.104	7.500	0.934	0.152	0.785	0.121	0.515
8820.641	0.260	7.494	0.839	0.196	0.785	0.140	0.498
8822.637	0.512	7.916	0.590	0.266	0.929	0.232	0.551
8823.613	0.636	8.036	0.599	0.236	0.969	0.178	0.619
8824.625	0.764	7.997	0.619	0.231	0.912	0.179	0.528
8826.615	0.015	7.363	1.046	0.135	0.731	0.091	0.509
9045.931	0.733	8.059	0.523	0.223	0.922	0.168	0.542
9051.917	0.489	7.842	0.654	0.247	0.928	0.205	0.543
9052.887	0.612	8.030	0.597	0.264	0.952	0.183	0.560
9053.906	0.741	8.053	0.606	0.229	0.925	0.198	0.539
9054.904	0.867	7.702	0.784	0.171	0.803	0.156	0.474
9175.610	0.122	7.496	0.835	0.178	0.791	0.163	0.472
		RY CMA	--	4.6784 DAYS			
8820.683	0.774	8.426	0.594	0.275	0.620	0.122	0.482
8822.694	0.204	8.036	0.788	0.214	0.541	0.067	0.503
8823.692	0.417	8.255	0.634	0.262	0.613	0.101	0.501
8825.669	0.840	8.252	0.736	0.216	0.563	0.138	0.443
9177.724	0.091	7.846	0.958	0.211	0.466	0.027	0.441
9178.708	0.302	8.076	0.649	0.273	0.572	0.105	0.479
9440.976	0.361	8.176	0.667	0.309	0.583	0.111	0.477
9445.967	0.428	8.235	0.660	0.236	0.627	0.120	0.500
		SU CAS	--	1.9493 DAYS			
8687.938	0.557	6.171	0.859	0.122	0.546	0.077	0.433
8688.817	0.008	5.774	1.127	0.137	0.421	0.008	0.443
8689.890	0.559	6.172	0.878	0.142	0.530	0.056	0.443
8691.831	0.555	6.179	0.866	0.159	0.524	0.065	0.466
8692.792	0.048	5.798	1.113	0.124	0.437	0.028	0.419

TABLE 6.1

(CONTINUED)

JD (2430000+)	PHASE	Y	C1	M1	B-Y	G	N
8693.935	0.634	6.157	0.861	0.149	0.528	0.043	0.462
9045.892	0.186	5.900	1.062	0.119	0.481	0.031	0.433
9051.872	0.253	5.971	0.960	0.155	0.480	0.041	0.438
9052.863	0.762	6.029	0.926	0.178	0.470	0.029	0.433
9053.897	0.292	6.006	0.938	0.173	0.483	0.057	0.431
9054.856	0.784	5.979	0.991	0.142	0.468	0.041	0.410
9176.627	0.252	5.944	1.003	0.153	0.478	0.0	0.0
9177.638	0.771	5.986	0.952	0.154	0.478	0.035	0.447
9440.770	0.756	6.033	0.971	0.131	0.485	0.037	0.423
9444.794	0.820	5.937	0.991	0.108	0.487	0.034	0.420
		TU CAS -- 2.1394 DAYS					
8687.888	0.687	7.946	0.718	0.215	0.441	0.123	0.408
8688.808	0.117	7.620	0.915	0.196	0.343	0.038	0.425
8689.852	0.605	8.005	0.732	0.222	0.459	0.089	0.427
8691.786	0.509	8.061	0.701	0.269	0.449	0.090	0.452
8692.747	0.958	7.515	1.017	0.193	0.308	0.012	0.415
8693.813	0.456	7.904	0.767	0.208	0.432	0.098	0.427
9045.813	0.985	7.197	1.183	0.182	0.223	-0.017	0.364
9046.821	0.457	7.994	0.726	0.242	0.462	0.103	0.440
9051.790	0.779	8.025	0.724	0.211	0.442	0.063	0.466
9052.775	0.240	7.834	0.794	0.215	0.433	0.065	0.434
9053.784	0.711	7.888	0.769	0.189	0.424	0.059	0.436
9054.837	0.204	7.716	0.835	0.224	0.364	0.008	0.438
9440.713	0.567	8.060	0.759	0.222	0.468	0.109	0.443
9443.731	0.977	7.180	1.244	0.174	0.222	-0.024	0.391
9444.712	0.436	8.015	0.768	0.216	0.484	0.129	0.412
9445.740	0.916	7.461	1.052	0.180	0.296	0.047	0.387
		DL CAS -- 8.0004 DAYS					
8691.800	0.975	8.707	0.882	0.122	0.742	0.017	0.524
8692.762	0.095	8.771	0.862	0.116	0.765	0.141	0.463
8693.823	0.228	8.867	0.800	0.212	0.743	0.156	0.520
9045.802	0.223	8.842	0.804	0.152	0.806	0.148	0.533
9051.799	0.973	8.712	0.896	0.145	0.714	0.090	0.469
9053.805	0.224	8.829	0.731	0.139	0.817	0.111	0.535
9443.740	0.963	8.714	0.912	0.122	0.732	0.105	0.523
9444.724	0.086	8.761	0.836	0.079	0.779	0.120	0.521
9445.767	0.216	8.823	0.769	0.178	0.792	0.125	0.604

TABLE 6.1

(CONTINUED)

JD (2430000+)	PHASE	Y	C1	M1	B-Y	G	N
		DELTA CEP -- 5.3662 DAYS					
8553.979	0.850	4.037	0.757	0.240	0.431	0.079	0.453
8554.961	0.032	3.542	1.084	0.185	0.311	0.015	0.437
8555.972	0.221	3.856	0.844	0.214	0.430	0.086	0.456
8687.783	0.784	4.268	0.626	0.294	0.493	0.138	0.462
8688.760	0.966	3.493	1.116	0.193	0.273	0.005	0.421
8689.775	0.155	3.755	0.891	0.212	0.394	0.040	0.452
8691.733	0.520	4.195	0.655	0.279	0.526	0.134	0.498
8692.691	0.699	4.357	0.597	0.314	0.542	0.152	0.503
8694.706	0.074	3.622	1.003	0.193	0.340	0.042	0.428
9046.738	0.675	4.331	0.599	0.308	0.554	0.160	0.510
9051.729	0.605	4.286	0.593	0.321	0.537	0.146	0.494
9052.744	0.795	4.236	0.628	0.289	0.499	0.120	0.482
9053.728	0.978	3.485	1.136	0.181	0.284	0.005	0.419
9054.702	0.159	3.743	0.875	0.216	0.396	0.071	0.437
9444.680	0.832	4.119	0.729	0.248	0.450	0.093	0.460
9445.676	0.018	3.517	1.101	0.196	0.293	0.029	0.409
		X CYG -- 16.3854 DAYS					
8688.697	0.185	6.193	0.645	0.306	0.743	0.173	0.574
8691.672	0.366	6.494	0.490	0.432	0.855	0.237	0.658
8692.645	0.426	6.613	0.404	0.478	0.886	0.263	0.697
9045.665	0.970	5.853	0.952	0.188	0.554	0.096	0.453
9046.692	0.033	5.937	0.851	0.228	0.595	0.114	0.497
9051.679	0.337	6.439	0.485	0.407	0.852	0.239	0.687
9053.681	0.460	6.659	0.425	0.478	0.911	0.268	0.767
9054.622	0.517	6.758	0.375	0.519	0.931	0.263	0.829
9440.626	0.075	6.001	0.777	0.228	0.658	0.129	0.486
9443.622	0.258	6.302	0.556	0.366	0.804	0.214	0.618
9444.622	0.319	6.394	0.501	0.414	0.848	0.245	0.697
9445.624	0.380	6.493	0.417	0.443	0.879	0.245	0.724
		SU CYG -- 3.8455 DAYS					
8553.854	0.305	6.909	0.695	0.209	0.403	0.082	0.418
8554.894	0.575	7.107	0.516	0.173	0.459	0.0	0.0
8555.774	0.804	7.080	0.604	0.185	0.415	0.042	0.474
8556.773	0.064	6.540	0.985	0.137	0.319	0.004	0.403
8557.784	0.327	6.954	0.656	0.188	0.407	0.056	0.475
8558.763	0.581	7.151	0.543	0.214	0.440	0.091	0.422
8559.781	0.846	6.944	0.678	0.191	0.368	0.065	0.437
8560.781	0.106	6.625	0.887	0.203	0.301	0.020	0.451
8561.767	0.362	6.994	0.638	0.187	0.423	0.100	0.430

TABLE 6.1

(CONTINUED)

JD (2430000+)	PHASE	Y	C1	M1	B-Y	G	N
8564.758	0.140	6.680	0.834	0.196	0.328	0.019	0.445
8565.782	0.407	7.030	0.594	0.203	0.424	0.066	0.438
8566.801	0.672	7.190	0.521	0.204	0.454	0.089	0.446
8693.642	0.656	7.173	0.541	0.195	0.450	0.102	0.456
		VZ CYG	--	4.8646 DAYS			
8555.957	0.479	8.832	0.440	0.315	0.562	0.120	0.534
8556.951	0.683	9.289	0.575	0.321	0.651	0.217	0.437
8557.962	0.891	8.830	0.794	0.240	0.490	0.006	0.510
8558.931	0.090	8.717	0.920	0.204	0.494	0.110	0.444
8559.941	0.298	8.958	0.685	0.231	0.637	0.156	0.403
8560.950	0.505	9.147	0.707	0.301	0.646	0.112	0.577
8561.944	0.710	9.288	0.608	0.256	0.680	0.095	0.588
8565.942	0.531	9.175	0.596	0.271	0.679	0.163	0.484
8566.910	0.730	9.259	0.586	0.349	0.627	0.152	0.455
8689.760	0.984	8.623	0.956	0.207	0.448	-0.002	0.484
8691.699	0.383	9.055	0.622	0.263	0.648	0.201	0.452
		DT CYG	--	2.4993 DAYS			
8553.875	0.066	5.626	0.963	0.194	0.303	0.026	0.421
8554.926	0.486	5.896	0.790	0.220	0.373	0.012	0.494
8555.855	0.858	5.713	0.901	0.191	0.319	0.028	0.420
8556.848	0.255	5.759	0.863	0.197	0.348	0.039	0.416
8557.935	0.690	5.883	0.842	0.209	0.352	0.054	0.441
8558.895	0.074	5.661	0.942	0.198	0.304	0.010	0.437
8559.924	0.486	5.911	0.816	0.198	0.392	0.069	0.454
8560.824	0.846	5.720	0.897	0.187	0.326	-0.003	0.454
8561.841	0.253	5.774	0.856	0.249	0.308	0.051	0.438
8564.915	0.483	5.902	0.809	0.202	0.374	0.048	0.452
8565.922	0.886	5.711	0.917	0.190	0.312	0.034	0.424
8687.740	0.627	5.853	0.809	0.189	0.383	0.064	0.434
8688.674	0.000	5.648	0.965	0.209	0.286	0.033	0.412
8689.665	0.397	5.873	0.826	0.210	0.369	0.055	0.437
8691.649	0.191	5.721	0.919	0.224	0.311	0.038	0.423
8692.653	0.593	5.940	0.791	0.230	0.365	0.079	0.425
8694.639	0.387	5.862	0.835	0.222	0.350	0.040	0.447
9443.633	0.068	5.653	0.946	0.193	0.312	0.024	0.437
9445.646	0.873	5.681	0.924	0.200	0.302	0.025	0.411

TABLE 6.1

(CONTINUED)

JD (2430000+)	PHASE	Y	C1	M1	B-Y	G	N
		ZETA GEM -- 10.1514 DAYS					
9052.983	0.714	3.917	0.561	0.333	0.482	0.120	0.484
9173.707	0.606	4.016	0.500	0.354	0.511	0.155	0.512
9174.765	0.710	3.906	0.627	0.317	0.471	0.132	0.482
9175.769	0.809	3.790	0.725	0.296	0.430	0.107	0.482
9177.814	0.011	3.706	0.712	0.319	0.410	0.109	0.471
9178.788	0.107	3.743	0.641	0.329	0.467	0.139	0.488
9432.008	0.051	3.720	0.671	0.328	0.434	0.111	0.472
9440.967	0.933	3.687	0.729	0.331	0.390	0.095	0.485
9441.969	0.032	3.705	0.719	0.271	0.450	0.0	0.0
9443.988	0.231	3.934	0.542	0.422	0.510	0.148	0.540
9444.950	0.326	4.060	0.490	0.443	0.559	0.197	0.570
9445.960	0.425	4.157	0.500	0.418	0.581	0.182	0.602
		W GEM -- 7.9136 DAYS					
8692.973	0.668	7.378	0.598	0.311	0.730	0.148	0.576
8820.747	0.814	7.200	0.708	0.260	0.633	0.129	0.506
8822.733	0.065	6.690	0.986	0.164	0.533	0.064	0.468
8823.740	0.192	6.780	0.853	0.214	0.564	0.073	0.492
8824.747	0.319	6.936	0.822	0.273	0.541	0.128	0.481
8825.692	0.439	7.090	0.680	0.243	0.694	0.152	0.525
8826.721	0.569	7.244	0.581	0.287	0.742	0.169	0.551
9045.999	0.278	6.751	0.869	0.186	0.590	0.112	0.480
9174.722	0.544	7.212	0.613	0.303	0.713	0.191	0.517
9175.730	0.671	7.365	0.619	0.290	0.744	0.189	0.531
9177.784	0.931	6.688	1.016	0.162	0.503	0.057	0.464
9178.766	0.055	6.634	0.992	0.177	0.519	0.052	0.473
9444.984	0.695	7.400	0.494	0.395	0.699	0.144	0.582
9445.937	0.816	7.222	0.667	0.244	0.643	0.139	0.496
		X LAC -- 5.4448 DAYS					
8555.965	0.925	8.276	1.105	0.152	0.564	0.0	0.0
8687.794	0.137	8.262	0.884	0.175	0.573	0.068	0.415
8688.769	0.316	8.426	0.761	0.205	0.630	0.123	0.515
8691.746	0.863	8.350	0.935	0.136	0.590	0.086	0.464
8692.699	0.038	8.236	0.956	0.187	0.532	0.033	0.483
9046.749	0.064	8.201	0.992	0.144	0.570	0.067	0.450
9051.736	0.980	8.189	0.983	0.107	0.585	0.060	0.437
9052.751	0.166	8.279	0.958	0.185	0.577	0.070	0.475
9053.754	0.350	8.472	0.867	0.174	0.635	0.129	0.434
9054.742	0.532	8.571	0.796	0.177	0.681	0.139	0.474
9440.701	0.418	8.498	0.822	0.195	0.653	0.116	0.468

TABLE 6.1

(CONTINUED)

JD (2430000+)	PHASE	Y	C1	M1	B-Y	G	N
9444.689	0.151	8.286	0.877	0.190	0.577	0.025	0.451
9445.690	0.334	8.414	0.879	0.165	0.655	0.104	0.475
		RS ORI -- 7.5668 DAYS					
8691.967	0.342	8.403	0.772	0.123	0.721	0.132	0.434
8692.962	0.474	8.613	0.650	0.240	0.744	0.156	0.543
8820.731	0.359	8.467	0.723	0.225	0.684	0.135	0.451
8822.724	0.623	8.796	0.637	0.215	0.800	0.156	0.509
8823.724	0.755	8.775	0.722	0.213	0.749	0.140	0.526
8824.735	0.888	8.347	0.883	0.161	0.611	0.047	0.462
8825.685	0.014	8.049	1.107	0.146	0.525	0.020	0.488
8826.705	0.149	8.230	0.955	0.153	0.615	0.067	0.479
9174.709	0.140	8.227	0.905	0.173	0.611	0.083	0.470
9175.702	0.271	8.212	0.826	0.187	0.636	0.081	0.511
9178.756	0.674	8.814	0.556	0.260	0.781	0.163	0.566
9444.973	0.857	8.489	0.648	0.262	0.618	0.096	0.525
9445.919	0.982	8.034	1.131	0.106	0.548	0.016	0.468
		AU PEG -- 2.3911 DAYS					
8555.947	0.062	9.010	0.744	0.218	0.498	0.085	0.532
8556.931	0.474	9.285	0.518	0.277	0.613	0.183	0.625
8557.910	0.883	9.189	0.707	0.192	0.532	0.095	0.539
8558.874	0.287	9.166	0.530	0.293	0.562	0.225	0.523
8559.909	0.719	9.417	0.535	0.264	0.600	0.124	0.568
8560.938	0.149	9.070	0.617	0.307	0.494	0.141	0.517
8561.917	0.559	9.387	0.626	0.202	0.656	0.190	0.583
8564.886	0.801	9.350	0.566	0.252	0.560	0.167	0.585
8565.954	0.247	9.142	0.588	0.264	0.528	0.142	0.518
8566.929	0.655	9.410	0.492	0.266	0.601	0.235	0.480
8688.651	0.561	9.419	0.507	0.313	0.577	0.044	0.661
8689.658	0.982	9.147	0.693	0.216	0.461	0.123	0.450
		AW PER -- 6.4635 DAYS					
8687.989	0.870	7.446	0.798	0.051	0.739	0.078	0.470
8688.939	0.017	7.122	1.101	0.072	0.628	0.033	0.459
8689.962	0.175	7.315	0.817	0.120	0.706	0.091	0.474
8691.913	0.477	7.698	0.579	0.086	0.850	0.141	0.512
8692.909	0.631	7.817	0.498	0.126	0.842	0.154	0.476
8693.981	0.797	7.762	0.585	0.118	0.797	0.085	0.533
8820.659	0.396	7.512	0.667	0.113	0.796	0.083	0.502
8822.658	0.706	7.888	0.515	0.144	0.829	0.133	0.558
8823.662	0.861	7.472	0.767	0.082	0.738	0.105	0.443

TABLE 6.1

(CONTINUED)

JD (2430000+)	PHASE	Y	C1	M1	B-Y	G	N
8824.665	0.016	7.088	1.068	0.056	0.653	0.049	0.446
8825.624	0.165	7.308	0.858	0.092	0.723	0.099	0.501
8826.657	0.324	7.454	0.762	0.090	0.774	0.075	0.506
9045.967	0.255	7.417	0.747	0.103	0.760	0.087	0.479
9052.936	0.333	7.456	0.675	0.118	0.778	0.112	0.486
9053.989	0.496	7.702	0.557	0.105	0.842	0.110	0.504
9174.641	0.163	7.286	0.870	0.061	0.731	0.075	0.455
9175.619	0.314	7.435	0.749	0.102	0.758	0.137	0.472
		SS SCT -- 3.6713 DAYS					
8555.886	0.578	8.407	0.609	0.205	0.726	0.189	0.439
8556.865	0.844	8.205	0.747	0.170	0.619	0.112	0.442
8557.849	0.112	8.058	0.782	0.212	0.578	0.102	0.466
8558.801	0.372	8.323	0.673	0.224	0.676	0.126	0.529
8559.844	0.656	8.468	0.682	0.232	0.674	0.165	0.537
8560.859	0.932	7.977	0.926	0.160	0.534	0.059	0.467
8561.863	0.206	8.145	0.754	0.165	0.649	0.152	0.468
8564.831	0.014	7.919	0.900	0.130	0.566	0.074	0.474
8565.856	0.293	8.246	0.701	0.200	0.666	0.166	0.481
8566.849	0.564	8.413	0.648	0.210	0.712	0.197	0.479
		S SGE -- 8.3821 DAYS					
8553.831	0.873	5.616	0.758	0.244	0.471	0.118	0.457
8554.833	0.993	5.267	0.994	0.186	0.412	0.047	0.444
8555.806	0.109	5.452	0.883	0.223	0.448	0.091	0.461
8556.810	0.229	5.372	0.850	0.230	0.452	0.072	0.460
8557.815	0.348	5.643	0.657	0.293	0.535	0.144	0.492
8558.850	0.472	5.777	0.657	0.288	0.602	0.173	0.511
8559.789	0.584	5.940	0.566	0.336	0.634	0.201	0.540
8560.810	0.706	6.037	0.601	0.334	0.607	0.168	0.539
8561.824	0.827	5.790	0.698	0.246	0.532	0.132	0.441
8564.785	0.180	5.409	0.875	0.199	0.460	0.074	0.482
8565.839	0.306	5.537	0.726	0.278	0.492	0.120	0.469
8566.787	0.419	5.716	0.665	0.310	0.560	0.148	0.512
8688.640	0.956	5.318	0.990	0.196	0.396	0.072	0.452
8689.649	0.076	5.400	0.915	0.232	0.432	0.078	0.450
9045.633	0.546	5.866	0.570	0.361	0.606	0.189	0.534
		ST TAU -- 4.0342 DAYS					
8691.959	0.998	7.813	1.173	0.108	0.475	0.012	0.434
8692.983	0.252	8.185	0.806	0.168	0.594	0.083	0.479
8820.698	0.910	7.948	1.037	0.137	0.484	-0.003	0.477

TABLE 6.1

(CONTINUED)

JD (2430000+)	PHASE	Y	C1	M1	B-Y	G	N
8822.711	0.409	8.356	0.734	0.150	0.681	0.140	0.484
8823.712	0.657	8.547	0.633	0.192	0.701	0.166	0.463
8824.703	0.902	7.985	1.023	0.134	0.493	0.013	0.426
8825.642	0.135	8.025	0.978	0.161	0.533	0.060	0.482
8826.679	0.392	8.342	0.677	0.231	0.640	0.130	0.446
9051.951	0.232	8.170	0.870	0.172	0.584	0.095	0.482
9173.662	0.402	8.312	0.644	0.219	0.655	0.0	0.0
9174.674	0.652	8.526	0.688	0.224	0.676	0.100	0.477
9175.679	0.901	7.982	1.008	0.119	0.509	0.042	0.452
9178.690	0.648	8.531	0.601	0.228	0.688	0.139	0.477
9444.906	0.637	8.555	0.653	0.247	0.673	0.0	0.0
		SW TAU -- 1.5836 DAYS					
8692.883	0.843	9.596	1.186	0.041	0.412	-0.012	0.402
8820.623	0.507	9.980	0.816	0.169	0.529	0.037	0.614
8822.626	0.772	10.140	0.846	0.144	0.497	-0.018	0.417
9053.957	0.851	9.548	1.272	0.090	0.366	-0.043	0.369
9176.667	0.339	9.801	1.022	0.150	0.441	0.0	0.0
9177.659	0.966	9.380	1.438	0.090	0.331	-0.038	0.394
9440.864	0.173	9.572	1.199	0.207	0.343	0.065	0.325
		SZ TAU -- 3.1487 DAYS					
8688.007	0.234	6.535	0.803	0.157	0.587	0.103	0.456
8689.989	0.863	6.406	0.901	0.189	0.506	0.048	0.466
8691.948	0.486	6.713	0.716	0.188	0.626	0.119	0.481
8822.676	0.003	6.402	0.935	0.164	0.506	0.050	0.461
8823.648	0.312	6.592	0.750	0.211	0.591	0.102	0.462
8824.649	0.630	6.642	0.796	0.184	0.578	0.096	0.480
8825.618	0.938	6.379	0.954	0.179	0.500	0.046	0.464
8826.633	0.260	6.574	0.776	0.193	0.583	0.097	0.468
9045.960	0.916	6.364	0.950	0.134	0.531	0.063	0.462
9051.933	0.813	6.454	0.895	0.163	0.524	0.058	0.460
9052.964	0.140	6.446	0.880	0.135	0.579	0.067	0.449
9053.981	0.463	6.683	0.746	0.207	0.617	0.119	0.495
9174.624	0.778	6.469	0.871	0.194	0.518	0.070	0.465
9175.656	0.106	6.408	0.905	0.164	0.545	0.078	0.464
9177.669	0.745	6.504	0.840	0.189	0.535	0.062	0.443
9178.629	0.050	6.388	0.940	0.158	0.533	0.060	0.448
9440.874	0.336	6.645	0.704	0.279	0.568	0.105	0.487

TABLE 6.1

(CONTINUED)

JD (2430000+)	PHASE	Y	C1	M1	B-Y	G	N
		AL VIR -- 10.3030 DAYS					
8819.971	0.728	9.824	1.046	0.099	0.400	0.108	0.343
8822.973	0.019	9.183	1.247	0.131	0.265	-0.017	0.376
8823.996	0.118	9.292	1.158	0.128	0.329	0.016	0.434
8824.965	0.212	9.475	0.967	0.180	0.411	0.049	0.465
8825.994	0.312	9.651	0.895	0.150	0.482	0.090	0.472
8826.964	0.406	9.788	0.829	0.233	0.473	0.061	0.481
9176.004	0.284	9.673	1.005	0.182	0.427	0.084	0.435
9177.987	0.476	9.943	0.749	0.220	0.486	0.134	0.441
		T VUL -- 4.4355 DAYS					
8553.865	0.501	5.944	0.643	0.277	0.470	0.127	0.466
8554.917	0.738	6.037	0.630	0.319	0.439	0.149	0.489
8555.847	0.947	5.442	1.053	0.161	0.298	0.015	0.422
8556.840	0.171	5.627	0.827	0.227	0.373	0.063	0.435
8557.928	0.417	5.887	0.665	0.271	0.458	0.113	0.462
8558.889	0.633	6.039	0.646	0.269	0.485	0.109	0.475
8559.917	0.865	5.718	0.832	0.224	0.352	0.047	0.429
8560.817	0.068	5.468	0.950	0.207	0.323	0.032	0.421
8561.833	0.297	5.787	0.715	0.261	0.421	0.079	0.450
8564.904	0.989	5.430	1.030	0.196	0.281	0.042	0.404
8565.915	0.217	5.704	0.783	0.236	0.392	0.080	0.440
8687.729	0.680	6.011	0.634	0.273	0.476	0.128	0.442
8688.667	0.892	5.583	0.940	0.208	0.306	0.044	0.404
9045.720	0.391	5.877	0.687	0.252	0.461	0.105	0.466
9445.632	0.552	5.980	0.666	0.290	0.465	0.126	0.482
		U VUL -- 7.9905 DAYS					
8555.815	0.107	6.916	0.960	0.121	0.826	0.106	0.491
8556.803	0.230	6.943	0.810	0.163	0.852	0.150	0.568
8557.808	0.356	7.161	0.726	0.177	0.940	0.184	0.507
8558.792	0.479	7.316	0.605	0.232	0.982	0.204	0.499
8559.773	0.602	7.464	0.640	0.217	1.008	0.213	0.510
8560.763	0.726	7.497	0.659	0.234	0.958	0.222	0.525
8561.790	0.855	7.158	0.725	0.194	0.870	0.104	0.497
8564.768	0.227	6.946	0.923	0.119	0.854	0.091	0.578
8565.767	0.352	7.139	0.717	0.169	0.938	0.179	0.522
8693.606	0.351	7.138	0.710	0.207	0.916	0.166	0.533

TABLE 6.2

CEPHEID PERIODS

Star	Epoch (+2430000JD)	P_p	Accuracy*10^6 [=0.01P/cycles]	GCVS Period P_c	Period Change $(P_p-P_c)*10^6$
		------- Photometric Results -------			
		----- Cδ Cepheids -----			
SU Cas	9445.144	$1^d.949338$	± 15	$1^d.949319$	+19
DT Cyg	9445.962	2.499303	± 9	2.49934	-40
SS Sct	8568.450	3.671272	± 25	3.671253	+19
RT Aur	9445.787	3.728134	± 21	3.728261	-127
SU Cyg	8694.965	3.845485	± 26	3.845664	-179
FF Aql	8692.667	4.470908	± 34	4.470959	-51
RY CMa	9448.643	4.678383	± 51	4.67804	+340
VZ Cyg	8694.701	4.864512	±121	4.864603	-91
δ Cep	9450.948	5.366235	± 43	5.366341	-106
X Lac	9449.314	5.444753	±109	5.44442	+330
FM Aql	8698.044	6.114191	± 63	6.11423	-40
AW Per	9180.053	6.463493	±176	6.46338	+110
V496 Aql	8569.872	6.807162	±115	6.8069	+300
U Aql	8567.947	7.024011	± 85	7.02393	+80
η Aql	9048.601	7.176712	± 82	7.176641	+71
RS Ori	9446.056	7.566781	±117	7.56681	-30
RX Cam	9182.555	7.912424	± 98	7.911848	+576
W Gem	9447.395	7.913602	±134	7.91467	-1070
DL Cas	9452.037	8.000406	±192	8.0003	+100
S Sge	9049.440	8.382126	±112	8.38216	-30

TABLE 6.2

(CONTINUED)

Star	Epoch (+2430000JD)	P_p	Accuracy*10^6 [=0.01P/cycles]	GCVS Period P_c	Period Change $(P_p-P_c)*10^6$
	------- Photometric Results -------				
ζ Gem	9451.794	10.151384	±156	10.15172	-330
X Cyg	9455.784	16.386080	±401	16.3866	-500
		----- C Cepheids -----			
SZ Tau	9442.965	3.148729	± 15	3.148987	-258
T Vul	9447.620	4.435521	± 29	4.435578	-57
U Vul	8698.790	7.990491	±188	7.990676	-185
		----- CW Cepheids -----			
SW Tau	9442.174	1.583598	± 4	1.583648	-50
TU Cas	9445.919	2.139438	± 17	2.13930	+140
AU Peg	8689.701	2.387012	± 10	2.39787	-10860
ST Tau	9446.370	4.034239	± 35	4.034229	+10
AL Vir	9183.384	10.303022	±170	10.299971	+3051

TABLE 6.3

CEPHEID COLOR EXCESSES DETERMINED USING THE RELATION

$$G_o = 0.543*(b-y)_o - 0.110$$

Star	Type	Period	Kelsall E(b-y)	Williams E(b-y)	Fernie 0.7*E(B-V)
η Aql	δC	7.177	0.156	0.100	0.15
U Aql	δC	7.024	0.359		0.29
FF Aql	δC	4.471	0.218	0.208	0.22
FM Aql	δC	6.114	0.581		0.46
V496 Aql	δC	6.807	0.300		0.44
RT Aur	δC	3.728	0.069	0.055	0.09
RX Cam	δC	7.912	0.474	0.409	0.40
RY CMa	δC	4.678	0.249		0.20
SU Cas	δC	1.949	0.273		0.21
δ Cep	δC	5.366	0.102	0.075	0.10
X Cyg	δC	16.385	0.283	0.241	0.25
SU Cyg	δC	3.846	0.112	0.112	0.13
VZ Cyg	δC	4.865	0.234		0.28
DT Cyg	δC	2.499	0.084		
ζ Gem	δC	10.151	0.035	0.029	0.10
W Gem	δC	7.914	0.269		0.28
X Lac	δC	5.445	0.327		0.27
RS Ori	δC	7.567	0.385		0.26:
AW Per	δC	6.464	0.526		0.21
S Sge	δC	8.382	0.112	0.113	0.14
SS Sct	δC	3.671	0.263		0.26

TABLE 6.3

(CONTINUED)

Star	Type	Period	Kelsall E(b-y)	Williams E(b-y)	Fernie 0.7*E(B-V)
SZ Tau	C	3.149	0.285	0.243	
T Vul	C	4.436	0.059	0.058	
U Vul	C	7.990	0.586		

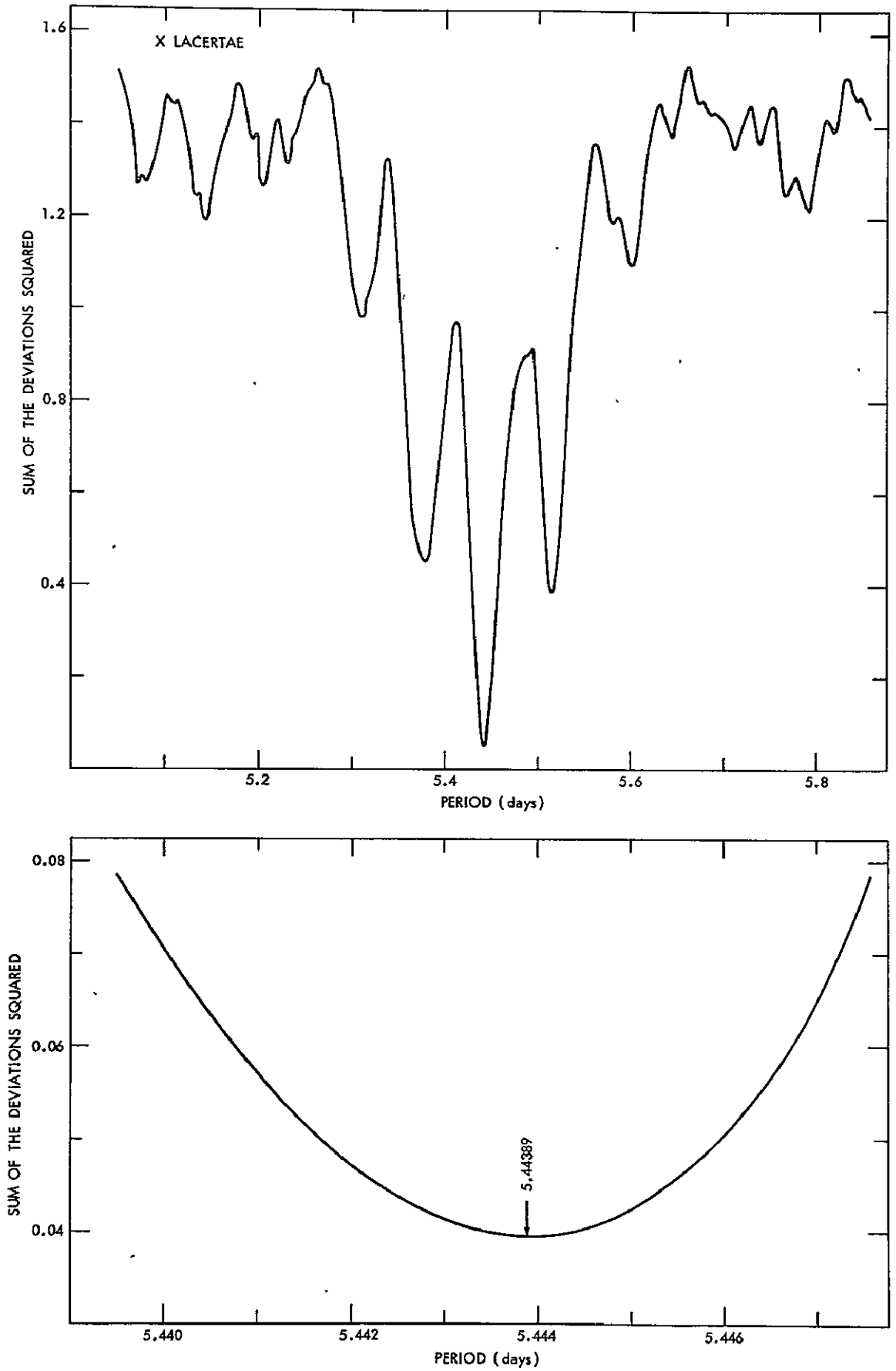

Fig. 6.1 Variation of the sum of the deviations squared for V with period for X Lacertae.

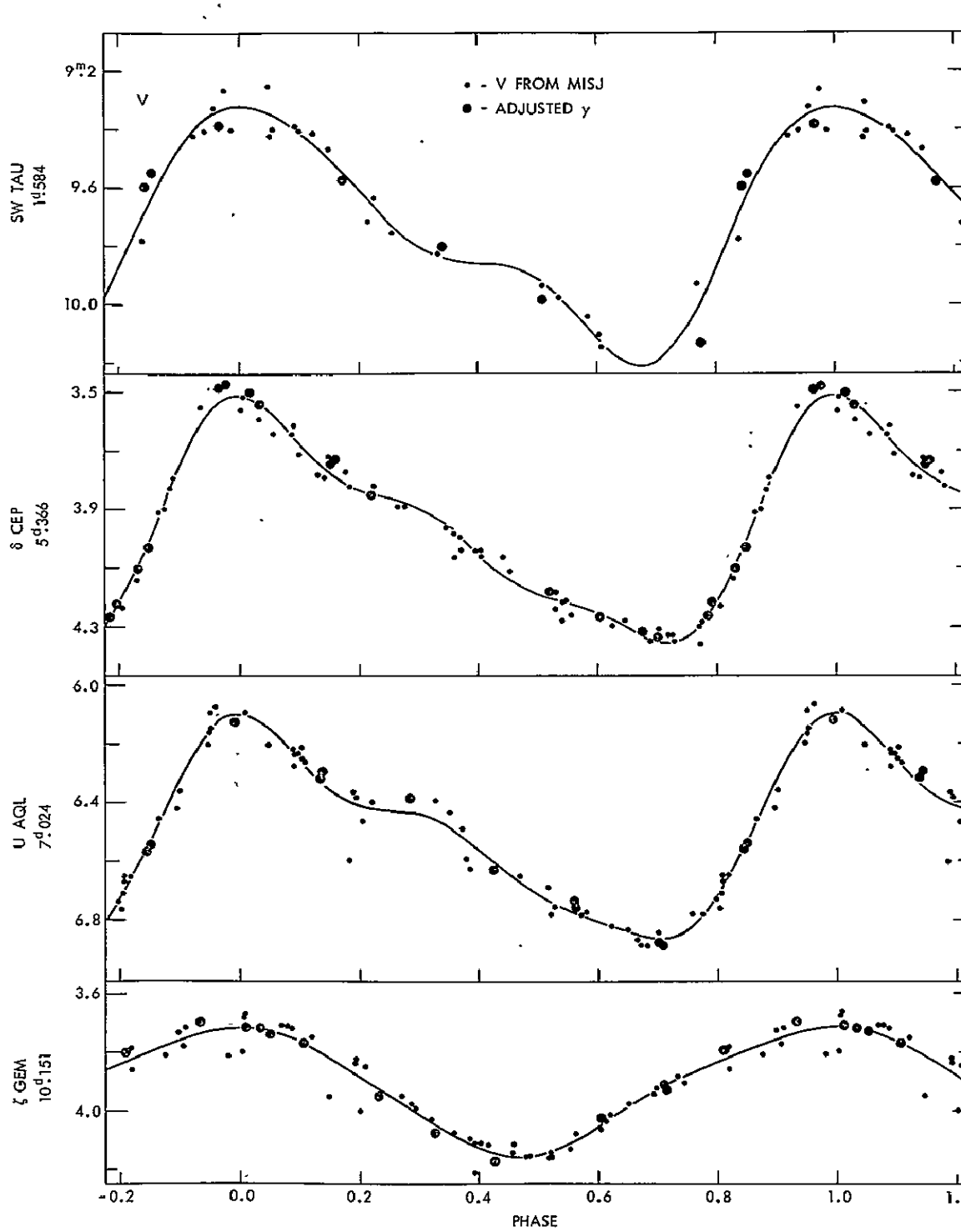

Fig. 6.2 The fits of the visual magnitudes for four representative cepheids.

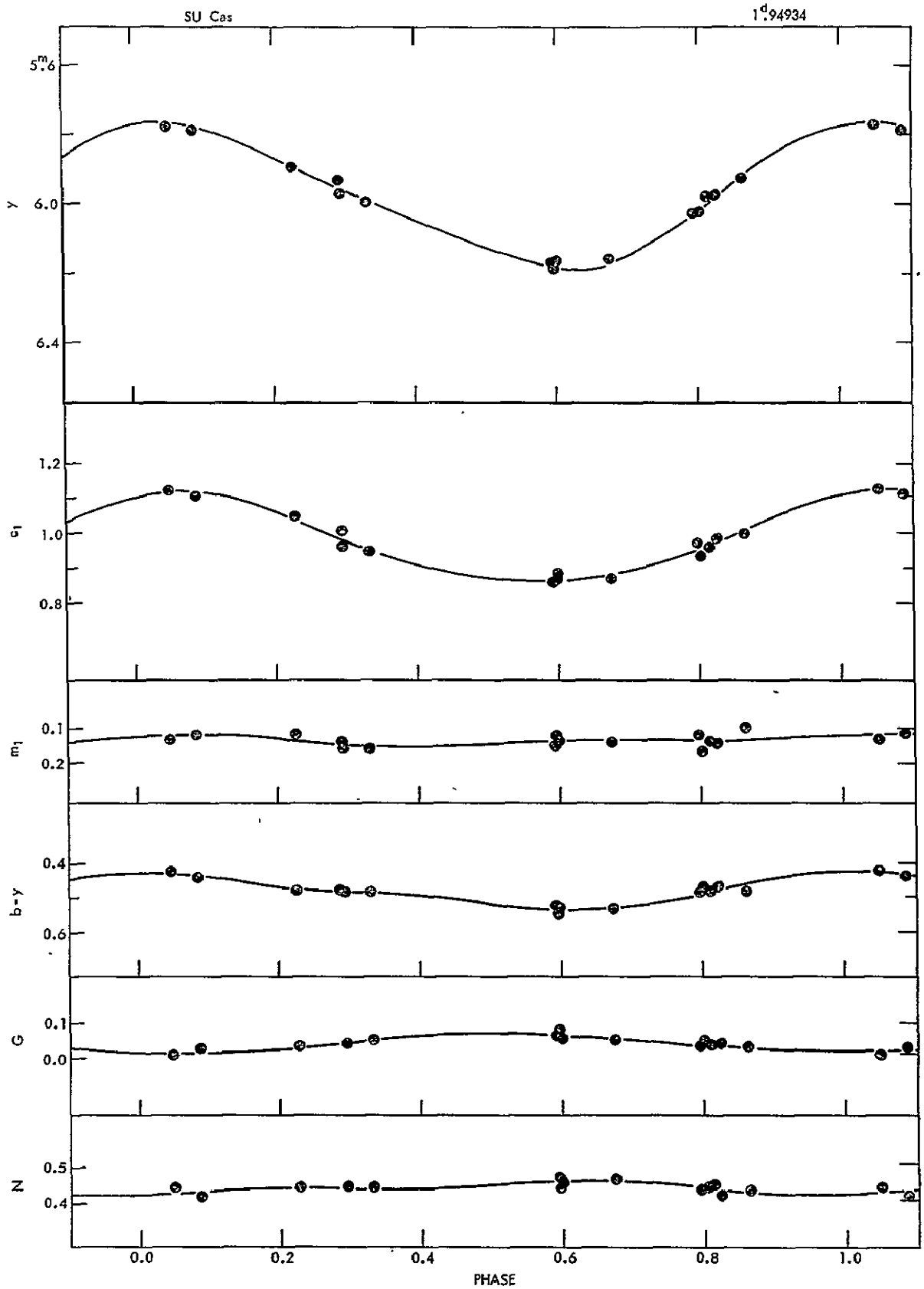

Fig. 6.3 Light and color variations with phase for SU Cas.

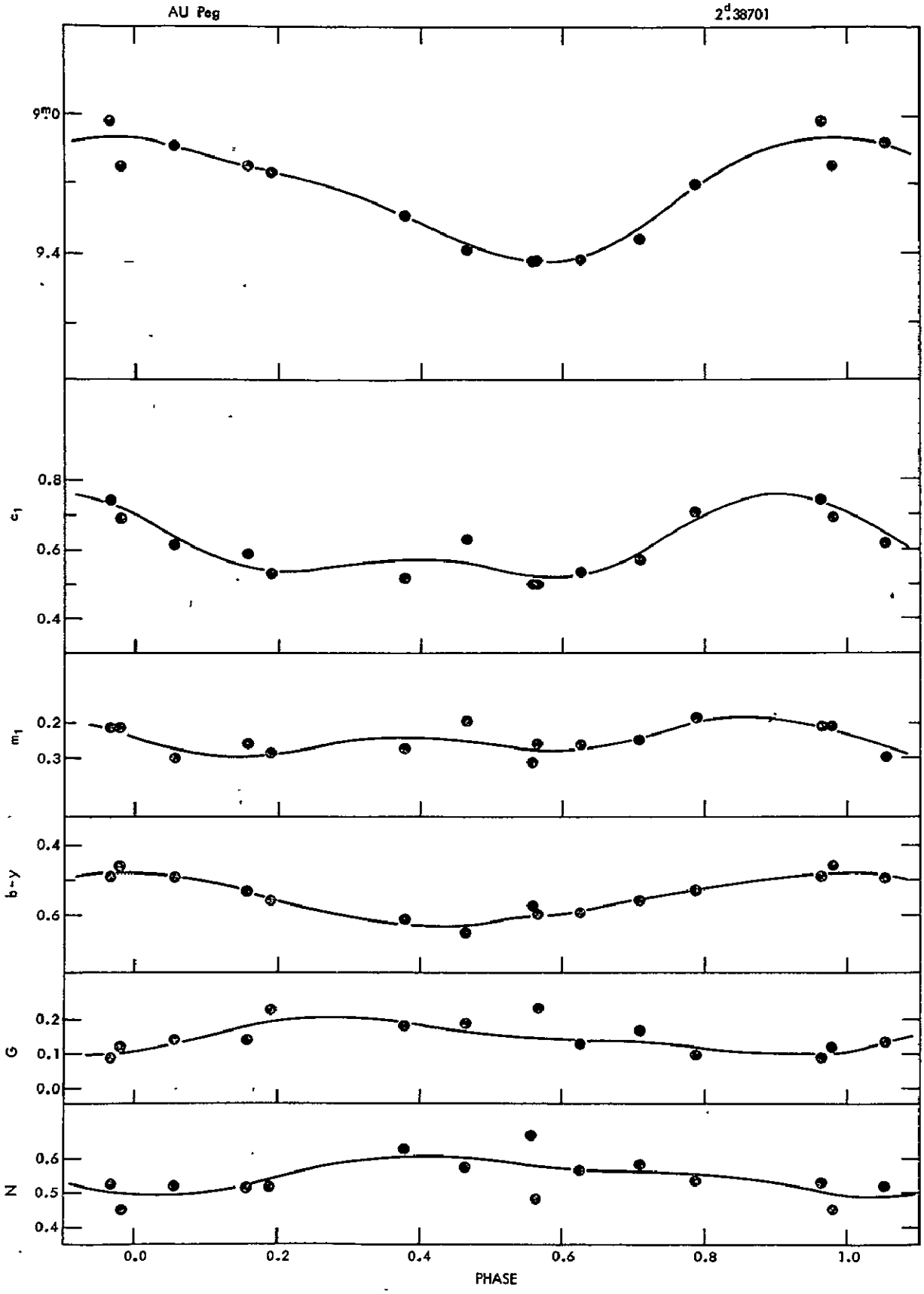

Fig. 6.4 Light and color variations with phase for AU Peg.

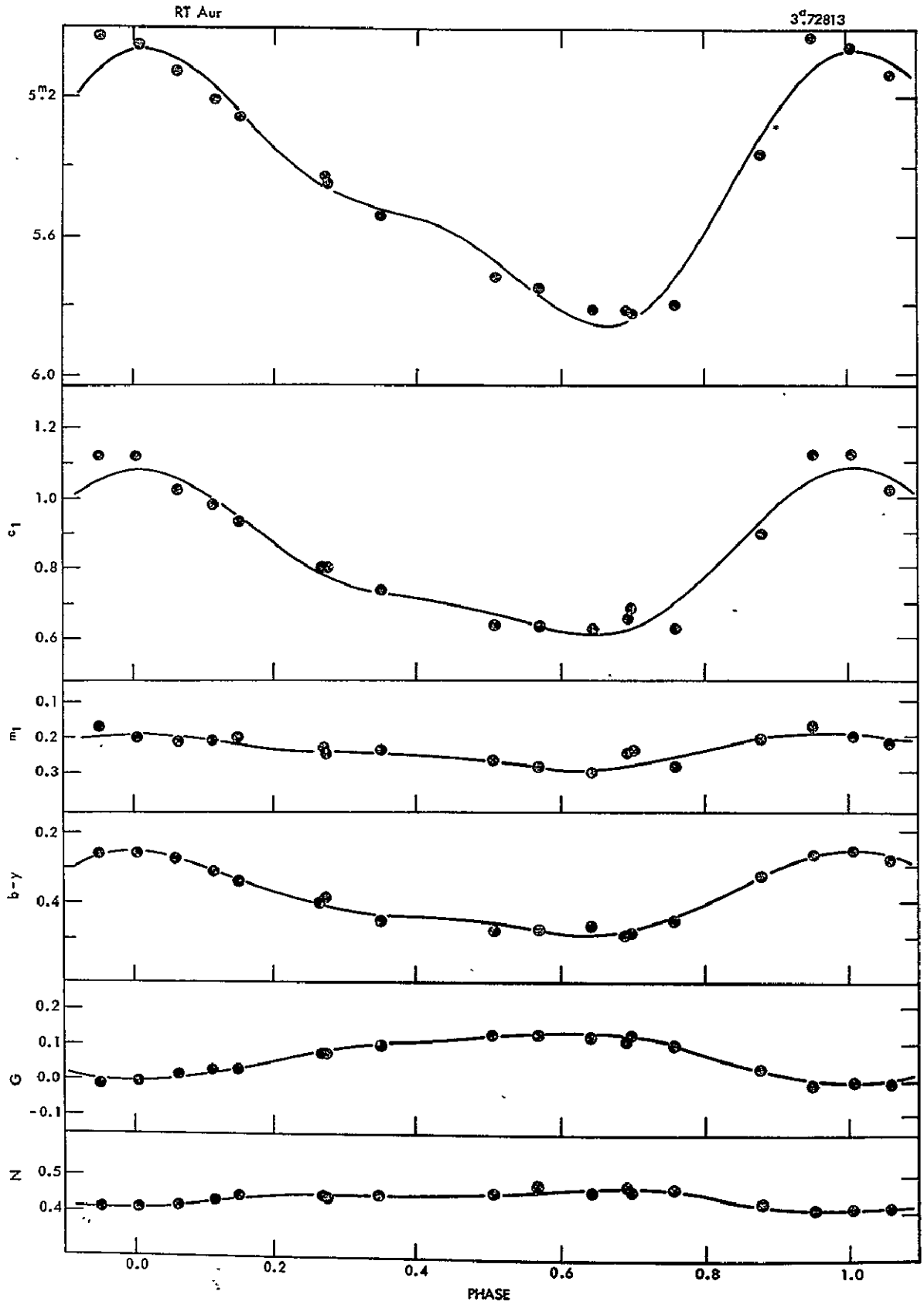

Fig. 6.5 Light and color variations with phase for RT Aur.

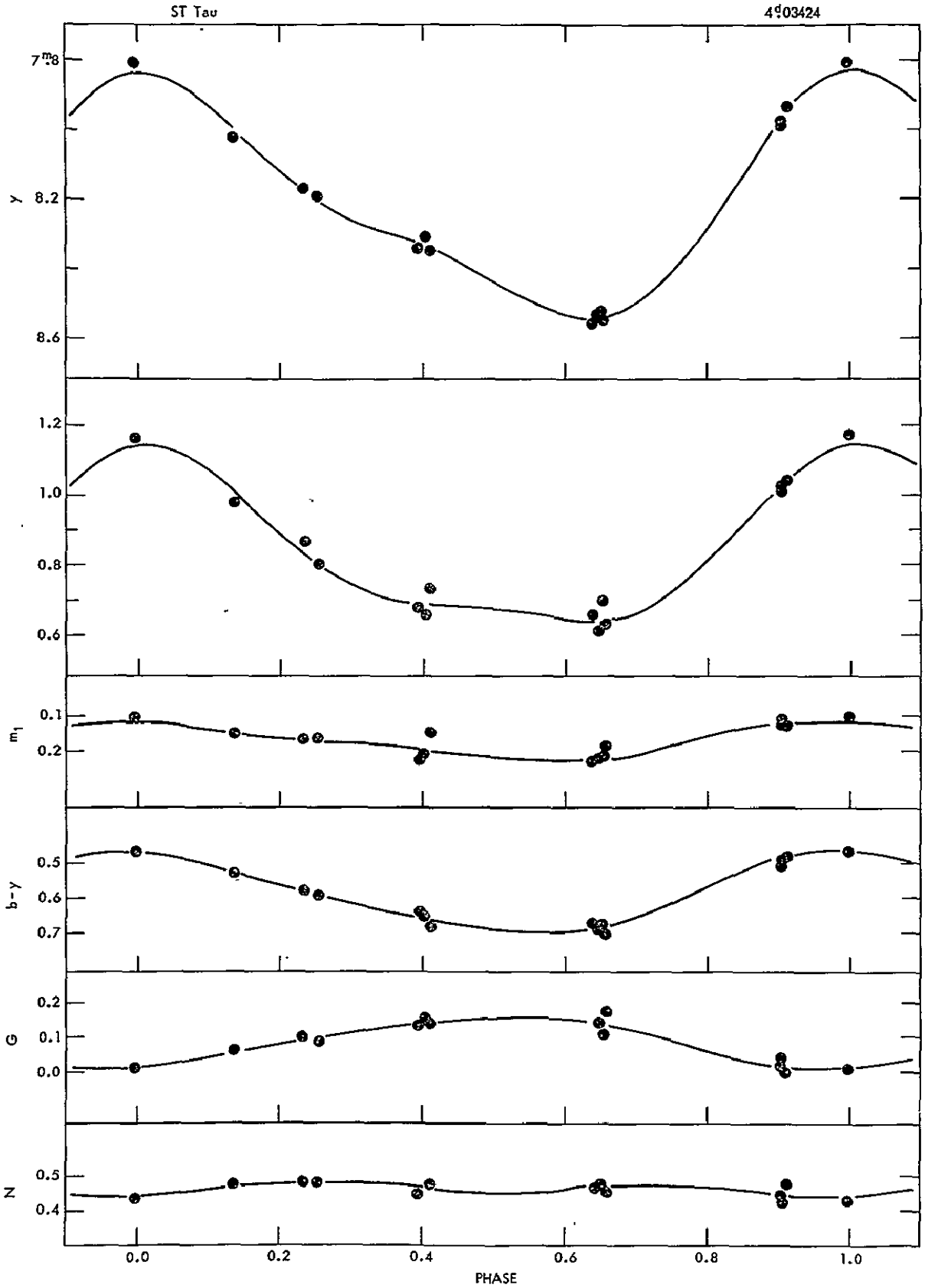

Fig. 6.6 Light and color variations with phase for ST Tau.

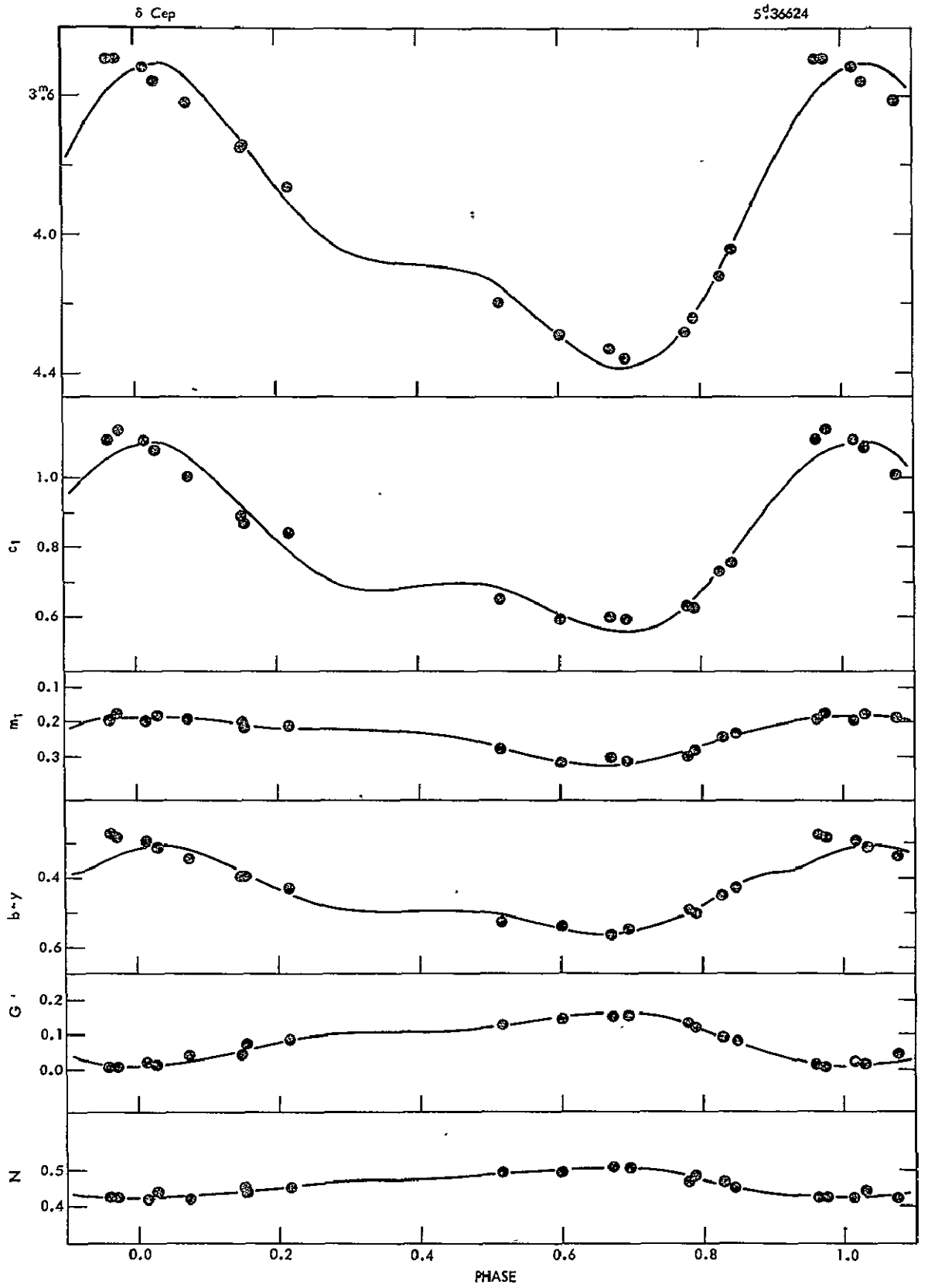

Fig. 6.7 Light and color variations with phase for δ Cep.

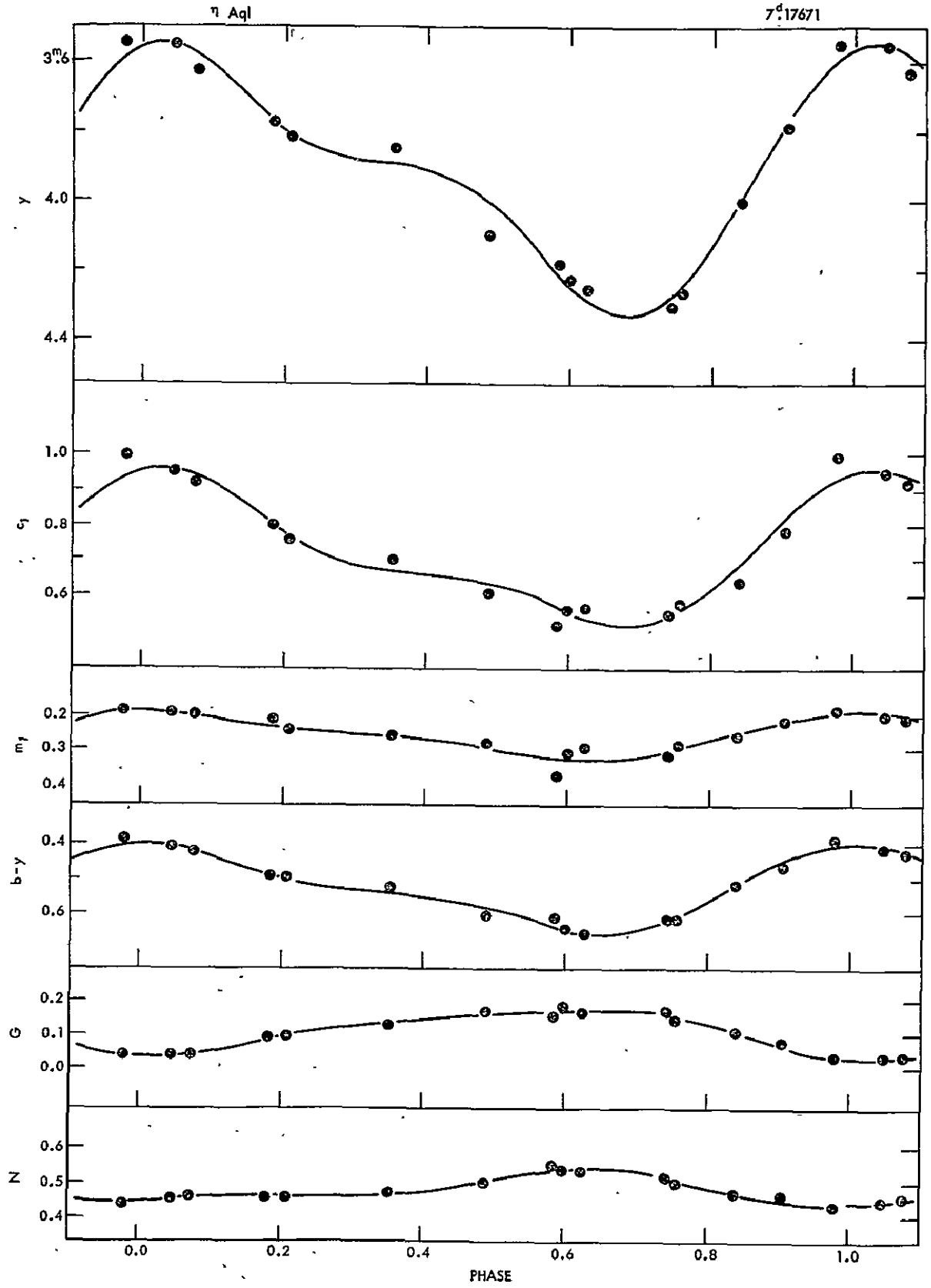

Fig. 6.8 Light and color variations with phase for η Aql.

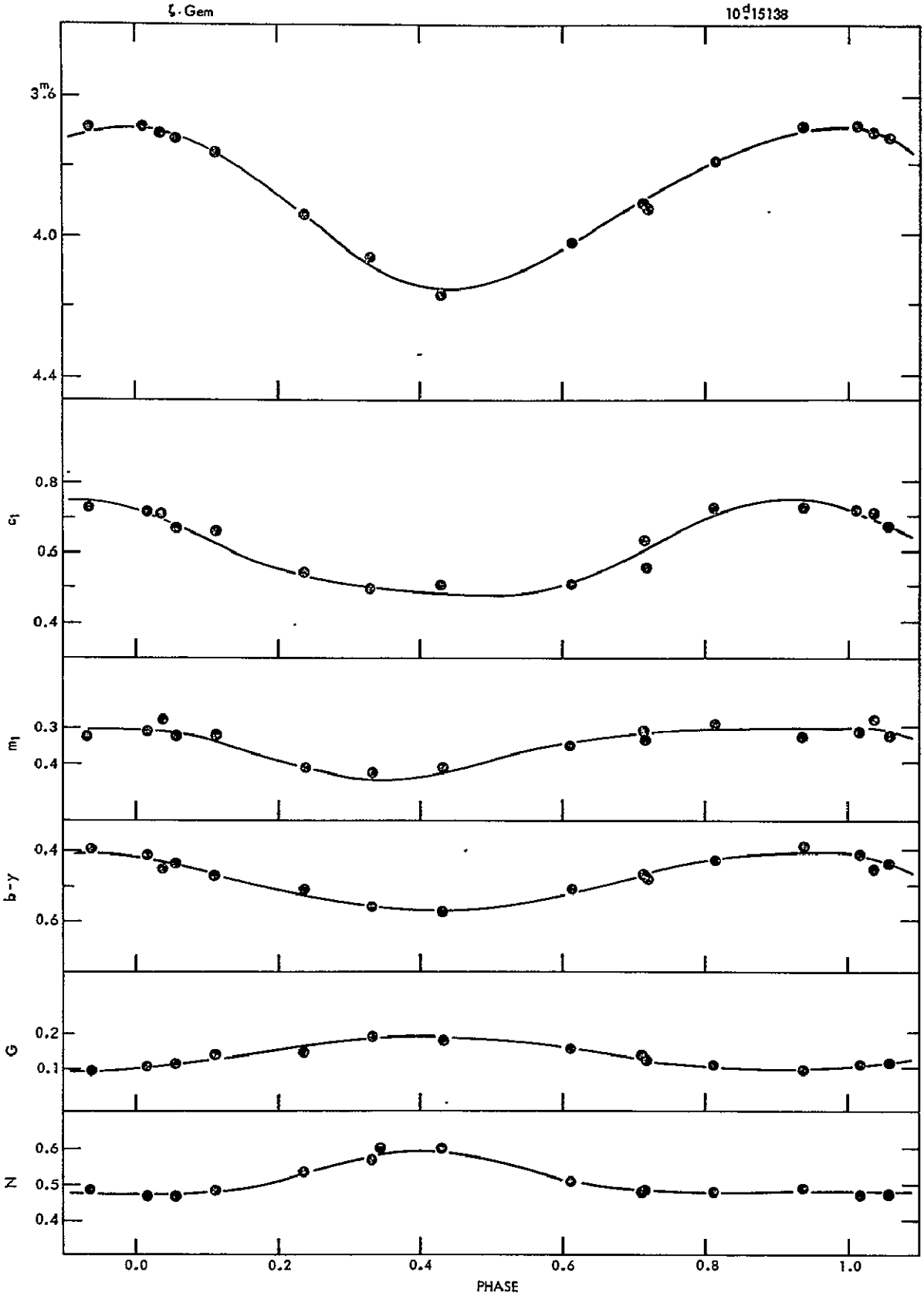

Fig. 6.9 Light and color variations with phase for ζ Gem.

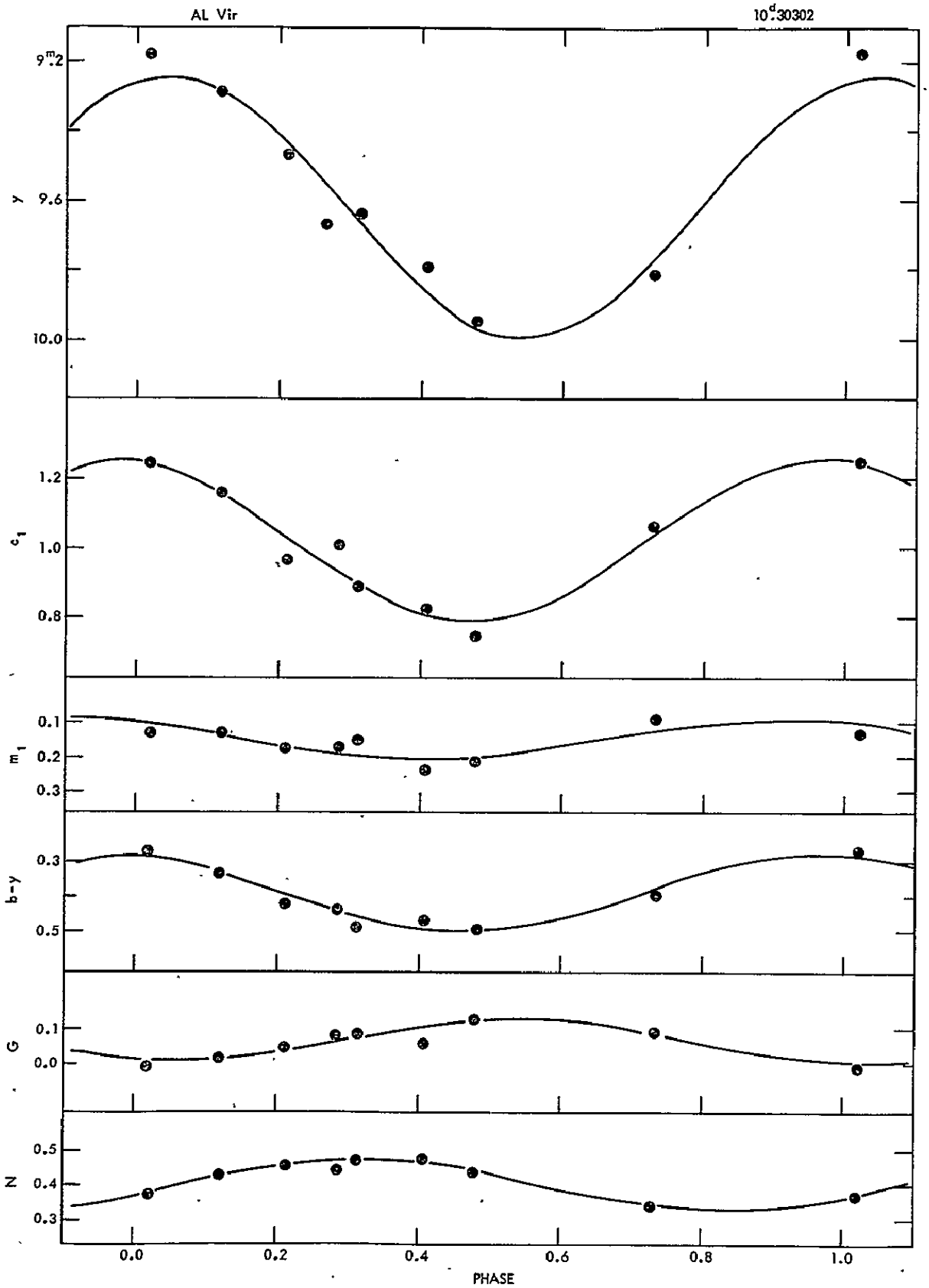

Fig. 6.10 Light and color variations with phase for AL Vir.

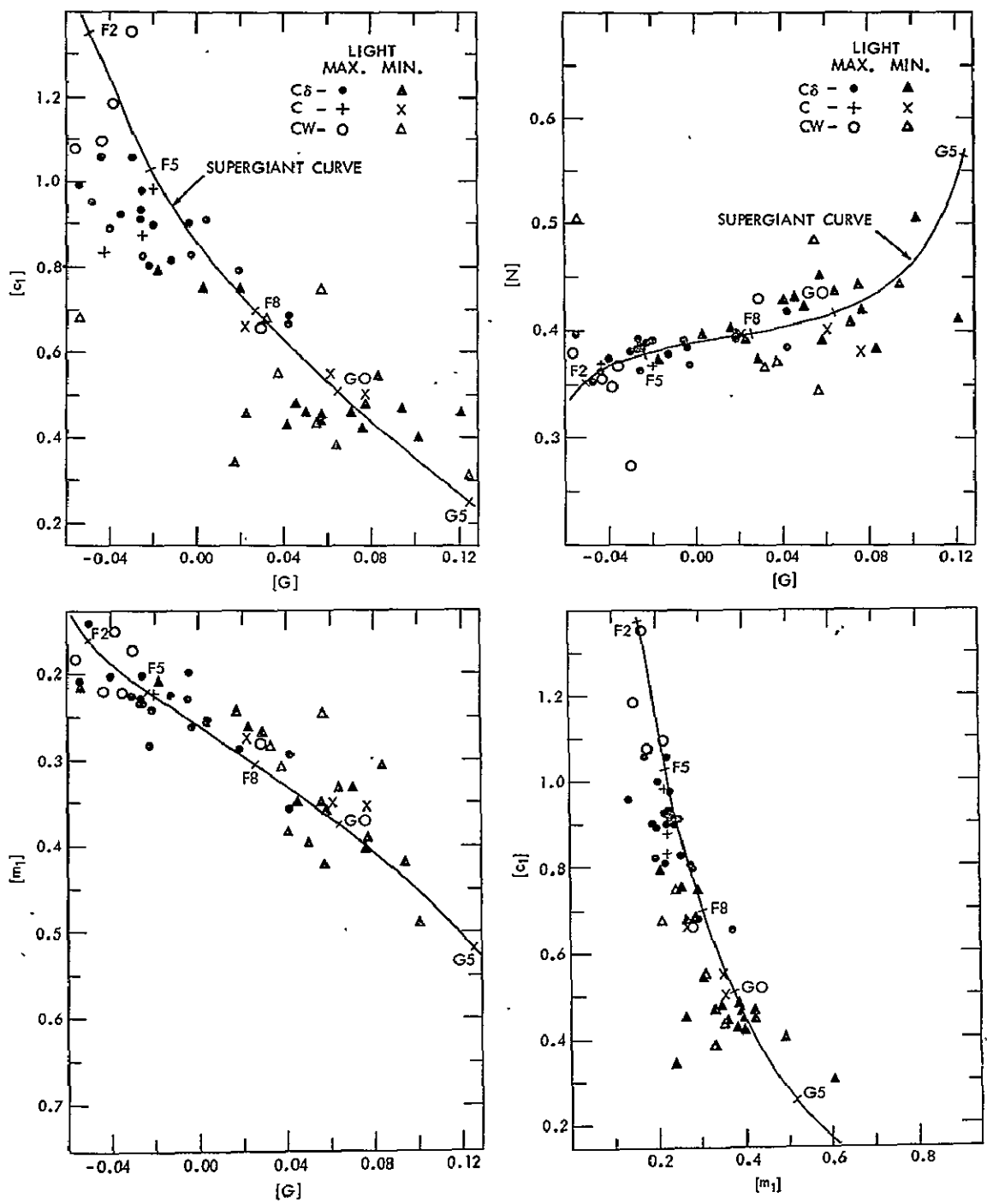

Fig. 6.11 Comparison of cepheids at maximum and minimum light to the mean supergiant results in various color-color plots.

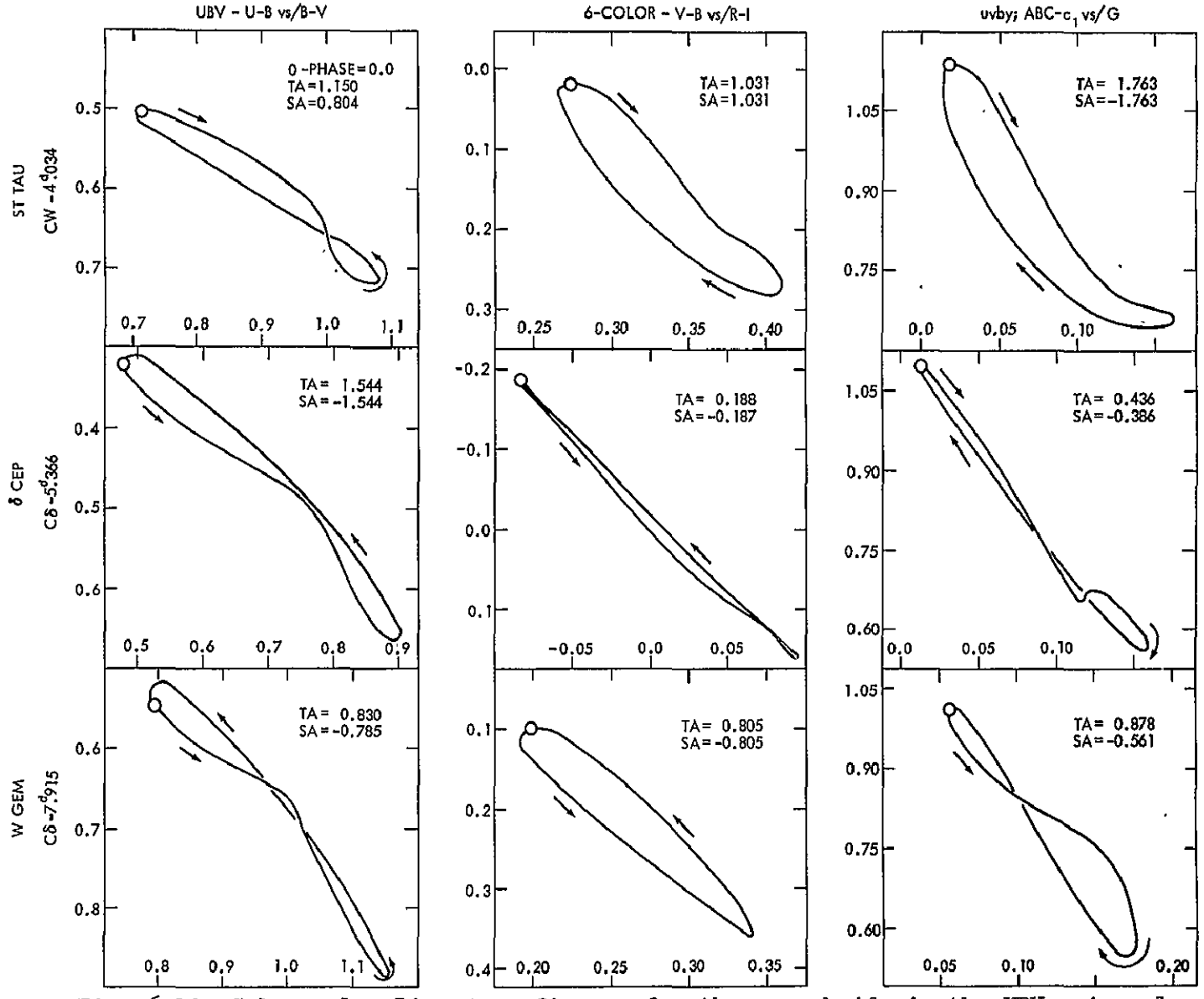

Fig. 6.12 Color-color Lissajous figures for three cepheids in the UBV, six-color, and uvby;ABC systems.

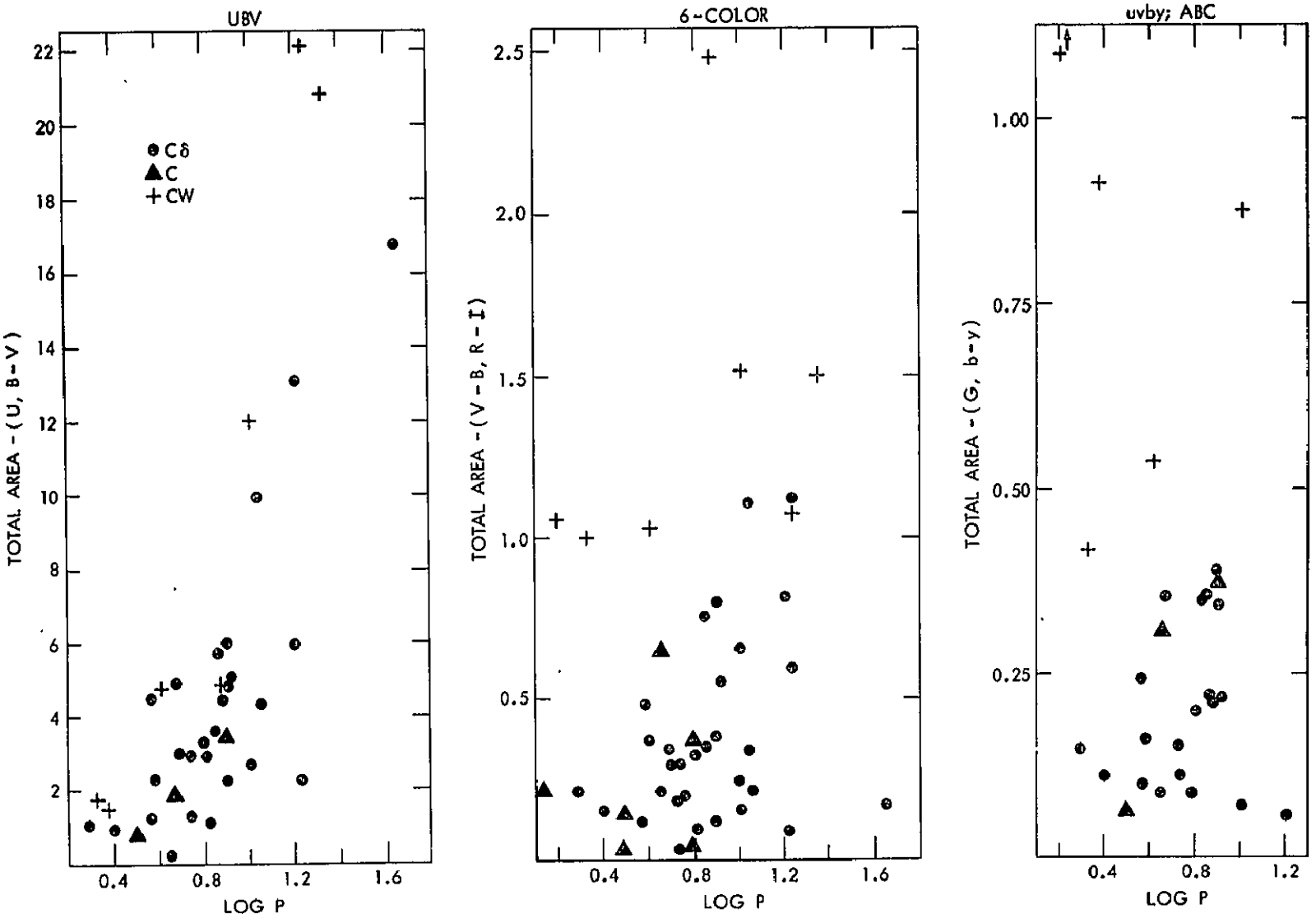

Fig. 6.13 Total areas of color-color loops versus period in three photometric systems.

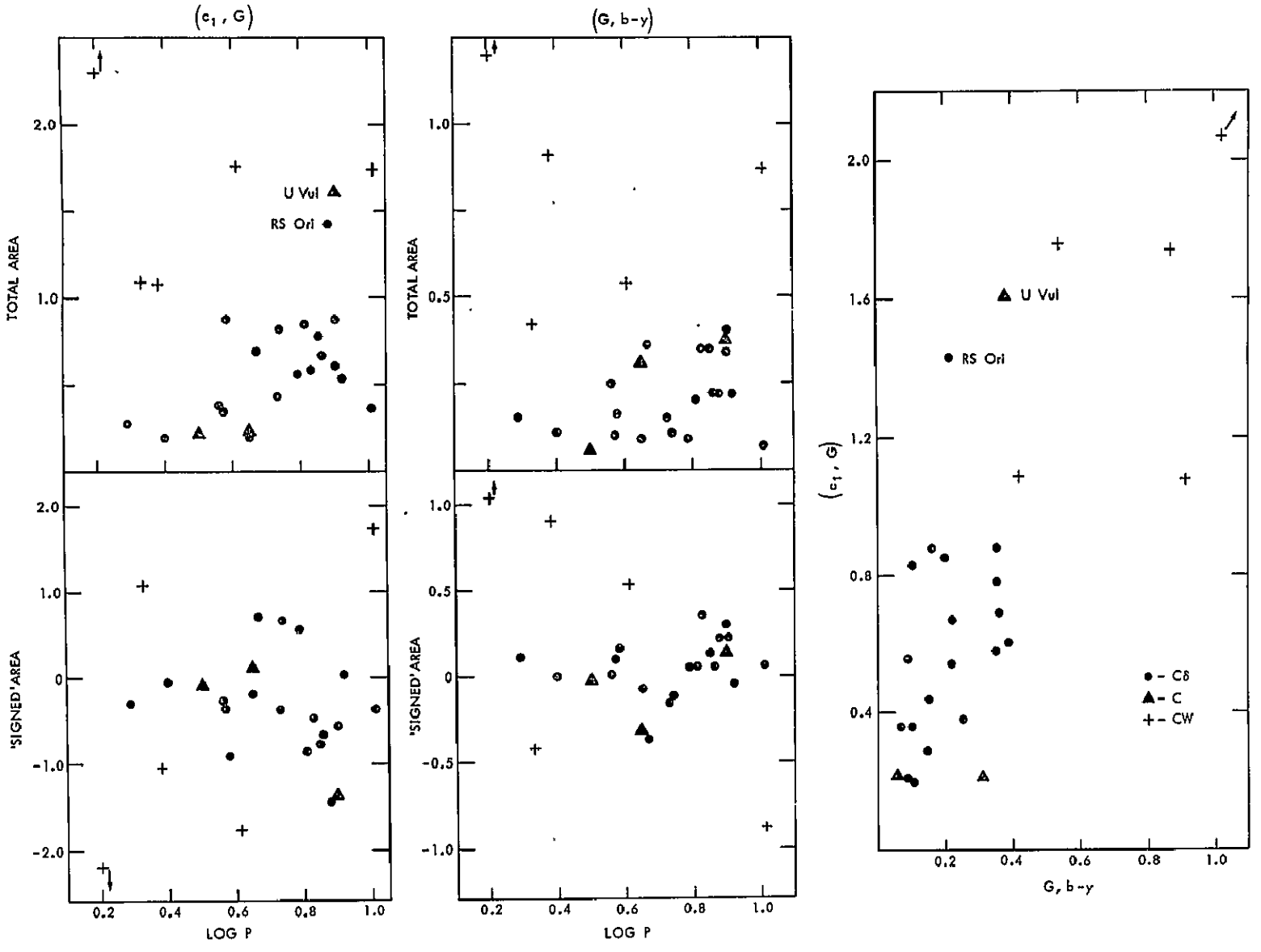

Fig. 6.14 The best total and signed color-color areas for population discrimination in our photometric system.

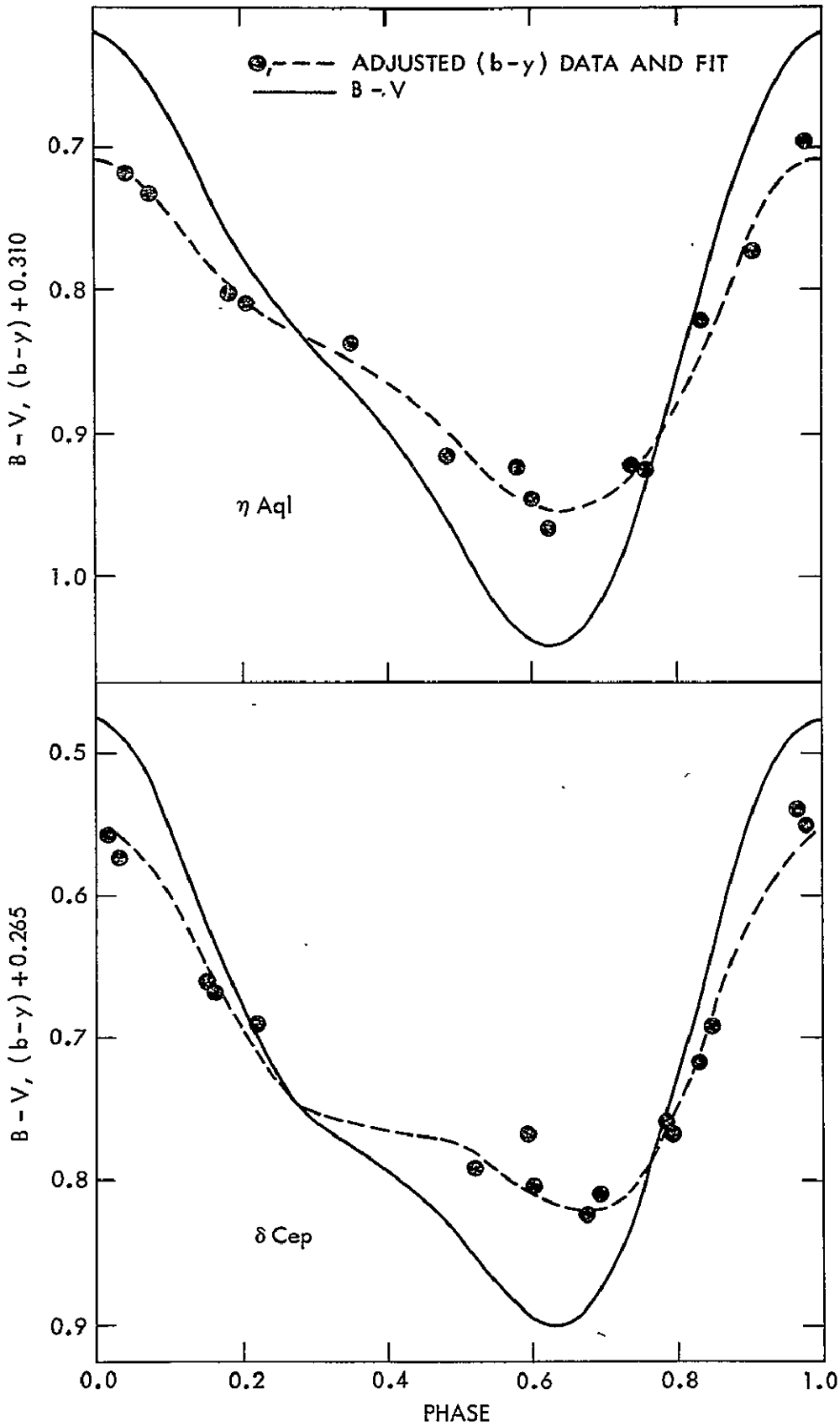

Fig. 6.15 $(B-V)$ and $(b-y)$ for η Aql and δ Cep, with $\langle b-y \rangle = \langle B-V \rangle$ for convenience.

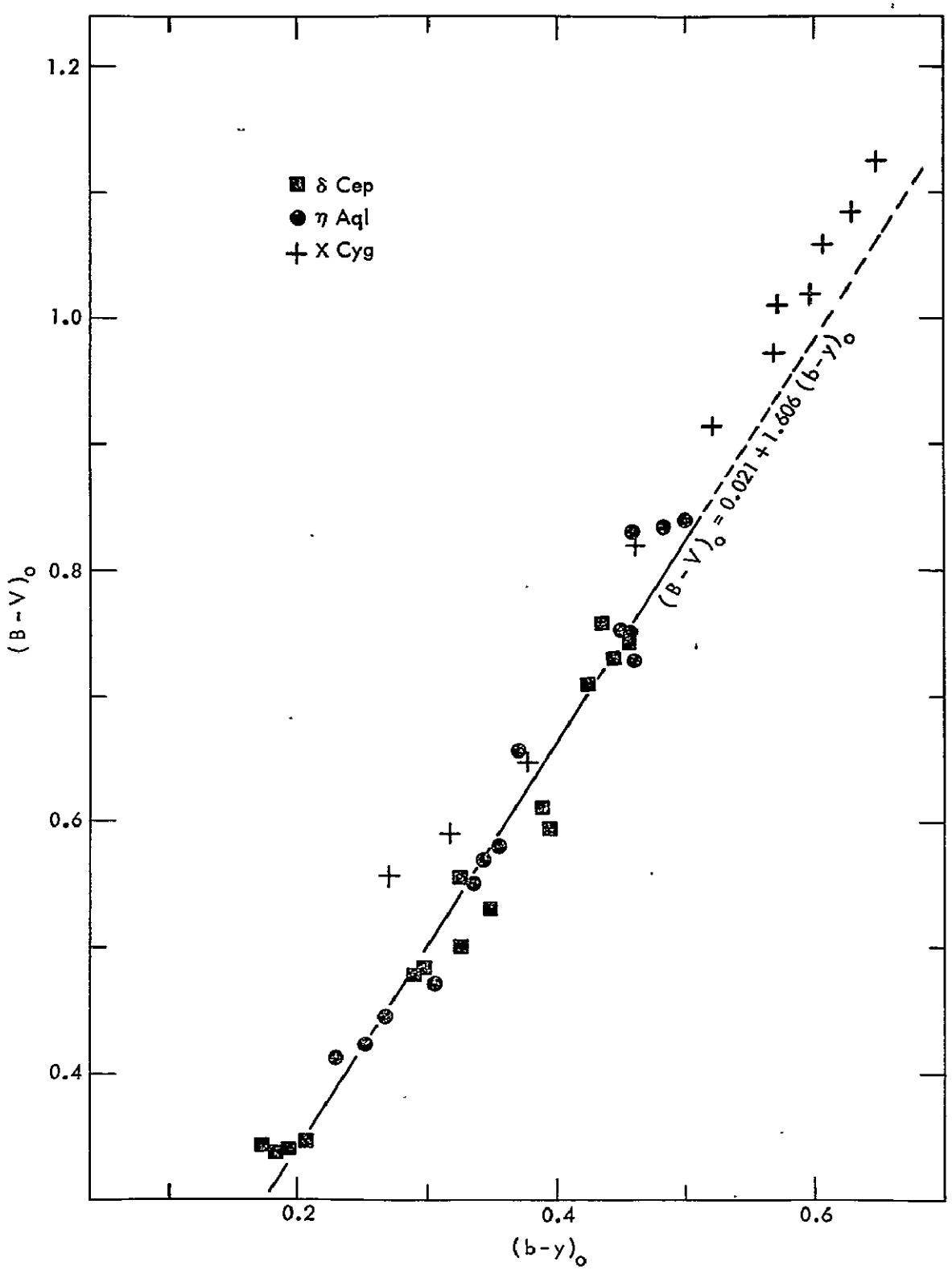

Fig. 6.16 Relation of the intrinsic colors $(B-V)_o$ and $(b-y)_o$.

CHAPTER VII

COMBINED CEPHEID-SUPERGIANT RESULTS

7-1. The 'Supercolor' Method

In section 5-4 we found it possible to construct two equations that map the mean, bracket-color lines over to the mean luminosity-class lines in a standard M_v, $\log T_e$ H-R diagram. We termed the results from these equations the M_v-supercolor and the $\log T_e$-supercolor. The structure of the supercolor equations contain no physical insight. In section 5-4 they are simple, fully-quadratic (color-color cross terms are included) expressions in all four, reddening-free colors. The coefficients for the color terms are found by least squares, using for data the mean colors at each spectral type for all luminosity classes. The information on M_v and $\log T_e$ comes from other investigations. The lack of good M_v data for particular supergiants forces our use of the mean colors. Restrictive as this is, the procedure at least complements the statistical nature of the class Ib M_v data. When the supercolor equations are applied to individual stars with colors near to the means for its spectral type and luminosity class, the supercolors resemble the physical quantities, M_v or $\log T_e$. Application to stars with colors, all or some, lying off the means for their spectral types and luminosity classes gives results beyond physical credence, particularly for M_v. This unstable characteristic of the supercolors would be more controlled if individual star data, covering the full range in spectral types and luminosity classes, could be used in determining the supercolor coefficients. For then dispersions in the colors and their relation to

the calibrating quantities is automatically included. However, we emphasize that the use of the supercolors is purely for discriminatory reasons, so that the colors can be used over their full range without necessary recourse to external information, such as spectral type or luminosity class. We feel this ability to discriminate is essential for a viable sky survey photometric system, which should be a totally self-contained entity. We also feel that the system of this investigation warrants consideration on this level.

A search was made for an M_V-supercolor, using the cepheids as a form of control. The idea was to find an M_V-supercolor which preserved luminosity class discrimination and also reasonably tracked the variation of M_V with phase for a group of representative cepheids. No such desirable situation was found. As the spectral type is not determined photometrically, the final decision is to create for a set of ranges in [G] an associated set of M_V-supercolor equations which minimize the dispersion in M_V for supergiants alone.

The full range of [G], -0.055 to 0.300, is broken up into segments of fixed length. The (n+1) segment overlaps the n^{th} segment by half. The length of the segments is varied over a wide range. For each segment length and position an M_V-supercolor equation is found, and the rms dispersion for the class Ib stars is found. From this analysis a set of contiguous [G] segments is selected that covers the full range in [G] such that the rms dispersion in M_V for the class Ib stars is in every segment less than $0^m.2$. To span the total range in [G] under this restriction requires six segments. The comparison of the M_V-supercolor (solid line) results to the M_V calibration (dashed curve) for the class Ib stars is shown in the left panel of Fig. 7.1. The application to all

luminosity classes is shown in the right panel of Fig. 7.1.

The $\log T_e$-supercolor is of much reduced form as compared to the M_V-supercolor. A single, fourth-order expression in [G] for the full range in [G] is sufficient.

The M_V-supercolor for a cepheid at any phase point can be striking. Answers ranging from -9 to +4 are found for a single cepheid. The $\log T_e$-supercolor makes no such wild excursions. The results are acceptable if the two supercolors are averaged over a full cycle. In Fig. 7.2 the averaged supercolors for the twenty-one Pop. I cepheids are shown in comparison with the cepheid instability strip given by Fernie (1967c). In detail the comparison is poor, but the basic positioning is correct - the cepheids appear to be what they really are. Most of the scatter results from the crudity of the M_V-supercolor. The $\log T_e$-supercolor introduces a minor systematic effect arising from the differences between Fernie's and our temperature scale (Johnson 1966).

A full H-R diagram is created by applying the supercolor formulas directly to the data of the individual stars. This is shown in Fig. 7.3, where the solid lines are the supercolor results when the mean bracket colors are used as input. Fig. 7.3 demonstrates the viability of the supercolor method as a supergiant discriminant, if applied to non-selective survey photometry. Even in this crude form better than two-thirds of the supergiants are separated from the other luminosity class stars. And the separation is effectively without bias to selected spectral type regions, a situation not realizable through use of the colors alone. The class V stars are also well separated. The I-II-III confusion is not resolved, but this may be amenable to a more sophisticated application of the supercolor idea.

7-2. Comparison of the Cepheid and Supergiant Mean Colors

For the cepheids we need to determine the mean bracket colors relative to some suitable photometric quantity as independent parameter. Following Williams' (1966) suggestion we choose as independent parameter the color [G]. The mean color lines for $[c_1]$, $[m_1]$, and [N] are constructed by a least squares analysis using a polynomial up to sixth order in [G]. In this analysis each cepheid is represented by twenty-five equally spaced phase points, and the colors at these points are calculated from the Fourier fits to the colors. The results are shown in Fig. 7.4. In these plots the Ib mean lines are shown for comparison. Except for $[c_1]$ the cepheid mean lines are strikingly similar to those of the supergiants.

Using the mean lines various correlations from the norm can be found in the deviations. The deviations from the mean lines are given in Tables 7.1 and 7.2 for the supergiants and cepheids, respectively. A most interesting correlation is that between $\delta[m_1] = [m_1]_* - [m_1]_{mean}$ and $\delta[N] = [N]_* - [N]_{mean}$ (a positive δ implies a greater than normal metallic or CN absorption). The correlations for the supergiants and cepheids are shown in the two panels of Fig. 7.5. The solid lines in the graphs represent the orientation of the semi-major axis of the correlation ellipses. This correlation was also noted by Williams for long period cepheids. He also notes the fact that it lacks theoretical basis. A second interesting finding is the lack of correlations between $\delta[c_1]$, $\delta[m_1]$ and $\delta[c_1]$, $\delta[N]$ for both supergiants and cepheids. The correlation plots are shown in Fig. 7.6. The fortunate insensitivity of $[c_1]$ to the strength of line blanketing enhances the possibility of calibration purely in terms of gravity, at any fixed temperature. This

point is also stressed by McNamara and Colton (1969) in their study of line blanketing effects on the uvby system for main-sequence stars and RR Lyrae variables.

7-3. Metal Content and Galactic Structure

One primary aim is to see if the metal index could delineate variations of metal content with galactic location. Plots of the $\delta[m_1]$'s versus galactic position are shown for supergiants and cepheids in the two panels of Fig. 7.7. As can be seen there is no obvious relationship between various groupings of the magnitudes of $\delta[m_1]$ and galactic position. In fact, for the cepheids there is no one star which greatly deviates from the mean. The radial distribution of the stars in this program is different from the distribution of the long period cepheids studied by Williams; and our conclusion is also different in that we find no great metallic differences, as indicated by deviations in $[m_1]$, as a function of galactic position.

7-4. Comments on Williams' Work

The discrepancy in our results can arise purely from differences in radial distribution, and some inherent characteristics of long period cepheids. In particular, there is the known correlation of long period cepheids ($P \geq 11^d$) with galactic arm location, which is distinct from the anti-correlation for shorter period cepheids (Fernie 1968a, Tammann 1970). However, on looking at Williams's listing of his data a number of peculiarities become obvious. For example, for KX Cyg the variations in c_1, N and G at nearby phase points, ϕ = 0.174 and 0.220, are fantastically large. We decided then to do a re-analysis of his data for cepheids with periods greater than eleven days.

As a first step the E(b-y)'s are calculated using his $G_o,(b-y)_o$ relationship. A number of errors are present here, as is clear upon comparing columns two and three of Table 7.3. Continuing, m_1 is corrected at each data point for the effects of interstellar reddening using both his interstellar reddening line and, as the filters in our two programs are nearly equivalent, the line used in this study. As can be noted in Table 4.6 Williams' m_1 reddening line differs from ours in slope by a factor of two. From these results new m_1 versus (b-y) relationships are developed using the stars SZ Aql, TT Aql, RX Aur, RW Cam, RW Cas, TY Cas, X Cyg, CD Cyg, W Sgr, A Sct, UZ Sct, and SV Vul. The results are given in Fig. 7.8, and as can be seen no glaring discrepancy exists. Once the mean $m_1,(b-y)$ relation is known the average δm_1's for each cepheid are found, and these are shown in columns four through six of Table 7.3. The same procedure is repeated for N, and these results are listed in columns seven through nine. The major points to be noted on the ten stars which show large δm_1's in Williams' original analysis are as follows:

YZ Aur - E(b-y) is poorly determined, and of the two data points only one is far from the norm;

CP Cep - still looks strange and there is good correlation between δm_1 and δN, but there are only two data points;

SZ Cyg - comment same as for CP Cep;

V396 Cyg - only one of the two data points is far from the norm;

V609 Cyg - comment same as for CP Cep;

VY Sgr - poor E(b-y), and the data show very large amplitude changes in the colors for nearby phase points, which is rather hard to understand;

AV Sgr - $\delta m_1,\delta N$ correlation is not so definite, and both become

"normal" when our reddening line is used;

RU Sct - still strange but the effect is reduced to high normal for δm_1 and δN if our reddening line is used;

TY Sct - comment same as for RU Sct;

DG Vul - δm_1 large but not correlated with δN.

So of the ten stars three can be dropped - YZ Aur, V396 Cyg, and VY Sgr - three have a high likelihood of being normal - AV Sgr, RU Sct, and TY Sct - and three rest on a paucity of data - CP Cep, SZ Cyg, and V609 Cyg. It thus appears that the discrepancy between our studies is probably not that pronounced.

7-5. Conclusions

The primary aims of this investigation are satisfied. Through an analysis and interpretation of the data we have developed eight distinct conclusions.

(1) The intrinsic G,(b-y) relations for both the supergiants and cepheids are found in Chapters IV and VI, respectively. These relations are adequately represented by simple linear equations. The simplicity of the relationships, and the accuracy of the photometry allow for precise determinations for the color excesses. These excesses are listed in Tables 4.1 and 6.3 for the supergiants and cepheids, respectively.

(2) In Chapter IV we developed our definition of the reddening free colors. From the present data the reddening free color relations for the supergiants with respect to spectral type are found. In Chapter V the comparison of the supergiant colors relative to those for all other luminosity classes is made. These color relations for all

luminosity classes as functions of spectral type are shown in Figs. 5.7 and 5.8. In Chapter VII we obtain the mean color relations for the cepheids. The cepheid mean colors are similar to those for the supergiants, as is shown in Fig. 7.4.

(3) The problem of distinguishing supergiants from other luminosity classes through a study of color-color plots is attacked in Chapter V. It is evident from the data that the positive separation of I from II is impossible. The segregation of I-II in the spectral type range F0 to G0 from the other luminosity classes is good using the plots $[c_1]$, [G] and [u-v], [G]. The confusion of luminosity classes is complete in the range G0 to G6. From G6 to K5 the discrimination of I-II is possible through the plots [N], $[m_1]$ and [N], [G].

(4) In Chapters V and VII the concept of supercolors is introduced. An application of the supercolor equations representing M_v and $\log T_e$ to the raw data produces a level of discrimination for the supergiants which is superior to the discrimination resulting from a study of colors. The procedure has the virtue of eliminating the I-II-III confusion to the point that approximately two-thirds of the supergiant stars are clearly separated, regardless of their spectral type through the whole range F0 to K5. The average values of M_v and $\log T_e$ derived from the supercolors for the cepheids are compatible with our current knowledge. These results are presented in Fig. 7.3.

(5) The population typing of cepheids does not appear possible on the basis of color information. However, in section 6-5 we find that the population type of cepheids can be deduced from an analysis of the areas of particular color-color loops. This is true both for the color system of this investigation, and the wide band six-color system. The

results of this study are given in Figs. 6.12 and 6.13. An advantage of the procedure is that it is unaffected by the amounts of interstellar reddening.

(6) There is a strong correlation between metallic line absorption and CN absorption for both supergiants and cepheids. The correlation lines are virtually identical for the two types of stars, as is seen in Fig. 7.6.

(7) The Balmer discontinuity index, $[c_1]$, for supergiants and cepheids is insensitive to the extent of line blanketing by metallic line or CN absorption (Fig. 7.6). We speculate that this feature will enable us to calibrate $[c_1]$ in terms of gravity with some precision.

(8) Finally, in Chapter VII we find no strong galactic position dependent features in the deviations from the mean $[m_1]$ values for supergiants or cepheids. This is shown in Fig. 7.7. We interpret the result to indicate that within the sampling volume there are no large scale regions, where stars are formed, which have distinctive metal anomalies. While the findings are in contradiction to the work of Williams, we show that most of the discrepancy is removed upon reinterpretation of Williams' data.

One unfortunate shortcoming of the investigation is our inability to calibrate the photometric quantities to physical parameters. This defect should disappear with further work similar to the investigations made by Bell (1970), Bell and Rodgers (1969), and Parsons (1970).

TABLE 7.1

DEVIATIONS OF THE F0 TO K0 SUPERGIANTS ABOUT THE MEAN COLOR LINES DEFINED WITH [G] AS INDEPENDENT COORDINATE

HD/BD	Spectral Type	ℓ^{II}	b^{II}	r‡	$\delta[c_1]$	$\delta[m_1]$	$\delta[N]$
4362	G0Ib	122°.4	-3°.3	0.9 kpc	0^m.040	-0^m.052	-0^m.065
6474	G0Ia	124.7	1.0	4.2	0.092	0.066	-0.026
7927	F0Ia	126.7	-4.4	2.3	0.190	-0.084	-0.048
8906	F3Ib	127.6	-2.5	1.3	0.126	-0.004	-0.024
8992	F6Ib	127.9	-3.7	1.7	-0.286	0.054	0.054
9250	G0Ib	127.5	1.1	1.0	-0.021	-0.006	-0.020
10494	F5Ia	129.1	-0.4	3.8	0.116	-0.063	-0.027
14662	F7Ia	135.9	-5.2	0.96	0.010	0.001	0.006
16901	G0Ib	143.3	-14.1	0.76	0.003	0.023	-0.007
17971	F5Ia	137.8	1.2		0.131	-0.054	-0.005
18391	G0Ia	139.5	-1.0		-0.061	0.104	-0.005
20902	F5Ib	146.6	-5.9	0.16	-0.028	0.014	0.002
25056	G0Ib	148.8	0.8	1.6	0.065	-0.048	-0.050
26630	G0Ib	154.0	-1.8	0.36	-0.025	-0.027	-0.003
31964	F0Iap	162.8	1.2		-0.031	-0.075	-0.034
31910	G0Ib	149.6	11.4	0.4	0.033	-0.026	-0.020
36673	F0Ib	219.2	-24.5	0.26	0.086	0.046	-0.024
36891	G3Ib	169.5	4.4		-0.011	-0.016	0.005
37819	F5Ib	179.6	-0.5	2.6	-0.635	0.099	0.056
38247	G8Iab	188.7	-5.4	2.1	-0.021	0.106	0.048
38808	G3Ib-II	184.5	-1.7		0.058	-0.094	-0.058

TABLE 7.1

(CONTINUED)

HD/BD	Spectral Type	ℓ^{II}	b^{II}	r‡	$\delta[c_1]$	$\delta[m_1]$	$\delta[N]$
39416	G3Ib-II	184.2	-0.5		-0.115	0.042	0.030
39949	G2Ib	182.7	1.3	1.7	-0.053	-0.005	0.021
43282	G5Ib-II	192.0	1.2	1.9	0.009	0.029	0.027
47731	G5Ib	186.5	10.4		0.039	-0.005	-0.032
48616	F5Ib	209.4	-0.1		-0.226	0.054	0.035
58526	G3Ib	220.8	5.6		-0.003	0.022	-0.014
67594	G2Ib	223.1	16.5		0.061	0.003	-0.069
74395	G2Ib	233.1	21.1	0.63	-0.129	0.003	0.013
77912	G8Ib-II	184.4	42.2		0.063	-0.032	-0.023
161796	F3Ib	77.2	30.9	1.8	0.615	-0.020	-0.018
163506	F2Ia	51.4	23.2	5.2	0.376	-0.077	-0.006
171635	F7Ib	86.2	25.0	0.60	0.093	0.028	0.010
172365	F9Ib	36.3	5.0	1.3	-0.037	-0.014	-0.009
174104	G0Ib	58.6	13.4	3.8	-0.083	-0.090	-0.041
179784	G5Ib	48.8	2.1		0.069	-0.071	-0.036
180028	F6Ib	41.0	-2.4	1.4	-0.032	-0.036	-0.007
180583	F6Ib-II	60.6	7.4	0.9	-0.328	0.039	0.021
182296	G3Ib	44.3	-3.1	1.4	-0.020	0.027	0.119
183864	G2Ib	59.6	3.2	2.9	-0.089	-0.049	-0.010
187203	G0Ib	49.1	-7.5	1.2	0.105	-0.065	-0.012
187299	G5Iab-Ib	61.5	-0.3	2	-0.227	0.045	0.065
190113	G5Ib	72.1	2.7	1.4	0.133	-0.074	-0.058

TABLE 7.1

(CONTINUED)

HD/BD	Spectral Type	ℓ^{II}	b^{II}	r‡	$\delta[c_1]$	$\delta[m_1]$	$\delta[N]$
331777	F8Ia	69.1	0.5	5.2	0.237	0.084	-0.017
190446	F6Ib	76.2	4.9	3.5	-0.124	-0.010	-0.046
190323	G0Ia-Iab	54.7	-8.6	1.1	0.171	0.082	0.040
191010	G3Ib	64.2	-3.5	2.8	0.027	-0.083	-0.027
37°3827	F3Ib	75.6	2.3	1.7	0.110	-0.035	-0.005
192713	G2Ib	63.5	-6.4	0.7	-0.128	0.033	0.063
192876	G3Ib	32.3	-24.2	0.5	-0.023	0.008	0.031
193370	F5Ib	73.4	-0.5	1.0	0.049	0.011	-0.003
194093	F8Ib	78.2	1.9	0.22	0.135	0.067	0.026
200102	G1Ib	86.2	-0.7	1.1	0.013	-0.057	-0.022
200805	F5Ib	86.8	-1.2	2.5	-0.129	0.062	0.015
202314	G2Ib	76.7	-12.9		0.062	-0.048	-0.061
204022	G0Ib	92.9	0.1	1.0	0.120	-0.022	-0.036
204867	G0Ib	49.6	-37.1	0.3	0.020	-0.020	0.001
206859	G5Ib	72.0	-26.5	0.4	0.070	-0.014	-0.021
207089	K0Ib	76.6	-22.8	0.6	0.022	0.007	-0.017
207489	F5Ib	88.3	-11.3	1.5	0.176	-0.035	0.002
207647	G4Ib	95.4	-3.2	1.4	-0.143	0.067	0.103
208606	G8Ib	103.5	5.5		-0.020	0.085	0.040
209750	G2Ib	61.0	-41.4	0.3	0.081	-0.001	-0.038
216206	G4Ib	104.1	-7.7	1.0	0.068	-0.039	-0.047
218356	K0Ibp	95.1	-31.7	0.5	-0.104	0.011	-0.096

TABLE 7.1

(CONTINUED)

HD/BD	Spectral Type	ℓ^{II}	b^{II}	r‡	$\delta[c_1]$	$\delta[m_1]$	$\delta[N]$
219135	G0Ib	109.6	-3.8	1.7	0.062	-0.067	-0.022
60°2532	F7Ib	112.8	0.4	1.4	-0.204	0.011	0.012
221861	K0Iab	116.9	9.7	1.2	-0.032	0.081	0.017
223047	G5Ib	111.4	-15.0	0.7	-0.146	0.050	0.079
224165	G8Ib	113.2	-14.5		0.038	0.006	-0.013

‡Distances [Buscombe (1964)] are only assigned to stars of good photometric quality.

TABLE 7.2

AVERAGE DEVIATIONS OF THE POP. I CEPHEIDS ABOUT THE MEAN COLOR LINES DEFINED WITH [G] AS INDEPENDENT COORDINATE

Star	ℓ^{II}	b^{II}	r	$\langle\delta[c_1]\rangle$	$\langle\delta[m_1]\rangle$	$\langle\delta[N]\rangle$
η Aql	40.9	-13.1	0.27kpc	0.018	0.003	0.004
U Aql	30.9	-11.6	0.65	0.020	-0.055	-0.007
FF Aql	49.2	6.4	0.39	0.062	0.014	0.009
FM Aql	44.3	0.9	1.00	-0.095	-0.020	0.017
V496 Aql	28.2	-7.1	0.92	0.070	-0.035	-0.046
RT Aur	183.1	8.9	0.46	0.046	0.008	-0.004
RX Cam	145.9	4.7	0.96	0.026	-0.002	-0.011
RY CMa	226.0	0.3	1.32	-0.070	0.037	-0.002
SU Cas	133.5	8.5	0.33	-0.005	-0.003	0.003
δ Cep	105.2	0.5	0.27	0.050	0.003	0.002
X Cyg	76.9	-4.3	1.08	0.070	0.043	0.069
SU Cyg	64.8	2.5	0.86	-0.143	-0.014	0.000
VZ Cyg	91.5	-8.5	1.70	-0.030	0.032	0.000
DT Cyg	76.5	-10.8	0.43	0.001	0.014	0.012
ζ Gem	195.7	11.9	0.36	0.036	0.036	0.018
W Gem	197.4	3.4	0.94	0.032	0.018	0.016
X Lac	106.6	-2.5	1.50	0.039	-0.012	-0.010
RS Ori	196.6	0.3	1.79:	-0.063	0.018	0.014
AW Per	166.6	-5.4	1.20	-0.228	-0.033	0.006
S Sge	55.2	-6.1	0.66	0.103	-0.012	-0.005
SS Sct	25.2	-1.8	1.10	0.039	-0.049	-0.019
SZ Tau	179.6	-19.0	0.5:	-0.023	0.003	0.004

TABLE 7.2

(CONTINUED)

Star	ℓ^{II}	b^{II}	r	$\langle\delta[c_1]\rangle$	$\langle\delta[m_1]\rangle$	$\langle\delta[N]\rangle$
T Vul	72.2	-10.0	0.6:	0.052	0.003	-0.009
U Vul	56.1	-0.3	0.6:	-0.086	0.015	-0.014

TABLE 7.3

REANALYSIS OF WILLIAMS' LONG PERIOD CEPHEID DATA

Star	Williams E(b-y)	Recalculated E(b-y)	$\sigma(E(b-y))$	$-\delta m_1^W$	δm_1^K	$\delta m_1^{K'}$	$-\delta N^W$	δN^K	$\delta N^{K'}$
SZ Aql	0.476	0.475	±0.041	-0.036	-0.034	-0.041	-0.044	-0.048	-0.050
TT Aql	0.394	0.393	±0.017	-0.005	-0.011	-0.011	-0.001	-0.005	-0.007
RX Aur	0.264	0.263	±0.030	0.028	0.020	0.028	0.018	0.014	0.016
YZ Aur	0.505	0.608	±0.207	0.122	0.162	0.144	0.030	0.052	0.058
ER Aur	0.504	0.602	±0.199	0.013	-0.029	-0.045	-0.175	0.446	0.510
RW Cam	0.668	0.644	±0.056	0.028	0.013	0.000	0.069	0.087	0.081
RW Cas	0.252	0.252	±0.080	-0.056	-0.068	-0.059	-0.057	-0.058	-0.052
RY Cas	0.486	0.486	±0.050	0.001	-0.002	-0.005	-0.022	-0.017	-0.014
SZ Cas	0.682	0.681	±0.105	-0.013	-0.019	-0.037	0.000	-0.005	-0.007
CY Cas	0.756	0.756	±0.104	-0.046	-0.053	-0.083	-0.020	0.000	0.009
CP Cep	0.473	0.473	±0.041	-0.093	-0.095	-0.094	-0.136	-0.108	-0.099
X Cyg	0.241	0.240	±0.040	0.006	0.000	0.005	0.001	-0.002	-0.002
SZ Cyg	0.395	0.395	±0.030	-0.128	-0.107	-0.113	-0.169	-0.109	-0.111

TABLE 7.3

(CONTINUED)

Star	Williams E(b-y)	Recalculated E(b-y)	σ(E(b-y))	$-\delta m_1^W$	δm_1^K	$\delta m_1^{K'}$	$-\delta N^W$	δN^K	$\delta N^{K'}$
TX Cyg	0.995	0.937	±0.097	0.044	0.020	0.018	-0.003	0.019	0.047
VX Cyg	0.595	0.594	±0.028	-0.020	-0.028	-0.033	-0.038	-0.045	-0.047
CD Cyg	0.386	0.386	±0.033	0.028	0.028	0.028	-0.038	-0.020	-0.017
KX Cyg	1.274	1.273	±0.317	-0.065	0.108	-0.003	0.093	0.066	0.092
V396 Cyg	0.849	0.848	±0.084	-0.076	-0.072	-0.075	-0.114	-0.090	-0.068
V609 Cyg	0.955	0.954	±0.013	-0.110	-0.118	-0.128	-0.069	-0.059	-0.063
AA Gem	0.399	0.399		0.042	0.036	0.034	0.030	0.010	0.005
T Mon	0.216	0.216	±0.069	-0.004	0.045	0.046	-0.001	0.026	0.021
SV Mon	0.201	0.201		-0.020	-0.026	-0.013	-0.019	-0.041	-0.038
Y Oph	0.494	0.493	±0.033	0.014	-0.016	-0.017	0.006	-0.018	-0.016
BM Per	0.897	0.992	±0.289	0.016	0.237	0.128	-0.051	0.350	0.441
VY Sgr	1.076	1.074	±0.203	0.091	0.224	0.129	-0.080	0.100	0.194
WZ Sgr	0.353	0.353	±0.045	-0.022	0.061	0.060	-0.006	0.071	0.070

TABLE 7.3

(CONTINUED)

Star	Williams E(b-y)	Recalculated E(b-y)	σ(E(b-y))	$-\delta m_1^W$	δm_1^K	$\delta m_1^{K'}$	$-\delta N^W$	δN^K	$\delta N^{K'}$
AV Sgr	0.922	0.920	±0.017	0.087	0.079	0.044	0.021	0.014	0.006
Z Sct	0.453	0.452	±0.157	-0.030	-0.049	-0.055	0.002	0.004	0.000
RU Sct	0.816	0.788	±0.052	0.106	0.084	0.061	0.066	0.028	0.020
TY Sct	0.852	0.851	±0.087	0.085	0.078	0.065	0.046	0.054	0.059
UZ Sct	0.784	0.753	±0.157	0.030	0.018	0.002	0.035	0.049	0.061
SV Vul	0.470	0.470	±0.064	-0.002	0.003	-0.002	-0.052	-0.036	-0.038
DG Vul	0.951	0.954	±0.026	-0.127	-0.115	-0.130	-0.026	-0.007	0.007

$-\delta m_1^W$ and $-\delta N^W$ are from Williams (1966).
δm_1^K and δN^K are recalculated values using Williams data and his $E(m_1)/E(b-y)$.
$\delta m_1^{K'}$ and $\delta N^{K'}$ are calculated from Williams data using $E(m_1)/E(b-y) = -0.125$.

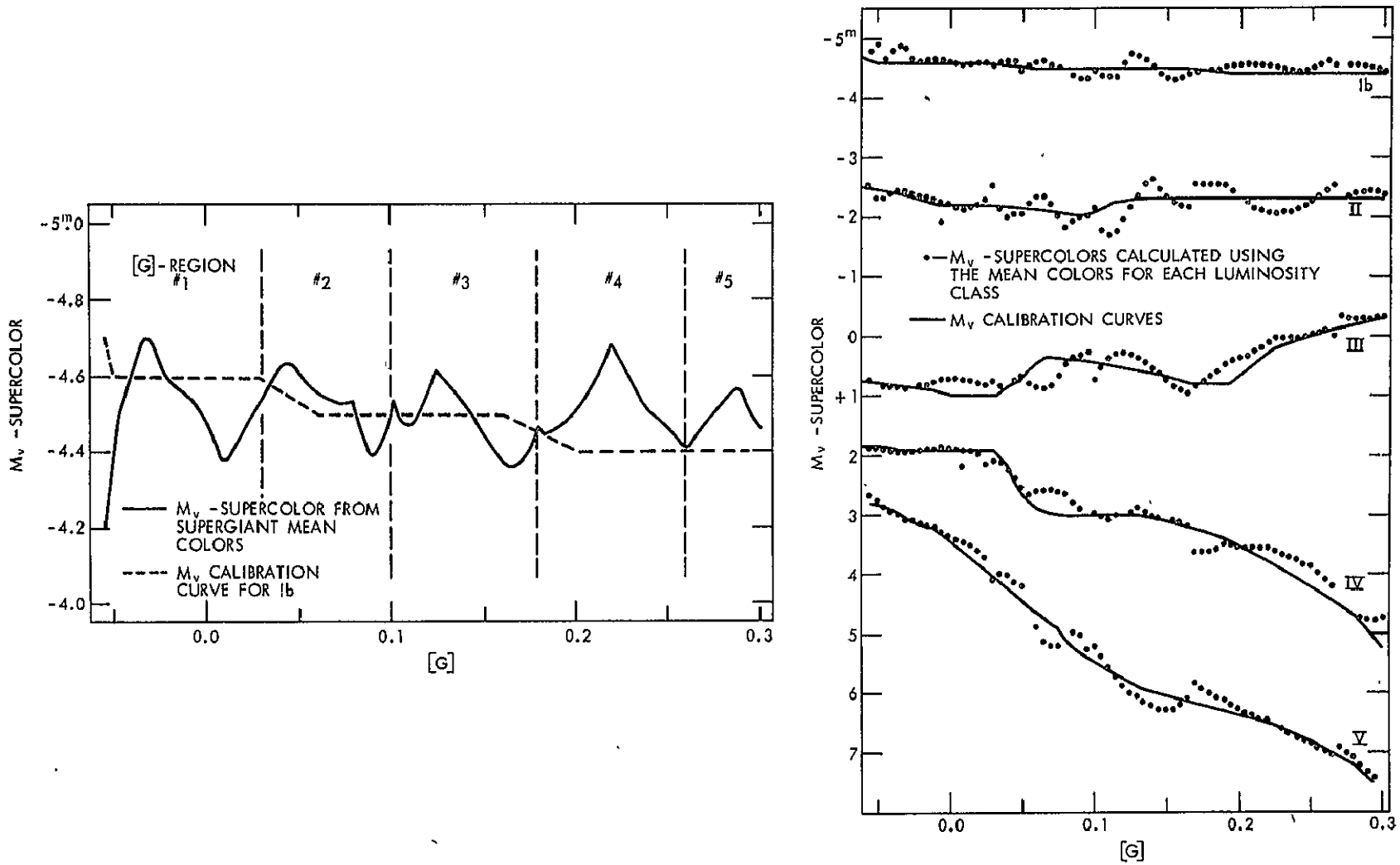

Fig. 7.1 M_V-supercolor for supergiants (left) and all luminosity classes (right) versus [G].

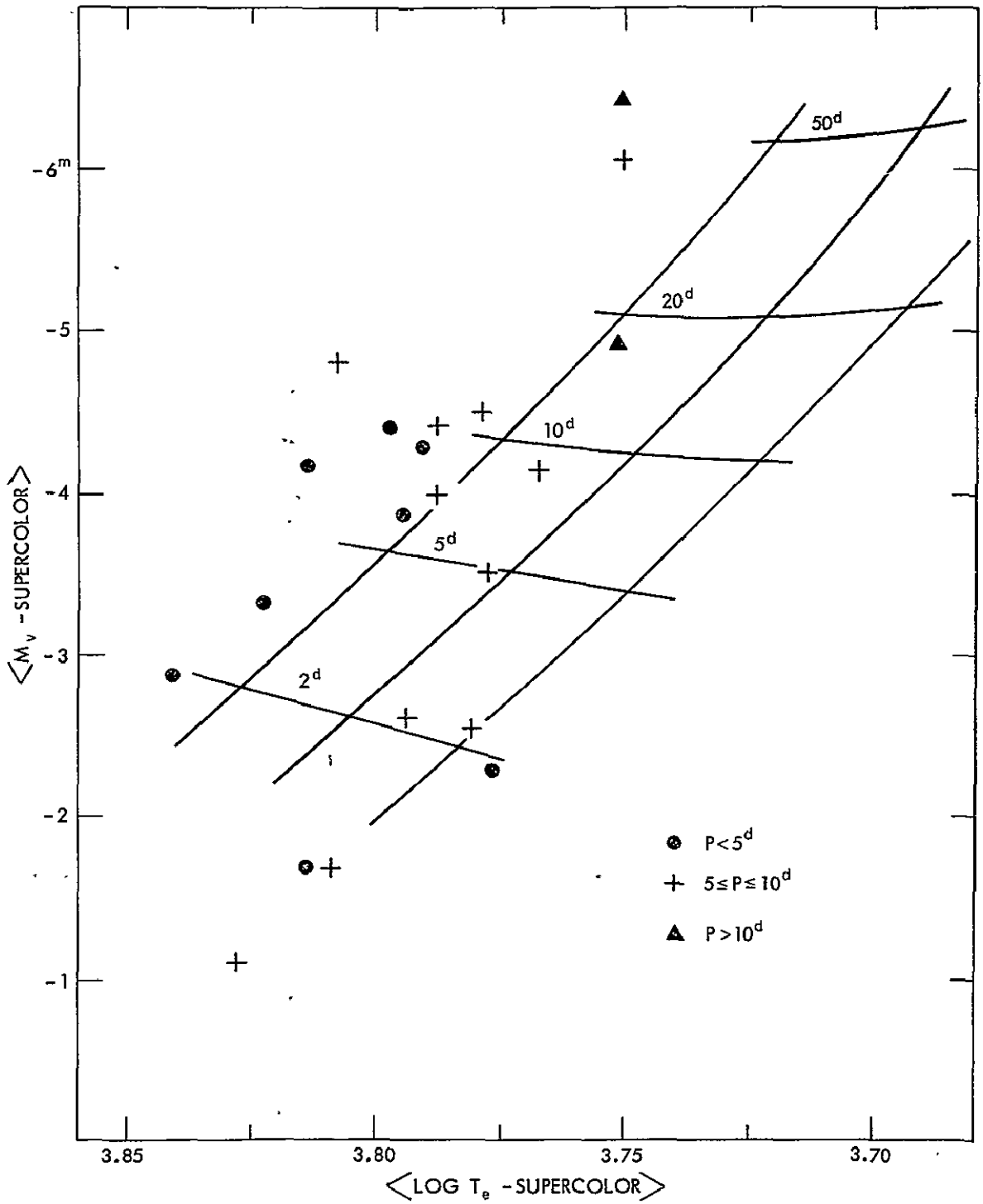

Fig. 7.2 The average M_V, $\log T_e$-supercolor diagram for cepheids. The location of the instability strip is by Fernie (1967c).

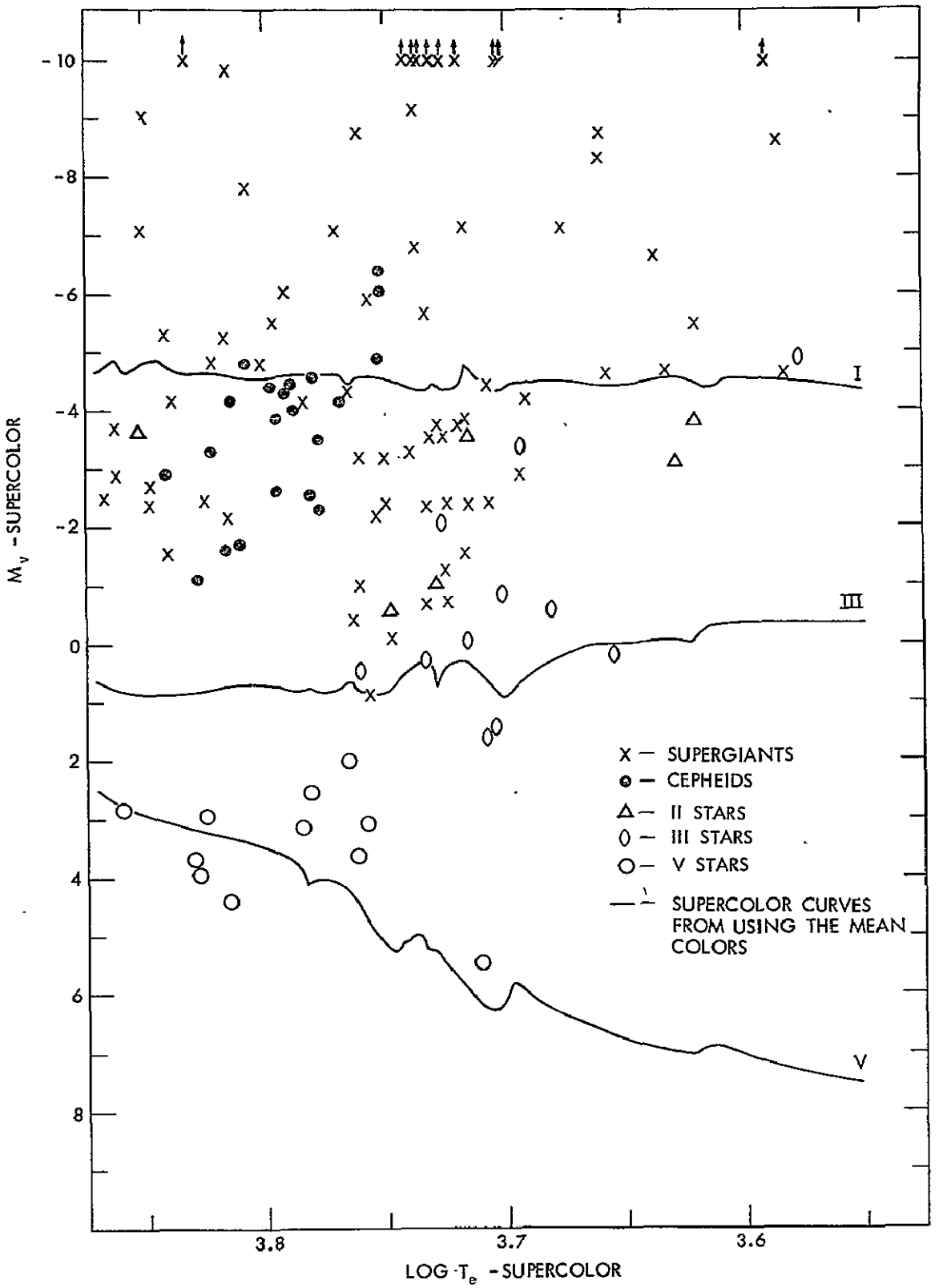

Fig. 7.3 The supercolor HR diagram created from data on individual stars of all luminosity classes.

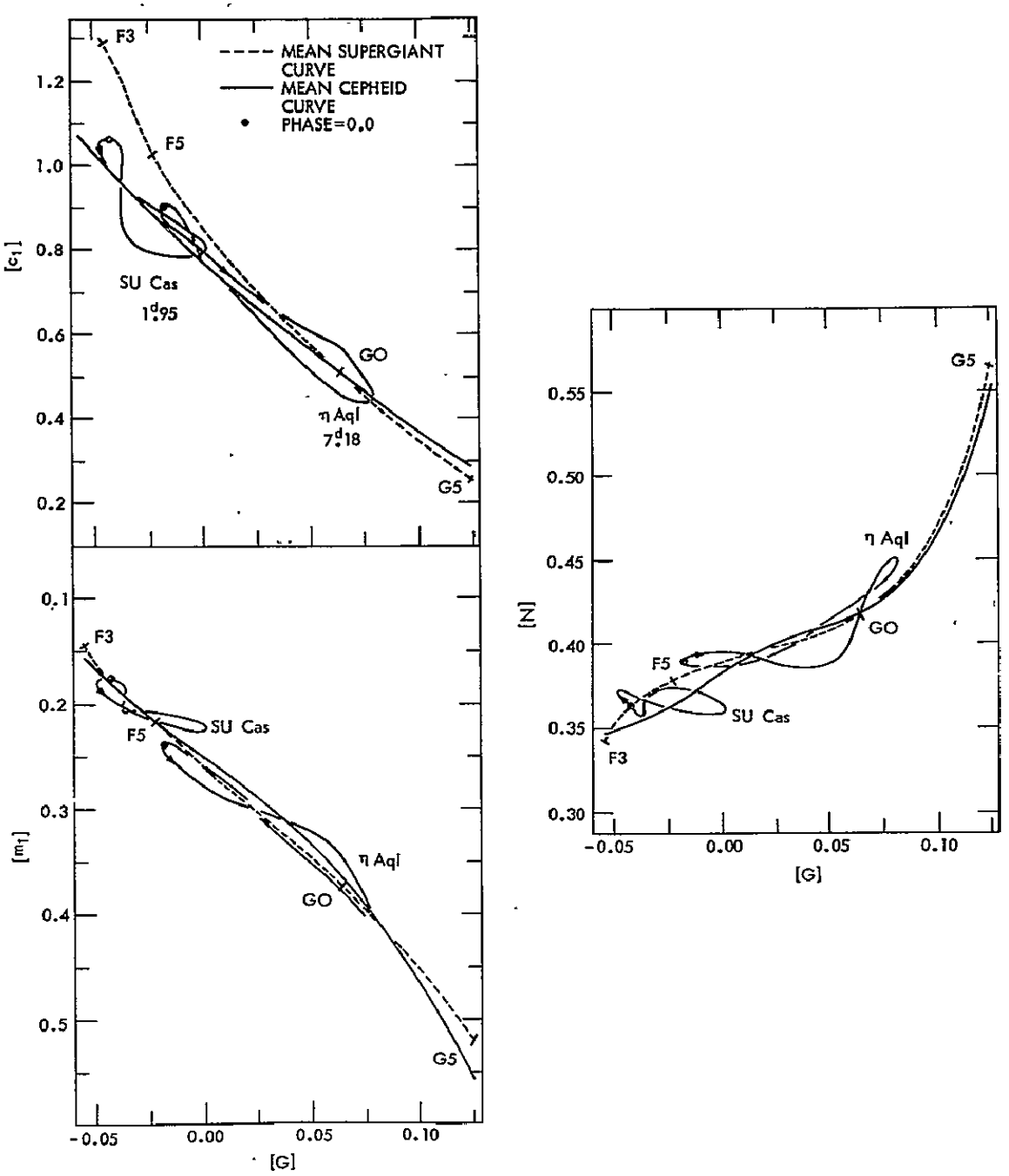

Fig. 7.4 A comparison between the mean color results for the cepheids and the supergiants.

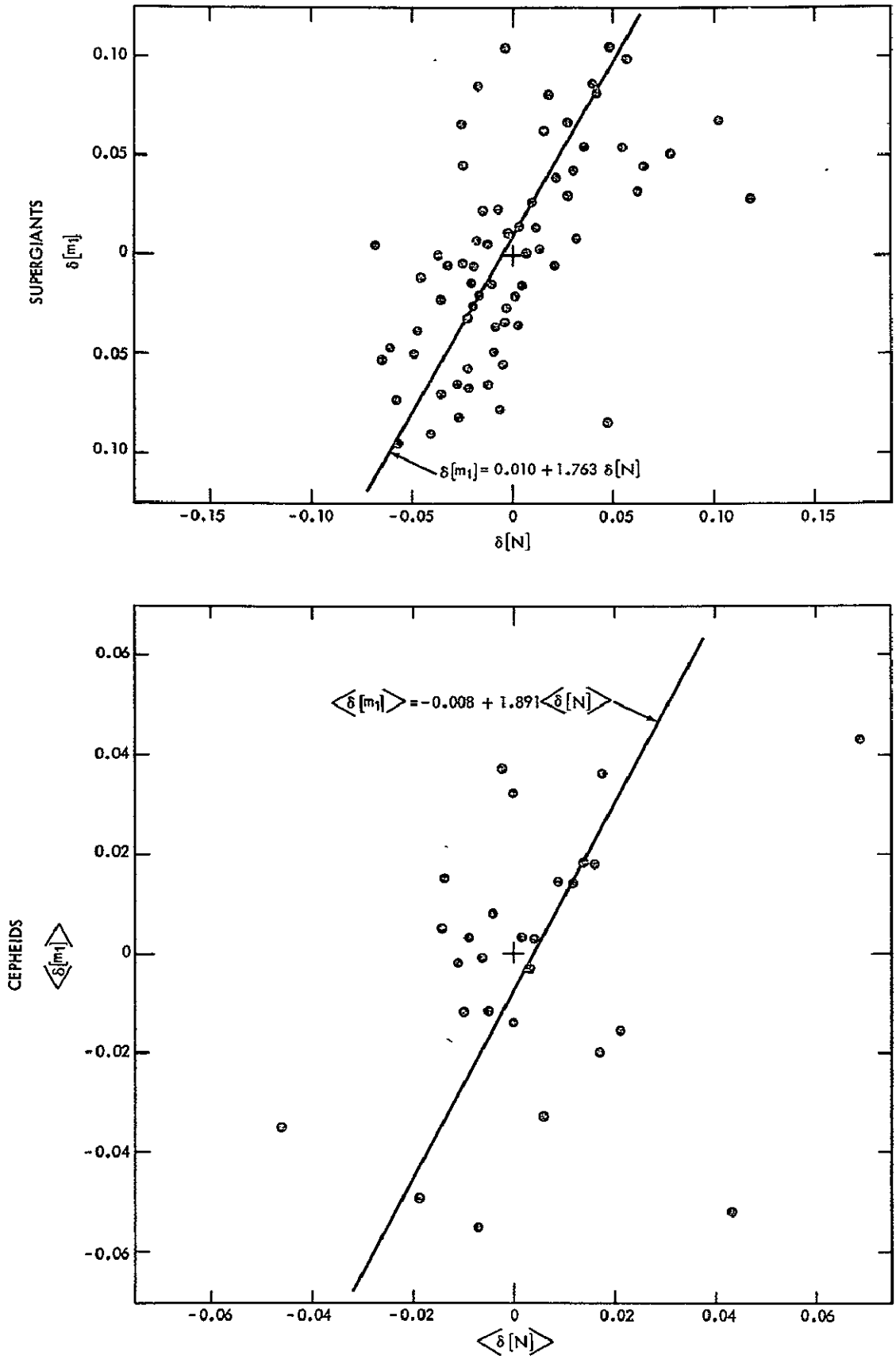

Fig. 7.5 Correlation plots of deviations in $[m_1]$ and $[N]$ from the mean for supergiants and cepheids.

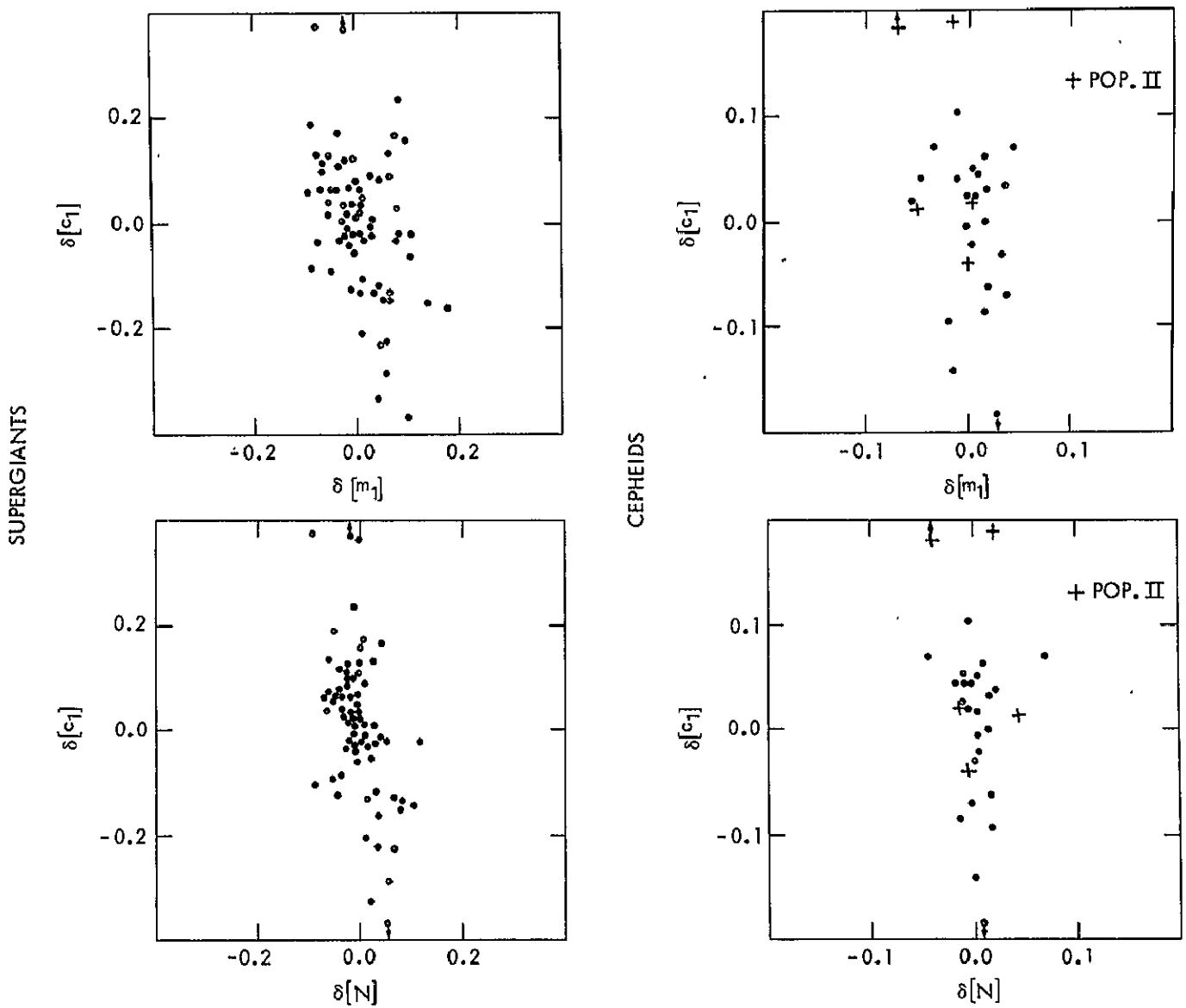

Fig. 7.6 Diagrams showing the insensitivity of $[c_1]$ on line blanketing in supergiants and cepheids.

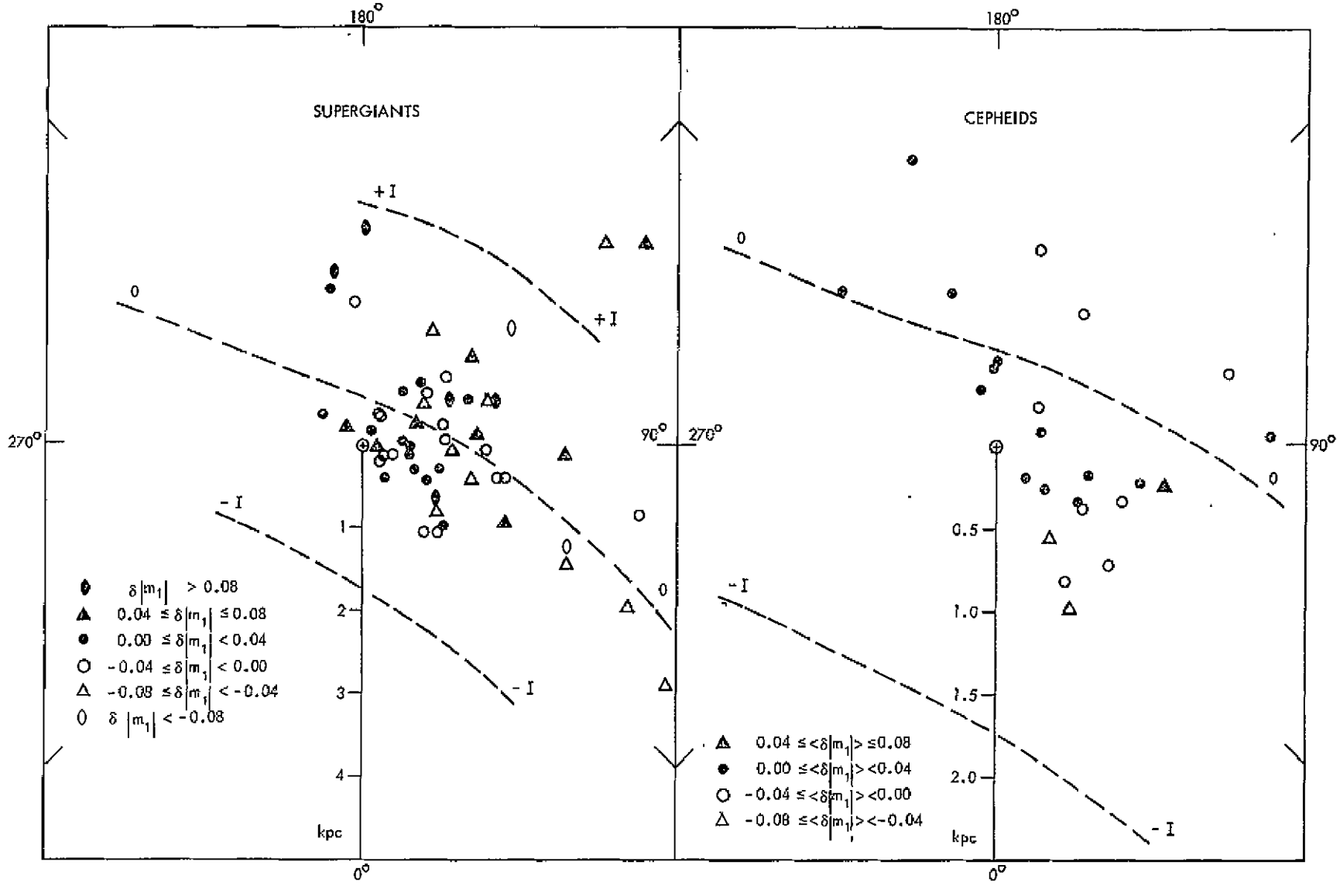

Fig. 7.7 Galactic distribution of deviations in $[m_1]$ from the mean.

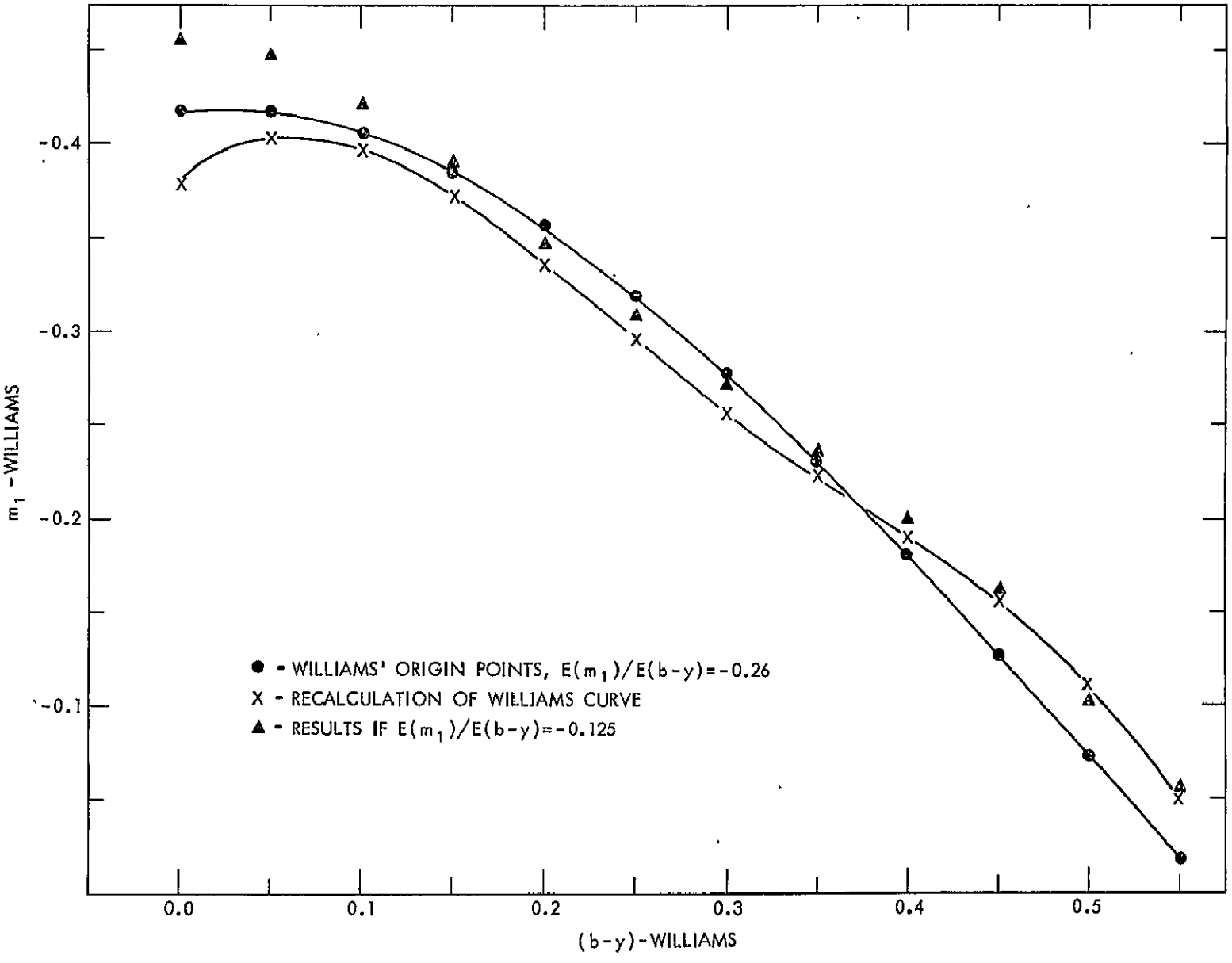

Fig. 7.8 Mean m_1 versus (b-y) relation for Williams' long period cepheids ($P>11^d$).

APPENDIX A

STAR IDENTIFICATIONS

We list in Table A.1 data which identifies each star in the observational program. The table gives the name, catalog numbers, spectral class, and equatorial and galactic coordinates for Epoch 1965.

TABLE A.1

CATALOG OF IDENTIFICATION DATA FOR THE PROGRAM STARS.

NAME			CATALOG NUMBERS HD	BD	GC	HR	SPECTRAL CLASS	R.A. (1965) H	M	S	DEC. D	M	S	LII DEG.	BII DEG.
							-- STANDARD STARS --								
22		AND	571	45 17	169	27	F2II	0	8	23	45	51	54	115.5	-16.2
33	θ	CAS	6961	54 236	1424	343	A7V	1	8	54	54	57	32	125.8	-7.6
50	υ	AND	9826	40 332	1948	458	F8V	1	34	36	41	13	18	132.0	-20.7
			10476	19 279	2080	493	K1V	1	40	36	20	5	57	138.9	-41.0
			18331	-4 502	3541	875	A1V	2	54	49	-3	51	22	178.3	-50.9
	ζ	PER	19373	49 857	3740	937	G0V	3	6	23	49	28	24	144.6	-7.4
1	ο	TAU	21120	8 511	4070	1030	G8III	3	22	56	8	54	25	174.1	-38.2
38	o^1	ERI	26574	-7 764	5056	1298	F2III	4	10	9	-6	55	39	197.3	-37.5
			27022	64 433	5199	1327	G5III	4	17	10	65	3	24	142.7	10.6
56	π^3	TAU	27309	21 623	5216	1341	A 5I	4	17	32	21	41	26	174.1	-19.8
1		ORI	30652	6 762	5875	1543	F6V	4	48	1	6	54	1	191.5	-23.1
3	ζ	AUR	31398	32 855	6029	1577	K3II	4	54	43	33	6	46	170.6	-6.2
54	χ	ORI	39587	20 1162	7419	2047	G0V	5	52	11	20	16	18	188.5	-2.8
27	ε	GEM	48329	25 1406	8786	2473	G8IB	6	41	43	25	10	7	189.6	9.6
66		AUR	57669	40 1852	9850	2805	K0III	7	21	43	40	46	15	177.7	23.2
3	β	CMI	58715	8 1774	9947	2845	B7V	7	25	12	8	21	45	209.5	11.7
62	ρ	GEM	58946	32 1562	9987	2852	F0V	7	26	52	31	51	20	187.2	21.3
77	κ	GEM	62345	24 1759	10403	2985	G8III	7	42	20	24	29	1	195.9	22.0
81		GEM	62721	18 1733	10456	3003	K5III	7	44	6	18	35	58	201.9	20.1
27		LYN	67006	51 1391	11018	3173	A2V	8	5	50	51	36	34	167.2	32.6
4	δ	HYA	73262	6 2001	11823	3410	A0V	8	35	49	5	49	37	220.3	26.2
14	τ	UMA	78362	64 723	12646	3624	F5+A5	9	8	3	63	39	27	151.2	39.4
18		UMA	79439	54 1285	12761	3662	A5V	9	13	41	54	10	4	163.1	42.7
11		LMI	82885	36 1979	13242	3815	G8IV-V	9	33	34	35	58	11	188.5	47.8
			83425	5 2207	13316	3834	K3III	9	36	38	4	48	30	230.2	38.9

TABLE A.1

(CONTINUED)

NAME		HD	CATALOG NUMBERS BD	GC	HR	SPECTRAL CLASS	R.A. (1965) H M S	DEC. D M S	LII DEG.	BII DEG.
γ	LEO	89484-5	20 2467	14177	4057	K0IIIP	10 17 59	20 1 27	216.6	54.6
47 ρ	LEO	91316	10 2166	14487	4133	B1IB	10 30 55	9 29 32	234.9	52.8
5 β	VIR	102870	2 2489	16215	4540	F8V	11 48 46	1 58 24	270.5	60.8
		103095	38 2285	16253	4550	G8VI	11 50 55	37 58 36	168.5	73.7
64 γ	UMI	103287	54 1475	16268	4554	A0V	11 51 51	53 53 22	140.9	61.4
95	LEO	103578	16 2319	16311	4564	A3V	11 53 52	15 50 29	251.7	72.7
16	VIR	107328	4 2604	16828	4695	K1III	12 18 34	3 30 27	284.3	65.0
31	COM	111812	28 2156	17455	4883	G0III	12 50 0	27 45 31	115.4	89.6
78	UMA	113139	57 1408	17664	4931	F2V	12 59 9	56 33 54	120.4	60.7
85 η	UMA	120315	50 2027	18643	5191	B3V	13 46 8	49 29 30	100.7	65.3
		122563	10 2617	18965	5270	G0VI	14 0 5	9 51 17	349.9	65.9
27 γ	BOO	127762	38 2565	19607	5435	A7III	14 30 40	38 27 38	67.3	66.2
		130109	2 286	19884	5511	A0V	14 44 23	2 2 54	355.3	52.7
41 γ	SER	142860	16 2849	21408	5933	F6IV-V	15 54 45	15 46 54	27.8	45.7
13 ε	CRB	143107	27 2558	21440	5947	K3III	15 56 6	26 59 0	43.7	48.8
15 ρ	CRB	143761	33 2663	21527	5968	G2V	15 59 38	33 24 48	53.5	48.9
23 β	DRA	159181	52 2065	23741	6536	G2II	17 29 37	52 19 38	79.6	33.3
30 δ	AQL	182640	2 3879	26816	7377	F0IV	19 23 38	3 2 12	39.6	-6.1
32 ν	AQL	182835	0 4206	26838	7387	F2IB	19 24 41	0 15 55	37.3	-7.6
5 α	SGE	185758	17 4042	27215	7479	G0II	19 38 26	17 55 48	54.5	-2.1
		186427	50 2848	27285	7504	G5V	19 40 53	50 25 54	83.4	13.2
50 γ	AQL	186791	10 4043	27354	7525	K3II	19 44 30	10 31 0	48.7	-7.1
17	CYG	187013	33 3587	27369	7534	F5V	19 45 1	33 38 30	68.8	4.4
30 α^1	CYG	192514	46 2881	28091	7730	A3III	20 12 8	46 42 6	82.7	6.9
22	VUL	192713	23 3944	28144	7741	G2IB	20 13 57	23 23 51	63.5	-6.4
37 γ	CYG	194093	39 4159	28338	7796	F8IB	20 20 56	40 8 26	78.2	1.9

TABLE A.1

(CONTINUED)

NAME	CATALOG NUMBERS HD	BD	GC	HR	SPECTRAL CLASS	R.A. (1965) H M S	DEC. D M S	LII DEG.	BII DEG.
64 ζ CYG	202109	29 4348	29661	8115	G8II	21 11 24	30 4 42	76.8	-12.4
24 ι PEG	210027	24 4533	30932	8430	F5V	22 5 16	25 9 42	82.2	-24.2
23 ε CEP	211336	56 2741	31135	8494	F0IV	22 13 39	56 51 24	102.9	0.4
35 PEG	212943	3 4710	31377	8551	K0III-IV	22 26 6	4 31 10	70.0	-42.9
51 PEG	217014	19 5036	32003	8729	G5V	22 55 48	20 35 30	90.1	-34.7
			-- ORDINARY STARS --						
	4362	58 101	926	207	G0IB	0 44 36	59 22 41	122.4	-3.3
	6474	63 141	1332		G0IA	1 4 45	63 35 12	124.7	1.0
34 φ CAS	7927	57 260	1594	382	F0IA	1 17 52	58 2 54	126.7	-4.4
	8906	59 258	1784		F3IB	1 26 53	59 51 1	127.6	-2.5
	8992	58 249			F6IB	1 27 32	58 35 0	127.9	-3.7
	9022	59 261	1803		K3III	1 28 0	59 36 6	127.8	-2.7
	9250	62 264	1851		G0IB	1 30 15	63 24 33	127.5	1.1
	9366	54 315	1873		K3IB	1 31 13	54 45 57	129.0	-7.4
	10494	61 316			F5IA	1 41 45	61 40 42	129.1	-0.4
	11092	64 243	2218		K5IAB-IB	1 48 44	64 40 55	129.3	2.7
	11800	59 363			K5IB	1 55 13	60 2 8	131.1	-1.6
		59 366			A0IB	1 55 56	59 52 8	131.2	-1.8
	12014	58 345			K0IB	1 57 23	58 59 2	131.6	-2.6
		59 389			F0IB	1 55 56	59 52 8	131.2	-1.8
	14662	54 535	2863	690	F7IB	2 21 21	55 12 7	135.9	-5.2
14 PER	16901	43 566	3278	800	G0IB	2 41 44	44 8 43	143.3	-14.1
-- --	17378	56 718	3370	825	A5IA	2 46 50	56 56 8	138.5	-2.2
15 η PER	17506	55 714	3390	834	K3IB	2 48 8	55 45 6	139.2	-3.2

TABLE A.1

(CONTINUED)

NAME	HD	BD	GC	HR	SPECTRAL CLASS	R.A. (1965) H M S	DEC. D M S	LII DEG.	BII DEG.
	17958	63 369	3497	861	K3IA	2 53 30	64 11 30	136.0	4.7
	17971	59 569			F5IA	2 53 14	60 14 58	137.8	1.2
	18391	57 672	3578		G0IA	2 57 9	57 31 29	139.5	-1.0
	20123	50 729	3883	969	G5II	3 13 41	50 48 34	144.9	-5.7
33 α PER	20902	49 917	4041	1017	F5IB	3 21 44	49 44 5	146.6	-5.9
41 υ PER	23230	42 815	4474	1135	F5II	3 42 44	42 28 0	153.8	-9.6
	25030	51 827			K1IB	3 58 25	52 4 11	149.8	-0.5
	25056	53 722	4797		G0IB	3 58 55	53 46 8	148.8	0.8
	25305	51 843			A2IB	4 1 7	51 47 58	150.3	-0.5
	25291	58 690	4858	1242	F0II	4 1 31	59 3 37	145.5	5.0
51 μ PER	26630	48 1063	5099	1303	G0IB	4 12 19	48 19 20	154.0	-1.8
	31118	43 1124	5979		K5IB	4 52 45	43 21 43	162.4	-0.0
7 ε AUR	31964	43 1166	6123	1605	F0IAP	4 59 23	43 46 20	162.8	1.2
10 β CAM	31910	60 856	6136	1603	G0IB	5 0 12	60 23 32	149.6	11.4
	33299	30 804	6319		K1IB	5 8 20	30 45 19	174.2	-5.3
11 α LEP	36673	-17 1166	6875	1865	F0IB	5 31 8	-17 50 48	219.2	-24.5
	36891	40 1346	6952	1884	G3IB	5 34 26	40 9 42	169.5	4.4
	37819	28 856			F5IB	5 40 20	28 59 4	179.6	-0.5
	38247	18 950	7187		G8IAB	5 43 5	18 41 26	188.7	-5.4
	38808	24 973			G3IB-II	5 47 15	24 13 30	184.5	-1.7
	39416	25 1020			G3IB-II	5 51 25	25 4 6	184.2	-0.5
	39866	28 952	7472	2066	A2IB	5 54 20	28 56 18	181.2	2.1
	39970	24 1033	7483	2074	A0IA	5 54 47	24 14 46	185.3	-0.2
	39949	27 923			G2IB	5 54 49	27 18 54	182.7	1.3
	40297	27 938	7545		A0IB	5 56 54	27 33 38	182.7	1.8
	43282	19 1281			G5IB-II	6 14 8	19 4 51	192.0	1.2

TABLE A.1

(CONTINUED)

NAME			CATALOG NUMBERS HD	BD	GC	HR	SPECTRAL CLASS	R.A. (1965) H	M	S	DEC. D	M	S	LII DEG.	BII DEG.
			44033	14 1247	8131	2269	K3IB	6	18	4	14	40	3	196.4	-0.1
		MON	44990	7 1273	8291	2310	F7IAB	6	23	20	7	6	23	203.6	-2.6
			45829	8 1367			K0IAB	6	28	8	7	56	30	203.5	-1.1
13		MON	46300	7 1337	8506	2385	A0IB	6	30	57	7	21	39	204.3	-0.8
25		GEM	47731	28 1207	8719	2453	G5IB	6	39	9	28	13	51	186.5	10.4
			48616	3 1379			F5IB	6	42	37	3	11	8	209.4	-0.1
			58439	-18 1825	9899	2831	A2IB	7	23	19	-18	56	32	232.0	-0.6
			58526	-5 2112	9923	2833	G3IB	7	24	8	-5	42	15	220.8	5.6
			59067	-11 1951	9979	2859	G8IB	7	26	13	-11	29	5	226.5	3.1
29	ζ	MON	67594	-2 2450	11051	3188	G2IB	8	6	50	-2	52	51	223.1	16.5
			71952	53 1259	11665	3351	K0IV	8	29	57	53	14	7	165.3	36.4
			74395	-6 2708	12006	3459	G2IB	8	41	57	-7	6	24	233.1	21.1
			77912	39 2200	12565	3612	G8IB-II	9	4	19	38	35	36	184.4	42.2
17	ε	LEO	84441	24 2129	13443	3873	G0II	9	43	49	23	56	27	206.8	48.2
30	η	LEO	87737	17 2171	13899	3975	A0IB	10	5	26	16	56	3	219.6	50.8
65		LEO	96436	2 2387	15282	4319	G7	11	5	7	2	8	45	253.7	54.5
			111631	0 2989	17435		M0.5V	12	48	55	0	34	27	302.6	63.3
			128750	18 2906	19726	5462	K2	14	36	37	18	26	58	18.8	63.9
45		BOO	134083	25 2873	20342	5634	F5V	15	5	46	25	0	16	36.5	59.5
			148743	-7 4305	22187	6144	A7IB	16	28	33	-7	26	16	8.8	27.2
13	ζ	OPH	149757	-10 4350	22332	6175	O9.5V	16	35	10	-10	30	0	7.2	24.2
			161796	50 2457	24113		F3IB	17	44	2	50	3	28	77.2	30.9
89		HER	163506	26 3120	24382	6685	F2IA	17	53	58	26	3	16	51.4	23.2
			163800	-22 4474	24456		O8	17	56	45	-22	31	0	8.0	1.2
			168913	29 3241	25056	6876	F9IB	18	19	36	29	50	28	57.4	19.2
45		DRA	171635	56 2113	25362	6978	F7IB	18	31	57	57	1	3	86.2	25.0

TABLE A.1

(CONTINUED)

NAME	HD	BD	GC	HR	SPECTRAL CLASS	R.A. (1965) H	M	S	DEC. D	M	S	LII DEG.	BII DEG.
	172365	5 3891	25520	7008	F9IB	18	37	50	5	13	48	36.3	5.0
	173638	-10 4797	25718	7055	F2IB-II	18	44	44	-10	9	54	23.7	-3.4
	174104	28 3085			G0IB	18	46	21	28	41	3	58.6	13.4
	179784	14 3829	26483		G5IB	19	11	40	14	58	29	48.8	2.1
	180028	5 4087	26514		F6IB	19	12	59	5	59	5	41.0	-2.4
	180583	27 3314	26562	7308	F6IB-II	19	14	33	27	51	43	60.6	7.4
	182296	8 4072			G3IB	19	22	0	8	35	28	44.3	-3.1
	183864	24 3768			G2IB	19	29	10	25	1	54	59.6	3.2
	187203	10 4058	27413	7542	G0IB	19	46	48	10	36	12	49.1	-7.5
	187299	24 3889			G5IAB-IB	19	46	56	24	54	52	61.5	-0.3
	226223	38 3790			F6IB	19	50	22	38	39	42	73.7	6.0
	190113	35 3920			G5IB	20	0	40	35	31	36	72.1	2.7
	331777	31 3907			F8IA	20	1	49	31	49	8	69.1	0.5
	190446	39 4020			F6IB	20	2	7	40	9	42	76.2	4.9
	190323	14 4158	27819		G0IA-IAB	20	2	10	14	52	49	54.7	-8.6
	190403	29 3873	27825		G5IB-II	20	2	19	29	53	23	67.5	-0.6
	191010	25 4103			G3IB	20	5	22	25	34	6	64.2	-3.5
	191423	42 3599			O9V	20	6	50	42	30	0	78.6	5.4
		37 3827			F3IB	20	11	28	38	16	40	75.6	2.3
32 o^2 CYG	192909	47 3059	28160	7751	K3IB-II	20	14	24	47	36	21	83.7	7.0
5 α^1 CAP	192876	-12 5683	28189	7747	G3IB	20	15	39	-12	37	15	32.3	-24.2
35 CYG	193370	34 3967	28242	7770	F5IB	20	17	16	34	52	9	73.4	-0.5
	193469	38 4003	28255		K5IB	20	17	41	38	53	36	76.8	1.7
41 CYG	195295	29 4057	28513	7834	F5II	20	27	55	30	14	50	70.9	-5.0
42 CYG	195324	35 4141	28515	7835	A1IB	20	28	0	36	20	14	75.9	-1.5
44 CYG	195593	36 4105	28551	7847	F5IAB	20	29	37	36	48	49	76.4	-1.4

TABLE A.1

(CONTINUED)

NAME	CATALOG NUMBERS HD	BD	GC	HR	SPECTRAL CLASS	R.A. (1965) H M S	DEC. D M S	LII DEG.	BII DEG.
47 CYG	196093	34 4079	28630	7866	K2IB	20 32 32	35 7 48	75.4	-2.9
8 θ DEL	196725	12 4411	28743	7892	K3IB	20 37 4	13 11 28	58.0	-16.6
	200102	44 3661	29323		G1IB	20 58 37	44 51 33	86.2	-0.7
	200805	44 3688			F5IB	21 2 53	45 0 12	86.8	-1.2
62 ξ CYG	200905	43 3800	29459	8079	K5IB	21 3 39	43 47 15	86.0	-2.1
	202314	29 4354	29695	8126	G2IB	21 12 40	29 45 20	76.7	-12.9
	204022	49 3516			G0IB	21 22 55	50 17 45	92.9	0.1
22 β AQR	204867	-6 5770	30137	8232	G0IB	21 29 40	-5 43 50	49.6	-37.1
	205349	45 3584	30189	8248	K1IB	21 31 57	45 41 37	90.8	-4.3
	206312	48 3457	30335		K1III	21 38 37	48 58 8	93.9	-2.6
8 ε PEG	206778	9 4891	30431	8308	K2IB	21 42 28	9 42 49	65.6	-31.5
9 PEG	206859	16 4582	30444	8313	G5IB	21 42 48	17 11 2	72.0	-26.5
12 PEG	207089	22 4472	30479	8321	K0IB	21 44 25	22 46 55	76.6	-22.8
10 ν CEP	207260	60 2288	30483	8334	A2IA	21 44 26	60 57 31	102.3	5.9
	207489	38 4611	30534		F5IB	21 46 49	38 47 17	88.3	-11.3
	207647	49 3631	30557		G4IB	21 47 47	49 30 49	95.4	-3.2
	207673	40 4648	30566	8345	A2IB	21 48 15	40 59 6	90.0	-9.8
	208606	60 2318	30702	8374	G8IB	21 54 18	61 22 31	103.5	5.5
14 CEP	209481	57 2441	30837	8406	O9V	22 1 2	57 49 0	102.0	2.2
34 α AQR	209750	-1 4246	30896	8414	G2IB	22 3 56	0 29 44	61.0	-41.4
	210221	52 3114	30958	8443	A3IB	22 6 7	53 8 9	99.8	-2.0
21 ζ CEP	210745	57 2475	31044	8465	K1IB	22 9 36	58 1 24	103.1	1.7
10 LAC	214680	38 4826	31626	8622	O9V	22 37 37	38 51 0	96.6	-17.0
	216206	49 3954	31858	8692	G4IB	22 48 37	50 29 9	104.1	-7.7
	216946	48 3887	31989	8726	K5IB	22 54 53	49 32 46	104.6	-9.0
	217476	56 2923	32063	8752	G0IA	22 58 34	56 45 7	108.2	-2.7

TABLE A.1

(CONTINUED)

NAME	HD	CATALOG NUMBERS BD	GC	HR	SPECTRAL CLASS	R.A. (1965) H M S	DEC. D M S	LII DEG.	BII DEG.
56 PEG	218356	24 4716	32201	8796	K0IBP	23 5 21	25 16 25	95.1	-31.7
	219135	55 2919	32322		G0IB	23 11 17	56 20 26	109.6	-3.8
		60 2532			F7IB	23 22 42	61 24 0	112.8	0.4
	221861	70 1327	32793	8952	K0IAB	23 33 24	71 26 35	116.9	9.7
	222574	-18 6358	32911	8982	G0II	23 39 54	-18 0 59	59.5	-71.4
20 ψ AND	223047	45 4321	32988	9003	G5IB	23 44 14	46 13 13	111.4	-15.0
7 ρ CAS	224014	56 3111	33160	9045	F8IAP	23 52 37	57 18 16	115.3	-4.5
	224165	46 4214	33183	9053	G8IB	23 53 47	47 9 40	113.2	-14.5
					-- VARIABLE STARS --				
TU CAS	2207	53 72			CW	0 24 22	51 4 48	118.9	-11.4
DL CAS		59 65			C-DELTA	0 27 58	60 1 14	120.3	-2.6
SU CAS	17463	68 200	3403	829	C-DELTA	2 48 44	68 44 24	133.5	8.5
RX CAM	25361	58 694			C-DELTA	4 1 59	58 33 48	145.9	4.7
SW TAU		3 601			CW	4 22 39	4 2 33	190.2	-29.9
SZ TAU	29260	18 661	5621		C	4 35 9	18 28 18	179.5	-18.8
AW PER	30282	36 937			C-DELTA	4 45 22	26 39 54	166.6	-5.4
ST TAU	38262	13 971			CW	5 43 1	13 33 42	193.1	-8.1
RS ORI	44415	14 1259			C-DELTA	6 20 10	14 41 48	196.6	0.3
RT AUR	45412	30 1238	8371	2332	C-DELTA	6 26 15	30 31 6	183.2	8.9
W GEM	46595	15 1246	8560		C-DELTA	6 32 54	15 21 42	197.4	3.4
ζ GEM	52973	20 1687	9313	2650	C-DELTA	7 2 2	20 38 23	195.8	11.9
RY CMA	56450	-11 1867			C-DELTA	7 14 57	-11 25 18	225.3	0.7
AL VIR	123984	-12 3993			CW	14 9 15	-13 8 49	331.2	45.4
SS SCT	173058	-7 4683			C-DELTA	18 41 46	-7 46 12	26.6	-1.1

TABLE A.1

(CONTINUED)

NAME	CATALOG NUMBERS HD	BD	GC	HR	SPECTRAL CLASS	R.A. (1965) H	M	S	DEC. D	M	S	LII DEG.	BII DEG.
FF AQL	176155	17 3799	26052	7165	C-DELTA	18	56	39	17	18	42	49.2	6.4
V496 AQL	178287	-7 3861			C-DELTA	19	6	24	-7	29	42	29.1	-6.7
FM AQL	178695	10 3800			C-DELTA	19	7	34	10	30	0	44.4	0.9
U AQL	183344	-7 4968	26905	7402	C-DELTA	19	27	24	-7	7	12	31.1	-11.5
U VUL	185059	20 4200	27119	7458	C	19	35	3	20	15	6	56.1	-0.3
SU CYG	186688	28 3460	27336	7518	C-DELTA	19	43	21	29	10	36	64.8	2.5
η AQL	187929	0 4337	27517	7570	C-DELTA	19	50	39	0	54	36	40.9	-13.1
S SGE	188727	16 4067	27601	7609	C-DELTA	19	54	24	16	32	24	55.2	-6.1
X CYG	197572	35 4234	28886	7932	C-DELTA	20	41	59	35	27	24	76.9	-4.3
T VUL	198726	27 3890	29089	7988	C	20	49	56	28	6	48	72.1	-10.2
DT CYG	201078	30 4318	29502	8084	C-DELTA	21	5	0	31	2	18	76.6	-10.8
AU PEG		17 4572			CW	21	22	20	18	7	24	69.1	-22.3
VZ CYG		42 4233			C-DELTA	21	50	14	42	57	54	91.5	-8.5
δ CEP	213306	57 2548	31421	8571	C-DELTA	22	27	49	58	13	48	105.2	0.5
X LAC	216105	55 2817			C-DELTA	22	47	34	56	14	18	106.6	-2.5

APPENDIX B

DATA FROM WILLIAMS AND STRÖMGREN

In Table B.1 we give data for the stars taken from Williams' (1966) study that were used in determining the mean color lines for luminosity classes V, IV, III and II. For each star we give its Henry Draper number, and its spectral type. The reddening-free color data is that derived from the original work, the same quantities transformed to our system according to the equations given in Chapter V, and the results from this investigation. The Table B.2 is of identical form, but here the data comes from the Strömgren-Perry catalog (1962).

TABLE B.1

COMPARISON OF WILLIAMS' ORIGINAL AND TRANSFORMED REDDENING-FREE COLORS TO THOSE OF KELSALL'S.

HD	SPECTRAL TYPE	STATE OF THE DATA	(C1)	(M1)	(G)	(N)
571	F2II	ORIGINAL	1.022	-0.546	-0.185	0.217
		TRANSFORMED	1.022	0.173	-0.041	0.357
		KELSALL	1.038	0.172	-0.039	0.357
7927	F0IA	ORIGINAL	1.152	-0.553	-0.185	0.197
		TRANSFORMED	1.180	0.168	-0.041	0.336
		KELSALL	1.403	0.109	-0.037	0.321
18331	A1V	ORIGINAL	1.161	-0.516	-0.262	0.208
		TRANSFORMED	1.192	0.194	-0.132	0.348
		KELSALL	1.033	0.170		
18391	G0IA	ORIGINAL	0.202	-0.172	-0.050	0.299
		TRANSFORMED	0.230	0.481	0.103	0.447
		KELSALL	0.355	0.523	0.084	0.435
20902	F5IB	ORIGINAL	1.002	-0.459	-0.162	0.242
		TRANSFORMED	0.998	0.236	-0.015	0.384
		KELSALL	1.049	0.228	-0.026	0.379
21120	G8III	ORIGINAL	0.368	-0.289	-0.050	0.303
		TRANSFORMED	0.361	0.374	0.103	0.451
		KELSALL	0.399	0.396	0.107	0.459
27022	G5III	ORIGINAL	0.362	-0.323	-0.076	0.284
		TRANSFORMED	0.356	0.345	0.077	0.430
		KELSALL	0.375	0.343	0.093	0.414
30652	F6V	ORIGINAL	0.476	-0.499	-0.155	0.201
		TRANSFORMED	0.454	0.207	-0.007	0.340
		KELSALL	0.357	0.221	-0.004	0.344
36673	F0IB	ORIGINAL	1.385	-0.501	-0.193	0.229
		TRANSFORMED	1.488	0.205	-0.050	0.370
		KELSALL	1.462	0.206	-0.050	0.329
38247	G8IAB	ORIGINAL	-0.057	0.160	0.066	0.543
		TRANSFORMED	0.055	0.834	0.210	0.724
		KELSALL	0.077	0.820	0.193	0.715
46300	A0IB	ORIGINAL	0.990	-0.646	-0.213	0.212
		TRANSFORMED	0.984	0.107	-0.073	0.352
		KELSALL	0.976	0.090	-0.064	0.360

TABLE B.1

(CONTINUED)

HD	SPECTRAL TYPE	STATE OF THE DATA	(C1)	(M1)	(G)	(N)
48329	G8IB	ORIGINAL	0.029	0.139	0.066	0.559
		TRANSFORMED	0.109	0.810	0.210	0.743
		KELSALL	0.098	0.810	0.198	0.744
58946	F0V	ORIGINAL	0.682	-0.513	-0.204	0.223
		TRANSFORMED	0.650	0.196	-0.063	0.364
		KELSALL	0.587	0.178	-0.062	0.362
67594	G2IB	ORIGINAL	0.343	-0.226	-0.041	0.320
		TRANSFORMED	0.340	0.430	0.112	0.470
		KELSALL	0.337	0.505	0.119	0.465
73262	A0V	ORIGINAL	1.197	-0.540	-0.247	0.205
		TRANSFORMED	1.237	0.177	-0.114	0.344
		KELSALL	1.062	0.171		
111812	G0III	ORIGINAL	0.362	-0.411	-0.103	0.180
		TRANSFORMED	0.356	0.273	0.049	0.317
		KELSALL	0.383	0.228	0.055	0.318
113139	F2V	ORIGINAL	0.667	-0.503	-0.183	0.215
		TRANSFORMED	0.635	0.204	-0.038	0.355
		KELSALL	0.533	0.208	-0.047	0.358
122563	G0VI	ORIGINAL	0.373	-0.493	-0.131	0.211
		TRANSFORMED	0.365	0.211	0.019	0.351
		KELSALL	0.458	0.189	0.026	0.351
142860	F6IV-V	ORIGINAL	0.483	-0.506	-0.143	0.190
		TRANSFORMED	0.460	0.201	0.006	0.328
		KELSALL	0.370	0.186	0.004	0.327
159181	G2II	ORIGINAL	0.338	-0.283	-0.056	0.265
		TRANSFORMED	0.336	0.379	0.097	0.410
		KELSALL	0.371	0.394	0.101	0.414
182835	F2IB	ORIGINAL	1.252	-0.551	-0.194	0.219
		TRANSFORMED	1.309	0.170	-0.051	0.359
		KELSALL	1.410	0.144	-0.065	0.365
185758	G0II	ORIGINAL	0.424	-0.363	-0.085	0.262
		TRANSFORMED	0.409	0.312	0.068	0.406
		KELSALL	0.434	0.315	0.071	0.411

TABLE B.1

(CONTINUED)

	SPECTRAL TYPE	STATE OF THE DATA	(C1)	(M1)	(G)	(N)
186427	G5V	ORIGINAL	0.408	-0.445	-0.076	0.159
		TRANSFORMED	0.395	0.247	0.077	0.295
		KELSALL	0.346	0.239	0.078	0.297
186791	K3II	ORIGINAL	0.001	0.243	0.119	0.479
		TRANSFORMED	0.091	0.935	0.253	0.650
		KELSALL	0.084	0.896	0.261	0.655
192713	G2IB	ORIGINAL	0.236	-0.195	-0.058	0.345
		TRANSFORMED	0.255	0.459	0.095	0.498
		KELSALL	0.232	0.483	0.098	0.527
193370	F5IB	ORIGINAL	0.873	-0.426	-0.148	0.248
		TRANSFORMED	0.851	0.261	0.001	0.391
		KELSALL	0.964	0.256	-0.008	0.383
200905	K5IB	ORIGINAL	-0.063	0.279	0.143	0.423
		TRANSFORMED	0.051	0.979	0.272	0.586
		KELSALL	-0.001	0.923	0.267	0.575
204867	G0IB	ORIGINAL	0.477	-0.285	-0.069	0.270
		TRANSFORMED	0.455	0.378	0.084	0.415
		KELSALL	0.503	0.367	0.070	0.424
206778	K2IB	ORIGINAL	-0.008	0.204	0.106	0.496
		TRANSFORMED	0.085	0.887	0.243	0.670
		KELSALL	0.043	0.940	0.256	0.671
206859	G5IB	ORIGINAL	0.191	-0.101	-0.014	0.433
		TRANSFORMED	0.222	0.550	0.138	0.597
		KELSALL	0.252	0.568	0.148	0.605
207673	A2IB	ORIGINAL	0.936	-0.649	-0.187	0.198
		TRANSFORMED	0.922	0.135	-0.043	0.337
		KELSALL	1.007	0.029		
211336	F0IV	ORIGINAL	0.853	-0.481	-0.223	0.227
		TRANSFORMED	0.829	0.220	-0.085	0.368
		KELSALL	0.729	0.228	-0.079	0.357
217014	G4V	ORIGINAL	0.437	-0.444	-0.089	0.167
		TRANSFORMED	0.420	0.248	0.063	0.303
		KELSALL	0.341	0.285	0.083	0.330

TABLE B.1

(CONTINUED)

	SPECTRAL TYPE	STATE OF THE DATA	(C1)	(M1)	(G)	(N)
217476	G0IA	ORIGINAL	0.326	-0.141	-0.070	0.287
		TRANSFORMED	0.326	0.511	0.083	0.434
		KELSALL	0.358	0.551	0.063	0.451

TABLE 8.2

COMPARISON OF STROMGREN'S ORIGINAL AND TRANSFORMED REDDENING-FREE COLORS TO THOSE OF KELSALL'S.

HD	SPECTRAL TYPE	STATE OF THE DATA	(C1)	(M1)
571	F2II	ORIGINAL	1.050	0.156
		TRANSFORMED	1.034	0.161
		KELSALL	1.038	0.172
6961	A7V	ORIGINAL	0.985	0.224
		TRANSFORMED	0.971	0.222
		KELSALL	0.946	0.245
9826	F8V	ORIGINAL	0.361	0.221
		TRANSFORMED	0.369	0.220
		KELSALL	0.390	0.202
10476	K1V	ORIGINAL	0.226	0.428
		TRANSFORMED	0.238	0.418
		KELSALL	0.309	0.364
17378	A5IA	ORIGINAL	1.321	-0.034
		TRANSFORMED	1.292	-0.000
		KELSALL	1.274	0.010
18331	A1V	ORIGINAL	1.054	0.172
		TRANSFORMED	1.038	0.175
		KELSALL	1.033	0.170
19373	G0V	ORIGINAL	0.325	0.248
		TRANSFORMED	0.334	0.244
		KELSALL	0.366	0.217
21120	G8III	ORIGINAL	0.348	0.402
		TRANSFORMED	0.356	0.392
		KELSALL	0.399	0.396
23230	F5II	ORIGINAL	0.936	0.218
		TRANSFORMED	0.924	0.217
		KELSALL	0.932	0.231
25291	F0II	ORIGINAL	1.440	0.155
		TRANSFORMED	1.405	0.160
		KELSALL	1.414	0.174
26574	F2III	ORIGINAL	0.766	0.222
		TRANSFORMED	0.761	0.221
		KELSALL	0.742	0.271

TABLE B.2

(CONTINUED)

HD	SPECTRAL TYPE	STATE OF THE DATA	(C1)	(M1)
27022	G5III	ORIGINAL	0.334	0.354
		TRANSFORMED	0.343	0.345
		KELSALL	0.375	0.343
27309	A SI	ORIGINAL	0.553	0.196
		TRANSFORMED	0.555	0.197
		KELSALL	0.535	0.198
30652	F6V	ORIGINAL	0.373	0.199
		TRANSFORMED	0.381	0.200
		KELSALL	0.357	0.221
31398	K3II	ORIGINAL	0.181	0.892
		TRANSFORMED	0.194	0.926
		KELSALL	0.102	0.935
39587	G0V	ORIGINAL	0.256	0.240
		TRANSFORMED	0.267	0.237
		KELSALL	0.283	0.226
39866	A2IB	ORIGINAL	1.436	0.046
		TRANSFORMED	1.401	0.066
		KELSALL	1.463	0.061
48329	G8IB	ORIGINAL	0.163	0.769
		TRANSFORMED	0.176	0.783
		KELSALL	0.098	0.810
58715	B7V	ORIGINAL	0.806	0.108
		TRANSFORMED	0.800	0.119
		KELSALL	0.787	0.109
58946	F0V	ORIGINAL	0.582	0.183
		TRANSFORMED	0.583	0.185
		KELSALL	0.587	0.178
62345	G8III	ORIGINAL	0.321	0.452
		TRANSFORMED	0.330	0.442
		KELSALL	0.348	0.435
62721	K5III	ORIGINAL	0.318	0.861
		TRANSFORMED	0.327	0.890
		KELSALL	0.308	0.881

TABLE B.2

(CONTINUED)

HD	SPECTRAL TYPE	STATE OF THE DATA	(C1)	(M1)
67006	A2V	ORIGINAL	1.096	0.153
		TRANSFORMED	1.078	0.158
		KELSALL	1.066	0.176
78362	F5+A5	ORIGINAL	0.694	0.265
		TRANSFORMED	0.692	0.260
		KELSALL	0.658	0.288
79439	A5V	ORIGINAL	0.877	0.210
		TRANSFORMED	0.868	0.210
		KELSALL	0.845	0.225
82885	G8IV-V	ORIGINAL	0.312	0.369
		TRANSFORMED	0.321	0.360
		KELSALL	0.356	0.304
84441	G0II	ORIGINAL	0.388	0.338
		TRANSFORMED	0.395	0.330
		KELSALL	0.416	0.332
D89484	K0IIIP	ORIGINAL	0.281	0.543
		TRANSFORMED	0.291	0.536
		KELSALL	0.308	0.533
91316	B1IB	ORIGINAL	-0.037	0.028
		TRANSFORMED	-0.020	0.051
		KELSALL	-0.058	0.014
102870	F8V	ORIGINAL	0.366	0.232
		TRANSFORMED	0.374	0.230
		KELSALL	0.397	0.206
103095	G8VI	ORIGINAL	0.124	0.272
		TRANSFORMED	0.138	0.267
		KELSALL	0.134	0.275
103287	A0V	ORIGINAL	1.110	0.171
		TRANSFORMED	1.091	0.174
		KELSALL	1.075	0.165
103578	A3V	ORIGINAL	1.099	0.176
		TRANSFORMED	1.081	0.179
		KELSALL	1.064	0.202

TABLE 8.2

(CONTINUED)

HD	SPECTRAL TYPE	STATE OF THE DATA	(C1)	(M1)
107328	K1III	ORIGINAL	0.418	0.572
		TRANSFORMED	0.424	0.566
		KELSALL	0.438	0.593
111812	G0III	ORIGINAL	0.349	0.247
		TRANSFORMED	0.357	0.244
		KELSALL	0.383	0.228
113139	F2V	ORIGINAL	0.544	0.200
		TRANSFORMED	0.547	0.200
		KELSALL	0.533	0.208
120315	B3V	ORIGINAL	0.309	0.086
		TRANSFORMED	0.318	0.100
		KELSALL	0.289	0.081
122563	G0VI	ORIGINAL	0.472	0.169
		TRANSFORMED	0.477	0.173
		KELSALL	0.458	0.189
127762	A7III	ORIGINAL	0.992	0.205
		TRANSFORMED	0.978	0.205
		KELSALL	0.965	0.218
130109	A0V	ORIGINAL	1.080	0.134
		TRANSFORMED	1.062	0.142
		KELSALL	1.044	0.154
134083	F5V	ORIGINAL	0.411	0.201
		TRANSFORMED	0.418	0.201
		KELSALL	0.415	0.180
142860	F6IV-V	ORIGINAL	0.360	0.193
		TRANSFORMED	0.368	0.194
		KELSALL	0.370	0.186
143107	K3III	ORIGINAL	0.313	0.666
		TRANSFORMED	0.322	0.668
		KELSALL	0.328	0.670
143761	G2V	ORIGINAL	0.269	0.232
		TRANSFORMED	0.279	0.230
		KELSALL	0.321	0.205

TABLE B.2

(CONTINUED)

HD	SPECTRAL TYPE	STATE OF THE DATA	(C1)	(M1)
159181	G2II	ORIGINAL	0.341	0.399
		TRANSFORMED	0.350	0.389
		KELSALL	0.371	0.394
182640	FQIV	ORIGINAL	0.685	0.191
		TRANSFORMED	0.683	0.192
		KELSALL	0.685	0.212
185758	G0II	ORIGINAL	0.398	0.323
		TRANSFORMED	0.405	0.315
		KELSALL	0.434	0.315
186427	G5V	ORIGINAL	0.298	0.278
		TRANSFORMED	0.308	0.272
		KELSALL	0.346	0.239
186791	K3II	ORIGINAL	0.173	0.880
		TRANSFORMED	0.186	0.912
		KELSALL	0.084	0.896
187013	F5V	ORIGINAL	0.392	0.194
		TRANSFORMED	0.399	0.195
		KELSALL	0.408	0.187
192514	A3III	ORIGINAL	1.301	0.158
		TRANSFORMED	1.273	0.163
		KELSALL	1.275	0.166
194093	F8IB	ORIGINAL	0.824	0.345
		TRANSFORMED	0.817	0.336
		KELSALL	0.862	0.365
207260	A2IA	ORIGINAL	0.958	-0.005
		TRANSFORMED	0.946	0.023
		KELSALL	0.908	0.018
210027	F5V	ORIGINAL	0.406	0.196
		TRANSFORMED	0.413	0.197
		KELSALL	0.402	0.211
210221	A3IB	ORIGINAL	1.294	0.044
		TRANSFORMED	1.266	0.064
		KELSALL	1.288	0.059

TABLE B.2

(CONTINUED)

HD	SPECTRAL TYPE	STATE OF THE DATA	(C1)	(M1)
211336	F0IV	ORIGINAL	0.768	0.216
		TRANSFORMED	0.763	0.215
		KELSALL	0.729	0.228
212943	K0III	ORIGINAL	0.322	0.507
		TRANSFORMED	0.331	0.498
		KELSALL	0.372	0.495
217014	G5V	ORIGINAL	0.308	0.284
		TRANSFORMED	0.317	0.278
		KELSALL	0.341	0.285

APPENDIX C

COEFFICIENTS OF THE SUPERCOLORS

We give here the coefficients for the supercolor expansions as they were used in Chapter VII. The $\mathrm{Log}T_e$-supercolor is a simple quartic in [G] --

$$\mathrm{Log}T_e\text{-supercolor} = 3.812 - 1.024[G] + 0.5973[G]^2 + 19.82[G]^3 - 66.67[G]^4.$$

The form of the M_v-supercolor is given in Eq. (5-1). The coefficients of the various terms in the expansion are listed in Table C.1.

TABLE C.1

THE MV-SUPERCOLOR COEFFICIENTS FOR THE VARIOUS (G) REGIONS.

	RANGES IN (G)					
THE TERM	-0.06 TO 0.03	0.03 TO 0.05	0.05 TO 0.10	0.10 TO 0.17	0.17 TO 0.27	0.27 TO 0.30
1.0	48.544	73.167	99.720	39.131	-58.784	16.364
(C1)	-41.279	196.14	-191.97	-66.904	171.97	237.28
(M1)	-49.856	-547.80	261.39	-1.5944	-125.86	179.28
(G)	-5.3417	2220.6	-770.13	47.952	668.52	-497.84
(N)	-117.12	-455.08	-391.94	-117.82	72.125	-123.52
(C1)**2	6.0328	41.535	-61.474	0.1357	-88.885	-238.77
(C1)(M1)	38.875	838.79	-614.72	210.60	357.48	121.82
(C1)(G)	-106.40	-1295.4	547.72	-388.63	-1229.6	-616.34
(C1)(N)	24.484	-1223.7	1046.5	23.059	-216.55	-167.98
(M1)**2	-342.08	-1597.1	-327.76	-361.74	72.439	-44.310
(M1)(G)	879.86	11291.	-616.03	1045.1	1.5574	-159.57
(M1)(N)	555.30	1586.5	542.70	212.41	-100.47	-100.46
(G)**2	-755.49	-14400.	3425.4	-1385.2	-883.73	824.24
(G)(N)	-606.93	-10231.	855.83	212.98	-24.561	362.45
(N)**2	-89.422	1405.4	-342.04	-31.594	22.614	94.076

REFERENCES

Abt, H. A. 1959a, Ap. J. 130, 769.

Abt, H. A. 1959b, Ap. J. 130, 824.

Abt, H. A., Osmer, P. S., and Kraft, R. P. 1966, Ap. J. 145, 479.

Allen, C. W. 1963, Astrophysical Quantities, (London: Athlone Press), p. 103.

Aller, L. H. 1954, Astrophysics: Nuclear Transformations, Stellar Interiors, and Nebulae, (New York: Ronald Press Company), p. 98.

Arp, H. C. 1961, A. J. 65, 404.

Baade, W. 1926, Astr. Nachr. 228, 359.

Baker, N. and Kippenhahn, R. 1965, Ap. J. 142, 868.

Barry, D. C. 1967, Ap. J. Lett. 148, L87.

Becker, W. 1938, Z. Astrophys. 15, 225.

Bell, R. A. 1970, M. N. 148, 25.

Bell, R. A. and Rodgers, A. W. 1969, M. N. 142, 161.

Blauuw, A. 1963, Basic Astronomical Data, ed. K. Aa. Strand (Chicago: University of Chicago Press), p. 383.

Boggess, A. and Borgman, J. 1964, Ap. J. 140, 1636.

Buscombe, W. 1964, Mount Stromlo Observatory Mimeograph No. 8.

Chaffee, F. H. 1970, Astron. Astrophys. 4, 291.

Christy, R. F. 1964, Rev. Mod. Phys. 36, 555.

Christy, R. F. 1966a, Ann. Rev. Astron. Astrophys. 4, 353.

Christy, R. F. 1966b, Ap. J. 145, 340.

Christy, R. F. 1968, Quart. J. Roy. Astron. Soc. 9, 13.

Conti, P. S. and Deutsch, A. J. 1966, Ap. J. 145, 742.

Conti, P. S. and Deutsch, A. J. 1967, Ap. J. 147, 368.

Cox, J. P. 1963, Ap. J. 138, 487.

Cox, J. P. and Whitney, C. A. 1958, Ap. J. 127, 561.

Crawford, D. 1961, A. J. 66, 281.

Eddington, A. 1930, The Internal Constitution of the Stars, (Cambridge: Cambridge University Press), p. 202.

Epstein, I. 1950, Ap. J. 112, 6.

Fernie, J. D. 1963, A. J. 68, 780.

Fernie, J. D. 1964, Ap. J. 140, 1482.

Fernie, J. D. 1965, Ap. J. 142, 1072.

Fernie, J. D. 1966a, A. J. 71, 119.

Fernie, J. D. 1966b, A. J. 71, 732.

Fernie, J. D. 1967a, A. J. 72, 422.

Fernie, J. D. 1967b, A. J. 72, 708.

Fernie, J. D. 1967c, A. J. 72, 1327.

Fernie, J. D. 1968a, A. J. 73, 995.

Fernie, J. D. 1968b, Ap. J. 151, 197.

Fernie, J. D. and Hube, J. O. 1967, P. A. S. P. 79, 95.

Franz, O. G. 1966, Lowell Obs. Bull. 6, 251.

Gascoigne, S. C. B. and Eggen, O. J. 1957, M. N. 117, 430.

Gascoigne, S. C. B. and Kron, G. E. 1965, M. N. 130, 333.

Geyer, U. 1970, Astron. Astrophys. 5, 116.

Griffin, R. F. 1967, Ap. J. 148, 465.

Griffin, R. F. 1969, M. N. 148, 211.

Griffin, R. F. and Redman, R. O. 1960, M. N. 120, 287.

Iben, I. 1965, Ap. J. 142, 1447.

Iben, I. 1966a, Ap. J. 143, 483.

Iben, I. 1966b, Ap. J. 143, 505.

Iben, I. 1966c, Ap. J. 143, 516.

Jaschek, C., Conde, H. and de Sierra, A. C. 1964, Observatorio Astronomico de la Universidad Nacional de la Plata 28, No. 2.

Johnson, H. L. 1962, Astronomical Techniques, ed. W. A. Hiltner (Chicago: University of Chicago Press), p. 157.

Johnson, H. L. 1966, Ann. Rev. Astron. Astrophys. 4, 193.

Kelsall, T. and Strömgren, B. 1966, Vistas in Astronomy, Vol. 8, ed. A. Beer and K. Aa. Strand (Oxford: Pergamon Press), p. 159.

Kraft, R. P. 1960, Stellar Atmospheres, ed. J. L. Greenstein (Chicago: University of Chicago Press), p. 370.

Kraft, R. P. 1961, Ap. J. 133, 39.

Kraft, R. P. 1963, Basic Astronomical Data, ed. K. Aa. Strand (Chicago: University of Chicago Press), p. 421.

Kraft, R. P. 1965, Galactic Structure, ed. A. Blaauw and M. Schmidt (Chicago: University of Chicago Press), p. 157.

Kraft, R. P. 1966, Ap. J. 144, 1008.

Kraft, R. P., Kuhi, L. V. and Kuhi, P. S. 1968, A. J. 73, 221.

Kron, G. E. 1958, P. A. S. P. 70, 561.

Kron, G. E. and Svolopoulos, S. 1959, P. A. S. P. 71, 126.

Kukarkin, B. V., Parenago, P. P., Ephremov, Y. I. and Kholopov, P. N. 1958, General Catalogue of Variable Stars, (Moscow: USSR Academy of Science).

Kwee, K. K. 1967, B. A. N. Suppl. 2, 97.

Lambert, D. L. 1968, Astrophys. Lett. 2, 37.

Ledoux, P. and Walraven, T. 1958, Handbuch der Physik, Vol. 51, ed. S. Flugge (Berlin: Springer), p. 353.

Leotta-Janin, C. 1967, B. A. N. 19, 169.

Lloyd Evans, T. 1968, M. N. 141, 109.

McNamara, D. H. 1967, P. A. S. P. 79, 434.

McNamara, D. H. and Colton, D. J. 1969, P. A. S. P. 81, 826.

Mitchell, R. I., Iriarte, B., Steinmetz, D. and Johnson, H. L. 1964, Tonantzintla Bulletin 3, 153.

Nandy, K. 1964, Publ. Roy. Obs. Edinburgh 3, 142.

Nandy, K. 1965, Publ. Roy. Obs. Edinburgh 5, 13.

Nandy, K. 1966, Publ. Roy. Obs. Edinburgh 5, 233.

Nandy, K. 1967, Publ. Roy. Obs. Edinburgh 6, 25.

Nikolov, N. S. 1967a, Soviet Astron. 10, 623.

Nikolov, N. S. 1967b, Soviet Astron. 11, 92.

Oke, J. B. 1961, Ap. J. 134, 214.

Oosterhoff, P. Th. 1964, B. A. N. 17, 448.

Parsons, S. B. 1970, Ap. J. 159, 951.

Payne-Gaposchkin, C. 1954, Variable Stars and Galactic Structure, (London: Athlone Press).

Payne-Gaposchkin, C. and Gaposchkin, S. 1938, Variable Stars, (Cambridge: The Observatory), p. 153.

Payne-Gaposchkin, C. and Gaposchkin, S. 1966, Smithsonian Contrib. Astrophys. 9, 1.

Rakos, K. D. 1965, Applied Optics 4, 1453.

Reddish, V. C. 1955, M. N. 115, 480.

Rodgers, A. W. and Bell, R. A. 1963, M. N. 125, 487.

Rodgers, A. W. and Bell, R. A. 1964, M. N. 127, 471.

Rodgers, A. W. and Bell, R. A. 1967, M. N. 136, 91.

Rodgers, A. W. and Bell, R. A. 1968a, M. N. 138, 23.

Rodgers, A. W. and Bell, R. A. 1968b, M. N. 139, 175.

Rosendhal, J. D. 1970, Ap. J. 160, 627.

Rosseland, S. 1954, The Pulsation Theory of Variable Stars, (Oxford: Clarendon Press).

Sandage, A. and Tammann, G. A. 1968, Ap. J. 151, 531.

Sandage, A. and Tammann, G. A. 1969, Ap. J. 157, 683.

Schwarzschild, M. 1938, Harvard Circ. 431.

Shapley, H. and Nicholson, S. B. 1919, Proc. Nat. Acad. Sci. 5, 417.

Stibbs, D. W. N. 1955, M. N. 115, 323.

Stobie, R. S. 1969a, M. N. 144, 461.

Stobie, R. S. 1969b, M. N. 144, 485.

Stobie, R. S. 1969c, M. N. 144, 511.

Strömgren, B. 1966, Ann. Rev. Astron. Astrophys. 4, 433.

Strömgren, B. and Perry, C. 1962, Institute for Advanced Study Preprint.

Tammann, G. A. 1970, I.A.U. Symposium No. 38, The Spiral Structure of Our Galaxy, ed. G. Contopoulos (Dordrecht: D. Reidel Publishing Company), p. 236.

Thiessen, G. 1956, Z. Astrophys. 39, 65.

Unno, W. 1967, P. A. S. Japan 19, 140.

Van den Bergh, S. and Sackmann, I. J. 1965, A. J. 70, 353.

Van Hoof, A. and Deurinck, R. 1952, Ap. J. 115, 166.

Vitrichenko, E. A. and Tsarevskii, G. S. 1969, Soviet Astron. 13, 159.

Walraven, T. and Walraven, J. H. 1960, B. A. N. 15, 67.

Wesselink, A. J. 1946, B. A. N. 10, 91.

Williams, J. A. 1966, A. J. 71, 615.

Worley, C. E. 1966, P. A. S. P. 78, 485.

Yale Catalog of Bright Stars 1964, ed. D. Hoffleit (New Haven: Yale University Observatory).

Zhevakin, S. A. 1963, Ann. Rev. Astron. Astrophys. 1, 367.